The apical polarity network in *Caenorhabditis elegans* larval epithelia

María Victoria García Castiglioni

"Theory is when you know everything but nothing works.
Practice is when everything works, but nobody knows why.
In our lab theory and practice are combined:
Nothing works and nobody knows why"

The apical polarity network in *Caenorhabditis elegans* larval epithelia

Het apicale polariteitsnetwerk in *Caenorhabditis elegans* larvale epithelia
(met een samenvatting in het Nederlands)

Proefschrift

ter verkrijging van de graad van doctor aan de
Universiteit Utrecht
op gezag van de
rector magnificus, prof.dr. H.R.B.M. Kummeling,
ingevolge het besluit van het college voor promoties
in het openbaar te verdedigen op

maandag 11 oktober 2021 des middags te 12.15 uur

door

María Victoria García Castiglioni

geboren op 14 september 1993
te Montevideo, Uruguay

Printed by: Ridderprint, Alblasserdam
Layout and design: Victoria García
Copyright © 2021 by V. García Castiglioni. All rights reserved.

Promoteren: Prof. dr. M. Boxem
Prof. dr. S.J.L. van den Heuvel

Para mi familia,

Table of contents

General introduction

Victoria G. Castiglioni[a]

"Build a man a fire, and he'll be warm for a day.
Set a man on fire, and he'll be warm for the rest of his life"

Terry Pratchett

[a] Developmental Biology, Institute of Biodynamics and Biocomplexity, Department of Biology, Faculty of Science, Utrecht University, Padualaan 8, 3584 CH, Utrecht, The Netherlands.

Cell polarity

Cell polarity – the unequal distribution of molecules and structures within the cell, creating a polarity axis along which cellular processes are differentially regulated – is a fundamental and universal feature of both unicellular and multicellular organisms. Evidence of cell polarity can be found in simple unicellular organisms, like *Escherichia coli*, where protein aggregates accumulate differentially during cell division. This unequal distribution ensures deleterious material is differentially inherited by the older cells, suggesting that cell polarity arose as a solution to the problem of lineage senescence. In slightly more complex organisms, such as *Saccharomyces cerevisiae*, cell polarity is implicated in several processes, such as spindle positioning, differential inheritance of cellular components and polarized growth, which is integral to both mating and budding. During mating, cells react to gradients of pheromones by forming a mating projection, and during budding, the polarized actin cytoskeleton is reoriented in response to the small GTPase Cdc42. In complex multicellular organisms, namely plants and animals, cell polarity is implicated in a wide range of processes such as cell differentiation and proliferation, cell adhesion and migration, epithelial barrier function and morphogenesis (Macara and Mili, 2008; Martin-Belmonte et al., 2016).

The establishment of cell polarity in metazoan cells can be divided into four different steps: (1) asymmetry breaking due to an external or internal cue, (2) the establishment of cortical domains with dedicated polarity determinants, (3) the polarization of the trafficking machinery and the cytoskeleton and (4) the maintenance of the polarized state, in which mechanical processes and chemical elements cooperate. A crucial step for polarization is the localization of polarity determinants, which are highly conserved across animal species. One example is the small GTPase Cdc42, which acts as a key polarity regulator of polarity establishment in many organisms, including yeast, *C. elegans*, Drosophila and mammalian systems (Etienne-Manneville, 2004), and another is the PAR complex, which regulate several aspects of polarity in metazoan cells, including polarity establishment during asymmetric cell division, the establishment of apical-basal polarity in epithelial cells, and the axon-dendrite polarity of neurons (Martin-Belmonte et al., 2016; Wen and Zhang, 2018).

Epithelial tissues

A simple epithelium is the most basic tissue type in metazoans and perhaps the first tissue that emerged during phylogenesis. It is also the first tissue type that emerges during the development of an organism, and is important for the morphogenesis and homeostasis of tissues and organs. Epithelial tissues are incredibly diverse and can be found, among many others, in the lining of the intestinal lumen, in the epidermis covering the skin, in secretory glands. Interestingly, epithelial tissues can even be found in non-metazoan

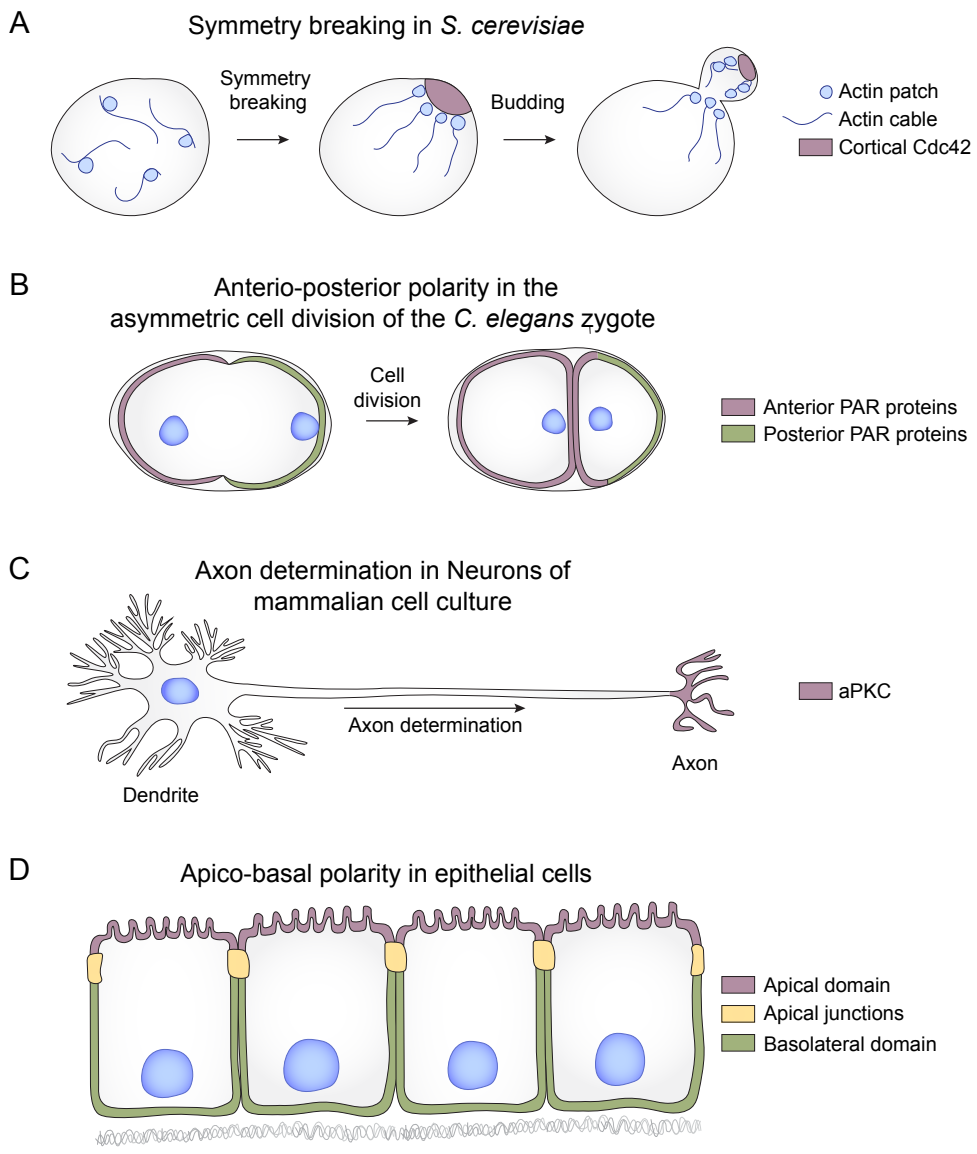

Figure 1. Cell polarization in diverse cell types. (A) Process of symmetry breaking in the budding yeast *S. cerevisiae*. During interphase actin is not polarized and Cdc42 is distributed symmetrically. Upon cell division entry, Cdc42 forms a polar cap resulting in actin polarization, leading to the formation of a bud. (B) Asymmetric cell division in the *C. elegans* zygote. Before cell division the embryo is polarized along an anterior-posterior axis, which influences the position of the mitotic spindle and the plane of cleavage. As a result, two unequal daughter cells are produced. (C) Polarization of mammalian primary-cultured neurons specifies one immature neurite as an axon. (D) Monolayered epithelia. Epithelial cells are polarized along an apical-basal axis.

organisms such as *D. discoideum*. A key feature of epithelial tissues is their capability of segregating the internal medium from the outside environment. As a result, epithelial tissues are the most common tissue that subdivides the body into different compartments. Moreover, epithelial tissues form selectively permeable barriers, blocking the transport of unwanted molecules and fluids from one side to the other. To perform these functions, epithelial cells must be highly polarized along an apical-basal axis and tightly bound together into sheets. The apical, basal and lateral domains established must be molecularly and functionally distinct. The apical domain typically faces either an internal cavity or the outside world, and can have specialized features such as cilia or the brush border of microvilli. The basolateral domain faces the neighboring cells and the basal membrane. The apical and basolateral domain are separated by cell junctions, which prevent proteins and lipids from diffusing between both domains, prevent the passage of molecules between cells, and provide mechanical strength and cohesion (Dickinson et al., 2011; Rodriguez-Boulan and Macara, 2014; Roignot et al., 2013; Weis et al., 2013).

The establishment and maintenance of polarity in epithelial cells is the result of complex interactions between several evolutionary conserved groups of cortical proteins. Apical domain establishment is mediated by the Partitioning defective (Par) and Crumbs complexes, which together with Scribble also control junction formation. Basolateral domain identity is promoted by the Scribble module, composed by Scribble, Dlg1 an Lgl1, the kinase Par1 and 14-3-3, and the complex made by Yurt, Coracle, Nrx-IV and Na+K+ATPase. Positive and negative interactions between these proteins leads to segregation of each member to its appropriate domain and is essential for cell polarization (Assémat et al., 2008). As well as cortical polarity proteins, protein trafficking, membrane lipid regulators and the actomyosin and microtubule cytoskeleton contribute to epithelial polarization and morphogenesis.

More details into the apical and basolateral polarity complexes, as well as their mutual interactions, can be found in Chapter 2.

The epithelial apical polarity network

Apical domain identity is established by the coordinated activities of the apical Par and Crumbs complexes. The Par complex functions in many different cell types to regulate cell polarity, whilst the Crb complex is more restricted to the organization of epithelial polarity. Positive and negative feedback interactions between proteins of these complexes, as well as context-dependent redundancies, are important to ensure a robust network and the ability to adapt to different requirements.

The apical Par complex includes two scaffold and adapter proteins, Par3 and Par6, the atypical protein kinase C (aPKC) and the small GTPase Cdc42, whilst the Crb complex consists of the transmembrane protein Crumbs, the

intracellular binding partner Pals1 and the Pals1 binding partner PatJ (Assémat et al., 2008).

A series of complex interactions between the apical polarity proteins takes place in order to ensure the correct localization and coordinated function of each protein. Of key importance is the activation of aPKC, which is essential for antagonizing proteins from the basolateral domain (Hong, 2018). As a result, a major role of the apical polarity proteins is to strictly regulate the localization and activity of aPKC. The main binding partner of aPKC is Par6, with which aPKC forms a stable subcomplex. aPKC and Par6 are interdependent for their localization, and they both individually interact with Par3, resulting in the formation of a Par3-Par6-aPKC complex. The interactions of Par6-aPKC with Par3 are dynamic and mediate the apical localization of Par6-aPKC (Franz and Riechmann, 2010; Hung and Kemphues, 1999; Izumi et al., 1998; Lin et al., 2000; Tabuse et al., 1998). When Par6-aPKC are associated with Par3, Par3 inhibits the kinase domain of aPKC. Association of Par6-aPKC with Cdc42, on the other hand, results in activation of the kinase domain of aPKC. Activated aPKC then phosphorylates Par3, which dissociates the complex formed by Par3/Par6/aPKC and results in Par3 segregation to the apical junctions. Junctional Par3 then mediates junction positioning and assembly (Laprise and Tepass, 2011; Morais-de-Sá et al., 2010) The interaction of Par6 with Cdc42 outcompetes Par3 for binding to Par6 and also mediates the apical localization of Par6-aPKC (Gao and Macara, 2004; Garrard et al., 2003; Joberty et al., 2000; Johansson et al., 2000). Moreover, Cdc42 induces a conformational switch in Par6 that greatly increases the affinity for Crb. The interaction between Par6-aPKC and Crumbs-Pals1 results in mutual stabilization of each other at the apical membrane domain and may also activate the kinase domain of aPKC (Almeida et al., 2019). The apical recruitment of Pals1, in the same way as the one of Par6-aPKC, can be mediated by a transient interaction with Par3 (Krahn et al., 2010b).

It is important to stress that the interactions described above are context dependent. For example, in *C. elegans* late embryos Cdc42 does not mediate the apical localization of aPKC (Zilberman et al., 2017b), and in the Drosophila follicular epithelium and adult mid gut epithelium, Par3 is dispensable for the localization of Par6 (Chen et al., 2018; Shahab et al., 2015). Moreover, aPKC has been recently shown to be able to localize apically independently of any protein-protein interaction, but through direct electrostatic binding to plasma membrane lipids PI4P and PIP2 (Dong et al., 2020). In the same study, it was shown that Par6 inhibits aPKC kinase activity, whilst several other studies have shown that Par6 can inhibit or activate aPKC kinase activity, and that interaction with other proteins, such as Cdc42 and Crb, are then necessary to activate aPKC (Atwood et al., 2007; Chabu and Doe, 2008; Dong et al., 2020; Graybill et al., 2012; Lin et al., 2000; Yamanaka et al., 2001). These alternative modes of polarity establishment indicate that several mechanisms may play

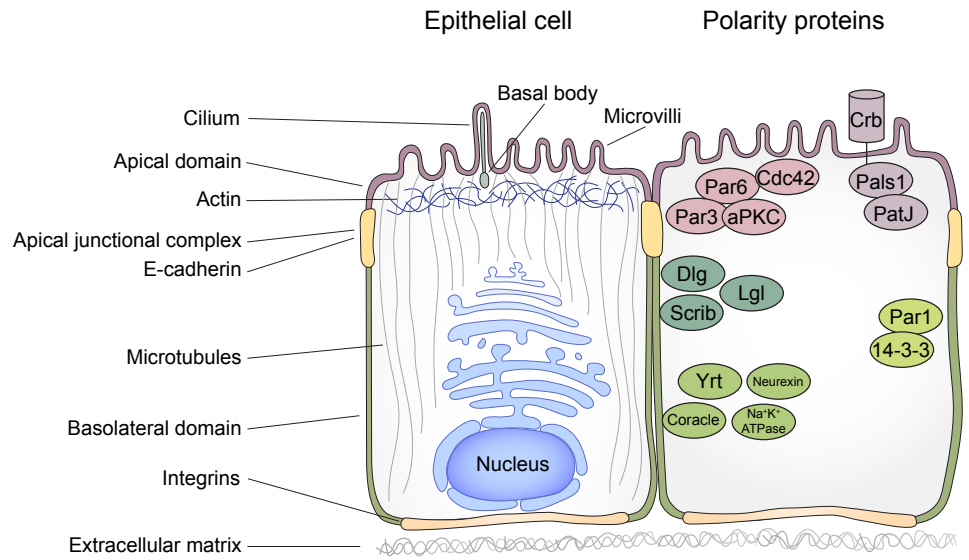

Figure 2. Apical-basal polarity in an epithelial cell. (A) A typical epithelial cell with the polarized cytoskeleton. (B) Approximate organization of the cortical polarity proteins.

specific roles in particular cell types, ensuring a robust network.

Protein interplay organizing apical-basal polarity

Establishment and maintenance of cell polarity relies on a complex series of interactions between apical and basolateral proteins. Mutual exclusion, mediated by the kinases aPKC and PAR-1, is of key importance in order to properly segregate each protein to its appropriate domain and to obtain a polarized cell.

The combined activity of the kinases PAR-1 and aPKC is critical for polarity establishment and maintenance. This is clear when examining Par3 regulation, which is excluded from both the apical and basolateral domains, and is therefore restricted to the apical junctions. On one hand, apical exclusion is mediated by phosphorylation of Par3 by aPKC, which weakens the association of Par3 with the cortex (Kullmann and Krahn, 2018; McKinley et al., 2012). On the other hand, basolateral exclusion is mediated by phosphorylation of Par3 by PAR-1, which prevents Par3 oligomerization, generates 14-3-3 binding sites and inhibits the formation of cortical Par3/Par6/aPKC clusters. Binding of 14-3-3 to Par3 also prevents oligomerization, which is important for Par3 stability. Phosophorylation of Par3 by PAR-1 ultimately prevents Par3 cluster formation, resulting in Par3 exclusion from the basolateral domain (Benton and St Johnston, 2003). The combined actions of aPKC and PAR-1, which exclude Par3 from the apical and the basolateral domain, restrict Par3 to the apical junc-

tions, where it has essential functions for junction assembly and functioning.

aPKC can also directly influence PAR-1 activity and localization through phosphorylation, essential to release PAR-1 autoinhibition and for its basolateral localization. When aPKC phosphorylates PAR-1, PAR-1 is restricted to the basolateral domain (Hurov et al., 2004; Suzuki et al., 2004) and undergoes a conformational change that allows PAR-1 binding to 14-3-3, an important downstream effector of PAR-1 (Kusakabe and Nishida, 2004). Together with aPKC phosphorylation, binding to the plasma membrane is also essential to release PAR-1 autoinhibition (Emptage et al., 2017; Folkmann and Seydoux, 2019).

Mutual interactions between aPKC and the basolateral protein Lgl are also important to establish apical-basal polarity. Lgl can be phosphorylated by aPKC, inhibiting its apical localization through inhibition of its polybasic domain. The polybasic domain of Lgl specifically targets it to the plasma membrane through electrostatic interactions. Polybasic domains are positively charged and the plasma membrane, due to its enrichement in polyphosphoinositides PI4P and PI(4,5)P2 (PIP2), is negatively charged. Upon phosphorylation by aPKC, the positive charges of Lgl's polybasic domain are neutralized, and thus the binding to the plasma membrane is prevented. As aPKC activity is restricted to the apical domain, binding to the plasma membrane is only prevented in the apical side (Bailey and Prehoda, 2015; Betschinger et al., 2003; Dong et al., 2015; Plant et al., 2003). Exclusion of Lgl from the apical domain is important for the activity of the apical PAR complex. Lgl can physically interact with Par6, blocking the formation of the Par3/Par6/aPKC complex, inhibiting aPKC kinase activity and preventing membrane association of Par6-aPKC (Betschinger et al., 2003; Hutterer et al., 2004; Yamanaka et al., 2003). In the lateral membrane, phosphorylated Lgl can interact with the consitutively basolateral protein Dlg, though the functional role of this interaction has not been elucidated (Zhu et al., 2014). Altogether, the feedback loop formed between aPKC/Par6 and Lgl is essential for correct apical-basal polarity.

Finally, the interplay between the lateral polarity protein Yurt and the apical polarity proteins Crumbs and aPKC is also critical for determining apical and basolateral domain sizes. Yurt and its mammalian orthologs stabilize the lateral membrane and restrict apical membrane growth (Gosens et al., 2007; Laprise et al., 2006). This is achieved through several interactions. Firstly, Yurt prevents Crb basolateral localization and limits Crb apical activity, regulating apical membrane size (Laprise et al., 2006; Laprise et al., 2009; Lee et al., 2007). Secondly, Yurt can directly bind and negatively inhibit aPKC activity. Finally, aPKC can phosphorylate Yurt, inhibiting Yurt's oligomerization and impairing the interaction between Yurt and Crb (Gamblin et al., 2014; Gamblin et al., 2018).

The interactions between apical and basolateral polarity determinants ultimately lead to a polarized state, key for several processes detailed below.

Effector pathways of cortical polarity

The establishment of apical-basal polarity is essential for multiple processes, such as polarized trafficking, lumen formation, cytoskeletal organization and rearrangements and spindle orientation during cell division. Cortical polarity must therefore be transduced to other cellular pathways through diverse interactions.

Membrane trafficking

Membrane trafficking, the movement of cargo using membrane-bound transport vesicles, is an essential process for the generation of epithelial polarity. Plasma membrane components, sorted in the trans-Golgi network, are delivered to specific membrane domains through exocytic pathways, driven by microtubule and actin-based motors. Once vesicles arrive to their destination, they are tethered through the exocyst complex. Fusion is mediated by t-SNARE complexes and syntaxins on the target membrane, and v-SNARE complexes on vesicle membranes. In order to maintain membrane homeostasis, cortical apical and basolateral cargoes are then endocytosed and either recycled or targeted for degradation. Endocytosis ensures there are proper levels of polarity proteins in the different plasma membrane domains, whilst recycling allows the repositioning of cargoes that are endocytosed but not targeted for degradation yet (Michaux et al., 2016; Oztan et al., 2007; Zuo et al., 2009).

Polarity regulators are essential for several aspects of membrane trafficking, and also depend on membrane trafficking for their correct localization and function. A good example of this is the Crumbs complex, which is necessary for apical localization of the exocyst complex (Pieczynski and Margolis, 2011; Wang et al., 2006), and at the same time depends on the exocyst complex for its apical localization (Blankenship et al., 2007; Campbell et al., 2009). Moreover, Crumbs is endocytosed to prevent apical membrane expansion, and later on recycled back to the apical domain through Rab11 recycling endosomes. Disruption of Rab11 function results in loss of Crumbs from the apical domain, ultimately leading to adherens junction disassembly (Roeth et al., 2009). Another clear example is the Par complex, which directly interacts with several exocyst components (Lalli, 2009; Rosse et al., 2009). The Par complex can function, directly or indirectly, as an apical exocyst receptor required for targeted protein delivery (Abrams and Nance, 2020; Ahmed and Macara, 2017; Rosse et al., 2009; Winter et al., 2012) and plays a role in cargo endocytosis and recycling (Balklava et al., 2007; Georgiou et al., 2008). Reciprocally, apical localization of Par proteins depends on the exocyst and is disrupted upon impaired vesicle fusion (Michaux et al., 2016; Rosse et al., 2009; Winter et al., 2012). A tight regulation of membrane trafficking by the Par complex is essential for downstream functions of cell polarity, including lumen formation, cell migration and differentiation, and ultimately, cell survival (Polgar and Fo-

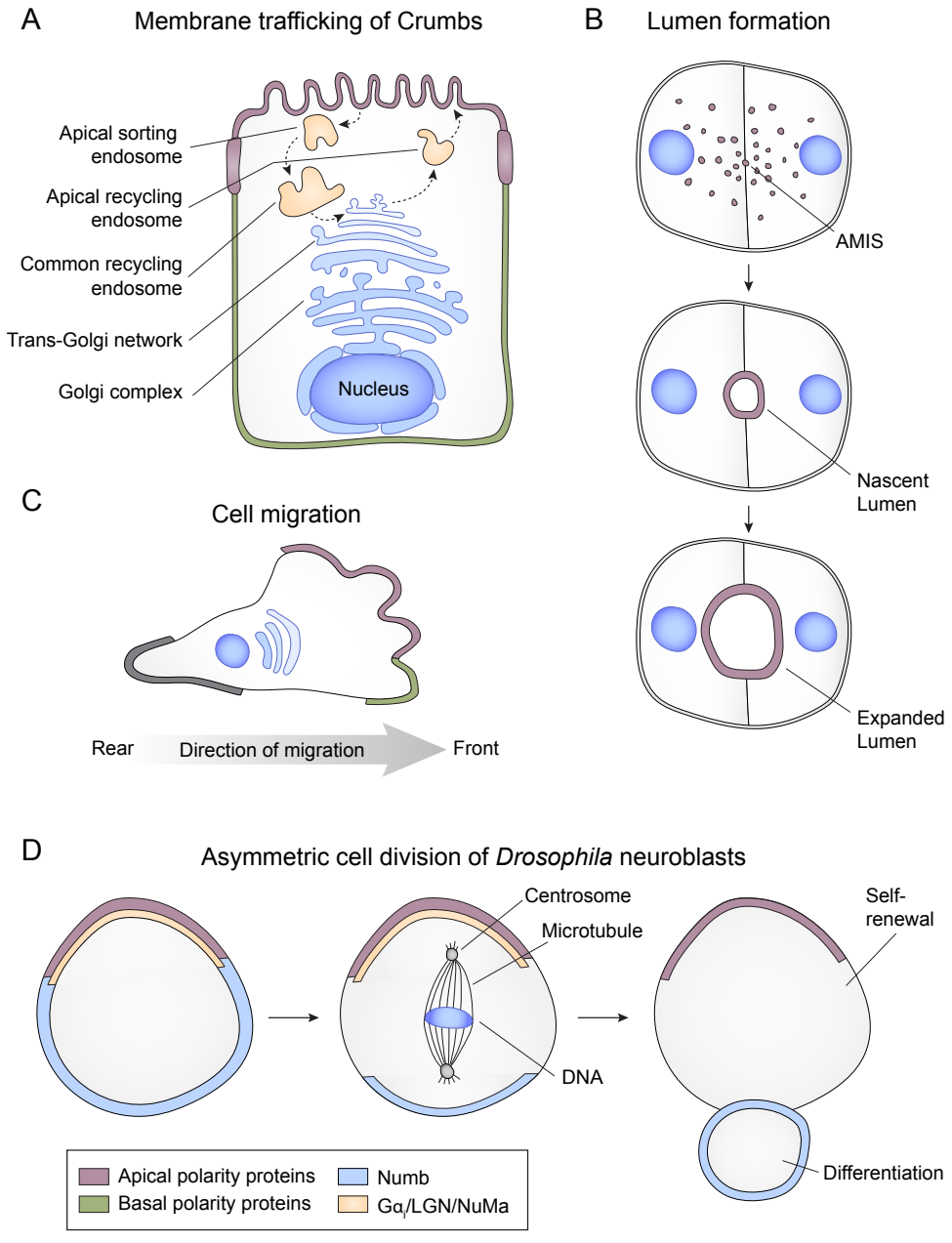

Figure 3. Effector pathways of cortical polarity. (A) The localization of Crumbs is regulated by membrane trafficking. Crumbs is endocytosed into apical sorting endosomes and later on recycled through common recycling endosomes, to the trans-Golgi network and into apical recycling endosomes, from where it can be recycled back to the apical cortex. (B) Lumen formation by hollowing. Intracellular vesicles containing apical membrane components are delivered to the region between cells. Once an apical membrane initiation site (AMIS) is formed, several processes promote the expansion of the lumen. (C) Cell migration is directed by the leading edge at the front of the cell. The apical Par proteins and Scribble are enriched at the leading edge. (D) Asymmetric cell division of Drosophila neuroblasts. The apical Par complex is connected to $G\alpha_i$/LGN/NuMA. During mitosis, the Par proteins direct the orientation of the mitotic spindle and the localization of the cell fate determinant Numb to the basal cortex. After cell division Numb is restricted to one daughter cell, where it prevents self-renewal and induces differentiation.

gelgren, 2018).

Lumen formation

Tubular epithelial structures are used to transport gases and fluids from one side of the body to another. Tubular epithelia consist of a lumen surrounded by epithelial cells. One way in which lumens are formed is by apical domain invasion of the cytoplasm, which requires an interplay between polarity complexes and membrane trafficking. Apical domain invasion relies on polarized delivery of vesicles containing apical domain components, which are needed to extend the luminal surface. These vesicles accumulate at the apical membrane initiation site (AMIS), which can be in the cytoplasm or at the contact site of several cells, and fuse to form an intracellular lumen. Finally the luminal space is expanded by pumps and channels (Bagnat et al., 2007; Ferrari et al., 2008). These mechanisms of forming a lumen are seen in Madin-Darby Canine Kidney (MDCK) cells cultured in a 3D extracellular matrix, in 3D endothelial cell cultures and in the *C. elegans* excretory cell. It's important to note that there are other ways in which lumens can be formed, reviewed by (Sigurbjörnsdóttir et al., 2014).

Cdc42 plays a central role in lumen formation and in the interplay between vesicular trafficking and cell polarity. Vesicular trafficking is necessary to localize Cdc42 at the apical membrane initiation site, where it is activated and recruits Par6/aPKC. Depending on the system, Par3 may also contribute to the recruitment of Par6/aPKC to the apical initiation site. The Par complex then cooperates with the exocyst complex to promote the delivery of apical components to the apical initiation site, through Rab11a/Rab8a positive vesicles (Bryant et al., 2010; Martin-Belmonte et al., 2007). One of the components that is delivered by Rab11a positive vesicles to the apical initiation site is the Crumbs complex, which then assists with the recruitment of Par6/aPKC and the exclusion of Par3 from the nascent apical surface, promoting the maturation of the apical luminal complex and apical junctions (Schlüter et al., 2009). The establishment of apical junctions, together with polarized fluid transport to the newly formed extracellular space mediated by ion and water channels, are necessary for lumen opening (Ferrari et al., 2008). Interestingly, once the lumen is formed, the Par and exocyst complexes are necessary for lumen extension and branching,

indicating that polarity proteins are not only necessary for lumen formation but also for its continued growth (Abrams and Nance, 2020; Jones et al., 2014).

Cell migration

Cell migration is fundamental to morphogenesis as well as to wound healing and immune responses. To migrate properly, cells must communicate with neighboring cells and respond to different environmental cues. A key process in cell migration is the ability of cells to polarize. Cell polarization in migrating cells can be on the level of the single cell or a cluster of cells in collective migration. Single cell migration requires the formation of new focal adhesions, the disassembly of the ones at the rear, and the detachment and retraction of the cell rear. All of these processes must be spatiotemporally controlled. The polarization of the microtubule network is key during migration, as it promotes vesicle trafficking and supports positive feedback loops between trafficking and polarity, and thereby stabilizing the polarized state. In collective cell migration an entire cell group polarizes in the direction of migration. Cohesive clusters are formed, and cells maintain cell to cell contacts. However, the position of the cells within the group is dynamic. Collective cell migration can maintain three polarity axes with respect to the group: front-back, apical-basal and inside-out (Allam et al., 2018; Montell et al., 2012).

In migrating cells, Cdc42 and the Par complex play an important role in the regulation of cell migration, and they are both located mainly at the leading edge (Nelson, 2009). Cdc42 is activated upon increased cellular tension, promoted by integrin signaling. At the leading edge, Cdc42 binds Par6, which recruits Smurf1. Smurf1 is a HECT domain E3 ubiquitin ligase, which regulates cell polarity and protusive activity. Upon recruitment by Par6, Smurf1 restricts RhoA activity to the rear of the cell, promoting the formation of new local adhesions (Etienne-Manneville and Hall, 2001; Wang et al., 2003). aPKC also inhibits the kinase GSK3β. GSK3β is involved in glycogen metabolism and is a positive regulator of epithelial-to-mesenchymal transition (EMT) (Plyte et al., 1992; Vijay et al., 2019, 3). When aPKC inhibits GSK3β, the inhibition of the microtubule organizer APC by GSK3β is released. APC is then recruited to the microtubules plus-end at the leading edge, promoting the localization of the microtubule organizing center at the leading edge, key for cell orientation (Etienne-Manneville and Hall, 2003; Schneikert and Behrens, 2007). By promoting microtubule organization, the Par complex also supports polarized trafficking. For example, the localization of the exocyst at the leading edge depends on aPKC (Rosse et al., 2009). Finally, Par3 and aPKC are important for establishing directional migration and maintaining cohesion during collective migration (Pinheiro and Montell, 2004).

Asymmetric cell division

Asymmetric cell division (ACD) enables cells to give rise to two daughter cells with unequal distribution of cellular components. ACD is a tightly regulated process and maintains the balance between stem cells and differentiation and is important during embryogenesis and organ development. Three steps are necessary for ACD: (1) a cell polarity axis is established, (2) cell polarity determines the asymmetric localization of cell fate determinants, and (3) the mitotic spindle aligns with the cell polarity axis, segregating cell fate determinants in one of the daughters.

ACD relies on cell polarity so that proteins, lipids or mRNA molecules can be asymmetrically localized in the cell during cleavage (Knoblich, 2010). In certain Drosophila cells, upon mitosis entry, the kinase Aurora A phosphorylates Par6, releasing the inhibiton on aPKC. aPKC then phosphorylates Lgl, which is displaced from the apical cortex and restricted to the basolateral domain. Par3 then forms a complex with Par6 and aPKC and binds the cell fate determinant Numb. Par3 may act as an adaptor between the kinase aPKC and the substrate Numb. Phosphorylation of Numb by aPKC neutralizes the positive charges in the amino terminus of Numb. As a result, Numb can no longer interact with plasma membrane phospholipids in the apical side, and is restricted to the basal side (Knoblich et al., 1997; Smith et al., 2007; Wirtz-Peitz et al., 2008). Similarly in the *C. elegans* embryo, asymmetric localization of the cell fate determinant MEX-5 is mediated by phosphorylation of MEX-5 by Par1 (Tenlen et al., 2008).

The positioning and orientation of the mitotic spindle during ACD is of key importance to regulate cell fate, epithelial homeostasis and tissue morphogenesis. Oriented cell division in most animal cell types involves the transmission of localized pulling forces by the dynein motor complex at the cell cortex to the astral microtubules to position the spindle. There are three main levels of regulation for spindle orientation: the cell cortex, the mechanisms that regulate the force generators and the astral microtubule network (di Pietro et al., 2016). The $G\alpha_i$/LGN/NuMa complex is a key regulator that polarizes cortical force generators. During mitosis this complex recruits the minus-end-directed microtubule motor dynein, generating pulling forces on the spindle poles and positioning the spindle. The localization of the $G\alpha_i$/LGN/NuMa complex therefore determines the site of force oncentration and the axis of spindle orientation (Morin and Bellaïche, 2011). Polarity proteins regulate the polarized distribution of the $G\alpha_i$/LGN/NuMa complex. The polarized localization of LGN, for example, relies heavily on polarity proteins: apical enrichment of the Drosophila homolog of LGN in Drosophila neuroblasts depends on Par3 and aPKC (Izumi et al., 2004; Wodarz et al., 2000; Yu et al., 2000), posterior localization of the *C. elegans* homolog of LGN during the first cell division depends on Par2 and Par3 (Gotta et al., 2003), and lateral localization during symmetric cell division in MDCK cells is mediated by phosphorylation of LGN by aPKC (Zheng et al.,

2010). Ultimately, the regulation of spindle positioning by polarity proteins can have effects on tissue homeostasis, as is the case in the mammalian epidermis, where aPKCλ/ι balances the orientation of cell division, controlling epidermal stem cell behavior and cell fate decisions (Niessen et al., 2013).

Cell polarity and disease

Cell polarity is a universal attribute of almost all cells and is tightly regulated and robust. Proper control of cell polarity is essential as loss of cell polarity leads to a wide range of cellular defects, ultimately leading to disease or cell death.

Loss of cell polarity is a hallmark of cancer and is correlated with malignancy: whilst most primary human carcinomas maintain epithelial characteristics such as intercellular adhesions and tight junctions, high-grade carcinomas usually lose apical-basal polarity and architectural organization. Cell polarity acts as a gatekeeper against cancer initiation and plays an active role in tumor development. When cell polarity is disrupted, essential processes such as differentiation, senescence and apoptosis may be circumvented, and thus hyperproliferation may occur. In addition, loss of cell polarity is associated with the disruption of cell junctions, which further disrupts the polarized state and can lead to a disruption of the 3D architecture of epithelial tissues, contributing to epithelial-to-mesenchymal transition (EMT), a crucial step in metastasis. Indeed, loss or downregulation of E-cadherin has been found in breast cancer and familial gastric cancers, respectively (Schrader et al., 2008). Moreover, loss of cell polarity can affect asymmetric cell division, impacting tissue homeostasis and eventually leading to tumorigenesis. This is the case with basolateral proteins Lgl, Dlg and Scrib, which were described as tumor supressors. In Drosophila, perturbations in asymmetric cell division due to mutant lgl, dlg or scrib lead to an abnormal accumulation of dividing cells, and ultimately tumor development in larval imaginal discs and brains (Albertson and Doe, 2003). Other polarity proteins, such as the Par complex, have been described as both tumor suppressors and oncogenes, although the mechanism by which this takes place is not fully elucidated yet. For instance, overexpression of aPKCλ is correlated with a poor tumor prognosis in a wide range of epithelial cancers, and its loss inhibits carcinogenesis in mice. However, in some contexts, loss of aPKCλ also promotes tumorigenesis (Reina-Campos et al., 2019). Similarly, Par3 promotes papilloma formation and basal cell carcinoma, but inhibit keratoacanthoma and human squamous cell carcinoma (Atwood et al., 2013; Iden et al., 2012; Ling et al., 2020; Vorhagen et al., 2018). It is important to note that loss of cell polarity predisposes cells to react more severely upon oncogenic stimuli and is most often accompanied by other oncogenic mutations.

Defects in the apical polarity complex Crb1 have also been associated with retinal problems. Loss of Crb1 or some of its intracellular interactors leads to morphological defects in photoreceptors, loss of adhesion between them

and light-induced photoreceptor degeneration (Mehalow et al., 2003). Indeed, mutations in Crb1 cause autosomal recessive retinitis pigmentosa and autosomal Leber congenital amaurosis (Hollander et al., 2004).

Moreover, consistently with the origin of cell polarity as a mechanism to ensure deleterious material is differentially inherited by aging cells, in metazoa, disruptions in cell polarity are linked to aging (Macara and Mili, 2008; Persa et al., 2021). For instance, loss of aPKC or Par3 can cause premature aging due to cell fate changes and premature skin aging phenotypes, including hair follicle stem cell weakening and hair loss (Ali et al., 2016; Niessen et al., 2013; Osada et al., 2015). The mechanisms by which aPKC and Par3 regulate aging are not clear, it may be through their regulation of spindle positioning, due to their interaction with extracellular collagens, or by preventing premature differentiation of epidermal stem cells. Ultimately, aging is big risk factor of cancer, and thus the mechanisms by which polarity proteins promote aging and cancer may be linked (Persa et al., 2021).

Finally, cell polarity is commonly targeted by pathogens in order to disrupt epithelial barrier function and structure. For example, enteropathogenic Escherichia coli (EPEC) infection, which causes diarrhea, leads to redistribution of the basolateral proteins Na+ K+ ATPase and B1-integrin to the apical domain. EPEC infection also causes the relocalization of junctional ZO-1, occludin, and claudin-1 to the lateral domain and the cytoplasm, and the EPEC effectors Map and Espf activate Cdc42 and bind 14-3-3, respectively. EPEC disrupts intestinal tight-junctions and the intestinal barrier function. The disruption in apical-basal polarity caused by EPEC infection is likely to contribute to EPEC pathophysiology (Tapia et al., 2017).

In summary, the disruption of apical-basal polarity is implicated in several pathologies. As a result, the polarity network must be tightly regulated and very robust.

Study of cell polarity in *C. elegans*

Discovery of the PAR proteins

The first genes involved in cell polarization, the *par* (partitioning defective) genes, were discovered in the *C. elegans* zygote (Kemphues et al., 1988). Mutations in the six *par* genes, *par-1* to *par-6*, caused abnormalities in the asymmetric divisions of the early embryo. These divisions are usually asymmetric, leading to daughters differing in size, cell division timing, cleavage pattern and eventually fate. Mutations in the *par* genes disrupted cell division timing, cleavage pattern and P granule distribution. Later on, it was shown that the PAR proteins are essential to establish anterior-posterior polarity in the zygote. PAR-3 and PAR-6 were placed in the same genetic pathway and, together with PKC-3, they formed the first polarity protein complex, the PAR-6/PAR-3/PKC-3 complex (Tabuse et al., 1998; Watts et al., 1996). Interestingly, the PAR proteins are conserved across metazoa.

Polarity in the early embryo

Since the discovery of the PAR proteins, the *C. elegans* one cell embryo has been extensively studied regarding polarity establishment and maintenance. The one cell embryo has an anterior and a posterior cortical domain. In the anterior domain there is an enrichment of cortical PAR-3, PAR-6, PKC-3 and CDC-42, whilst in the posterior domain there is an enrichment of PAR-1, PAR-2, LGL-1 and CHIN-1 (Beatty et al., 2010; Beatty et al., 2013; Boyd et al., 1996; Etemad-Moghadam et al., 1995; Guo and Kemphues, 1995; Guo and Kemphues, 1995; Hoege et al., 2010; Motegi and Sugimoto, 2006; Tabuse et al., 1998; Watts et al., 1996). Mutual exclusion between these cortical proteins ensures that each of them is excluded from the opposite domain.

Before polarity is established, PAR-3, PAR-6 and PKC-3 localize uniformly to the cortex, whilst PAR-1 and PAR-2 are cytoplasmic (Cuenca et al., 2003; Hung and Kemphues, 1999). The posterior side of the embryo is determined by the position of the paternal pronucleus and its associated centrosome after meiosis (Goldstein and Hird). Symmetry breaking is achieved by two partially redundant mechanisms: an actomyosin cortical flow, which causes accumulation of PAR-3/PAR-6/PKC-3 in the anterior pole, and microtubule-mediated PAR- 2 loading on the posterior cortex (Hao et al., 2006; Munro et al., 2004; Shelton et al., 1999; Zonies et al., 2010). PAR-2 recruits PAR-1 and LGL-1 to the cortex, and PAR-1 phosphorylates PAR-3, causing its dissociation from the posterior cortex and allowing the posterior domain to expand (Boyd et al., 1996; Motegi et al., 2011). Mutual exclusion as well as a positive feedback loop at either sides ensures polarity is maintained. Mutual exclusion is mediated by phosphorylation by the kinases PAR-1 and PKC-3 and by inhibition of CDC-42 by CHIN-1: (1) phosphorylation of PAR-3 by PAR-1 keeps

the anterior PAR complex away from the posterior cortex, (2) phosphorylation of PAR-1 and PAR-2 by PKC-3 keeps them away from the cortex in the anterior pole (Hao et al., 2006; Motegi et al., 2011), and (3) local inhibiton of CDC-42 by the GTPase-activating protein CHIN-1 on the posterior domain restricts CDC-42 activity to the anterior domain, where PAR-6/PKC-3 locally inhibits the accumulation of CHIN-1 (Beatty et al., 2013; Kumfer et al., 2010; Sailer et al., 2015). In the anterior domain, two different complexes can be formed with PAR-6/PKC-3: a complex with PAR-3, which responds to polarity cues and segregates PAR-6/PKC-3 to the anterior cortex, where PKC-3 is inactive, and a complex with CDC-42, where PKC-3 is active but diffuse (Rodriguez et al., 2017). CDC-42 also mediates a positive feedback loop which stabilizes PAR-6 at the anterior cortex (Aceto et al., 2006; Schonegg and Hyman, 2006). In the posterior cortex, PAR-2 mediates a positive feedback loop that promotes the recruitment of cytoplasmic PAR-2 and also promotes PAR-1 recruitment (Hao et al., 2006; Motegi et al., 2011). A balance is established between the levels of these proteins, and the absence of one regulator can be partially rescued by reducing the levels of another regulators. For example, par-2 null mutants can be partially rescued by decreasing the levels of PAR-6 or increasing those of LGL-1 (Motegi and Seydoux, 2013).

The asymmetric localization of the PAR proteins is essential for the first asymmetric division, causing the spindle to migrate off center in mitosis, and during later divisions (Cowan and Hyman, 2004). By the end of the 4-cell stage, anteriorly localized proteins migrate to the contact-free outer domain, and posteriorly localized proteins migrate to cell contacts on the inner side, establishing radial polarity. PAR-3 and PAR-6 are expressed in the outer domain, and are important during these stages for the establishment and function of radial polarity, as well as for cell adhesion and cell ingression during gastrulation (Nance et al., 2003). Asymmetric localization of PAR-6 during these stages depends on CDC-42, which is activated by the Rho guanine nucleotide exchange factors CGEF-1 and ECT-2 in the outer domain (Chan and Nance, 2013). Activated CDC-42 then actively recruits PAR-6 to the outer membrane domain. Exclusion from cell contacts is mediated by the Rho GTPase activating protein PAC-1, which inactivates CDC-42 at these sites and thus excludes PAR-6 from cell contacts (Anderson et al., 2008).

Polarized epithelial tissues

C. elegans contains several epithelial tissues, such as the intestine, epidermis, pharynx, vulva and spermatheca. These tissues contain an apical and a basal domain, as well as an apical junctional complex that links cells together and prevents paracellular passage of molecules (Michaux et al., 2001). The *C. elegans* apical junctional complex consists of one electron-dense structure, in contrast to the two structures observed in mammalian systems, the tight and adherens junctions (Costa et al., 1998; McMahon et al., 2001). Development

of some of these tissues, such as the intestine and the epidermis, begins during embryogenesis, whilst the vulva and spermatheca develop during larval stages. I will give a brief overview of the different epithelial tissues of *C. elegans* and go more in detail on the intestine and the epidermis.

The pharynx

The pharynx is a complex organ used for pumping food into the gut, and contains seven cell types: muscles, epithelia, neurons, glands, valves, arcade cells and marginal cells. A basement membrane separates the pharynx from the rest of the animal, and the lumen is lined with a cuticle that connects with the cuticle of the epidermis (Albertson and Thomson, 1976). Commitment to the pharyngeal fate is determined by pharyngeal regulators such as pha-4 in early stages of embryogenesis. During later embryogenesis, the pharyngeal precursors undergo reorganization and a mesenchymal to epithelial transition, forming the lumen (Mango, 2007). The polarization of the arcade cells, which generate an epithelium late in embryogenesis and form an epithelial bridge between the intestine and the epidermis, depends on the cytoskeletal regulator and kinesin ZEN-4/MKLP1 and on PAR-6, but not on E-cadherin or B-integrin (Von Stetina and Mango, 2015; Von Stetina et al., 2017).

The excretory system

The excretory system is a simple organ that functions in secretion and osmoregulation, and contains three unicellular tubes (canal, duct, and pore), connected to form a continuous lumen, a secretory gland, and two neurons. Development of the excretory canal starts during embryogenesis. Tube elongation is concomitant with embryo elongation and continues as worms grow in size during larval and adult stages. The excretory tubes are joined to each other by ring-shaped apical junctions and have the apical domain facing the inside of the cell, where CRB-1, the PAR proteins and actin are enriched (Sundaram and Buechner, 2016). PAR-6 and PKC-3, and PAR-3 to a lesser extent, function within the excretory canal to promote lumen extension and to recruit the exocyst to the lumen (Abrams and Nance, 2020).

The vulva

The hermaphrodite vulva connects the developing uterus to the external environment, is necessary for egg-laying and for copulation with males. The vulva is formed during larval development and is derived from epithelial cells of the P lineage. For the vulva to become accessible to egg-laying and sperm entry, anchor cell invasion, invagination and connection to the uterus at the L4 to adult molt are necessary (Sternberg, 2005). Although Wnt signalling is necessary for cell orientation (Green et al., 2008; Minor and Sternberg, 2019; Minor et al., 2013) and vulval cells are apical-basal polarized, the functioning

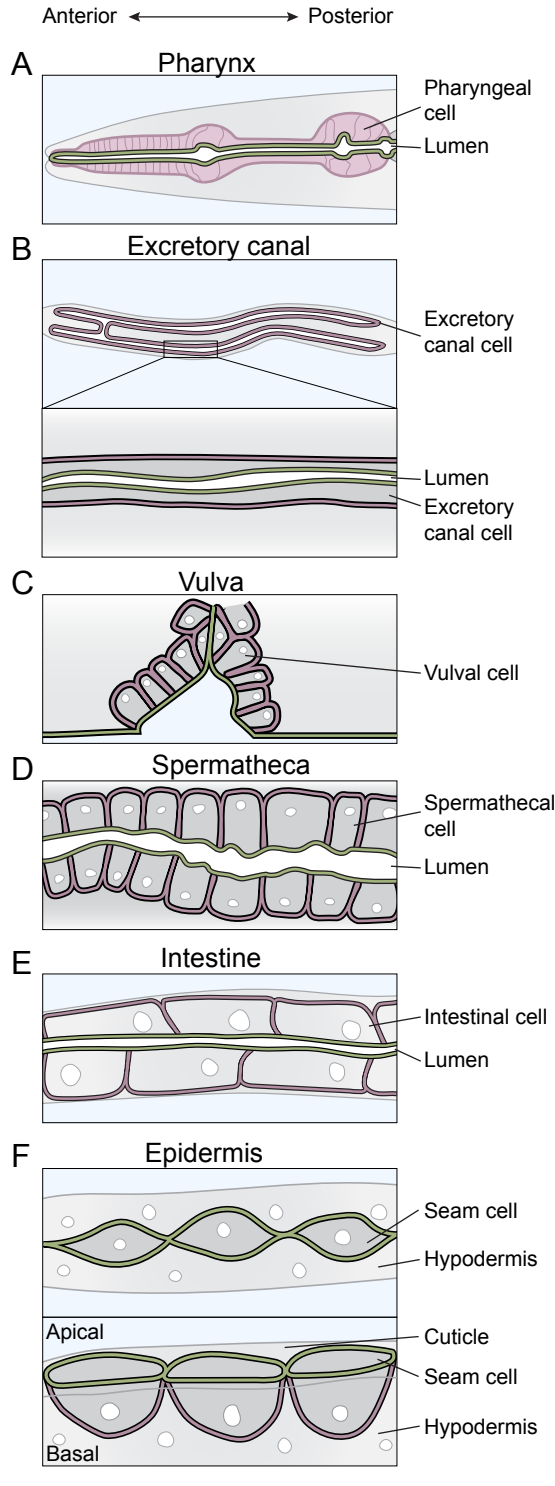

Figure 4. Apical-basal polarized epithelial tissues in *C. elegans*. Graphical representation of the organization of epithelial tissues. Green indicates the localization of the apical domain and dark pink indicates the localization of the basolateral domain. Light blue indicates the exterior environment.

of the polarity regulators in this tissue is not well defined.

The spermatheca

The spermatheca is a myoepithelial tube where sperm is stored. The function of the spermatheca is to fertilize oocytes before they are delivered to the uterus, for which it is essential that the tissue undergoes cycles of stretching and constriction (McCarter et al., 1999; Yin et al., 2004). Development of the spermatheca takes place during larval development. In spermathecal precursor cells, the PAR proteins are transiently expressed and localize asymmetrically. PAR-3 and PKC-3 have been shown to be essential for the function of the spermatheca. PAR-3 activity is required for spermathecal cell polarization as well as tissue organization, and defective development of the spermatheca due to PAR-3 absence results in ovulation defects (Aono et al., 2004). PKC-3, in turn, is necessary for junction stability, and its inactivation results in sterility (Montoyo-Rosario et al., 2020).

The intestine

The *C. elegans* intestine is specialized in nutrient absorption and digestion, but also fat storage, defense against pathogens, immunity, longevity and even detoxification of metals. In hermaphrodites, the intestine also produces yolk lipoprotein for developing oocytes. The intestine is a tube, connected on the anterior end to the pharynx and on the posterior end to the rectum. Food is directed to the intestine due to pumping of the pharynx and peristalsis through its lumen, and mechanically broken by the grinder at the posterior end of the pharynx. A valve separates the grinder from the intestine. The intestine consists of 20 large cells, which are arranged in 9 rings, and are polarized along an apical-basal axis. The basal side is surrounded by a basement membrane facing the pseudocoelomic space, whilst the apical side forms a lumen lined with microvilli that form the brush border. In the luminal side of the microvilli is the glycocalyx, a glycoprotein-rich region where digestive enzymes encounter macromolecules. The glycocalyx also filters intestinal absorption and provides a physical barrier from pathogens. At the posterior end, the intestine and the hindgut are connected through the intestinal-rectal valve, through which waste is disposed of (Dimov and Maduro, 2019).

The development of the intestine starts during early embryogenesis from the E blastomere. Specification of E is essential for intestinal development and is temporaly controlled by a gene regulatory network of maternal and zygotic transcription factors. Apicobasal cell polarization begins at 16E stage, and is mediated by PAR-3 (Achilleos et al., 2010). At this stage, the centrosomes and nuceli of intestinal cells move towards the apical membrane, and a non-centrosomal microtubule organizer center (ncMTOC) is established. PAR-3 is also essential in this process, as it provides a positional cue without which centrosomes fail to migrate apically, and microtubule organization is disrupted (Achilleos et al., 2010; Feldman and Priess, 2012). As part of the process of polarity establishment, junctional components localized apically migrate to the junctions. PAR-6 is involved in junction formation and is essential for epithelial cell adhesion, as well as for a correct cytoskeletal organization (Totong et al., 2007). Concomitant with junctional formation is lumen growth. Interestingly, PAR-6 is still necessary after polarity has been established and junctions have been formed, as the absence of PAR-6 after E16 causes the lumen to develop bulges and lose contiguity, the ncMTOC gets fragmented, and ultimately causes larval lethality (Sallee et al., 2020).

The epidermis

The *C. elegans* epidermis covers the worm's exterior surface and separates it from the outside world, acting as a structural and permeability barrier. The epidermis also plays essential roles in different physiological functions, such as mechanosensation, innate immunity and wound healing, as well as endocrine and exocrine secretion. Morphogenesis of the epidermis begins

during embryogenesis and continues during the larval stages and into adulthood (Chisholm and Hsiao, 2012; Chisholm and Xu, 2012).

There are several epidermal cell types: postmitotic epidermal syncytia, seam cells, ventral epidermal cells and interfacial epidermal cells (Gendreau et al., 1994; Page et al., 1997). Most of the epidermis is composed of postmitotic syncytia, formed by the fusion of epidermal precursors in mid-embryogenesis. hyp1-5 and hyp8-11 form the head and the tail, respectively, and do not increase their nuclei number during post-embryonic development. By contrast, the hyp7, which covers most of the worm's surface, starts with 23 nuclei. Through endoduplication and cell fusion, hyp7 ends up with 139 nuclei in adults. The bilateral seam cells form cuticular specializations, the lateral alae and are essential for elongation and molting. The seam cells form two rows along the long axis of the body and, with the exception of H0, undergo stem cell-like divisions in post-embryonic development. During the larval-to-adult transition, the seam cells undergo fusion, become bilateral syncytia, and enter persistent cell-cycle quiescence. The ventral epidermal cells (P1-12) play important roles in embryonic patterning, vulva or male tail development, contribute to the hyp7 nuclei and form neuroblasts. Finally, the interfacial epidermal cells make rings of specialized epidermal cells which line the orifices of the mouth, rectum, and the hermaphrodite vulva (Chisholm and Hsiao, 2012).

The epidermis is covered on its apical and basal side by specialized extracellular matrices. The apical side is covered by the cuticle, a multi-layered apical matrix composed of collagen, lipids and glycoproteins, patterned with circumferential furrows. The cuticle is produced by the underlying cells and syncytia. During post-embryonic development, the cuticles are shed and replaced with a larger structures during each of the four molts (Cohen and Sundaram, 2020). The basal side is covered by the basal lamina, which maintains epithelial integrity by creating adhesion between the muscles and the epidermis, and allows force transmission between these tissues as well as cell and axon migration (Altun and Hall, 2009; Carvalho and Broday, 2020).

Morphogenesis of the epidermis begins during embryogenesis on the dorsal side of the embryo, where epidermal cells are generated. Epidermal cell fate is specified by transcriptional regulators, with ELT-1 acting as a master regulator. After specification, dorsal epidermal cells rearrange in a process known as dorsal intercalation, which involves polarization and formation of directed protrusions of the dorsal cells. Following intercalation, the actin and microtubule cytoskeleton are arranged into circumferential arrays and the nuclei of the epidermal cells migrate contralaterally. The epidermal sheet is then spread over lateral and ventral cells to meet at the ventral midline, a process described as ventral enclosure. The actin cytoskeleton and calcium signaling contribute to the process of ventral enclosure. Cadherin mediated adhesion is necessary when the leading cells meet at the ventral midline. Immediately after enclosure, the embryo elongates dramatically from a bean shape to an elongated

worm. The cytoskeleton and the contraction of the underlying body wall muscles drive the process of elongation. After elongation the first cuticle is formed, which maintains the elongated form of the larvae (Carvalho and Broday, 2020; Chisholm and Hsiao, 2012).

During larval development, the volume of a worm increases 32-fold (Knight et al., 2002). To sustain this growth, hyp7 nuclear number and DNA volume increase significantly. The increase in nuclear number is due to several factors. Firstly, seam cells divide asymmetrically during each larval stage, and the anterior daughters fuse with the hyp7 syncytium. Secondly, seam cell number is doubled during the second larval stage due to a symmetric seam-cell division that precedes the asymmetric division. Thirdly, right before hyp7 fusion, seam-derived hyp7 nuclei undergo one round of DNA endoduplication. Finally, Pn.p cells and their daughters fuse with the hyp7 in the L1 or L3 stages. As a result of all these events, the hyp7 syncytium contains 139 nuclei in adults (Chisholm and Hardin, 2005).

Epidermal cells are polarized along an apical-basal axis. Due to the dynamic nature of the epidermis, polarity complexes, such as the PAR complex, play a role in a diverse number of processes during development. PAR-6 and PAR-3, for instance, are required for dorsal intercalation and apical junction formation, but not for apical-basal polarity during the embryonic development of the epidermis (Achilleos et al., 2010; Montoyo-Rosario et al., 2020; Totong et al., 2007; Walck-Shannon et al., 2016). CDC-42 is also required during early stages of morphogenesis for cell intercalation, as well as for junction remodeling during the later process of elongation (Walck-Shannon et al., 2016; Zilberman et al., 2017). During larval development and adulthood, not much is known about the role of the polarity complexes, apart from a requirement of CDC-42 and PAR-6 for epidermal development through unclear mechanisms (Welchman et al., 2007). Due to the complex nature of the epidermis, and the need to integrate several processes such as cell division, migration, cytoskeletal rearrangements and secretion, the epidermis presents itself as a great model to understand the interplay between cell polarity and downstream cellular processes.

Scope of this thesis

Polarization of epithelial cells is orchestrated by a network of conserved polarity regulators that establish opposing cortical domains through mutually antagonistic interactions and positive feedback loops. While our understanding is still far from complete, the molecular details behind these interactions continue to be worked out. In Chapter 2, we highlight recent findings on the mechanisms that control the activity and localization of apical–basal polarity regulators, including oligomerization and higher-order complex formation, auto-inhibitory interactions, and electrostatic interactions with the plasma membrane.

In Chapters 3-5 we study in detail the functions of the apical polarity complexes in *C. elegans* larval tissues. We start with the apical PAR proteins, which are conserved from *C. elegans* to higher organisms. In *C. elegans*, PAR-3/PAR-6/PKC-3 are involved in anterior-posterior polarity establishment and maintenance, as well as apical basal polarity establishment in the embryonic intestine, pharynx and epidermis, and in the larval spermatheca. A role for the apical PAR proteins in other larval tissues has not been established, probably due to the difficulty of studying these essential proteins: mutants die during embryogenesis and RNAi is not penetrant enough. In Chapter 3 we overcome this difficulty by degrading the proteins using the Auxin-Inducible Degradation (AID) system. We observe that PAR-6 and PKC-3, but not PAR-3, are essential for larval growth. Moreover, the proteins are required in the epidermis, but not in the intestine. Absence of the PAR-6/PKC-3 disrupts cell polarity and apical junctions, as well as the process of molting and seam cell division and differentiation. Ultimately, the absence of PAR-6 and PKC-3 in the epidermis results in larval lethality. Finally, we describe the interaction between PAR-6 and the microtubule organizer NOCA-1, and a direct role of PAR-6 in microtubule organization.

In Chapter 4 we characterize the conservation of composition and functioning of the Crumbs complex in *C. elegans*. The composition of the Crumbs complex in *C. elegans* has not been investigated yet. Here we characterize the homolog of Pals1, magu-2, which is highly conserved. MAGU-2 is enriched in the apical domain and, just as the three Crumbs homologs, is not necessary for epithelial polarity establishment or maintenance. We also describe an interaction between MAGU-2 and the homolog of PatJ, *mpz-1*. Finally, in order to gain more insight into the functioning of the Crumbs complex, we look at the effect of overexpressing the homologs of CRB2 and CRB3, *eat-20* and *crb-3*, respectively. Overexpression of EAT-20 and CRB-3 results in an enlarged apical domain, indicating that the role of the Crumbs proteins in promoting apical domain identity are conserved in *C. elegans*.

Finally, in Chapter 5, we examine more in detail the function of the three Crumbs homologs, which are not essential for polarity establishment in *C. elegans*. This non-essential role could be due to redundancies in the apical polarity network. To explore this possibility and gain insights into the functions of the Crumbs complex, we perform a genetic screen for synthetic interaction with the triple Crumbs knock-out. We identify synthetic defects between the triple Crumbs knock-out and a nonsense mutation in a serine-protease inhibitor, *ZK287.4*. The combined mutants are small in size, have reduced progeny numbers and have apical morphology defects, indicating that the Crumbs complex is involved in apical establishment/maintenance.

Final perspective

Our understanding of how cells become polarized, and how this polarization interacts with downstream pathways, is far from complete. In this thesis we focus on the functions of the apical polarity regulators in the *C. elegans* larval epithelia. We gain insights in the function of PAR-6 and PKC-3 in the epidermis, characterize more in detail the composition of the Crumbs complex and try to shed light into the elusive function of the Crumbs complex in *C. elegans*. Altogether, the work described in this thesis contributes to our understanding of the apical polarity network and its functions during *C. elegans* larval development.

*“I was gratified to be able to answer promptly, and I did.
I said I didn’t know.”*

Mark Twain

New insights into apical-basal polarization in epithelia

Amalia Riga[1]*, Victoria G. Castiglioni[1]*, and Mike Boxem[1]

Current Opinion in Cell Biology 2020, 62:1–8

[1] Developmental Biology, Institute of Biodynamics and Biocomplexity, Department of Biology, Faculty of Science, Utrecht University, Padualaan 8, 3584 CH, Utrecht, The Netherlands.

* These authors contributed equally, and the order of their names was determined by coin toss.

Summary

The establishment of an apical–basal axis of polarity is essential for the organization and functioning of epithelial cells. Polarization of epithelial cells is orchestrated by a network of conserved polarity regulators that establish opposing cortical domains through mutually antagonistic interactions and positive feedback loops. While our understanding is still far from complete, the molecular details behind these interactions continue to be worked out. Here, we highlight recent findings on the mechanisms that control the activity and localization of apical–basal polarity regulators, including oligomerization and higher-order complex formation, auto-inhibitory interactions, and electrostatic interactions with the plasma membrane.

Introduction

Cell polarity lies at the heart of the establishment of proper cellular architecture and function. To be able to form selectively permeable barriers, epithelial cells polarize along an apical–basal axis and establish molecularly and functionally distinct apical, basal and lateral membrane domains. At the interface between apical and lateral domains, adherens junctions (AJs) provide mechanical strength and cohesion, while occluding junctions – tight junctions (TJs) in vertebrates and septate junctions (SJs) in invertebrates – prevent the passage of molecules between cells and help maintain the segregation of apical and basolateral membrane components. Epithelial polarization and morphogenesis are controlled by an epithelial polarity program in which polarity proteins, protein trafficking, membrane lipid regulators, and actomyosin and microtubule cytoskeletons all contribute important roles (Rodriguez-Boulan and Macara, 2014; Roignot et al., 2013). The establishment of opposing cortical domains is the result of a complex web of interactions between a series of evolutionary conserved polarity proteins, most of which were identified through genetic studies in *Caenorhabditis elegans* and *Drosophila melanogaster* (Figure 1) (St Johnston and Ahringer, 2010; Tepass, 2012). Members of the *Par*titioning defective (Par) and Crumbs complexes function together in a semi-redundant fashion to establish the apical domain and position cell junctions at the apical/lateral border, while basolateral identity is promoted by the Scribble group proteins, the kinase PAR-1, and the phospho-protein interacting 14-3-3 protein Par5. More recent studies in Drosophila added the band 4.1-Ezrin-Radixin-Moesin (FERM) domain proteins Yurt and Coracle, and the membrane proteins Neurexin IV (Nrx-IV) and Na^+K^+-ATPase to the roster of proteins regulating epithelial polarity. In this review, we will highlight recent advances in our understanding of the molecular mechanisms that underpin the interactions that result in the correct spatial segregation of these components.

The apical polarity network

Apical domain identity is established by the coordinated activities of Par proteins and the Crumbs complex (Rodriguez-Boulan and Macara, 2014; Tepass, 2012). The apical PAR proteins include Par3 (Bazooka or Baz in Drosophila) and Par6, the small GTPase Cdc42, and the atypical protein kinase C (aPKC) (Goldstein and Macara, 2007). The Crumbs complex consists of the transmembrane protein Crumbs (Crb in Drosophila, CRB1-3 in mammals), the intracellular binding partner Stardust (Sdt, known as protein associated with Lin-7 – PALS1 – in vertebrates), and the Sdt binding partners PATJ (protein associated with tight junctions) and Lin-7 (Bulgakova and Knust, 2009). The proteins in these groups engage in complex and interdependent interactions, and together form an apical polarization network (Figure 2). Par6, aPKC, and the Crumbs proteins co-localize at the apical membrane domain. Par3 engages

in transient interactions with Sdt and with Par6–aPKC to mediate their apical localization (Franz and Riechmann, 2010; Krahn et al., 2010b; Morais-de-Sá et al., 2010). However, in mature Drosophila epithelia and in mammalian epithelial cells, the bulk of Par3/Baz segregates to the apical/lateral border, where it plays an essential role in the positioning and assembly of AJs in Drosophila and TJs in mammalian cells (Ebnet et al., 2008; Laprise and Tepass, 2011). Cdc42 plays a central role in the recruitment of Par6–aPKC, but has many other effector proteins important in epithelial morphogenesis, and its activity is controlled by numerous regulatory proteins (Pichaud et al., 2019).

The kinase activity of aPKC is central to the mutual antagonism between cortical polarity regulators, and a major role of the apical polarity proteins is to tightly control aPKC localization and activity. aPKC is complexed with the adapter protein Par6, which mediates most of the physical interactions that localize aPKC. In addition, Par6 controls the kinase activity of aPKC. It is still unclear, however, whether Par6 acts as an activator or an inhibitor, as studies into the effects of Par6 on aPKC kinase activity have yielded conflicting results (Dong et al., 2019; Graybill et al., 2012; Hong, 2018).

The localization of Par6–aPKC to the apical membrane is mediated by physical interactions with Par3, the active GTP-bound version of Cdc42, and Crumbs (Laprise and Tepass, 2011). The Par3–Par6–aPKC complex is thought to be inactive, which would help to prevent inappropriate phosphorylation of target proteins by aPKC (David et al., 2013; Graybill et al., 2012; Lin et al., 2000; Rodriguez et al., 2017; Soriano et al., 2016). Inhibition of aPKC was reported to be mediated by formation of high affinity interactions of two motifs within the Par3 conserved region 3 (CR3) with the aPKC kinase domain, blocking substrate access (Soriano et al., 2016). However, the effects on catalytic activity and its relevance *in vivo* are a point of contention (Holly and Prehoda, 2019; Thompson and McDonald, 2019). As discussed below, Par3 is an aPKC substrate itself, and its phosphorylation is required for junctional localization. How to reconcile roles of Par3 as both an inhibitor and a substrate of aPKC is an important future challenge.

The Par3–Par6 association was reported to involve a non-canonical interaction between the Par3 PDZ1 domain and Par6 Crib-PDZ domains (Joberty et al., 2000; Li et al., 2010a; Lin et al., 2000). However, recent data indicate that, at least in Drosophila and mammals, the Par3–Par6 association is mediated by interaction of the Par3 PDZ1 and PDZ3 domains with a PDZ binding motif (PBM) at the N-terminus of Par6 (Renschler et al., 2018). Par3 could interact simultaneously with two Par6 proteins, potentially facilitating higher order complex formation, though this has not been shown to occur *in vivo*. The PBM domain is absent from *C. elegans* PAR-6 (Renschler et al., 2018), hence the mode of the Par3–Par6 interaction is not fully resolved.

At least two mechanisms can contribute to membrane localization of Par3. First, the N-terminal conserved region (CR1) mediates homo-oligomeri-

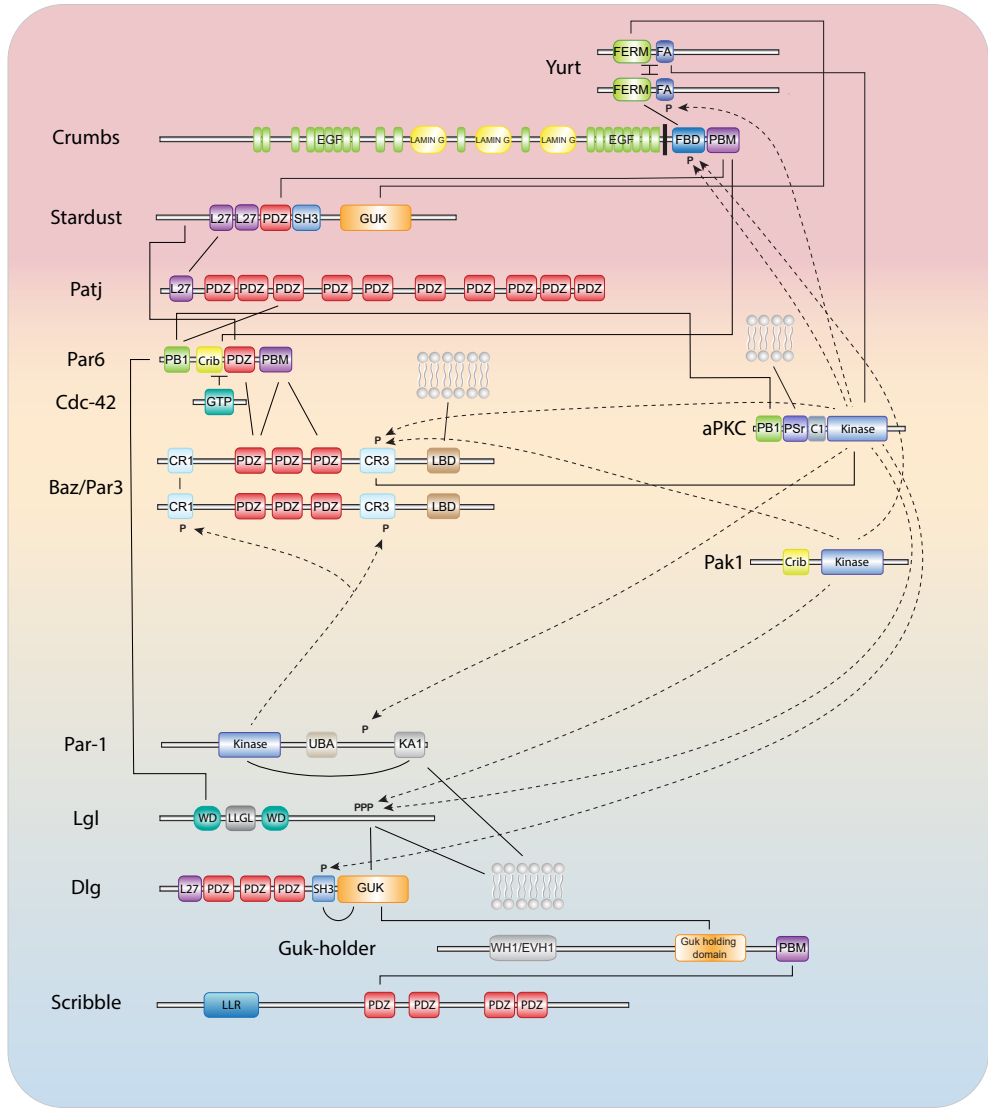

Figure 1. Cell polarity is established and maintained by a complex web of interactions between apical and basolateral polarity regulators. Solid lines indicate physical interactions. Dashed lines indicate phosphorylation events. Canonical domain organizations are shown. Abbreviations: FERM, 4.1-Ezrin-Radixin-Moesin; FA, FERM-adjacent (FA) domain; EGF, epidermal growth factor domain; L27, Lin-2 and Lin-7 domain; SH3, SRC homology 3 domain; GUK, guanylate kinase-like; FBD, FERM binding domain; PBM, PDZ domain-binding motif; PB1, Phox and Bem1 domain; Crib, Cdc42- and Rac-interactive binding motif; CR1, CR3, conserved region 1 and 3; LBD, lipid binding domain; KA1, kinase associated domain; WD, WD40 repeat; LLGL, lethal giant larvae specific domain; WH1/EVH1, Enabled/VASP homology 1; LLR, leucine rich repeat domain.

zation of Par3/Baz, which promotes the formation of cortical Par3–Par6–aPKC clusters and has been reported to be essential for Par3 localization (Dickinson et al., 2017; Harris, 2017; Kono et al., 2019; Rodriguez et al., 2017; Wang et al., 2017). Second, a C-terminal lipid binding (LB) domain promotes membrane localization through binding to phospholipids (Claret et al., 2014; Horikoshi et al., 2011; Krahn et al., 2010a). Recent studies in Drosophila indicate that oligomerization and phospholipid binding can contribute redundantly to the membrane association of Baz (Kullmann and Krahn, 2018; McKinley et al., 2012). How Par3 is transported apically is not completely clear. Dynein-mediated transport is important for Baz positioning in Drosophila epithelia and oocytes (Harris and Peifer, 2005; Jouette et al., 2019; McKinley and Harris, 2012), but based on other systems reaction–diffusion processes and advective transport play roles as well (Goehring and Grill, 2013). It is also not clear yet to what extent Par6–aPKC is transported apically in a complex with Par3, versus being recruited from the cytoplasm by previously localized Par3.

At the apical domain, the release of Par3/Baz from Par6–aPKC and Sdt critically depends on phosphorylation of Par3 by aPKC on a conserved Serine residue within the conserved region three (CR3), which reduces the affinity of Par3 for aPKC and Sdt (Hirose et al., 2002; Krahn et al., 2010b; Morais-de-Sá et al., 2010; Nagai-Tamai et al., 2002; Walther and Pichaud, 2010). Phosphorylation by aPKC alone is, however, not sufficient for the segregation of Par3 from Par6–aPKC, possibly due to the association of Par3 with Par6, and further depends on interactions of Par6 with GTP-Cdc42 and with Crb (Almeida et al., 2019; Harris and Peifer, 2005; Krahn et al., 2010b; Morais-de-Sá et al., 2010; Walther and Pichaud, 2010). GTP-Cdc42 may outcompete Par3 for binding to Par6, and furthermore induces a conformational switch in the Par6 PDZ domain that greatly increases the affinity for the C-terminal PBM in Crumbs (Peterson et al., 2004; Whitney et al., 2011; Whitney et al., 2016). In a recent preprint publication, Nunes de Almeida *et al*. used a series of Par6 alleles that specifically disrupt binding to Cdc42, Crb, or aPKC to investigate the order of events in Drosophila photoreceptor cells and follicle epithelium (Almeida et al., 2019). Their results support a model in which recruitment of Par6–aPKC by GTP-Cdc42 promotes the subsequent binding of Par6 to Crb, which results in mutual stabilization of both Par6–aPKC and Crb at the apical membrane.

The shuttling of aPKC between an inactive Par3 complex that promotes localization and a Par3-independent active complex appears to be a common feature of polarized cells. In the one-cell *C. elegans* embryo, PKC-3 shuttles between an inactive PAR-3/PAR-6/PKC-3 complex that promotes anterior segregation, and an active CDC-42/PAR-6/PKC-3 complex (Aceto et al., 2006; Beers and Kemphues, 2006; Rodriguez et al., 2017; Wang et al., 2017). An important difference however is the role of aPKC. While in Drosophila epithelia aPKC phosphorylates Par3/Baz to promote its release from the complex, in *C. elegans* aPKC activity was required to couple the behavior of PAR-3 and PAR-

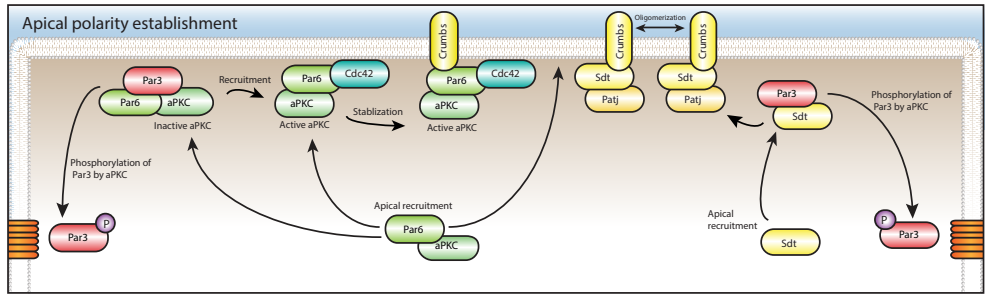

Figure 2. The apical domain is established by coordinated interactions between proteins of the Par and Crumbs complexes.

6/PKC-3 (Rodriguez et al., 2017). A similar observation was recently made in Drosophila neuroblasts, where acute inhibition of aPKC resulted in uncoupling of the localizations of Baz and aPKC–Par6 (Hannaford et al., 2019). These observations may reflect differences between epithelial cells and asymmetrically dividing cells. For example, in non-epithelial cells which lack apical junctions, phosphorylation of Par3 by aPKC is not essential. However, it may also reflect an incomplete understanding of a common underlying mechanism.

The relative importance of the interactions with Par6–aPKC described above are cell context dependent. For example, in the follicular epithelium and adult mid gut epithelium, Baz is dispensable for the localization of Par6 (Chen et al., 2018; Shahab et al., 2015), while in the follicular cells of stage 10 Drosophila embryos, Crb is not required for apical enrichment of aPKC (Sherrard and Fehon, 2015). In these cells, direct recruitment of Par6–aPKC by Cdc42 may be the dominant mechanism. However, in the *C. elegans* embryonic epidermis, Cdc42 was found to be dispensable for polarization and for apical localization of PAR-6, indicating that Cdc42 is not essential under all conditions (Zilberman et al., 2017). Interestingly, a recent preprint proposes an alternative localization mechanism for Drosophila and mammalian aPKC, based on direct binding of a polybasic domain within the aPKC pseudosubstrate region to the membrane lipids PI4P and PIP2 (Dong et al., 2019). This interaction did not require Cdc42, but does depend on binding to Par6, which the authors postulate induces an allosteric change that exposes the polybasic domain (Dong et al., 2019). The same study also finds that the binding of Crb activates the kinase activity of aPKC, although this cannot represent a general mechanism as aPKC is also active in cell types that do not express Crumbs.

A recent study in MDCK cells points to yet another mechanism that may contribute to the apical segregation of Par6–aPKC (Zihni et al., 2017). In these cells, apical activation of Cdc42 stimulates actomyosin contractility, while aPKC inhibits actomysosin contractility at the level of cell junctions, potentially setting up a contractility gradient. Interfering with apical actomyosin contractility blocked the separation of Par3 from Par6–aPKC, suggesting that

cortical contractility mediates the segregation of Par6–aPKC. How cortical contractility promotes Par3 segregation in this cell type, however, is unclear (Zihni et al., 2017). Taken together, it is evident that the localization and activation of aPKC can be controlled by several mechanisms that may act together or play specific roles in particular cell types.

Basolateral polarity regulators

The main basolateral determinants are the PAR-1/MARK serine/threonine kinases, which mediate exclusion of proteins from the basolateral domain through phosphorylation, and the Scribble group proteins Scribble (Scrib), Discs large (Dlg) and Lethal giant larvae (Lgl), which exclude apical proteins from the basolateral domain by virtue of the ability of Lgl to inhibit aPKC (Bonello and Peifer, 2019a; Stephens et al., 2018; Wu and Griffin, 2017; Yamanaka and Ohno, 2008). In addition, the Scribble module may regulate the polarized trafficking of proteins. In Drosophila, the Scribble module was shown to regulate trafficking of Crumbs and other cargo from early endosomes to the Golgi system through the retromer pathway (de Vreede et al., 2014). In the *C. elegans* intestine, the Scrib homolog LET-413 acts as a Rab5 effector, to promote the activation of RAB-10 and endocytic recycling (Liu et al., 2018). Scrib, Dlg, and Lgl each contain multiple protein–protein interaction domains, and scaffold a bewildering array of proteins linked to many processes besides cell polarity, including tissue growth, differentiation, and cell migration (Stephens et al., 2018).

In Drosophila, the Scribble proteins are dependent on each other for their localization and act in a common pathway to restrict apical determinants to the apical domain, control AJ formation and regulate cell growth (Yamanaka and Ohno, 2008). With respect to its role in junction formation, a recent preprint unexpectedly identified a very early role in organizing AJs in the developing Drosophila embryo, upstream of other polarity regulators including Baz/par3 (Bonello and Peifer, 2019b). Recently, the hierarchy in the relationships between Scrib, Dlg, and Lgl was elucidated in the midgut of adult Drosophila, a tissue in which the Scribble proteins are present at septate junctions but not essential for polarization (Chen et al., 2018). In these cells, Scrib recruits Dlg to the septate junctions, which in turn recruits Lgl. In *C. elegans* and mammalian systems, the Scribble proteins also play key roles in cell polarity, but the importance of their contribution varies, and the proteins often only partially overlap in localization (Bonello and Peifer, 2019a). Unlike the apical polarity determinants, few physical interactions have been identified within the Scribble module. In mammalian cells, Lgl2 directly interacts with the GUK domain of Dlg4 when phosphorylated by aPKC on one of three conserved serine residues (Zhu et al., 2014). In the synapses of Drosophila neurons, Dlg was also shown to indirectly associate with Scrib through the linker protein GUK-holder (Gukh) (Mathew et al., 2002). Recently, the Scrib PDZ1 domain was shown to interact

with a PDZ binding motif in C-terminus of Gukh (Caria et al., 2018). The same study also provides evidence for a broader role for Gukh in controlling epithelial polarity, and it will be important to investigate the role of Gukh homologs in other organisms in epithelial morphogenesis.

Mechanisms of mutual exclusion

The major mutual antagonistic interactions in epithelial cells are mediated by the kinases aPKC and PAR-1, and by Lgl. aPKC phosphorylates PAR-1, Par3, and Lgl to mediate their exclusion from the apical domain (Hong, 2018). Conversely, Lgl inhibits aPKC by binding to Par6–aPKC, which competes with Par3 binding, inhibits aPKC kinase activity, and prevents membrane association of Par6–aPKC (Bonello and Peifer, 2019a; Stephens et al., 2018). Crumbs has also been shown to be a target for phosphorylation by aPKC (Sotillos et al., 2004), but the importance of this is unclear as mutating the aPKC target sites does not appear to affect Crb localization, epithelial polarization, or viability in Drosophila (Cao et al., 2017). In the basolateral domain, the main target of PAR-1 is Par3. PAR-1 phosphorylates Baz/Par3 on two conserved serine residues, which prevents oligomerization, creates a binding site for the 14-3-3 protein Par5, and prevents binding of aPKC, all of which contribute to the exclusion of Baz/Par3 from the basolateral domain (Benton and St Johnston, 2003; Krahn et al., 2009). The combined activities of aPKC and PAR-1 thus position Par3 at the apical/lateral border, which is critical for the correct positioning and assembly of junctional complexes.

The mechanism of exclusion of Lgl is now well established. Several aPKC target proteins, including Lgl, the cell fate regulators Mira and Numb, and the *C. elegans* polarity protein PAR-2, localize to the plasma membrane via electrostatic interactions between basic and hydrophobic (BH) motifs and phospholipids (Bailey and Prehoda, 2015; Dong et al., 2015). Phosphorylation of aPKC consensus sites within BH motifs is thought to prevent membrane association by neutralizing positive charges (Bailey and Prehoda, 2015; Dong et al., 2015). Recent studies on *C. elegans* LGL-1 and human Lgl2 confirm this model and further show that aPKC phosphorylation counteracts formation of a membrane-binding α-helix conformation of the BH motif (Almagor et al., 2019; Visco et al., 2016). In mitotic divisions of epithelial cells, the cell-cycle kinases Aurora A and B also phosphorylate Lgl on target sites within the BH motif to induce a complete loss from the cortex (Bell et al., 2015; Carvalho et al., 2015). At the end of mitosis, when cells need to repolarize, the phosphatase PP1 dephosphorylates these sites (Moreira et al., 2019).

The mechanisms that mediate plasma membrane localization and exclusion of PAR-1 are also becoming increasingly clear. PAR-1 proteins contain a kinase domain, a linker region that harbors a conserved aPKC phosphorylation site, and a C-terminal kinase associated (KA1) domain that can mediate membrane association by binding to acidic phospholipids (Wu and Griffin,

2017). Phosphorylation by aPKC results in exclusion from the membrane by creating a binding site for the 14-3-3 protein Par5, and has also been reported to reduce PAR-1 kinase activity (Hurov et al., 2004; Kusakabe and Nishida, 2004; Motegi et al., 2011; Suzuki et al., 2004). A second level of control over PAR-1 activity is exerted by the KA1 domain, which had been suggested to form an auto-inhibitory interaction with the kinase domain (Wu and Griffin, 2017). Recent investigations of the human PAR-1 kinase MARK1 revealed that the KA1 domain can indeed bind to the kinase domain, blocking substrate access, thereby rendering the kinase inactive (Emptage et al., 2017; Emptage et al., 2018). Binding of MARK1 to the plasma membrane via the KA1 domain releases this interaction, resulting in kinase activation (Emptage et al., 2017; Emptage et al., 2018). Recent data in *C. elegans* confirm an inhibitory role for the KA1 domain and furthermore indicate that inhibition of PAR-1 activity by aPKC/PKC-3 and the KA1 domain act in parallel to restrict PAR-1 activity to the posterior domain (Folkmann and Seydoux, 2019).

In addition to aPKC, PAR-1, and Lgl, the FERM domain protein Yurt plays a role in determining apical and basolateral domain sizes in Drosophila, zebrafish and cultured mammalian cells (Gamblin et al., 2014; Hsu et al., 2006; Laprise et al., 2006; Laprise et al., 2009; Lee et al., 2007; Schell et al., 2017). Yurt physically interacts with and negatively regulates Crumbs and aPKC, and is itself a target for inactivation by aPKC (Gamblin et al., 2014; Hsu et al., 2006; Laprise et al., 2006; Laprise et al., 2009). In developing Drosophila embryos, Yurt displays a dynamic localization and activity pattern, initially preventing Crumbs localization to the basolateral domain, and later acting at the apical domain to limit Crumbs activity and prevent apical overexpansion (Gamblin et al., 2014; Laprise et al., 2006; Laprise et al., 2009). How Yurt inhibits aPKC is not known, but the binding to Crumbs was recently shown to depend on Yurt oligomerization (Gamblin et al., 2018). Phosphorylation of Yurt by aPKC prevents this oligomerization, explaining at least in part how aPKC counteracts Yurt (Gamblin et al., 2018).

Finally, aPKC may not be the only kinase involved in excluding proteins from the apical domain. A recent study reported that, in the Drosophila follicular epithelium, the kinase Pak1 may act redundantly with aPKC downstream of Cdc42, and phosphorylates an overlapping set of substrates (Aguilar-Aragon et al., 2018). Inhibition of Pak1 also resulted in polarity defects in mammalian cell cultures, indicating that the role of Pak1 may be conserved (Aguilar-Aragon et al., 2018).

Conclusion

The past couple of years have seen great progress in our understanding of the regulatory interactions between polarity proteins, and several novel mechanisms of control have emerged. It is clear that polarity proteins are regulated at multiple levels, as evidenced by the dual control over PAR-1 activity by aPKC and membrane association, the redundant control over Baz/Par3 membrane association by oligomerization and phospholipid binding, and the multiple mechanisms involved in targeting aPKC to the apical domain. While we have highlighted commonalities, the organization of cell polarity is not the same in all tissues and organisms. In Drosophila, *C. elegans*, and mouse embryos the requirements for Par3, Par6, Cdc42, aPKC and Crumbs all vary between epithelial tissues (Achilleos et al., 2010; Hirose et al., 2006; Shahab et al., 2015; Tepass and Knust, 1990; Totong et al., 2007; Waaijers et al., 2015; Zilberman et al., 2017), and recent investigations in the Drosophila midgut point to polarization mechanisms that do not rely on Par or Crumbs proteins at all (Chen et al., 2018). For the future, it will be important to clarify how conserved and generally used each mechanism of regulation is in different organisms and polarized cell types.

Acknowledgements

We thank Helena R. Pires, João J. Ramalho, Jorian J. Sepers and Nathan W. Goehring for critical reading of the manuscript. This work has received funding from the European Union's Horizon 2020 research and innovation programme under the Marie Skłodowska-Curie grant agreement No. 675407 – PolarNet, and from the Netherlands Organization for Scientific Research (NWO): earth and life sciences (ALW), Innovational Research Incentives Scheme grant 016.VICI.170.165.

"A day without sunshine is like, you know, night"

Steve Martin

Epidermal PAR-6 and PKC-3 are essential for larval development of *C. elegans* and organize non-centrosomal microtubules

Victoria G. Castiglioni[1]*, Helena R. Pires[1]*, Rodrigo Rosas Bertolini[1], Amalia Riga[1], Jana Kerver[1], Mike Boxem[1*]

eLife 2020;9:e62067

[1] Division of Developmental Biology, Institute of Biodynamics and Biocomplexity, Department of Biology, Faculty of Science, Utrecht University, Utrecht, The Netherlands

Short title: Essential roles for PAR-6 and PKC-3 in larval *C. elegans* epidermal epithelia

Keywords: cell polarity; Par3; Par6; aPKC; microtubule; NOCA-1

* These authors contributed equally to this work.

Summary
PAR-6 and PKC-3/aPKC are essential for postembryonic development of *C. elegans* and control the organization of non-centrosomal microtubule bundles in the epidermis, likely through recruitment of NOCA-1/Ninein.

Abstract
The cortical polarity regulators PAR-6, PKC-3, and PAR-3 are essential for the polarization of a broad variety of cell types in multicellular animals. In *C. elegans*, the roles of the PAR proteins in embryonic development have been extensively studied, yet little is known about their functions during larval development. Using inducible protein degradation, we show that PAR-6 and PKC-3, but not PAR-3, are essential for postembryonic development. PAR-6 and PKC-3 are required in the epidermal epithelium for animal growth, molting, and the proper pattern of seam-cell divisions. Finally, we uncovered a novel role for PAR-6 in organizing non-centrosomal microtubule arrays in the epidermis. PAR-6 was required for the localization of the microtubule organizer NOCA-1/Ninein, and defects in a *noca-1* mutant are highly similar to those caused by epidermal PAR-6 depletion. As NOCA-1 physically interacts with PAR-6, we propose that PAR-6 promotes non-centrosomal microtubule organization through localization of NOCA-1/Ninein.

Introduction
Polarity is a near universal property of cells that is essential for establishing proper cellular architecture and function. Epithelial cells – one of the major polarized animal cell types – polarize along an apical–basal axis and establish molecularly and functionally distinct apical, basal, and lateral membrane domains. The boundary between apical and lateral domains is marked by the presence of cell–cell junctions that provide adhesion between cells and prevent unwanted paracellular passage of molecules. The polarization of epithelial cells is orchestrated by conserved cortical polarity regulators that establish opposing membrane domains through mutually antagonistic interactions. In metazoans, the partitioning defective (PAR) proteins Par3, Par6, and atypical protein kinase C (aPKC) play a central role in the establishment of epithelial cell polarity. These highly conserved polarity regulators are essential determinants of apical domain identity, and are required for the positioning, maturation, and maintenance of apical cell junctions (Achilleos et al., 2010; Franz and Riechmann, 2010; Georgiou et al., 2008; Harris and Peifer, 2004; Harris and Peifer, 2005; Harris and Tepass, 2008; Hutterer et al., 2004; Izumi et al., 1998; Joberty et al., 2000; Leibfried et al., 2008; Lin et al., 2000; Totong et al., 2007; Wodarz et al., 2000; Yamanaka et al., 2001).

Par6 and Par3 are both PDZ domain containing scaffold proteins that can interact with each other, with aPKC, and with numerous other proteins. Par6 and aPKC form a stable subcomplex by interacting through their PB1 domains (Hirano et al., 2005; Wilson et al., 2003). The association of Par6–aPKC with Par3 is dynamic. In *C. elegans* zygotes, PAR-6/PKC-3 shuttle between a kinase inactive complex with PAR-3 that promotes anterior segregation, and an active complex with the small GTPase CDC-42 (Aceto et al., 2006; Beers and Kemphues, 2006; Rodriguez et al., 2017; Wang et al., 2017). In epithelia, Par3 can promote the apical recruitment of Par6–aPKC (Franz and Riechmann, 2010; Harris and Peifer, 2005; Hutterer et al., 2004; Joberty et al., 2000; Lin et al., 2000; Wodarz et al., 2000). In mature epithelia, however, the bulk of Par3 segregates to the apical/lateral border, where it plays an essential role in the positioning and assembly of apical junctions (Achilleos et al., 2010; Georgiou et al., 2008; Harris and Peifer, 2004; Harris and Tepass, 2008; Izumi et al., 1998; Leibfried et al., 2008; Totong et al., 2007; Yamanaka et al., 2001). The segregation of Par3 from Par6–aPKC in epithelia depends on phosphorylation of Par3 by aPKC, and involves handoff of Par6–aPKC to Cdc42 and the epithelial specific Crumbs polarity complex (Bilder et al., 2003; Harris and Peifer, 2005; Hong et al., 2003; Krahn et al., 2010b; Morais-de-Sá et al., 2010; Nagai-Tamai et al., 2002; Almeida et al., 2019; Walther and Pichaud, 2010).

In addition to interactions that mediate the subcellular localization of Par6–aPKC or Par3, both Par6 and Par3 can interact with effector proteins to connect cortical polarity with downstream pathways (McCaffrey and Macara, 2009). For example, Par3 modulates phospholipid levels by recruiting the lipid

phosphatase PTEN to cell junctions (Feng et al., 2008; Martin-Belmonte et al., 2007; Pinal et al., 2006; von Stein et al., 2005), inhibits Rac activity by binding to and inactivating the RacGEF Tiam1 (Chen and Macara, 2005, 1; Mertens et al., 2005, 1), and mediates spindle positioning in Drosophila neuroblasts through recruitment of Inscuteable (Schober et al., 1999; Wodarz et al., 1999). For Par6, fewer downstream targets have been described. In mammals, Par6 can recruit the E3 ubiquitin ligase Smurf1 to promote degradation of the small GTPase RhoA, causing dissolution of tight junctions (Ozdamar et al., 2005; Sánchez and Barnett, 2012; Wang et al., 2003). Par6 can also bind to the nucleotide exchange factor ECT2 to regulate epithelial polarization and control actin assembly at metaphase in dividing epithelial cells (Liu et al., 2004; Liu et al., 2006; Rosa et al., 2015). As high-throughput studies have identified multiple candidate binding partners that have not yet been investigated (Boxem et al., 2008; Brajenovic et al., 2004; Giot et al., 2003; Grossmann et al., 2015; Hein et al., 2015; Huttlin et al., 2015; Lenfant et al., 2010; Luck et al., 2020; Waaijers et al., 2016), additional interactions important for the functioning of Par6 and for linking cortical polarity to other processes involved in epithelial polarization likely remain to be discovered.

Despite the conserved requirements for Par6–aPKC and Par3 in epithelial cells there are important context and cell-type dependent differences in the functioning of these polarity proteins (Pickett et al., 2019; St Johnston, 2018). For example, in Drosophila, Bazooka (Par3) is not required for junction positioning or polarization of cells in the follicular epithelium (Pickett et al., 2019; Shahab et al., 2015), and in the adult Drosophila midgut, the canonical Par, Crumbs, and Scribble polarity modules are not essential for apical–basal polarity (Chen et al., 2018). In *C. elegans*, requirements for PAR-3 and PAR-6 in embryonic epithelia also vary. PAR-6 appears to be required for apical junction formation in all epithelia, including the epidermis, intestine, foregut, and pharyngeal arcade cells (Montoyo-Rosario et al., 2020; Totong et al., 2007; Von Stetina and Mango, 2015; Von Stetina et al., 2017). However, while arcade cells show a complete lack of polarization upon PAR-6 loss, foregut, intestinal, and epidermal epithelial cells still establish an apical domain (Totong et al., 2007; Von Stetina and Mango, 2015). PAR-3 is required for apical junction formation in embryonic intestinal and pharyngeal epithelia, but not in epidermal epithelial cells (Achilleos et al., 2010).

Studies of PAR-6, PKC-3, and PAR-3 in *C. elegans* have largely focused on embryonic tissues. Here, we make use of targeted protein degradation to investigate the role of PAR-6, PKC-3, and PAR-3 in larval epithelia of *C. elegans*. Ubiquitous depletion of PAR-6 and PKC-3, but not PAR-3, resulted in a larval growth arrest, demonstrating that these proteins are required for larval development. Through tissue-specific depletion, we identified an essential role for PAR-6 and PKC-3 in the *C. elegans* epidermis. Depletion in this tissue caused growth arrest, a failure to undergo molting, and severe defects in the division

pattern of the epidermal seam cells. We also observed defects in the maintenance of apical cell junctions, and a failure to exclude LGL-1 from the apical domain. Finally, we identified a novel role for PAR-6 in organizing non-centrosomal microtubule arrays in the epidermis. Epidermal depletion of PAR-6 led to defects in the localization of the microtubule organizer NOCA-1/Ninein, as well as of the γ-tubulin ring complex component GIP-1, and of the sole Patronin/CAMSAP/Nezha homolog PTRN-1. Microtubule defects in a *noca-1* mutant closely resembled those in PAR-6 depleted animals, including the loss of GIP-1 localization. As NOCA-1 physically interacts with PAR-6, we conclude that PAR-6 likely organizes non-centrosomal microtubule arrays through localization of NOCA-1.

Results

PAR-6 and PKC-3 are essential for larval development

To investigate the role of PAR-6, PKC-3, and PAR-3 in larval development, we made use of the auxin-inducible degradation (AID) system. The AID system enables targeted degradation of AID-degron tagged proteins through expression of the plant-derived auxin-dependent E3 ubiquitin ligase specificity factor TIR1 (Nishimura et al., 2009; Zhang et al., 2015) (Figure 1A). Using CRISPR/Cas9, we inserted sequences encoding the AID-degron and the green fluorescent protein (GFP) into the endogenous *par-6, pkc-3,* and *par-3* loci, such that all known isoforms of each protein are tagged (Figure 1B). PAR-6 was tagged at the shared C-terminus, and PKC-3 at the N-terminus. The *par-3* locus encodes two groups of splice variants that use two alternative start sites, termed PAR-3L (for long) and PAR-3S (for short) (Achilleos et al., 2010; Li et al., 2010b). PAR-3L isoforms are expressed maternally and in larval stages, but not or at low levels in the embryo, while PAR-3S isoforms are expressed zygotically and in larval stages, but not maternally (Achilleos et al., 2010; Li et al., 2010b). To deplete both PAR-3L and PAR-3S isoforms, we inserted the GFP–AID tag at both start sites. To examine if the presence of the GFP–AID tags interfered with protein function, we examined the growth rates of the tagged strains. Homozygous animals were viable and showed the same growth rates as wild-type, indicating that the proteins are still functional (Figure 1C–E). Each protein was enriched at the apical membrane domain of epithelial tissues, including the pharynx, excretory canal, intestine and epidermis (Figure 1F, G). This matches previous observations in *C. elegans* larvae (Li et al., 2010a; Li et al., 2010b), and further indicates that the GFP–AID tag does not interfere with protein functioning. In the epidermis, we sometimes observed higher levels of fluorescence at the seam–seam junctions than at the seam–hyp7 junctions. Similar planar polarization of the PAR module was recently observed in the lateral epidermis of the elongating embryo (Gillard et al., 2019). However, in the larval epider-

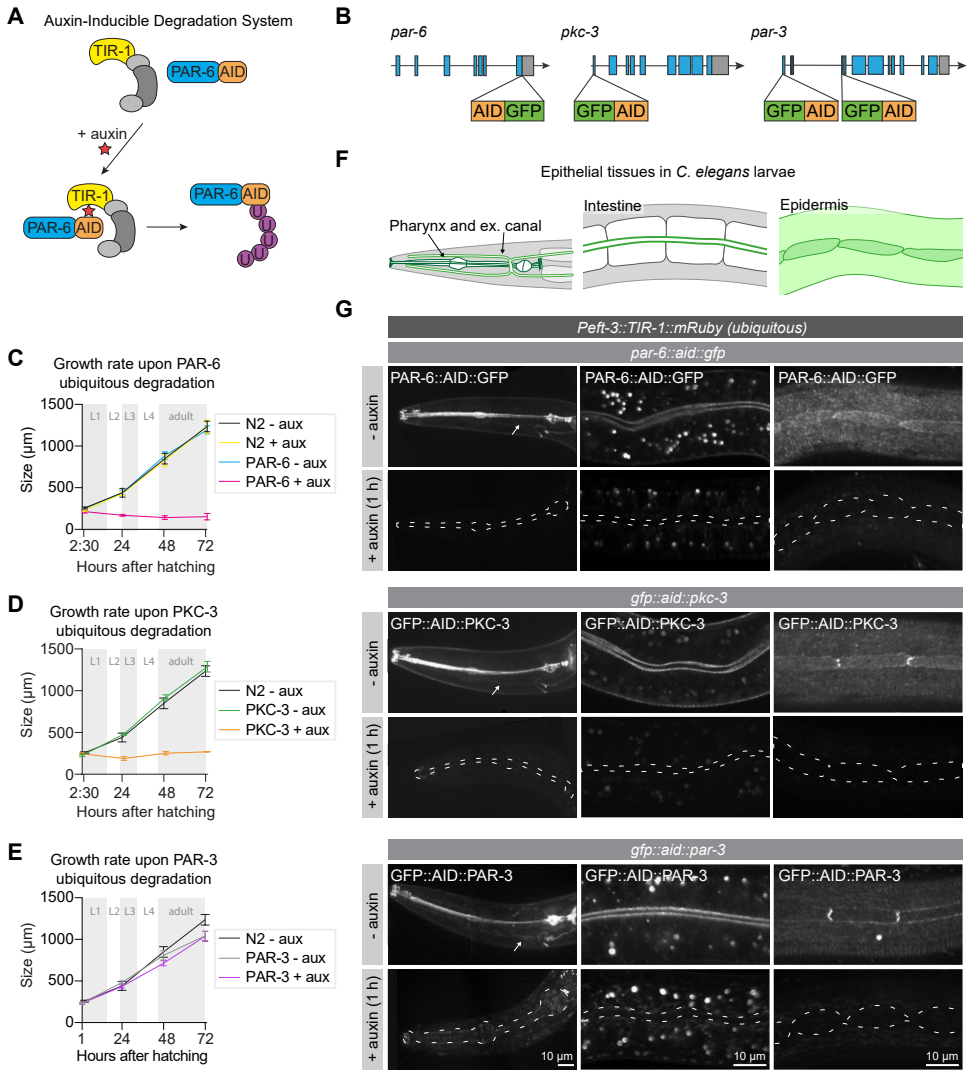

Figure 1. PAR-6 and PKC-3 are essential for larval development. (A) Overview of the AID system, which enables targeted degradation of AID-tagged proteins by the plant-derived E3 ubiquitin ligase specificity factor TIR1 upon addition of auxin. **(B)** Schematic representation of endogenous tagging of *par-6, pkc-3,* and *par-3* loci with sequences encoding a green fluorescent protein (GFP) and auxin-inducible degradation degron (AID) tag. **(C–E)** Growth curves of N2, *par-6::aid::gfp, gfp::aid::pkc-3*, and *gfp::aid::par-3* animals in absence (- aux) or presence (+ aux) of 4 mM auxin from hatching. Data show mean ± SD. Shading indicates the developmental stage of control animals. *n* = 6, 7, 8, and 8 for N2 - aux; 6, 7, 9, and 9 for N2 + aux; 7, 6, 9, and 9 for PAR-6 - aux; 8, 6, 7, and 9 for PAR-6 + aux; 22, 11, 10, and 14 for PKC-3 - aux; 19, 14, 9, and 10 for PKC-3 + aux; 10, 10, 10, and 10 for PAR-3 - aux, and 10, 10, 10, and 10 for PAR-3 + aux. **(F)** Graphical representation of larval epithelial tissues in *C. elegans*. Green indicates localization of PAR-6, PKC-3, and PAR-3. **(G)** Distribution of GFP::AID-tagged PAR-6, PKC-3, and PAR-3 in different larval tissues in absence (- auxin) or presence (+ auxin) of 4 mM auxin for 1 hour. Images are maximum intensity projections, and images of the pharynx are stitched montages. Dashed lines in - auxin panels outline pharynx (left panel), intestinal lumen (middle panel) or seam cells (right panel). White arrows point to the excretory canals.

mis we only observed planar enrichment in a subset of animals. Whether this pattern is functionally significant remains to be determined. Finally, to further investigate potential isoform specific expression of PAR-3, we examined the expression of the PAR-3L isoforms alone during larval development (Figure 1—Figure supplement 1). PAR-3L was expressed in the intestine, where it localized to the apical domain, but we observed little or no expression in the pharynx or epidermis (Figure 1—Figure supplement 1D). Thus, PAR-3S appears to be the predominant isoform group in larval tissues.

To investigate the role of PAR-3, PAR-6 and PKC-3 in larval development we degraded each protein using a ubiquitously expressed TIR1 under the control of the *eft-3* promoter (Zhang et al., 2015). We tested the efficiency of protein degradation by exposing synchronized L3 larvae to auxin and examining protein expression. Apical enrichment of PAR-3, PAR-6, and PKC-3 became indistinguishable from background fluorescence within one hour of exposure to 4 mM auxin in the pharynx, excretory canal, intestine, and epidermis (Figure 1G). To examine if the depletion of PAR-6, PKC-3, or PAR-3 affected larval development, we degraded each protein by addition of auxin at hatching and measured animal growth rates. Ubiquitous degradation of PAR-3 did not cause a defect in larval growth, and animals developed into morphologically normal and fertile adults (Figure 1E). To determine if the lack of phenotype was due to an inherent technical problem with our approach, we also depleted PAR-3 in the germline and early embryos using *Pgld-1* driven TIR1. Addition of auxin to L4-stage animals resulted in 100% embryonic lethality in the next generation (n = 378), compared to 3.2% in non-auxin-treated controls (n = 591). Thus, the lack of a visible phenotype upon larval degradation indicate that the functions of PAR-3 are not essential for larval development. Alternatively, despite visual absence of GFP::AID::PAR-3, degradation may be incomplete, or animals may express unpredicted non-tagged larval-specific protein isoforms. In contrast to PAR-3, depletion of PAR-6 or PKC-3 from hatching caused a striking growth arrest with animals not developing beyond L1 size (Figure 1C, D). Thus, PAR-6 and PKC-3 are essential for early larval development, and we focused our further analysis on PAR-6 and PKC-3.

PAR-6 and PKC-3 are essential in the larval epidermis, but not in the intestine

We next wanted to determine which larval tissue or tissues are severely affected by the loss of PAR-6/PKC-3 and contribute to the growth arrest. We focused on the two major epithelial organs: the intestine and the epidermis. The intestine is an epithelial tube formed in embryogenesis by 20 cells, which do not divide during larval development. PAR-6 and PKC-3 are highly enriched at the apical luminal domain (Figure 2A). The epidermis consists of two cell types: hypodermal cells and seam cells. The syncytial hypodermal cell hyp7 covers most of the body. Embedded within hyp7 are two lateral rows of epithelial seam cells, which contribute multiple nuclei to hyp7 through asymmetric divisions in each larval stage. PAR-6 and PKC-3 localize to the apical domain of the seam cells and hyp7 and are enriched at the seam–seam and seam–hyp7 junctions (Figure 2B).

To enable tissue-specific depletion of PAR-6 and PKC-3, we generated single-copy integrant lines expressing TIR1 in the intestine and epidermal lineages, using the tissue-specific promoters *Pelt-2* and *Pwrt-2*, respectively. In both tissues, protein depletion occurred within one hour of addition of 1 mM auxin (Figure 2A–F). To determine the contribution of the intestine and epidermis to the larval growth defects we observed above, we measured the growth rate of animals depleted of PAR-6 or PKC-3 from hatching in each tissue. Depletion of either protein from the intestine did not result in a growth delay or in obvious defects in morphology of the intestine (Figure 2G, H). These results are in contrast to the embryonic intestine, where PAR-6 has been shown to be required to maintain apical and junctional integrity (Sallee et al., 2020; Totong et al., 2007). Simultaneous depletion of PAR-6 and PKC-3 also did not result in a growth delay or visible abnormalities in the intestine (Figure 2—figure supplement 1A). These data indicate that PAR-6 and PKC-3 are not essential for the functioning and homeostasis of the larval intestine, though we cannot exclude that very low protein levels that we were not able to detect by fluorescence microscopy are sufficient in this tissue.

In contrast to the intestine, depletion of PAR-6 or PKC-3 from hatching in the epidermis caused an early larval growth arrest, as observed with ubiquitous degradation (Figure 2I, J). Thus, PAR-6 and PKC-3 play an essential role in the functioning and/or development of epidermal larval epithelia. We also noticed a small delay in growth in PAR-6::AID::GFP animals not exposed to auxin. One explanation is that TIR1 causes leaky degradation of PAR-6. However, no growth delay was observed in the absence of auxin when using ubiquitously expressed TIR1. Hence, the delayed growth may be due to other differences in genetic background. Finally, animals with ubiquitous PAR-6 or PKC-3 depletion have a more sick appearance than epidermal depleted animals, indicating that the functions of PAR-6 and PKC-3 are not limited to the epidermis. Indeed PAR-6 and PKC-3 were recently shown to be required for lumen formation in

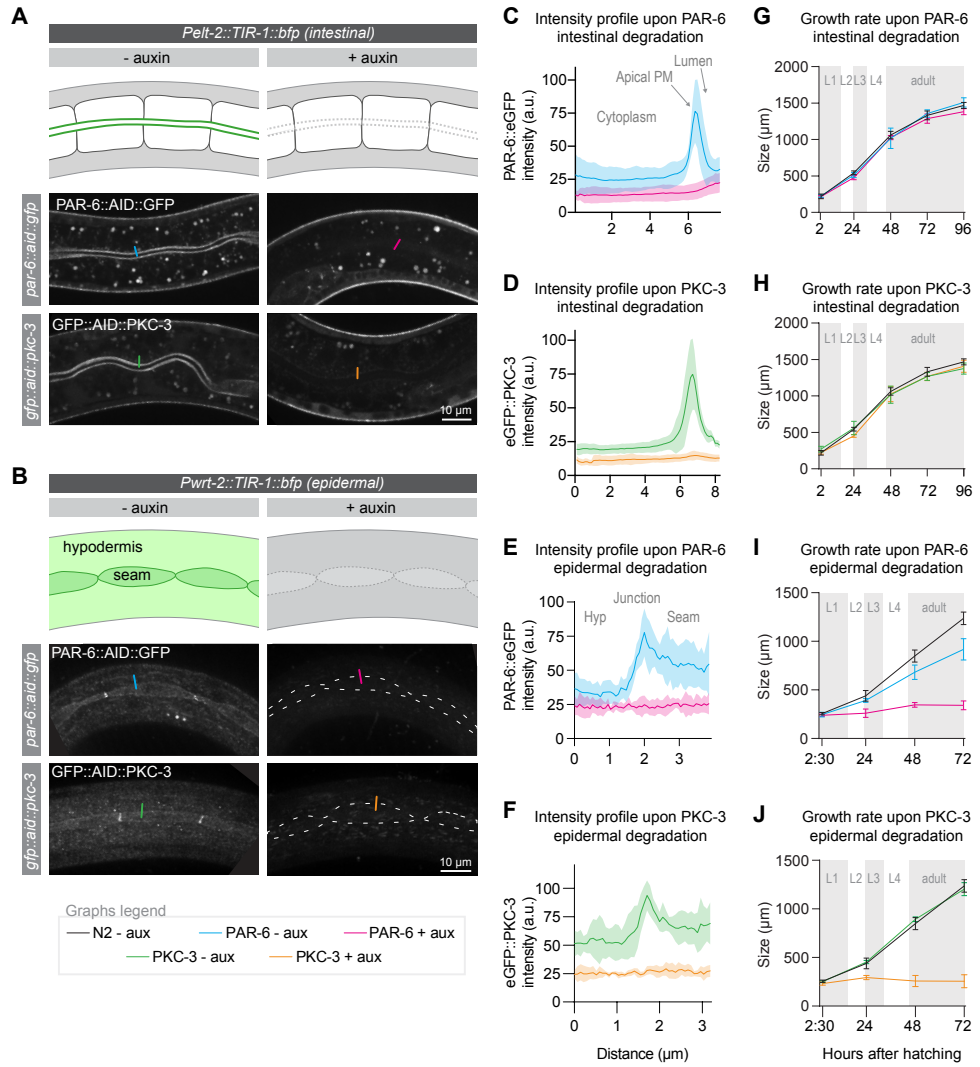

Figure 2. PAR-6 and PKC-3 are essential in the epidermis to support larval growth. **(A, B)** Distribution of PAR-6::AID::GFP and GFP::AID::PKC-3 in the intestine (A) and epidermis (B) in absence (- auxin) or presence (+ auxin) of 1 mM auxin for 1 h. Images are maximum intensity projections of the luminal domain for the intestine, and the apical domain for the epidermis. Drawings are schematic representation of the area imaged, with the localization of PAR-6 and PKC-3 indicated in green shades. Greys indicate absence of PAR-6 and PKC-3. Short colored lines indicate the area quantified in C–F. **(C–F)** Quantification of apical GFP fluorescence intensity at the intestinal lumen and the hyp7–seam cell junction in *par-6::aid::gfp* and *gfp::aid::pkc-3* animals in the absence (- aux) or presence (+ aux) of 1 mM auxin for 1 h. Solid lines and shading represent mean ± SD. For the intestine, n = 10 animals for PAR-6 - aux, PAR-6 + aux, PKC-3 - aux, and PKC-3 + aux. For the epidermis, n = 8 animals for PAR-6 - aux, 6 for

PAR-6 + aux, 5 for PKC-3 + aux, and 5 for PKC-3 - aux. **(G–J)** Growth curves of N2, *par-6::aid::gfp,* and *gfp::aid::pkc-3* animals in absence (- aux) or presence (+ aux) of 4 mM auxin from hatching. Solid lines and shading represent mean ± SD. In G and H, degradation was induced in the intestine, and in I and J in the epidermis. In the intestine, n = 13, 10, 13, 14, and 12 for N2 - aux; 7, 7, 7, 5, and 9 for PAR-6 - aux; 6, 6, 6, 5, and 7 for PAR-6 + aux; 8, 7, 8, 4, and 9 for PKC-3 - aux; and 8, 7, 8, 8, and 8 for PKC-3 + aux. In the epidermis, *n* = 6, 7, 8, and 8 for N2 - aux; 6, 5, 11, and 8 for PAR-6 - aux; 5, 10, 8, and 9 for PAR-6 + aux; 7, 7, 10, and 8 for PKC-3 - aux; and 8, 7, 12, and 13 for PKC-3 + aux.

the excretory canal using a ZF degron-based protein degradation approach (Abrams and Nance, 2020).

Cell autonomous and non-autonomous roles for PAR-6 and PKC-3 in growth, molting, seam cell divisions and seam cell morphology

To characterize the growth arrest of PAR-6 and PKC-3 depleted animals in more detail, we examined arrested animals by Nomarski differential interference contrast (DIC) microscopy. We observed incompletely released cuticles 30 hours past exposure to auxin, indicative of molting defects (Figure 3A). To examine molting progression in more detail, we used a transcriptional reporter expressing GFP from the *mlt-10* promoter (Meli et al., 2010). *mlt-10* expression cycles, increasing during molting and decreasing during the inter-molt. Upon epidermal degradation of PAR-6 from hatching, *mlt-10* driven GFP levels remained low (Figure 3B, C), indicating that these animals fail to go through the L1/L2 molt.

To determine if the growth arrest and molting defects reflect a complete developmental arrest, we next examined the effects of PAR-6 depletion on the stereotypical division pattern of the seam cells. In every larval stage, an asymmetric cell division creates a new seam cell daughter and a cell that differentiates to form neurons or fuse with hyp7 (Chisholm and Hsiao, 2012) (Figure 3E, blue shaded lineage tree). In the second larval stage, a symmetric division precedes the asymmetric division to double the number of seam cells. Depletion of PAR-6 from hatching did not disrupt the L1 asymmetric divisions, indicating that these animals are not developmentally arrested. As an additional marker of L1 development, we followed outgrowth of the excretory canals. During L1 development, both the anterior and posterior canals elongate from their initial positions at hatching to their final positions near the head and tail (Figure 3 —figure supplement 1A) (Buechner et al., 2020). Canal elongation still took place in PAR-6 depleted animals, with only a minor reduction in final length of the posterior canals (Figure 3 —figure supplement 1B). Thus, PAR-6 depleted animals appear to continue the L1 developmental program, despite the lack of growth.

In contrast to L1 seam cell divisions, the divisions that normally take

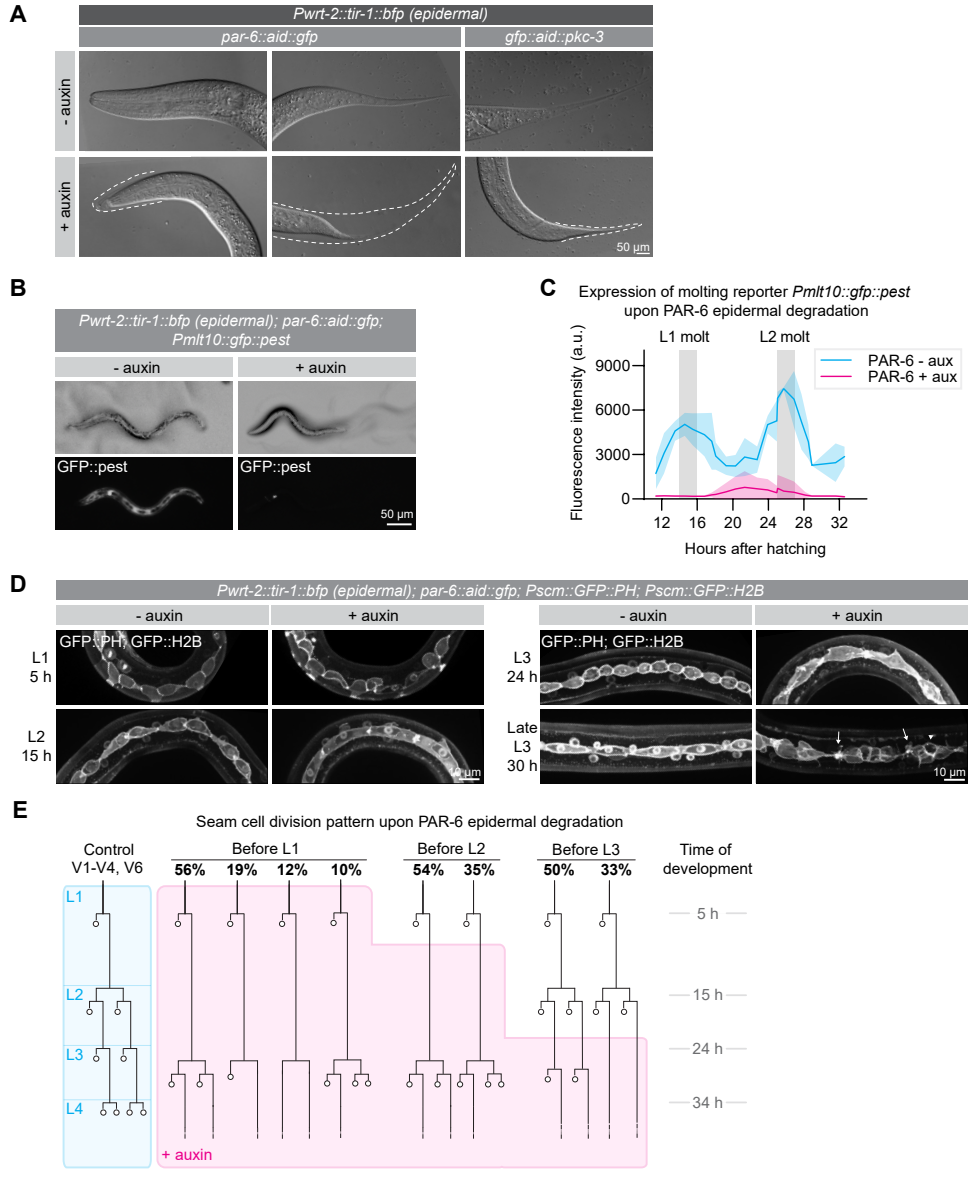

Figure 3. PAR-6 and PKC-3 are required in the epidermis for molting and seam cell development. (A) DIC microscopy images of molting defects upon epidermal depletion of PAR-6 or PKC-3. Animals were grown in absence (-auxin) or presence (+auxin) of 1 mM auxin from hatching, and images were taken 30 h after hatching. Dotted lines outline detached but unreleased cuticle in the pharynx and in the tail. Defects are observed in ~50% of the animals. Images are stitched montages. **(B)** Expression of the molting reporter *Pmlt-10::gfp::pest* in *par-6::aid::gfp* animals in the absence (- auxin) or presence (+ auxin) of 1 mM auxin from hatching. Images were taken at 22 h of post-embryonic development. **(C)** Quantification of *Pmlt-10::gfp::pest* expression

from 11 h to 32 h of post-embryonic development (mean fluorescence intensity ± SD) in *par-6::aid::gfp* animals in absence (- aux) or presence from hatching (+ aux) of 1 mM auxin from hatching. Measurements were done every hour. Each data point is an average of 3–12 measurements, with an average of 8 measurements per data point. **(D)** Examples of seam cell division and morphology defects observed upon depletion of PAR-6::GFP::AID from hatching. Seam cells are visualized by expression of nuclear H2B::GFP and membrane-bound PH::GFP markers (Wildwater et al., 2011). Arrows indicate membrane protrusions and arrowhead indicates abnormal division plane orientation. Images are maximum intensity projections. **(E)** Seam cell division pattern in *par-6::aid::gfp* animals in absence (control, blue) or presence (+ auxin, magenta) of 1 mM auxin. Auxin was added after hatching, before L2 divisions or before L3 divisions. For the control, *n* = 14, 75, 40, and 28 animals for the L1, L2, L3 and L4 divisions. For before L1, n = 17 animals for the L1 and 143 animals for the delayed L2 divisions. For before L2, n = 91 animals. For before L3, n = 40 animals.

place in the L2 stage were severely delayed (Figure 3D, E). At the time when control animals were already undergoing the L3 divisions, L2-stage divisions had still not taken place in PAR-6 depleted animals. Eventually, a next round of divisions did take place, but we observed various deviations from the normal L2 division pattern, including division failures and abnormal differentiation and fusion with hyp7. We did not observe any further divisions (Figure 3E). Following the delayed seam cell divisions, we also observed numerous morphological abnormalities such as membrane protrusions, blebs, and abnormal division plane orientation (Figure 3D). Exposure of synchronized populations to auxin starting after the L1 or L2 divisions resulted in similar defects, indicating that seam cell divisions require the functioning of PAR-6 throughout development (Figure 3E).

Expression of TIR1 under the *wrt-2* promoter results in degradation of target proteins in both the syncytial hypodermis and the seam cells. As the hypodermis is essential for molting and is involved in the control of larval growth (Chisholm and Hsiao, 2012; Chisholm and Xu, 2012; Lažetić and Fay, 2017), it is possible that the seam cell defects are a secondary consequence of defects in the hypodermis. To address this, we expressed an exogenous copy of *par-6::mCherry* lacking the degron sequence using the hypodermis-specific *dpy-7* promoter (Gilleard et al., 1997). In combination with auxin-induced depletion of PAR-6::GFP::AID by *wrt-2* driven TIR-1, this results in absence of PAR-6 only from the seam cells. Hypodermal specific expression of *par-6::mCherry* rescued the molting defects and seam cell division delay observed upon PAR-6 epidermal degradation, and partially rescued the growth arrest (Figure 3—figure supplement 1A–D). However, seam cell morphology defects and the abnormal cell division plane were not restored (Figure 3—figure supplement 1C).

To confirm that abnormalities in the hypodermis can affect seam cell divisions, we used a CRISPR-tagged NEKL-2::AID strain that arrests growth and

molting upon auxin addition (Joseph et al., 2020). Indeed, NEKL-2 depletion caused defects in the morphology of seam cells, as well as a partially penetrant reduction in seam cell divisions, confirming that abnormalities in the hypodermis can affect the seam cells (Figure 3—figure supplement 1E, F).

Taken together, our data show that PAR-6 is essential in the *C. elegans* hypodermis to support animal growth and molting. Whether the growth and molting phenotypes reflect separate functions of PAR-6, or are caused by the same underlying defect is difficult to establish, as molting is required for animal growth, but has also been reported to be governed by a size threshold (Chisholm and Hsiao, 2012; Lažetić and Fay, 2017; Uppaluri and Brangwynne, 2015). The seam cell division timing defects we observed appear to be a secondary consequence of hypodermal or molting defects. However, the fact that the growth arrest and seam abnormalities were not fully rescued by expression of PAR-6 in the hypodermis may indicate cell autonomous roles for PAR-6 in the seam, or alternatively that the *Pdpy-7::par-6::mCherry* rescue construct is not fully functional.

PAR-6 and PKC-3 mediate apical LGL-1 exclusion and promote junction integrity in the larval epidermis

As one of the major functions of the apical PAR complex is to mediate the exclusion of basolateral proteins from the apical domain, we next examined the effects of PKC-3 depletion on two key aPKC target genes: LGL-1/Lgl and PAR-1. Both proteins are direct aPKC targets in epithelia, and in the *C. elegans* zygote their anterior exclusion is mediated by PKC-3 (Beatty et al., 2010; Betschinger et al., 2003; Doerflinger et al., 2010; Hoege et al., 2010; Hurov et al., 2004; Motegi et al., 2011; Plant et al., 2003; Ramanujam et al., 2018; Yamanaka et al., 2003). For these experiments we made use of integrated LGL-1::GFP transgene (Waaijers et al., 2015) and an endogenously tagged PAR-1::GFP fusion.

Depletion of PKC-3 in the intestine did not result in apical invasion of LGL-1 (Figure 4—figure supplement 1A). In contrast, degradation of PKC-3 in the epidermis resulted in clear apical LGL-1 localization in the seam cells within 6 hours of auxin addition (Figure 4A, B). Degradation of PKC-3 in the epidermis did not result in apical PAR-1 localization (Figure 4C, D). Instead, prolonged depletion of PKC-3 for 24h resulted in fragmentation of the normally contiguous PAR-1 signal at cell junctions, which may reflect an indirect effect of PKC-3 on junction organization (Figure 4C). These results demonstrate that PKC-3 is necessary to maintain the basolateral localization of LGL-1 in the seam cells, but not the intestine. In contrast, the apical exclusion of PAR-1 is not solely mediated by aPKC.

In embryonic epithelia, PAR-6 and PKC-3 are essential for proper junction formation, with loss of either protein resulting in fragmented cell junc-

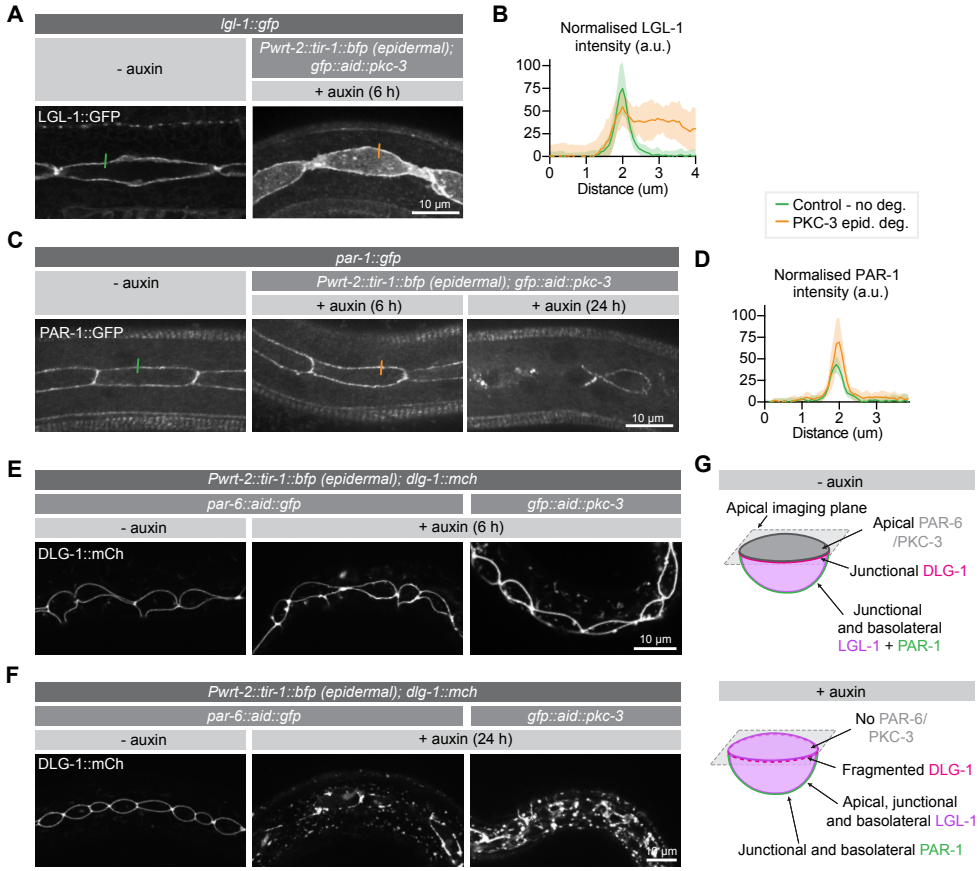

Figure 4. PKC-3 excludes LGL-1 from the apical cortex and, together with PAR-6, regulates junctions. (A, B) Distribution and quantification of LGL-1::GFP in the epidermis of *lgl-1::gfp* animals without auxin and in *lgl-1::gfp; gfp::aid::pkc-3; Pwrt-2::tir-1::bfp* animals in the presence of 4mM auxin for 6 hours. Images are maximum intensity projections of the apical domain. Quantifications shows mean apical GFP fluorescence intensity ± SD at the hyp7–seam cell junction, normalized to background intensity of each animal measured in the hypodermis. n = 7 animals for both conditions. Short colored lines in A indicate the area quantified in B. **(C, D)** Distribution and quantification of PAR-1::GFP in the epidermis in *par-1::gfp* animals without auxin and in *par-1::gfp; gfp::aid::pkc-3; Pwrt-2::tir-1::bfp* animals in the presence of 4mM auxin for 6 or 24 hours. Images are maximum intensity projections of the apical domain. Quantifications show mean apical GFP fluorescence intensity ± SD at the hyp7–seam cell junction, normalized to the background intensity of each animal measured in the hypodermis. n = 6 animals for both conditions. Short colored lines in C indicate the area quantified in D. **(E, F)** Junction organization visualized by DLG-1::mCherry expression in *par-6::aid::gfp* or *gfp::aid::pkc-3* animals in the absence (- auxin) or presence (+ auxin) of 1 mM auxin for 6 (E) or 24 (F) hours. Images are maximum intensity projections of the junctional domain. **(G)** Graphical representation of junctional defects in the seam cells upon PAR-6 or PKC-3 degradation.

tions (Montoyo-Rosario et al., 2020; Totong et al., 2007). To investigate the requirement for PAR-6 and PKC-3 in junction integrity in larval epithelia, we assessed the localization of an endogenous mCherry fusion of the junctional protein DLG-1/Discs large upon degradation of PAR-6 or PKC-3 from hatching. In control animals not exposed to auxin, DLG-1 displays the typical ladder-like intestinal junction pattern and forms a continuous apical belt around the seam cells (Figure 4–figure supplement 1B and 4E, F). Upon degradation of PAR-6 in the intestine, we did not observe junctional defects (Figure 4—figure supplement 1B). We also did not observe any changes to the DLG-1 localization pattern in the epidermis after 6 hours of PAR-6 or PKC-3 depletion (Figure 4E). However, after 24 h of degradation, DLG-1 no longer localized in a uniform band around the seam cells but appeared fragmented, with aggregates of bright DLG-1 interspersed with areas lacking fluorescent signal (Figure 4F). We also observed fluorescent aggregates in the hypodermis (Figure 4F). Thus, as in the embryo, PAR-6 and PKC-3 are essential for junction integrity in the epidermis. The fact that junctional defects took 24 h to develop, compared to 6 h for LGL-1 mislocalization, points to an inherent stability of cell junctions.

Finally, we investigated the localization dependencies between PAR-6 and PKC-3. Several studies demonstrated that PAR-6 and PKC-3 co-localize throughout development, and are mutually dependent on each other for their asymmetric localization (Bossinger et al., 2001; Leung et al., 1999; McMahon et al., 2001; Nance and Priess, 2002; Nance et al., 2003; Tabuse et al., 1998; Totong et al., 2007). Moreover, binding of PAR-6 to PKC-3 is required for apical localization of PAR-6, including in larval epithelia (Li et al., 2010a). Degradation of PAR-6 in the intestine resulted in the rapid loss of PKC-3 from the apical membrane domain, and degradation of PKC-3 similarly disrupted PAR-6 localization (Figure 4—figure supplement 2A, B). When we followed the apical loss of PKC-3 in the intestine over time, we observed similar dynamics of PAR-6 depletion and PKC-3 loss (Video 1). In the epidermis, the levels of PAR-6 and PKC-3 are more difficult to determine accurately, due to the low levels of expression of these proteins and the aggregation due to the mCherry reporters used. Nevertheless, depletion of PAR-6 resulted in a loss of the junctional enrichment of PKC-3, and vice versa (Figure 4—figure supplement 2C-D). These disruptions occurred rapidly, within 1 h of auxin addition. Our results thus confirm the interdependency between PAR-6 and PKC-3.

PAR-6 and PKC-3 control the organization of non-centrosomal microtubule arrays in the hypodermis

The loss of PAR-6 or PKC-3 affected several epidermal processes in which cytoskeletal elements play important roles, including molting, seam cell divisions, and maintaining proper seam cell morphology. The PAR proteins play essential roles in organizing the actomyosin cytoskeleton and microtubules in

different settings, including asymmetric cell division, neuronal differentiation, and epithelial polarization (Goldstein and Macara, 2007; Rodriguez-Boulan and Macara, 2014; St Johnston, 2018). We therefore investigated if PAR-6 degradation affects the organization of actin or microtubules in the epidermis. To assess the organization of the actin cytoskeleton we used an epidermal transgene expressing the actin-binding-domain of *vab-10* fused to *mCherry* (Gally et al., 2009). We depleted PAR-6 from hatching and examined actin organization after 24 h, when control larvae are in late L2 stage. Consistent with previous observations (Costa et al., 1997), we observed prominent circumferential actin bundles in hyp7, strong enrichment of actin along the hyp7–seam junctions, and largely anterior/posteriorly organized actin within the seam cells of control animals at this stage (Figure 5A). Upon PAR-6 depletion, actin organization appeared largely undisturbed in both the seam cells and hypodermis (Figure 5A), and actin bundles in hyp7 remained perpendicular to the seam cells (Figure 5B). These data indicate that PAR-6 does not play a major role in regulating the actin cytoskeleton in the *C. elegans* larval epidermis.

We next inspected the organization of the microtubule cytoskeleton using an endogenously GFP tagged variant of the microtubule-binding protein MAPH-1.1 (Waaijers et al., 2016). We degraded PAR-6 in the epidermis from hatching and assessed the organization of epidermal microtubule arrays. In control animals, we observed highly ordered circumferential microtubule bundles in the dorsal and ventral sections of hyp7 underlying the muscle quadrants, and a microtubule meshwork in the lateral sections of hyp7 abutting the seam cells, as previously reported (Chuang et al., 2016; Costa et al., 1997; Taffoni et al., 2020; Wang et al., 2015) (Figure 5C). In the seam cells the microtubule network was less well defined but also forms a meshwork (Figure 5C). In PAR-6 depleted animals, after 24h of development we observed a significant reduction in the density of circumferential microtubule bundles in the hypodermis (Figure 5C, D). Epidermal depletion of PKC-3 resulted in similar defects (Figure 5C, D). To understand the cause of the reduced microtubule density, we investigated microtubule dynamics using an endogenous fusion of the microtubule plus-end tracking protein EBP-2^{EB1} to GFP (Videos 2 and 3). In control animals, EB1 comets moved predominantly in a circumferential direction, consistent with the organization of microtubule bundles in the epidermis, and both comet density and growth rates matched previous reports (Figure 5 E–H) (Chuang et al., 2016; Taffoni et al., 2020; Wang et al., 2015). Already within 1 h of inducing depletion of PAR-6, we observed reduced microtubule dynamics (Figure 5E–G). The density of growing MTs was reduced by 56% (Figure 5F), and microtubule growth rate was reduced by 14% in hyp7 and by 16% in the seam cells (Figure 5G). These results suggest that the reduced density of microtubule bundles upon depletion of PAR-6 is the result of reduced growth of microtubules. We also observed a defect in the directionality of microtubule growth. While 54% of the comets in control animals travel perpendicular to

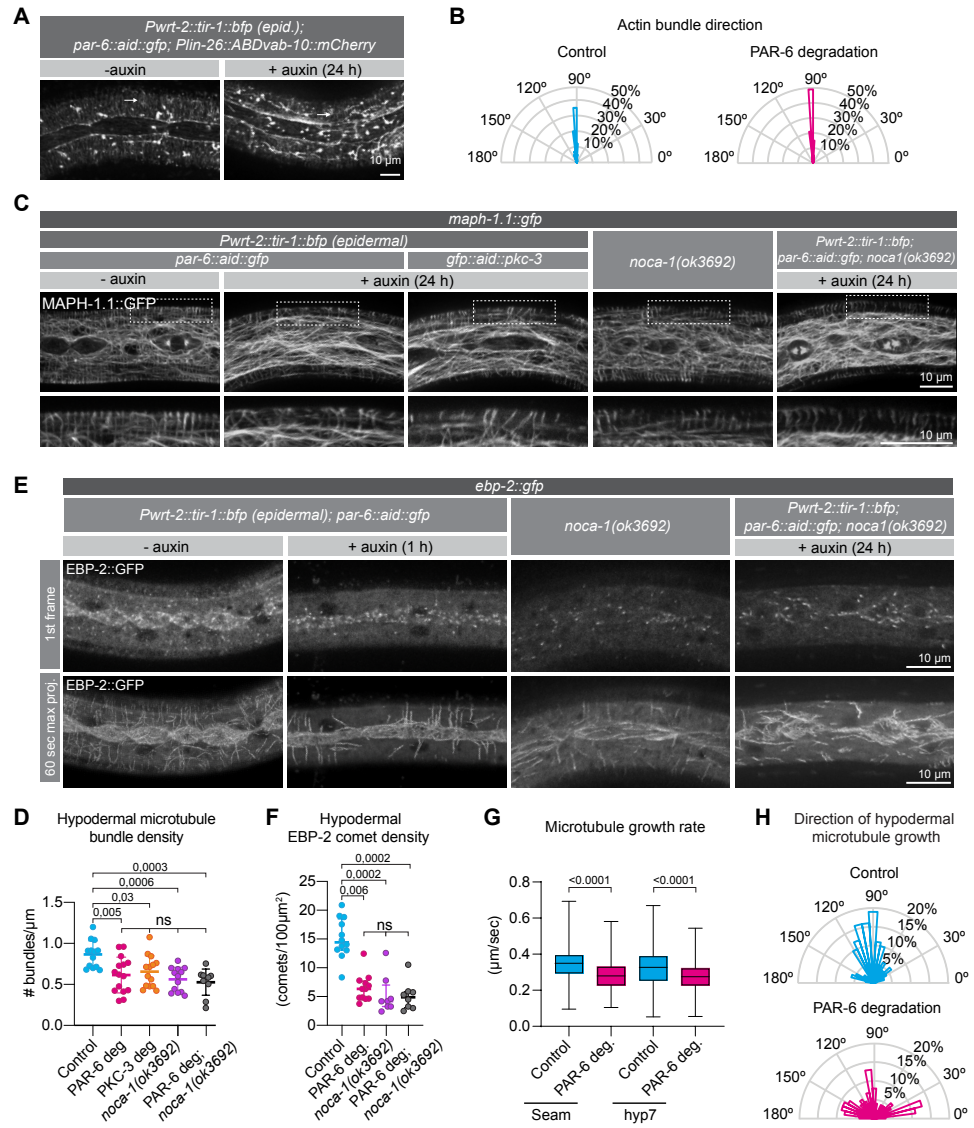

Figure 5. PAR-6 and PKC-3 control microtubule organization in the *C. elegans* epidermis. (A) Actin organization visualized by the *Plin-26::ABDvab-10::mCherry* reporter in *par-6::aid::gfp* animals in absence (- auxin) or presence (+ auxin) of 1 mM auxin for 24 hours. Images are maximum intensity projections. **(B)** Quantification of actin bundle orientation. Angle is measured relative to the anterior (180°) – posterior (0°) axis. n = 100 bundles in 5 animals per condition. **(C)** Microtubule organization of the indicated genotypes visualized by MAPH-1.1::GFP in absence (- auxin) or presence (+ auxin) of 1 mM auxin for 24 hours. Images are maximum intensity projections. **(D)** Hypodermal microtubule bundle density. n = 13 animals for control, 15 for PAR-6 deg, 14 for PKC-3 deg, 13 for *noca-1(ok3692)*, and 10 for PAR-6 deg. in *noca-1(ok3692)*. Bars show

mean ± SD. **(E)** Microtubule growth visualized by the plus end marker EBP-2::GFP in absence (- auxin) or presence (+ auxin) of 1 mM auxin for 1 h. Images are a single frame or a 60 second maximum projection (1 frame/second). To match the age of animals in (C), we depleted PAR-6 for 1 h starting with 23 h old L2 animals. **(F)** EBP-2 comet density in hyp7 in 24 h old animals. n = 12 animals for control and PAR-6 deg, 8 for *noca-1(ok3692),* and 10 for PAR-6 deg in *noca-1(ok3692)*. Auxin was present for 1 h, from 23–24 h of development. Bars show mean ± SD **(G)** Microtubule growth rate in 24 h old animals. n > 400 comets in 2 animals (seam), 4 animals (hyp7 control), or 5 animals (hyp7 + auxin). Auxin was present for 1 h, from 23–24 h of development. Bars = mean ± SD **(H)** Quantification of microtubule growth orientation in hyp7 in 24 h old animals. Auxin was present for 1 h, from 23–24 h of development. Vertical axis: left/right orientation; horizontal axis: anterior/posterior orientation. n = 150 comets. Bars = mean ± SD. Tests of significance: Tukey's multiple comparisons test for D, and Dunn's multiple comparisons test for F and G. ns = not significant.

the seam cells (70–110°), this number is reduced to 24% upon PAR-6 degradation (Figure 5H), consistent with the defects in organization observed with GFP::MAPH-1.1.

PAR-6 controls microtubule organization through its interaction partner NOCA-1/Ninein and the γ-tubulin ring complex

Two large-scale protein–protein interaction mapping studies in *C. elegans* had identified the microtubule organizing protein NOCA-1 as an interaction partner of PAR-6 (Boxem et al., 2008; Lenfant et al., 2010). Affinity purification experiments showed that PAR-6 interacts with NOCA-1 through its PDZ domain (Lenfant et al., 2010), and we were able to confirm the PAR-6 PDZ interaction with NOCA-1 by yeast two-hybrid (Figure 6—figure supplement 1). NOCA-1 functions together with γ-tubulin to assemble non-centrosomal microtubule arrays in multiple tissues, including the epidermis, and is thought to be a functional homolog of the vertebrate microtubule organizer Ninein (Green et al., 2011; Wang et al., 2015). NOCA-1 localizes to the apical cortex in seam cells, similar to the localization of PAR-6 (Figs 1G, 6A), but the mechanisms that mediate apical localization of NOCA-1 are currently not known. The physical interaction between PAR-6 and NOCA-1 prompted us to investigate if PAR-6 regulates non-centrosomal microtubule arrays through NOCA-1.

We first examined the effect of epidermal PAR-6 depletion on the localization of NOCA-1. To visualize NOCA-1 we made use of an existing transgenic line that expresses the epidermis specific NOCA-1d and e isoforms fused to GFP from their endogenous promoter (Wang et al., 2015). In untreated control animals, we observed punctate localization of NOCA-1 in the epidermis, mostly clustered at the seam–seam and seam–hyp7 junctions, as previously observed (Figure 6A) (Wang et al., 2015). Addition of auxin to induce epidermal PAR-6 degradation led to a 61% reduction in junctional levels of NOCA-1

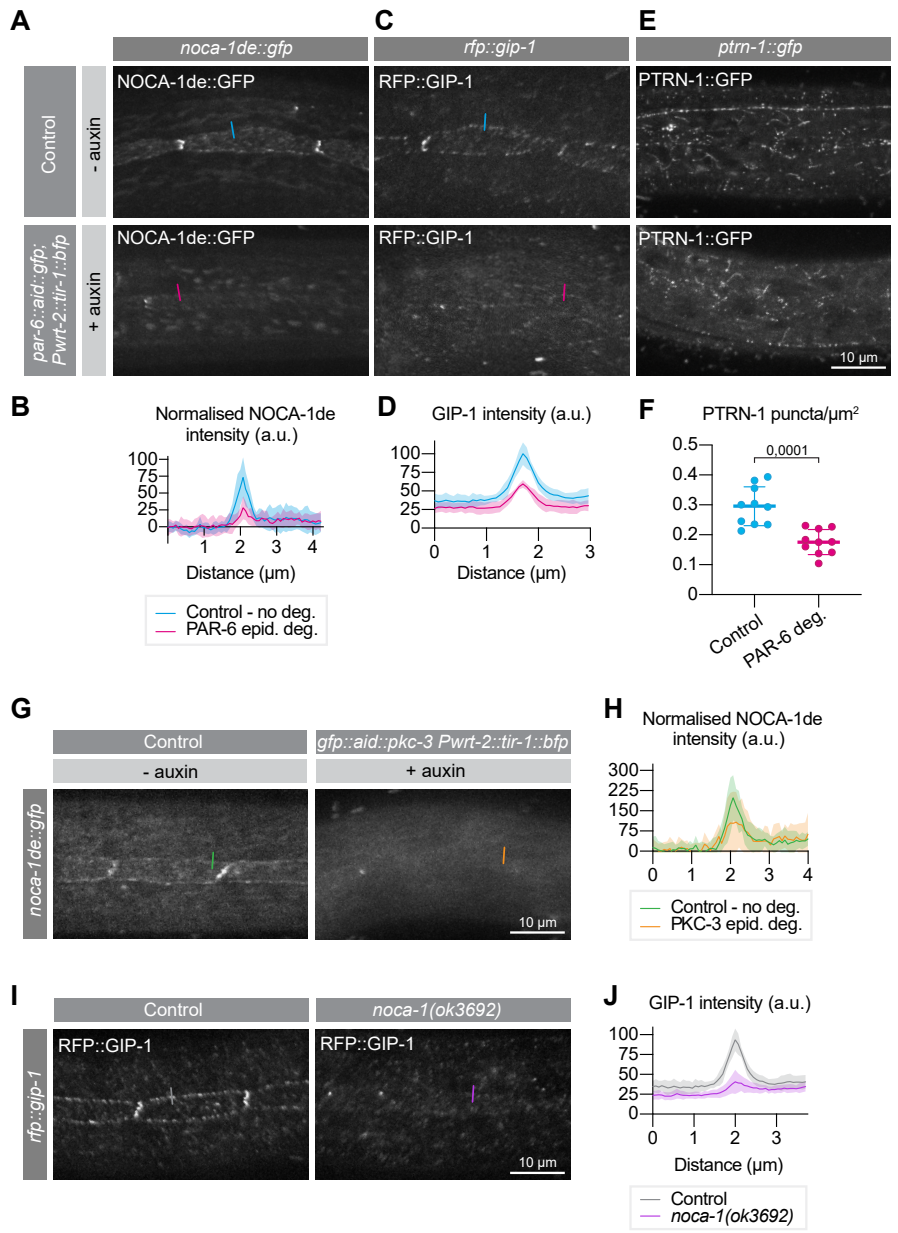

Figure 6. PAR-6 promotes the localization of its binding partner NOCA-1, as well as of GIP-1 and PTRN-1. (A, B) Distribution and quantification of NOCA-1de::GFP in the epidermis of *noca-1de::gfp* animals without auxin, and *noca-1de::gfp; par-6::aid::gfp; Pwrt-2::tir-1::bfp* animals in the presence of 4mM auxin for 6 hours. n = 9 animals for Control, and 10 for PAR-6 epid. deg. Short colored lines in A indicate the area quantified in B. **(C, D)** Distribution and quantification of GIP-1::RFP in the epidermis of *gip-1::rfp* animals without auxin, and *gip-1::rfp; par-6::aid::gfp; Pwrt-2::tir-1::bfp* animals in the presence of 4mM auxin for 6 hours. n = 6 for Control and 6 for PAR-6

epid. deg. Short colored lines in C indicate the area quantified in D. **(E, F)** Distribution and quantification of PTRN-1::GFP in the hyp7 and seam cells of *ptrn-1::gfp* animals without auxin, and *ptrn-1::gfp; par-6::aid::gfp; Pwrt-2::tir-1::bfp* animals in the presence of 4mM auxin for 6 hours. n = 10 for Control and 10 for PAR-6 deg. Short colored lines in E indicate the area quantified in F. **(G, H)** NOCA-1de::GFP in the epidermis of *noca-1de::gfp* animals without auxin, and *noca-1de::gfp; gfp::aid::pkc-3; Pwrt-2::tir-1::bfp* animals in the presence of 4mM auxin for 6 hours. n = 10 for Control and 10 for PKC-3 epid. deg. Short colored lines in G indicate the area quantified in H. **(I, J)** Distribution and quantification of GIP-1::RFP in the epidermis of *gip-1::rfp* animals and *gip-1::rfp; noca-1(ok3692)*. n = 6 for Control and 6 for *noca-1(ok3692)*. Short colored lines in I indicate the area quantified in J. All images are maximum intensity projections of the apical domain. Quantifications in B, D, H and J show mean apical GFP fluorescence intensity ± SD at the hyp7-seam cell junction (indicated by colored lines), normalized to background intensity of each animal measured in the hypodermis. Quantification in F shows mean PTRN-1::GFP puncta density ± SD. Tests of significance: unpaired t-test for F.

within 6 hours (Figure 6A, B). Depletion of PKC-3 resulted in a similar reduction in NOCA-1, (Figure 6G, H). These results demonstrate that PAR-6 and PKC-3 promote the apical localization of NOCA-1. Because of the physical interaction between PAR-6 and NOCA-1, we hypothesize that the loss of PKC-3 indirectly affects NOCA-1 through loss of PAR-6 localization.

NOCA-1 was reported to work together with γ-tubulin and redundantly with Patronin/PTRN-1 in controlling circumferential microtubule bundle organization in the hypodermis (Wang et al., 2015). We therefore examined the effect of PAR-6 depletion on the localization of PTRN-1 and GIP-1, a core component of the γ-tubulin ring complex (γ-TuRC) required to localize other γ-TuRC components to the apical non-centrosomal microtubule organizing center (ncMTOC) in the embryonic intestine (Sallee et al., 2018). To visualize PTRN-1 and GIP-1 we used endogenous PTRN-1::GFP and RFP::GIP-1 fusion proteins. GIP-1 localized in a punctate pattern at the seam–seam and seam–hyp7 junctions, similar to NOCA-1 (Figure 6C) (Sallee et al., 2018; Wang et al., 2015). PTRN-1 also localized in a punctate pattern, but dispersed through the epidermis and lacking the junctional enrichment seen for NOCA-1 and GIP-1 (Figure 6E) (Wang et al., 2015). Upon PAR-6 degradation, junctional GIP-1 levels were strongly reduced (Figure 6C, D), similarly to NOCA-1. We also observed that PAR-6 depletion resulted in a decrease in the number of PTRN-1 puncta in the epidermis (Figure 6E, F). As NOCA-1 is a direct interaction partner of PAR-6, we examined if the loss of GIP-1 is due to the loss of NOCA-1 localization. Indeed, in a *noca-1(ok3692)* deletion mutation GIP-1 levels were significantly reduced (Figure 6I, J), suggesting that NOCA-1 acts upstream of GIP-1 in the *C. elegans* larval epidermis.

Finally, we examined if the failure to properly localize NOCA-1 could explain the microtubule defects we observed upon PAR-6 depletion. We determined microtubule bundle density, EB1 comet density, and microtubule growth rate in *noca-1(ok3692)* animals. In the *noca-1(ok3692)* deletion mutant, we observed a significant reduction in the density of circumferential microtubule bundles in the hypodermis (Figure 5C, D). As reported in a previous study (Wang et al., 2015), we also observed reduced microtubule dynamics, with the density of growing MTs reduced by 65%, and microtubule growth rates reduced by 65 % (Figure 5E, G). These values are all very similar to those we observed upon PAR-6 depletion. To further determine if *par-6* and *noca-1* act in a linear pathway, we degraded PAR-6 in *noca-1(ok3692)* mutant animals. Both microtubule bundle density and microtubule dynamics were reduced to a similar extent as in PAR-6 depleted or *noca-1* mutant animals alone (Figure 5C–F). These data are consistent with a model in which the microtubule defects caused by PAR-6 depletion are a result of the requirement of PAR-6 in localizing NOCA-1. The effects on PTRN-1 may be a secondary consequence of microtubule defects caused by NOCA-1 loss.

Discussion

Par6 and aPKC are essential for apical–basal polarization across animal species. Most studies of the apical PAR proteins in *C. elegans* have focused on embryonic tissues, and their roles during postembryonic development remain unclear. Here, we used inducible protein degradation to identify essential roles for PAR-6 and PKC-3 in larval development. The depletion of PAR-6 or PKC-3 caused several developmental defects. When depleted from hatching, the first abnormality we observed is a severe growth defect, with animals barely increasing in length beyond their size at hatching. Surprisingly, the growth arrest is not the result of a complete developmental arrest, as the L1-stage seam cell divisions take place at their normal time of development and the posterior exretory canal undergo normal L1 elongation. The next developmental defect to become apparent was the failure to complete the L1/L2 molt, indicated by incompletely released cuticles and the lack of expression of the molting marker *Pmlt-10::gfp::pest*. Both the growth defect and molting defect were rescued by expressing a non-degradable copy of PAR-6 in the hypodermis, demonstrating that PAR-6 plays an essential role in this cell type required for organismal growth and molting. Determining the cause or causes underlying the molting and growth defects will require further study. Following the L1/L2 molt we observed severe defects in the normally stereotypical pattern of seam cell divisions, including a long delay before the next round of cell divisions. However, these defects are likely in large part a secondary consequence of the growth and molting defect, as expression of PAR-6 in the hypodermis was sufficient to restore the timing of divisions, and inducing growth and molting defects by degradation of NEKL-2 similarly induced seam-cell division defects.

In addition to these developmental defects we found that PAR-6 reg-

ulates the assembly of microtubule bundles through its interaction partner NOCA-1/Ninein. Already within 1 h of inducing PAR-6 degradation, we observed reduced numbers of growing microtubules. This makes it unlikely that the microtubule defects are a secondary consequence of the growth or molting defects. Vice versa, a *noca-1* mutant displaying very similar microtubule defects does not display the developmental defects observed upon PAR-6 depletion. Hence, the microtubule defects are most likely independent of the growth and molting defects. The finding that depletion of PAR-6 or PKC-3 causes multiple defects likely reflects the versatility of the PAR polarity in coordinating polarity with other cellular pathways.

An essential role in postembryonic development for PAR-6 or PKC-3 has not been described. Depletion of *par-6, pkc-3,* or *par-3* by RNAi in larval stages caused defects in polarization of spermathecal cells and in ovulation, but not in larval development (Aono et al., 2004). Similar results were recently observed using a temperature sensitive *pkc-3* allele grown at non-permissive temperature (Montoyo-Rosario et al., 2020). More severe phenotypes were observed in hatching progeny (escapers) of *par-6, pkc-3,* or *par-3* RNAi-treated mothers, which showed partially penetrant defects in outgrowth of vulval precursor and seam cells, migrations of neuroblasts and axons, and the development of the somatic gonad (Welchman et al., 2007). The lack of a growth arrest phenotype in these studies presumably reflects incomplete gene inactivation.

Auxin-inducible protein depletion of PAR proteins

The auxin-inducible degradation approach allowed us to bypass embryonic requirements and examine the roles of PAR-6, PKC-3, and PAR-3 in specific epithelial tissues during larval development. Despite these advantages, one drawback of all protein degradation approaches is that it remains difficult to draw conclusions from negative results. Although we tagged all known PAR-3 protein isoforms and observed efficient protein depletion, ubiquitous depletion of PAR-3 did not cause obvious defects in larvae. Thus, PAR-3 may not be essential in larval tissues, and the L1 lethality previously observed for the *par-3(tm2010)* null allele (Achilleos et al., 2010; Li et al., 2010b) may be the consequence of defects in embryonic development. In support of this interpretation, PAR-3 was recently found to be largely dispensable for lumen extension of the excretory canals, in contrast to PAR-6 and PKC-3 (Abrams and Nance, 2020). Nevertheless, it is possible that very low levels of PAR-3 are sufficient for its functioning, or that unpredicted splicing events cause the expression of non-degron tagged PAR-3 isoforms. One approach to counteract the latter possibility would be to replace the endogenous gene with a re-engineered copy that is unlikely to express alternative splice variants, e.g. by replacing natural introns with artificial ones and removing internal promoters. However, removing this level of regulation and expressing only one isoform may affect the functioning of *par-3* and cause unintended side effects. We also did not

detect phenotypes upon depletion of PAR-6 or PKC-3 in the larval intestine. Similar caveats as for PAR-3 depletion apply here, though PAR-6 depletion did lead to complete loss of PKC-3 from the apical domain, and epidermal depletion caused severe phenotypes. These observations make it less likely that the lack of a phenotype is due to the expression of unknown isoforms. PAR-6 and PKC-3 are likely to play non-essential or redundant roles in the intestine, as a previous study found that PAR-6 contributes to endosome positioning in this tissue (Winter et al., 2012).

Another advantage of inducible protein degradation is that the time it takes for defects to appear can give information on the role of the targeted protein in a particular process or structure. Processes highly dependent on the degraded protein likely show defects sooner after auxin addition than processes in which low levels of the protein suffice. Similarly, the speed at which molecular assemblies display defects will depend on whether the targeted protein is a core component of the assembly, or only required for its initial formation. For example, upon depletion of PAR-6, we observed defects in microtubule growth within 1 h using a plus-end-binding marker, while defects in circumferential microtubule bundles visualized with a microtubule-binding protein took ~24 h to become apparent. This indicates that PAR-6 regulates the formation of new microtubules but is not essential for the maintenance of already existing microtubule bundles. Similarly, junctional defects in the epidermis appeared ~24 after PAR-6 or PKC-3 depletion started, indicating that PAR-6 and PKC-3 are important for the assembly of new junctions, but are not integral components.

Roles of PAR-6 and PKC-3 in junction formation and cell polarity

Depletion of PAR-6 and PKC-3 in the epidermis resulted in a fragmented appearance of the hyp7–seam and seam–seam junctions (Fig. 4E, F), similar to previous observations in embryonic epithelia (Montoyo-Rosario et al., 2020; Totong et al., 2007; Von Stetina and Mango, 2015; Von Stetina et al., 2017). Localization of PAR-6 and PKC-3 were mutually dependent in both the epidermis and intestine. This result was not surprising, as Par6 and aPKC act as a dimer and have been shown to be mutually dependent in other *C. elegans* tissues (Hung and Kemphues, 1999; Li et al., 2010b; Nance et al., 2003; Tabuse et al., 1998; Totong et al., 2007). We also examined if PKC-3 functions to exclude the basolateral polarity proteins PAR-1 and LGL-1 from the apical domain. In the epidermis, PKC-3 depletion caused a rapid invasion of LGL-1 in the apical domain of the seam cells, while PAR-1 remained junctional and basal. Thus PKC-3 functions to exclude LGL-1 in the seam cells. A recent study found that LGL-1 can suppress sterility of a temperature sensitive *pkc-3* allele, further indicating that the interaction between LGL-1 and PKC-3 is functionally relevant (Montoyo-Rosario et al., 2020).

In contrast to the epidermis, LGL-1 localization in the intestine remained unchanged upon PKC-3 depletion, and we observed no obvious ab-

normalities in the intestine upon PAR-6 or PKC-3 depletion. Thus, while PAR-6 and PKC-3 are essential for development of the embryonic intestine (Totong et al., 2007), they do not appear to be essential in the larval intestine. Other cellular systems, such as polarized protein trafficking, may suffice to maintain cell polarity in the absence of the apical PAR proteins (Shafaq-Zadah et al., 2012; Zhang et al., 2011; Zhang et al., 2012). An analogous situation exists in the Drosophila midgut, where integrins, but not the apical PAR proteins, are essential for polarization (Chen et al., 2018). The lack of LGL-1 mislocalization also points to the existence of possible redundancies in polarization of cortical polarity regulators, which may be uncovered through enhancer screens in PAR-6 or PKC-3 depleted backgrounds.

In embryonic epithelia, the requirements of the apical PAR proteins also vary between tissues. Intestinal and epidermal cells depleted of PAR-6 or PKC-3 using the ZF1 system still show apicobasal polarization, as evidenced by apical localization of junctional and cytoskeletal proteins (Montoyo-Rosario et al., 2020; Totong et al., 2007). However, in the arcade cells of the pharynx, most PAR-6 depleted animals show no apical enrichment of junctional or apical cytoskeletal markers (Von Stetina and Mango, 2015). These data further highlight that the requirements for PAR-6 and PKC-3 can vary between tissues.

A novel role for PAR-6 in epidermal microtubule organization

Epidermal specific depletion uncovered a novel role for PAR-6 in organizing non-centrosomal microtubule bundles. In epithelial cells, apical non-centrosomal microtubule organizing centers (ncMTOCs) assemble apical–basal microtubule arrays. ncMTOCs contain proteins and complexes involved in microtubule anchoring, microtubule stabilization, and microtubule nucleation — such as the γ-tubulin ring complex (γ-TuRC) (Sanchez and Feldman, 2017). How apical ncMTOCs are organized is not well understood, but several studies indicate an important role for apical PAR proteins in this process. In the cellularizing Drosophila embryo, aPKC is required for the transition from centrosome emanated asters to non-centrosome associated apical–basal bundles (Harris and Peifer, 2007). In the developing embryonic intestine of *C. elegans*, PAR-3 is needed for the redistribution of γ-tubulin and other microtubule regulators from the centrosomes to the apical domain of the cell (Feldman and Priess, 2012). A role for Par6 in regulating microtubule organizing centers may not be limited to epithelial ncMTOCs. For example, in several mammalian cultured cell lines Par6 is a component of centrosomes and regulates centrosomal protein composition (Dormoy et al., 2013; Kodani et al., 2010).

Epidermal depletion of PAR-6 resulted in reduced numbers of circumferential microtubule bundles, as well as a reduced microtubule growth rate and EB1 comet density. Moreover, depletion of PAR-6 led to a loss of apical NOCA-1 enrichment at seam–seam and seam–hyp7 junctions. The effects of PAR-6 depletion on microtubule organization and dynamics are very similar

to those we observed in a *noca-1* mutant, and their severity did not increase when combining PAR-6 depletion with the *noca-1* mutant. While other models are possible, these data are consistent with PAR-6 acting through NOCA-1 to control microtubule organization in the epidermis. The reduced microtubule growth rate and EB1 comet density we observed in *noca-1* mutant animals have been reported previously (Wang et al., 2015). However, no defects in circumferential microtubule bundle density were observed in that study, despite using the same *noca-1(ok3692)* allele. The observed difference may be a result of a difference in exact experimental procedure or the precise genetic background used. For example, whereas we used the microtubule-binding protein GFP::MAPH-1.1 to label microtubules, the study by Wang *et al.* used a GFP::β-tubulin fusion. However, it is not immediately clear how the markers would differentially affect microtubule density in *noca-1(ok3692)* animals, as both appear to label all microtubules, and in control animals we observe a similar microtubule density as observed by Wang *et al*.

We also found that, in the epidermis, the localization of GIP-1 is dependent on NOCA-1. The relationship between NOCA-1 and γ-TuRC components has been examined previously in two different tissues (Sallee et al., 2018; Wang et al., 2015, 1). In the germline, NOCA-1 co-localizes with γ-tubulin to non-centrosomal microtubule arrays but is not required for the localization of γ-tubulin (Wang et al., 2015). In fact, in this tissue the localization of a short NOCA-1 protein lacking isoform-specific N-terminal extensions is dependent for its localization on γ-tubulin. The longer NOCA-1h isoform, however, localizes independently of γ-tubulin, indicating the presence of multiple NOCA-1 localization signals (Wang et al., 2015). In the embryonic intestine, the localization of NOCA-1 was not altered by the depletion of GIP-1 (Sallee et al., 2018). However, microtubule organization in the intestine is regulated differently from the epidermis, as apical microtubule organization was largely normal even in *ptrn-1* mutant animals depleted of intestinal NOCA-1 and GIP-1 (Sallee et al., 2018). Thus, differential effects of γ-TuRC component loss may reflect differences in the mechanisms of microtubule regulation. Whether PAR-6 plays a role in ncMTOC assembly and microtubule organization in tissues other than the epidermis remains to be investigated.

In addition to the effects on NOCA-1 and GIP-1, PAR-6 depletion resulted in a reduced number of PTRN-1 puncta in the epidermis. PTRN-1 is a member of the Patronin/CAMSAP/Nezha family of minus end-associated proteins, which stabilize and protect uncapped microtubule minus ends (Atherton et al., 2019; Goodwin and Vale, 2010; Hendershott and Vale, 2014; Jiang et al., 2014). NOCA-1 was previously shown to act in parallel with PTRN-1 in organizing circumferential microtubule arrays in the *C. elegans* epidermis (Wang et al., 2015). The mechanistic details of the relationship between NOCA-1 and PTRN-1 have not been resolved, but their distinct localization patterns suggest that they act on distinct pools of microtubules. Our data does not reveal why

PAR-6 depletion results in a reduced number of PTRN-1 foci.

Mechanisms of larval growth arrest and molting defects

The depletion of PAR-6 or PKC-3 in the epidermis led to a rapid growth arrest and failure to molt. What causes these dramatic effects? The junctional defects we observed are unlikely to be the primary consequence of either the growth or molting defects, as effects on cell junctions appeared only after 24 h of exposure to auxin. The effects on LGL-1 were more rapid but are also not likely to explain the defects, as *lgl-1* mutants are viable (Beatty et al., 2010; Hoege et al., 2010). The effects on the microtubule cytoskeleton are likely to contribute to the growth arrest and molting defects. However, *noca-1* mutants displayed similar microtubule defects as PAR-6 depletion yet develop to adulthood. Interestingly, *noca-1; ptrn-1* double mutant animals do grow slowly and frequently die before reaching adulthood (Wang et al., 2015). Thus, the combined defects in NOCA-1 and PTRN-1 localization we observed upon PAR-6 depletion may partially explain the growth defects. The roles of PTRN-1 may not be limited to microtubule regulation, as a recent study demonstrated that PTRN-1 stimulates actin polymerization during endocytic recycling in the intestine (Gong et al., 2018, 1).

Whether and how the growth and molting defects are related is difficult to establish. The molting defect may contribute to the growth arrest, as failure to molt can cause a growth arrest (Brooks et al., 2003; Lažetić and Fay, 2017; Russel et al., 2011; Yochem et al., 1999). PAR-6 and PKC-3 could affect molting through intracellular trafficking. Molting requires the coordinated activity of the endocytic and exocytic machineries (Lažetić and Fay, 2017), and several links between cortical polarity regulators and the polarized trafficking machinery have been uncovered (Rodriguez-Boulan and Macara, 2014). In *C. elegans*, *par-3, par-6,* and *pkc-3* were all found to be required for endocytic trafficking in oocytes, and RNAi for *par-3* and *par-6* causes scattering of multiple endosome types in the intestine (Balklava et al., 2007; Winter et al., 2012). It is possible, therefore, that PAR-6 and PKC-3 regulate vesicle trafficking in molting as well. Such regulation may be indirect, through regulation of cytoskeletal components, or through more direct mechanisms remaining to be uncovered. However, the fact that animals in which PAR-6 or PKC-3 is depleted from hatching lack any cell growth, rather than arresting at the L1 molt, suggests that the molting defect is not the sole cause of the growth defect. Alternatively, the growth defect may contribute to the molting defect. Diet restricted animals that grow very slowly delay the L1–L2 molt until a certain body size is reached, suggesting that molting is subject to a size threshold (Uppaluri and Brangwynne, 2015).

In summary, our data supports that PAR-6 and PKC-3 have multiple roles in the epidermis that support larval development and molting. We have

also uncovered an important role for PAR-6 in regulating the microtubule cytoskeleton, while additional mechanisms through which PAR-6 and PKC-3 control growth and/or molting likely remain to be discovered.

Materials and Methods

C. elegans strains

All C. elegans strains used in this study are derived from the N2 Bristol strain, and are listed in the Key resources table. All strains were maintained at 20 °C on Nematode Growth Medium (NGM) plates seeded with Escherichiae coli OP50 bacteria under standard conditions (Brenner, 1974).

CRISPR/Cas9 genome engineering

All gene editing was done by homology-directed repair of CRISPR/Cas9-induced DNA double-strand breaks, using plasmid-based expression of Cas9 and sgRNAs. All edits were made in an N2 background, with the exception of 2x*(egfp::aid)::par-3*, for which *egfp::aid::par-3* was used as the starting background. All fusions were repaired using a plasmid-based template with 190–600 bp homology arms and containing a self-excising cassette (SEC) for selection (Dickinson et al., 2015). The homology arms included mutations of the sgRNA recognition sites to prevent re-cutting after repair. The *par-6::aid::egfp, par-6::mCherry, dlg-1::mCherry* and *ebp-2::egfp* vectors were cloned using Gibson assembly and vector pJJR82 (Addgene #75027) (Gibson et al., 2009; Ramalho et al., 2020) as the backbone. The *2x(egfp::aid)::par-3*, *Pwrt-2::tir-1::bfp* and *Pelt-2::tir-1::bfp* vectors were cloned using SapTrap assembly into vector pMLS257 (Addgene #73716) (Schwartz and Jorgensen, 2016), and the *egfp::aid::pkc-3* and *mCherry::pkc-3* vectors were cloned using SapTrap assembly into vector pDD379 (Addgene #91834) (Dickinson et al., 2018). The sgRNAs were expressed from a plasmid under control of a U6 promoter. To generate sgRNA vectors, antisense oligonucleotide pairs were annealed and ligated into BbsI-linearized pJJR50 (Addgene #75026) (Waaijers et al., 2016), with the exception of the *pkc-3* fusions, in which the sgRNA was incorporated into assembly vector pDD379 using SapTrap assembly. The targeted sequences can be found in Table 2. Injection mixes were prepared in MilliQ H_2O and contained 50 ng/µl *Peft-3::cas9* (Addgene ID #46168) (Friedland et al., 2013), 50–100 ng/µl *U6::sgRNA*, 50 ng/µl of repair template, with the exception of the *pkc-3* fusions, in which the sgRNA-repair-template vector was used at a concentration of 65 ng/µl. All mixes also contained 2.5 ng/µl of the co-injection pharyngeal marker *Pmyo-2::GFP* or *Pmyo-2::tdTomato* to aid in visual selection of transgenic strains. Young

adult hermaphrodites were injected in the germline using an inverted micro-injection setup (Eppendorf FemtoJet 4x mounted on a Zeiss Axio Observer A.1 equipped with an Eppendorf Transferman 4r). Candidate edited progeny were selected on plates containing 250 ng/µl of hygromycin (Dickinson et al., 2015), and correct genome editing was confirmed by Sanger sequencing (Macrogen Europe) of PCR amplicons encompassing the edited genomic region. From correctly edited strains, the hygromycin selection cassette was excised by a heat shock of L1 larvae at 34 °C for 1 h in a water bath. Correct excision was confirmed by Sanger sequencing. Sequence files of the final gene fusions in Genbank format are in Supplementary File 1.

C. elegans synchronization

In order to obtain synchronized worm populations, plates with eggs were carefully washed with M9 (0.22 M KH_2PO_4, 0.42 M Na_2HPO_4, 0.85 M NaCl, 0.001 M $MgSO_4$) buffer in order to remove larvae and adults but leave the eggs behind. Plates were washed again using M9 buffer after an hour, to collect larvae hatched within that time span.

Auxin Inducible Degradation

Auxin treatment was performed by placing synchronized populations of worms on NGP plates seeded with *E. coli* OP50 and containing 1 or 4 mM auxin. To prepare plates, auxin (Alfa Aesar A10556) was diluted into the autoclaved NGM agar medium after cooling to 60 °C prior to plate pouring. Plates were kept for a maximum of 2 weeks in the dark at 4 °C.

C. elegans growth curves

To measure growth curves, L1 animals synchronized as described above were placed on NGM plates seeded with *E. coli* OP50 and either lacking auxin or containing 4 mM auxin. Images were taken in 24 h intervals up to 96 h, using a Zeiss Axio Zoom.V16 equipped with a PlanNeoFluar Z 1x/0.25 objective and Axiocam 506 color camera, driven by Zen Pro software. Animal length was quantified in ImageJ(FIJI) software by drawing a spline along the center line of the animal (Rueden et al., 2017; Schindelin et al., 2012).

Molting assay

Synchronized L1 animals were placed on NGM plates seeded with *E. coli* OP50 and either lacking auxin or containing 1 mM auxin. Fluorescence images were taken in 1 h intervals from 11 h to 32 h of development, using a Zeiss Axio Zoom.V16 equipped with a PlanNeoFluar Z 1x/0.25 objective and Axiocam 506 color camera, driven by

Zen Pro software. Expression levels of the *Pmlt-10::gfp::pest* reporter were quantified in ImageJ(FIJI) software (see image analysis).

Microscopy

Live imaging of *C. elegans* larvae was done by mounting larvae on 5% agarose pads in a 10 mM Tetramisole solution in M9 buffer to induce paralysis. DIC imaging was performed with an upright Zeiss AxioImager Z2 microscope using a 63× 1.4 NA objective and a Zeiss AxioCam 503 monochrome camera, driven by Zeiss Zen software. Spinning disk confocal imaging was performed using a Nikon Ti-U microscope driven by MetaMorph Microscopy Automation & Image Analysis Software (Molecular Devices) and equipped with a Yokogawa CSU-X1-M1 confocal head and an Andor iXon DU-885 camera, using 60× or 100× 1.4 NA objectives. All stacks along the z-axis were obtained at 0.25 µm intervals, and all images were analyzed and processed using ImageJ(FIJI) and Adobe Photoshop. For quantifications, the same laser power and exposure times were used within experiments.

Quantitative image analysis

All image analysis was done in using ImageJ (FIJI). For intensity profile measurements of spinning disk microscopy data, background values were subtracted from the intensity measurements. Mean background intensity was quantified on a circular region in an area not containing any animals, except in quantifications in Figure 4A, 4C and 6A, where background intensity was quantified on a circular region in an area with no fluorescence inside the worm.

For the intensity profiles in the epidermis, except those of RFP::GIP-1, a 10 px-wide line was drawn in the apical focal plane, from the hyp7 cytoplasm to the seam cell cytoplasm. The position of the line was chosen to avoid fluorescent signals present in neighboring tissues, notably the intestine and excretory canal. Additionally, mCherry tagged proteins tend to aggregate, as is evident from comparison with the otherwise identical GFP tagged variants. Hence, for mCherry intensity profiles lines were positioned to avoid aggregates. The RFP::GIP-1 fusion proteins localizes in a punctate pattern. To accurately capture the average intensity of this marker protein, we drew 10 separate 20-px wide lines per cell, which covers 25–50 % of the total seam cell circumference. Intensity values were manually aligned at their peak values, and then averaged to obtain a single intensity profile per cell. For the intensity profiles in the intestine, we drew 8 separate 50 px-wide lines from the intestinal lumen to the cytoplasm of the intestinal cells, which were aligned at their peak values and averaged to obtain a single value per worm. The intensity profiles from multiple animals were manually aligned at thepeak values for analysis and display.

To quantify the fluorescence intensity for the molting assay, whole worm fluorescence was quantified. A region of interest (ROI) of each whole worm was created by drawing a freehand line around the worm using the transmitted light channel. The corresponding fluorescence of the ROI was measured in the GFP channel.

Microtubule bundles were counted manually as follows: a 5-px-wide freehand line was drawn through an ~80 µm stretch of microtubule bundles at the dorsal or ventral region of an animal, and the intensity profile was plotted. The number of fluorescent peaks was counted, and the microtubule bundle density was calculated by dividing the number of peaks by the measured distance.

EBP-2::GFP comet counting was done manually as follows: an ROI was drawn around the area of hyp7 visible in the camera field of view (corresponding to 300–500 μm^2). The entire width of hyp7 was included, from the outside of the animal up to (but excluding) the seam cells. Either the ventral or dorsal hypodermis was analyzed. Comets were counted manually within the ROI, and density was calculated by dividing the number of EBP-2::GFP comets by the surface of the area analyzed.

PTRN-1::GFP puncta counting was done manually. The entire epidermal area visible in the camera field of view was analyzed, and puncta in both the seam cells and the hypodermis were counted. Puncta density was calculated by dividing the number of PTRN-1::GFP puncta by the surface of the area analyzed.

Microtubule growth rate was calculated in an automated manner using the ImageJ plug-in 'TrackMate' (Tinevez et al., 2017). An ROI was drawn around either the seam cells or hyp7 visible in the camera field of view. For hyp7 either the ventral or dorsal area was analyzed. The following parameters were chosen: estimated blob diameter = 0.700 um; threshold = 200,000; simple LAP tracker; linking max distance = 1.5 um; gap-closing max distance = 1.5 um; gap-closing max frame gap = 3; duration of track = 10. The mean speed of the comets was averaged to obtain the average microtubule growth rate. Comets in both the seam cells and the hypodermis were measured and represented separately.

To determine the directionality of the actin bundles and microtubule growth, images or movies were rotated to orient the seam cells horizontally. Lines were drawn along the microtubule or actin bundles, and the angle of these lines was calculated relative to the horizontal axis. Per animal, an area containing 20 actin bundles or 30 microtubule bundles was analyzed (all bundles in the area were analyzed). Movies of EBP-2 were used to calculate the directionality of microtubule growth, where the direction of growth of individual comets was annotated manually. Maximum intensity projections of EBP-2 movies were used to calculate the directionality of microtubule growth. Rose plots were generated using MatLAB.

Relative excretory canal outgrowth

To quantify relative canal outgrowth in the excretory canal cell, synchronized animals were placed on NGM plates seeded with *E. coli* OP50 and either lacking auxin or containing 4 mM auxin. Animals were placed on plates immediately after hatching. The distance between the cell body and either the anterior distal body tip or the anus was determined by tracing a segmented line along the center of the animal. The length of each individual canal was measured with a segmented line from the anterior-posterior bifurcation points close to the cell body until the canal tip. Relative outgrowth was calculated as the fraction of canal length over the distance between the cell body and the anterior distal tip or the anus.

Seam lineage analysis

To generate the seam cell lineage, synchronized animals were placed on NGM plates seeded with *E. coli* OP50 and either lacking auxin or containing 1 mM auxin. Animals were placed on plates immediately after hatching (before L1 degradation), at 7 h of development (before L2 degradation) or at 19 h of development (before L3 degradation). At 1 h intervals, 5–10 animals were randomly picked and transferred to a microcopy slide. The number of seam cells and hyp7 nuclei were determined manually based on expression of the dual color marker *ouIs10[scmp::NLS::tdTomato; dpy-7p::2xNLS::YFP;wrt-2p::GFP::PH]* that marks the seam nuclei in red and the hypodermal nuclei in green. Divisions of V5 were excluded from the analysis as V5 follows a different division pattern at the L2 stage, in which the anterior daughter becomes a neuroblast that generates a sensory structure termed the posterior deirid sensillium. V5 cells are readily recognized based on their position in the row of the seam cells, and in L2 stage additionally on their division pattern. Animals were classified according to showing a wild-type seam cell division pattern, having developmental defects such as delayed or arrested seam cell divisions, or having inappropriate seam cell differentiation. Control animals were classified at each larval stage. PAR-6 depleted animals were classified after they had undergone the delayed L2-stage divisions. From the total number of worms analyzed, the percentages of worms in each category were calculated.

PAR-6::mCherry transgenic array

The *Pdpy-7::par-6::mCherry* plasmid used for PAR-6 hypodermal rescue was cloned into the pBSK(+) vector using Gibson assembly. The promoter of *dpy7*, which is expressed in hyp7 but not in the seam cells (Gilleard et al., 1997; Myers and Greenwald, 2005), was amplified from *C. elegans* genomic DNA using primers Pdpy-7_F and Pdpy-7_R. A fragment of 5.3 kb containing the entire genomic sequence of *par-6* and a

fragment of 402 bp of the *par-6* 3′ UTR were amplified from *C. elegans* N2 genomic DNA using primers par-6_F1 and par-6_R1, and par-6_UTR_F and par-6_UTR_R, respectively. mCherry was amplified from pJJR83 (Addgene #75028) using primers mCherry_F and mCherry_R. Correct amplification and assembly were confirmed by Sanger sequencing. The plasmid generated can be found in Supplementary File 1. See Key resources table for primer sequences. To generate transgenic lines young adult hermaphrodites were injected in the germline with 30 ng/µl of *Pdpy-7::par-6::mCherry*. mCherry fluorescence was used to select stable transgenic lines.

Yeast two-hybrid analysis

Sequences encoding the PAR-6 PDZ domain and full-length NOCA-1d were PCR amplified from a mixed-stage cDNA library using primers par-6_F2 and par-6_R2, and noca-1d_F and noca-1d_R. See Key resources table for primer sequences. PCR products were digested with AscI and NotI, and cloned into Gal4-DB vector pMB28 and Gal4-AD vector pMB29, respectively (Koorman et al., 2016). The resulting plasmids were transformed into *Saccharomyces cerevisiae* strains Y8930 (MATα) and Y8800 (MAT**a**) (Yu et al., 2008) using the Te/LiAc transformation method (Schiestl and Gietz, 1989). DB::PAR-6/AD::NOCA-1 diploid yeast was generated by mating, and plated on synthetic defined (SD) medium plates lacking leucine, tryptophan, and histidine containing 2 mM 3-Amino-1,2,4-triazole (3-AT); and lacking leucine, tryptophan, and adenine to assess the presence of an interaction, and on an SD plate lacking leucine and histidine containing 1 mg/ml cycloheximide to test for self-activation by the DB::PAR-6 plasmid in the absence of the AD::NOCA-1 plasmid. Controls of known reporter activation strength and behavior on cycloheximide were also added to all plates.

Statistical analysis

All statistical analyses were performed using GraphPad Prism 8. For population comparisons, a D'Agostino & Pearson test of normality was first performed to determine if the data was sampled from a Gaussian distribution. For data drawn from a Gaussian distribution, comparisons between two populations were done using an unpaired t test, with Welch's correction if the SDs of the populations differ significantly, and comparisons between >2 populations were done using a one-way ANOVA, or a Welch's ANOVA if the SDs of the populations differ significantly. For data not drawn from a Gaussian distribution, a non-parametric test was used (Mann-Whitney for 2 populations and Kruskal-Wallis for >2 populations). ANOVA and non-parametric tests were followed up with multiple comparison tests of significance (Dunnett's, Tukey's, Dunnett's T3 or Dunn's). Tests of significance used and sample sizes are indicated in the figure legends. No statistical method was used to pre-determine sample sizes.

No samples or animals were excluded from analysis. The experiments were not randomized, and the investigators were not blinded to allocation during experiments and outcome assessment.

Key resources table

Reagent type (species) or resource	Designation	Source or reference	Additional information
Strain (C. elegans)	*BOX289*	*This paper*	*par-6(mib30[par-6::aid::egfp-loxp]) I; ieSi57[eft-3p::TIR1::mRuby::unc-54 3′UTR + Cbr-unc-119(+)] II*
Strain (C. elegans)	*BOX570*	*This paper*	*pkc-3(mib78[egfp-loxp::aid::pkc-3]) II; ieSi57[eft-3p::TIR1::mRuby::unc-54 3′UTR + Cbr-unc-119(+)] II*
Strain (C. elegans)	*BOX292*	*This paper*	*ieSi57[eft-3p::TIR1::mRuby::unc-54 3′UTR + Cbr-unc-119(+)] II; par-3(mib-68[eGFP-Lox2272::AID::par-3b+eGF-P(noIntrons)-LoxP::AID::par-3g]) III*
Strain (C. elegans)	*BOX276*	*This paper*	*par-3b(mib65[eG-FP-Lox2272::AID::par-3b]) III*
Strain (C. elegans)	*BOX667*	*This paper*	*par-3(mib68[eGFP-Lox-2272::AID::par-3b+eGFP(noIn-trons)-LoxP::AID::par-3g]) III; ieSi64 [gld-1p::TIR1::mRuby::gld-1 3′UTR + Cbr-unc-119(+)] II*
Strain (C. elegans)	*BOX409*	*This paper*	*par-6(mib30[par-6::aid::egfp-loxp]) I; mibIs49[Pwrt-2::TIR-1::tagBFP2-Lox511::tbb-2-3′UTR, IV:5014740-5014802 (cxTi10882 site)]) IV*
Strain (C. elegans)	*BOX607*	*This paper*	*pkc-3(mib78[egfp-loxp::aid::pkc-3]) II; mibIs49[Pwrt-2::TIR-1::tagBFP2-Lox511::tbb-2-3′UTR, IV:5014740-5014802 (cxTi10882 site)]) IV*
Strain (C. elegans)	*BOX444*	*This paper*	*pkc-3(mib78[egfp-loxp::aid::pkc-3]) II; mibIs48[Pelt-2::TIR-1::tagBFP2-Lox511::tbb-2-3′UTR, IV:5014740-5014802 (cxTi10882 site)]) IV*
Strain (C. elegans)	*BOX285*	*This paper*	*par-6(mib30[par-6::aid::egfp-loxp]) I; mibIs48[Pelt-2::TIR-1::tagBFP2-Lox511::tbb-2-3′UTR, IV:5014740-5014802 (cxTi10882 site)]) IV*
Strain (C. elegans)	*BOX506*	*This paper*	*par-6(mib30[par-6::aid::egfp-loxp]) I; mibIs49[Pwrt-2::TIR-1::tagBFP2-Lox511::tbb-2-3′UTR, IV:5014740-5014802 (cxTi10882 site)]) IV; dlg-1(mib23[dlg-1::mCherry-LoxP]) X; mgIs49[mlt-10::gfp-pest]*

Strain (C. elegans)	*BOX412*	*This paper*	*par-6(mib30[par-6::aid::egfp-loxp]) I; mibIs49[Pwrt-2::TIR-1::tagBFP2-Lox511::tbb-2-3′UTR, IV:5014740-5014802 (cxTi10882 site)]) IV; heIs63[Pwrt-2::GFP::PH, Pwrt-2::GF-P::H2B, Plin-48::mCherry]V*
Strain (C. elegans)	*BOX490*	*This paper*	*ouIs10[Pscm::NLS::tdToma-to(pAW584)+Pwrt2::GF-P::PH(pAW561)+Pdpy-7::2x-NLS::YFP(pAW516)] I; par-6(mib30[par-6::aid::egfp-loxp]) I; mibIs49[Pwrt-2::TIR-1::tagBFP2-Lox511::tbb-2-3′UTR, IV:5014740-5014802 (cxTi10882 site)]) IV*
Strain (C. elegans)	*BOX041*	*This paper*	*mibIs23 [lgl-1::GFP-2TEV-Avi 10ng + Pmyo-3::mCherry 10ng + lambda DNA 60ng] V*
Strain (C. elegans)	*BOX553*	*This paper*	*pkc-3(mib78[egfp-loxp::aid::pkc-3]) II; mibIs49[Pwrt-2::TIR-1::tagBFP2-Lox511::tbb-2-3′UTR, IV:5014740-5014802 (cxTi10882 site)]) IV; mibIs23 [lgl-1::GFP-2TEV-Avi 10ng + Pmyo-3::mCherry 10ng + lambda DNA 60ng] V*
Strain (C. elegans)	*BOX554*	*This paper*	*pkc-3(mib78[egfp-loxp::aid::pkc-3]) II; mibIs49[Pwrt-2::TIR-1::tagBFP2-Lox511::tbb-2-3′UTR, IV:5014740-5014802 (cxTi10882 site)]) IV; par-1(it324[par-1::gfp::par-1 exon 11a])*
Strain (C. elegans)	*BOX493*	*This paper*	*pkc-3(mib78[egfp-loxp::aid::pkc-3]) II; mibIs49[Pwrt-2::TIR-1::tagBFP2-Lox511::tbb-2-3′UTR, IV:5014740-5014802 (cxTi10882 site)]) IV; dlg-1(mib23[dlg-1::mCherry-LoxP]) X*
Strain (C. elegans)	*BOX402*	*This paper*	*par-6(mib30[par-6::aid::egfp-loxp]) I; mibIs49[Pwrt-2::TIR-1::tagBFP2-Lox511::tbb-2-3′UTR, IV:5014740-5014802 (cxTi10882 site)]) IV; dlg-1(mib23[dlg-1::mCherry-LoxP]) X*
Strain (C. elegans)	*BOX494*	*This paper*	*mcIs40 [Plin-26::ABDvab-10::mCherry + Pmyo-2::GFP]; par-6(mib30[par-6::aid::egfp-loxp]) I; mibIs49[Pwrt-2::TIR-1::tagBFP2-Lox511::tbb-2-3′UTR, IV:5014740-5014802 (cxTi10882 site)]) IV; heIs63[Pwrt-2::GFP::PH, Pwrt-2::GFP::H2B, Plin-48::mCherry] V*

Strain (C. elegans)	*BOX483*	*This paper*	*par-6(mib30[par-6::aid::egfp-loxp]) I; maph-1.1(mib12[egfp::maph-1.1]) I; mibIs49[Pwrt-2::TIR-1::tagBFP2-Lox511::tbb-2-3'UTR, IV:5014740-5014802 (cxTi10882 site)]) IV; dlg-1(mib23[dlg-1::mCherry-LoxP]) X*
Strain (C. elegans)	*BOX505*	*This paper*	*maph-1.1(mib12[egfp::maph-1.1]) I; pkc-3(mib78[egfp-loxp::aid::pkc-3]) II; mibIs49[Pwrt-2::TIR-1::tagBFP2-Lox511::tbb-2-3'UTR, IV:5014740-5014802 (cxTi10882 site)]) IV; dlg-1(mib23[dlg-1::mCherry-LoxP]) X*
Strain (C. elegans)	*BOX592*	*This paper*	*maph-1.1(mib12[egfp::maph-1.1]) I; noca-1(ok3692)V/nT1[qIs51](IV;V)*
Strain (C. elegans)	*BOX658*	*This paper*	*maph-1.1(mib12)I; par-6(mib24[par-6::egfp-loxp] I; mibIs49[Pwrt-2::TIR-1::tagBFP2-Lox511::tbb-2-3'UTR, IV:5014740-5014802 (cxTi10882 site)]) IV; noca-1(ok3692)V/nT1[qIs51](IV;V)*
Strain (C. elegans)	*BOX487*	*This paper*	*par-6(mib25[par-6::mCherry-LoxP]) I; ebp-2(he293[ebp-2::egfp]) II; mibIs49[Pwrt-2::TIR-1::tagBFP2-Lox511::tbb-2-3'UTR, IV:5014740-5014802 (cxTi10882 site)]) IV*
Strain (C. elegans)	*BOX580*	*This paper*	*ebp-2(he293[ebp-2::egfp]) II; noca-1(ok3692)V/nT1[qIs51](IV;V)*
Strain (C. elegans)	*BOX659*	*This paper*	*par-6(mib24[par-6::egfp-loxp] I; ebp-2(he293[ebp-2::egfp]) II; mibIs49[Pwrt-2::TIR-1::tagBFP2-Lox511::tbb-2-3'UTR, IV:5014740-5014802 (cxTi10882 site)]) IV; noca-1(ok3692)V/nT1[qIs51](IV;V)*
Strain (C. elegans)	*BOX567*	*This paper*	*par-6(mib30[par-6::aid::egfp-loxp]) I; ltSi540[pOD1343/pSW160; Pnoca-1de::noca-1de::sfGFP; cb-unc-119(+)]II; unc-119(ed3)III; mibIs49[Pwrt-2::TIR-1::tagBFP2-Lox511::tbb-2-3'UTR, IV:5014740-5014802 (cxTi10882 site)]) IV*
Strain (C. elegans)	*BOX355*	*This paper*	*par-6(mib30[par-6::aid::egfp-loxp]) I; ltSi540[pOD1343/pSW160; Pnoca-1de::noca-1de::sfGFP; cb-unc-119(+)]II; unc-119(ed3)III; ieSi57[eft-3p::TIR1::mRuby::unc-54 3'UTR + Cbr-unc-119(+)] II*

Strain (C. elegans)	*BOX568*	*This paper*	*par-6(mib30[par-6::aid::egfp-loxp]) I; gip-1(wow25[tagRFP-t::3xMyc::gip-1]) III; mibIs49[Pwrt-2::TIR-1::tagBFP2-Lox511::tbb-2-3'UTR, IV:5014740-5014802 (cxTi10882 site)]) IV*
Strain (C. elegans)	*BOX502*	*This paper*	*par-6(mib30[par-6::aid::egfp-loxp]) I; mibIs49[Pwrt-2::TIR-1::tagBFP2-Lox511::tbb-2-3'UTR, IV:5014740-5014802 (cxTi10882 site)]) IV; dlg-1(mib23[dlg-1::mCherry-LoxP]) X; ptrn-1(wow4[PTRN-1::GFP]) X*
Strain (C. elegans)	*BOX657*	*This paper*	*pkc-3(mib78[egfp-loxp::aid::pkc-3]) II; Pnoca-1de::noca-1de::superfolderG-FP; cb-unc-119(+)]II; unc-119(ed3) III; mibIs49[Pwrt-2::TIR-1::tagBFP2-Lox511::tbb-2-3'UTR, IV:5014740-5014802 (cxTi10882 site)]) IV*
Strain (C. elegans)	*BOX579*	*This paper*	*gip-1(wow25[tagRFP-t::3xMyc::gip-1]) III; noca-1(ok3692)V/nT1[qIs51](IV;V)*
Strain (C. elegans)	*BOX561*	*This paper*	*par-6(mib30[par-6::aid::egfp-loxp]) I; mibIs49[Pwrt-2::TIR-1::tagBFP2-Lox511::tbb-2-3'UTR, IV:5014740-5014802 (cxTi10882 site)]) IV; mibEx-221(Pdpy-7::par-6::mch)*
Strain (C. elegans)	*BOX563*	*This paper*	*par-6(mib30[par-6::aid::egfp-loxp]) I; mibIs49[Pwrt-2::TIR-1::tagBFP2-Lox511::tbb-2-3'UTR, IV:5014740-5014802 (cxTi10882 site)]) IV; heIs63[Pwrt-2::GFP::PH, Pwrt-2::GFP::H2B, Plin-48::mCherry] V; mibEx-222(Pdpy-7::par-6::mch; Pmyo-2::egfp)*
Strain (C. elegans)	*BOX608*	*This paper*	*pw27[nekl-2::aid];pwSi10[phyp7::bfp::tir-1];pw17[chc-1::GFP]; mibEx-223(Pwrt-2::mCh::H2B; Pwrt-2::mCh::PH)*
Strain (C. elegans)	*BOX447*	*This paper*	*pkc-3(mib78[egfp-loxp::aid::pkc-3]) II; mibIs48[Pelt-2::TIR-1::tagBFP2-Lox511::tbb-2-3'UTR, IV:5014740-5014802 (cxTi10882 site)]) IV; mibIs23 [lgl-1::GFP-2TEV-Avi 10ng + Pmyo-3::mCherry 10ng + lambda DNA 60ng] V*

Strain (C. elegans)	*BOX431*	*This paper*	*par-6(mib30[par-6::aid::egfp-loxp]) I; mibIs48[Pelt-2::TIR-1::tagBFP2-Lox511::tbb-2-3'UTR, IV:5014740-5014802 (cxTi10882 site)]) IV; dlg-1(mib23[dlg-1::mCherry-LoxP]) X*
Strain (C. elegans)	*BOX406*	*This paper*	*par-6(mib30[par-6::aid::egfp-loxp]) I; pkc-3(mib80[mcherry-loxp::pkc-3]) II; mibIs48[Pelt-2::TIR-1::tagBFP2-Lox511::tbb-2-3'UTR, IV:5014740-5014802 (cxTi10882 site)]) IV*
Strain (C. elegans)	*BOX653*	*This paper*	*par-6(mib24[par-6::egfp-loxp] I; pkc-3(mib78[egfp-loxp::aid::pkc-3]) II; mibIs48[Pelt-2::TIR-1::tagBFP2-Lox511::tbb-2-3'UTR, IV:5014740-5014802 (cxTi10882 site)]) IV*
Strain (C. elegans)	*BOX411*	*This paper*	*par-6(mib30[par-6::aid::egfp-loxp]) I; pkc-3(mib80[mcherry-loxp::pkc-3]) II; mibIs49[Pwrt-2::TIR-1::tagBFP2-Lox511::tbb-2-3'UTR, IV:5014740-5014802 (cxTi10882 site)]) IV*
Strain (C. elegans)	*BOX578*	*This paper*	*par-6(mib30[par-6::aid::egfp-loxp]) I; par-3(it300[par-3::mcherry]) III; mibIs49[Pwrt-2::TIR-1::tagBFP2-Lox511::tbb-2-3'UTR, IV:5014740-5014802 (cxTi10882 site)]) IV*
Strain (C. elegans)	*BOX484*	*This paper*	*par-6(mib25[par-6::mCherry-LoxP]) I; pkc-3(mib78[egfp-loxp::aid::pkc-3]) II; mibIs49[Pwrt-2::TIR-1::tagBFP2-Lox511::tbb-2-3'UTR, IV:5014740-5014802 (cxTi10882 site)]) IV*
Strain (C. elegans)	*BOX485*	*This paper*	*pkc-3(mib78[egfp-loxp::aid::pkc-3]) II; par-3(it300[par-3::mcherry]) III; mibIs49[Pwrt-2::TIR-1::tagBFP2-Lox511::tbb-2-3'UTR, IV:5014740-5014802 (cxTi10882 site)]) IV*
Strain (C. elegans)	*BOX486*	*This paper*	*par-6(mib25[par-6::mCherry-LoxP]) I; par-3(mib68[eGFP-Lox2272::AID::par-3b+eGFP(noIntrons)-LoxP::AID::par-3g]) III; mibIs49[Pwrt-2::TIR-1::tagBFP2-Lox511::tbb-2-3'UTR, IV:5014740-5014802 (cxTi10882 site)]) IV*

Strain (C. elegans)	*BOX492*	*This paper*	*pkc-3(it309[GFP::pkc-3]) II; par-3(mib68[eGFP-Lox2272::AID::par-3b+eGFP(noIntrons)-LoxP::AID::par-3g]) III; mibIs49[Pwrt-2::TIR-1::tagBFP2-Lox511::tbb-2-3'UTR, IV:5014740-5014802 (cxTi10882 site)]) IV*
Strain (C. elegans)	*AW1015*	*(Hughes et al., 2014)*	*ouIs10[Pscm::NLS::tdTomato(pAW584)+Pwrt2::GFP::PH(pAW561)+Pdpy-7::2xNLS::YFP(pAW516)] I*
Strain (C. elegans)	*BOX188*	*(Waaijers et al., 2016)*	*maph-1.1(mib12[egfp::maph-1.1]) I*
Strain (C. elegans)	*CA1200*	*CGC*	*ieSi57[eft-3p::TIR1::mRuby::unc-54 3'UTR + Cbr-unc-119(+)] II; unc-119(ed3) III*
Strain (C. elegans)	*GR1395*	*(Hayes et al., 2006)*	*mgIs49 [mlt-10::GFP-pest; ttx-1::GFP]*
Strain (C. elegans)	*JLF15*	*Jessica Feldman*	*ptrn-1(wow4[PTRN-1::GFP]) X*
Strain (C. elegans)	*JLF173*	*Jessica Feldman*	*gip-1(wow25[tagRFP-t::3xMyc::gip-1]) III*
Strain (C. elegans)	*KK1218*	*CGC*	*par-3(it300[par-3::mCherry]) III*
Strain (C. elegans)	*KK1228*	*CGC*	*pkc-3(it309[GFP::pkc-3]) II*
Strain (C. elegans)	*KK1262*	*CGC*	*par-1 (it324[par-1::gfp::par-1 exon 11a])*
Strain (C. elegans)	*ML916*	*CGC*	*mcIs40 [Plin-26::ABDvab-10::mCherry + Pmyo-2::GFP]*
Strain (C. elegans)	*OD1652*	*Karen Oegema*	*ltSi540[pOD1343/pSW160; Pnoca-1de::noca-1de::sfGFP; cb-unc-119(+)]II; unc-119(ed3)III*
Strain (C. elegans)	*RT3638*	*David Fay*	*pw27[nekl-2::aid];pwSi10[phyp7::bfp::tir-1];pw17[chc-1::GFP]*
Strain (C. elegans)	*SV1009*	*(Wildwater et al., 2011)*	*heIs63[Pwrt-2::GFP::PH, Pwrt-2::GFP::H2B, Plin-48::mCherry]V*
Strain (C. elegans)	*SV1937*	*Sander van den Heuvel*	*ebp-2(he293[ebp-2::egfp]) II*
Strain (C. elegans)	*VC2998*	*CGC*	*noca-1(ok3692)V/nT1[qIs51](IV;V)*
Strain (C. elegans)	*CA1352*		*ieSi64 [gld-1p::TIR1::mRuby::gld-1 3'UTR + Cbr-unc-119(+)] II*

Strain (C. elegans)	*STR320*	*Martin Harter-ink*	*maph-1.1(mib15[GFPKI]);hrtEx-110[Pptrn-1::ebp-2::mKate2; Pmyo-2::tdTom]*
Recombinant DNA reagent	*Plasmid: pJJR82*	*Addgene #75027*	*EGFP^SEC^3xFlag vector with ccdB markers for cloning homology arms*
Recombinant DNA reagent	*Plasmid: pJJR83*	*Addgene #75028*	*mCherry^SEC^3xFlag vector with ccdB markers for cloning homology arms*
Recombinant DNA reagent	*Plasmid: pMLS257*	*Addgene #73716*	*SapTrap destination vector for building repair template only vectors*
Recombinant DNA reagent	*Plasmid: pDD379*	*Addgene #91834*	*SapTrap destination vector for building combined sgRNA expression + repair template vectors, using the F+E sgRNA scaffold*
Recombinant DNA reagent	*Plasmid: pJJR50*	*Addgene #75026*	*U6 promoter driven flipped + extended sgRNA expression vector*
Recombinant DNA reagent	*Plasmid: Peft-3::cas9*	*Addgene #46168*	*codon optimized Cas9_SV40 NLS with intron*
Recombinant DNA reagent	*Plasmid: Pdpy-7::par-6::mCherry*	*This paper*	*Expression of PAR-6::mCherry in the hypodermis. Full sequence in Supplementary File 1*
Recombinant DNA reagent	*Plasmid: PAR-6 PDZ in pMB28*	*This paper*	*Yeast expression plasmid of PAR-6 PDZ fused to Gal4 DNA binding domain. Full sequence in Supplementary File 1*
Recombinant DNA reagent	*Plasmid: NOCA-1d in pMB29*	*This paper*	*Yeast expression plasmid of NOCA-1d fused to Gal4 activation domain. Full sequence in Supplementary File 1*
Sequence-based reagent	*par-6 sgRNA*	*gacgcaaatga-cagtgatagTGG*	*sgRNA target site. PAM site in uppercase.*
Sequence-based reagent	*pkc-3 sgRNA*	*tgggtctccgacat-cattagAGG*	*sgRNA target site. PAM site in uppercase.*
Sequence-based reagent	*par-3 sgRNA 1*	*tttcagatcgatcat-catgtCGG*	*sgRNA target site. PAM site in uppercase.*
Sequence-based reagent	*par-3 sgRNA 2*	*cacatgcataacg-gtcgtggTGG*	*sgRNA target site. PAM site in uppercase.*
Sequence-based reagent	*dlg-1 sgRNA*	*gccacgtcatt-agatgaaatTGG*	*sgRNA target site. PAM site in uppercase.*
Sequence-based reagent	*mos IV01390..5015700 sgRNA*	*agctcaatcgtg-tacttgcgTGG*	*sgRNA target site for LG IV position 5013690..5015700. PAM site in uppercase.*
Sequence-based reagent	*ebp-2 sgRNA 1*	*gcaggcaaatctg-gacgataCGG*	*sgRNA target site*
Sequence-based reagent	*ebp-2 sgRNA 2*	*tacggggatagga-taagcaaTGG*	*sgRNA target site*

Sequence-based reagent	*Pdpy-7_F*	*This paper*	*TGTAATACGACTCACTATAGGGC-GAATTGGctcattccacgatttctcgc*
Sequence-based reagent	*Pdpy-7_R*	*This paper*	*tctggaacaaaatgtaagaatattc*
Sequence-based reagent	*par-6_F1*	*This paper*	*tttaagaatattcttacattttgttccagaAT-GTCCTACAACGGCTCCTA*
Sequence-based reagent	*par-6_R1*	*This paper*	*GGCCATGTTGTCCTCCTCTCCCTTG-GACATGTCCTCTCCACTGTCCGAAT*
Sequence-based reagent	*par-6_UTR_F*	*This paper*	*CACTCCACCGGAGGAATGGAC-GAGCTCTACTGAaaaactcttttcagcca*
Sequence-based reagent	*par-6_UTR_R*	*This paper*	*TAAAGGGAACAAAAGCTGGAGCTC-CACCGCgaaataaataatttattctc*
Sequence-based reagent	*mCherry_F*	*This paper*	*TCCAAGGGAGAGGAGGACAA*
Sequence-based reagent	*mCherry_R*	*This paper*	*GTAGAGCTCGTCCATTCCTC*
Sequence-based reagent	*par-6_F2*	*This paper*	*ggaggcgcgccATGATTGTGC-CAGAAGCTCATCG*
Sequence-based reagent	*par-6_R2*	*This paper*	*ggagcggccgcTCAGGCGTTCGGT-GTTCCTTGTT*
Sequence-based reagent	*noca-1d_F*	*This paper*	*ggaggcgcgccATGAATATTTGTTGTTGT-GG*
Sequence-based reagent	*noca-1d_R*	*This paper*	*ggagcggccgcCTATTGAACTCTGCATA-CAT*

Supplementary figures

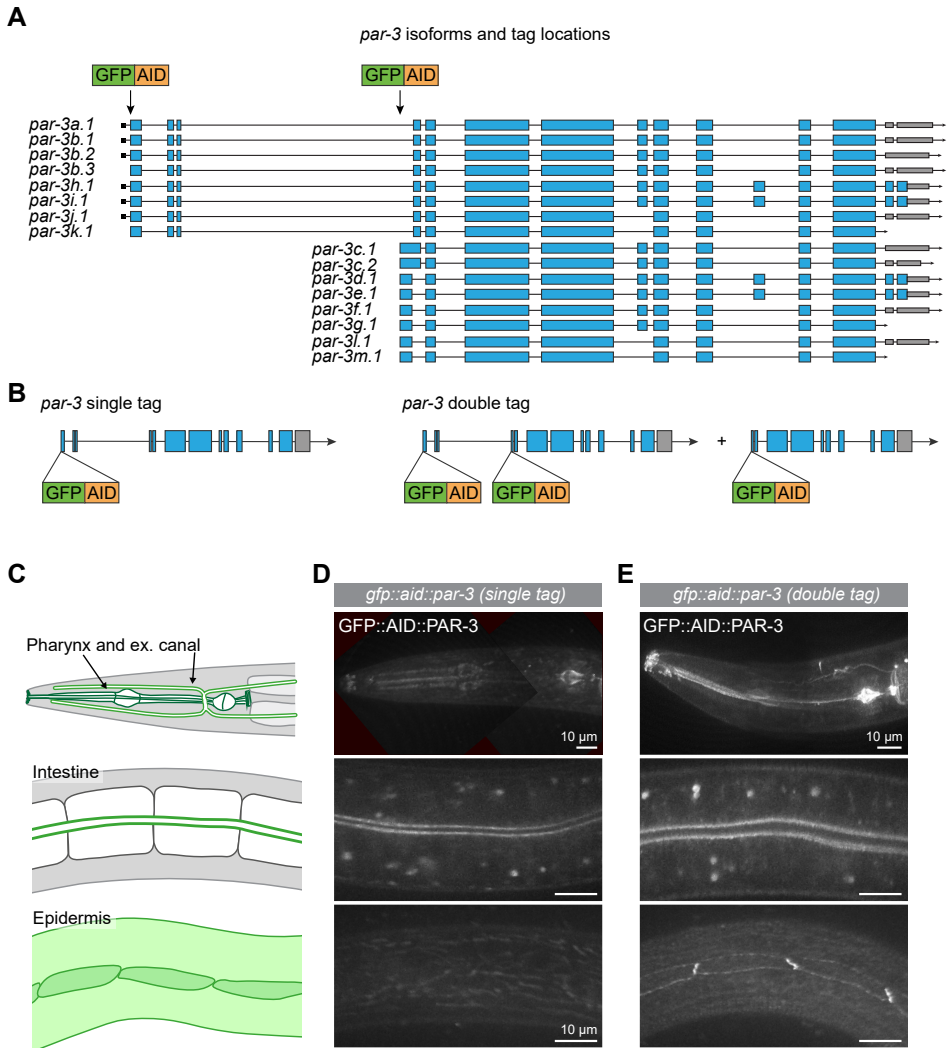

Figure 1—figure supplement 1. Isoform-specific expression pattern of PAR-3. (A, B) Schematic representation of endogenous tagging of *par-3* isoforms with sequences encoding a green fluorescent protein (GFP) and auxin-inducible degradation degron (AID) tag. **(C)** Graphical representation of larval epithelial tissues in *C. elegans*. Green indicates localization of PAR-3 (all isoforms combined). **(D)** Distribution of the long isoforms of PAR-3 tagged with GFP::AID. **(E)** Distribution of all PAR-3 isoforms tagged with GFP::AID. Images of the pharynx are stitched montages.

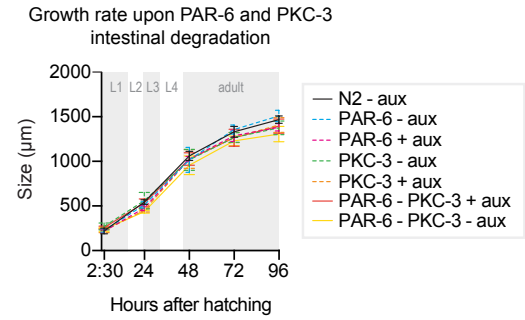

Figure 2—figure supplement 1. PKC-3 does not act redundantly with PAR-6 in the *C. elegans* intestine. Growth curves of N2, *par-6::aid::gfp, gfp::aid::pkc-3*, and *par-6::aid::gfp; gfp::aid::pkc-3* (double depletion) animals in absence (- aux) or presence (+ aux) of 4 mM auxin from hatching. Data of single PAR-6 and PKC-3 depletions (dashed lines) are repeated from Figure 1 for comparison. Data show mean ± SD. *n* = 13, 10, 13, 14, and 12 for N2 - aux; 7, 7, 7, 5, and 9 for PAR-6 - aux; 6, 6, 6, 5, and 7 for PAR-6 + aux; 8, 7, 8, 4, and 9 for PKC-3 – aux; 8, 7, 8, 8, and 8 for PKC-3 + aux; 5, 8, 6, 8, and 7 for PAR-6–PKC-3 – aux; and 11, 7, 10, 7, and 8 for PAR-6–PKC-3 + aux. Data show mean ± SD. *n* = 13, 10, 13, 14, and 12 for Control – empty vector; 8, 7, 8, 4, and 9 for PKC-3 – aux and 8, 7, 8, 8, and 8 for PKC-3 + aux.

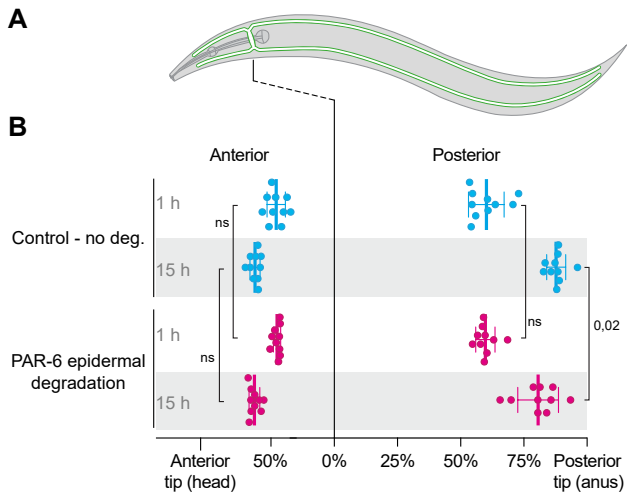

Figure 3—figure supplement 1. Effect of PAR-6 epidermal degradation on canal outgrowth. (A) Schematic drawing of the excretory canal system in an L2 animal. Green indicates localization of PAR-6. **(B)** Quantification of excretory canal outgrowth in L1 and L2 animals. One anterior and one posterior branch were measured per animal. n = 10 animals per condition. Bars represent mean ± SD. Test of significance: two-sided student's T-test. ns = not significant.

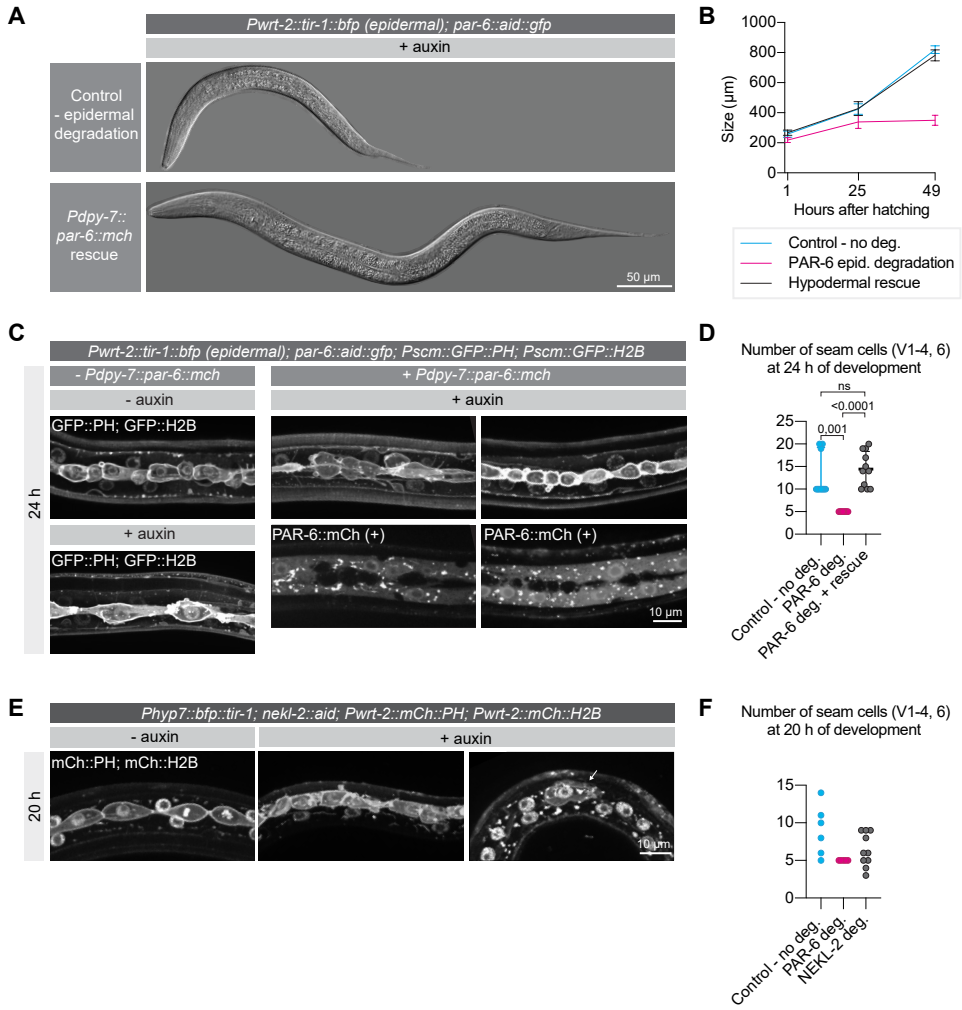

Figure 3—figure supplement 2. Hypodermal expression of PAR-6 is necessary for larval development. (A) DIC microscopy images of *par-6::aid::gfp; Pwrt-2::tir-1::bfp* animals carrying (*Pdpy-7::par-6::mCherry*) or lacking (Control) an extrachromosomal array expressing PAR-6 in the hypodermis. Worms were grown in presence (+ auxin) of 4 mM auxin from hatching. Images taken 30 h after hatching. Images are stitched montages. **(B)** Growth curves of animals treated as in (A). Lengths were measured at 1, 25, and 49 h after hatching. *n* = 5 animals per condition and data point. Data shows mean ± SD. **(C)** Seam cells visualized by nuclear H2B::GFP and membrane-bound PH::GFP at 24 h of post-embryonic development in *par-6::aid::gfp* animals carrying (*Pdpy-7::par-6::mCherry*) or lacking (Controls) an extrachromosomal array expressing PAR-6 in the hypodermis. Worms were grown in presence (+ auxin) of 4 mM auxin from hatching. Images are maximum intensity projections. **(D)** Number of seam cells (V1–4, 6) at 24 h of post-embryonic development in absence (- auxin) or presence (+ auxin) of 4 mM auxin from hatching and with or without PAR-6 hypodermal res-

cue. *n* = 10 for control, and 11 for PAR-6 deg and PAR-6 deg + rescue. Bars represent median ± interquartile range. **(E)** Seam cells visualized by nuclear H2B::mCherry and membrane-bound PH::mCherry at 20 h of post-embryonic development in *nekl-2::aid; Phyp7::bfp::tir-1* animals in absence (- aux) or presence (+ aux) of 4 mM auxin from hatching. Images are maximum intensity projections. **(F)** Number of seam cells (V1–4, 6) at 20 h of post-embryonic development in *nekl-2::aid; Phyp7::bfp::tir-1* animals in absence (Control – no deg) or presence (NEKL-2 deg.) of 4 mM auxin and in *par-6::aid::gfp; Pwrt-2::tir-1::bfp* animals in presence (PAR-6 deg.) of 4 mM auxin from hatching. *n* = 6 for Control, 5 for PAR-6 deg, and 10 for NEKL-2 deg. . Test of significance: Dunn's test of significance for D. ns = not significant.

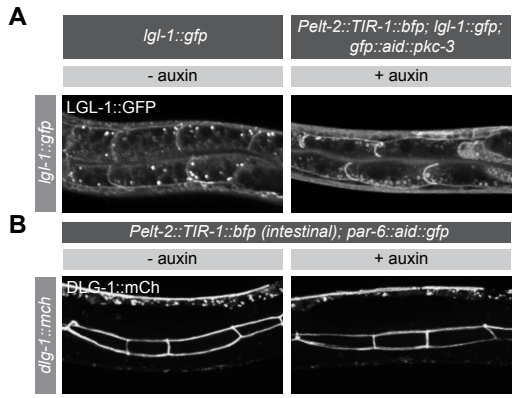

Figure 4—figure supplement 1. PAR-6 and PKC-3 are not essential for LGL-1 localization or junction maintenance in the larval intestine. (A) Distribution of LGL-1::GFP, in *lgl-1::gfp* animals without auxin and in *lgl-1::gfp; gfp::aid::pkc-3; Pelt-2::tir-1::bfp* animals in presence of 4 mM auxin from hatching. Images are maximum intensity projections covering the whole intestinal cells. **(B)** Distribution of DLG-1::mCherry in *par-6::aid::gfp; Pelt-2::tir-1::bfp* animals in absence (- auxin) or presence (+ auxin) of 4 mM auxin from hatching. Images are maximum intensity projections of the luminal domain for the intestine.

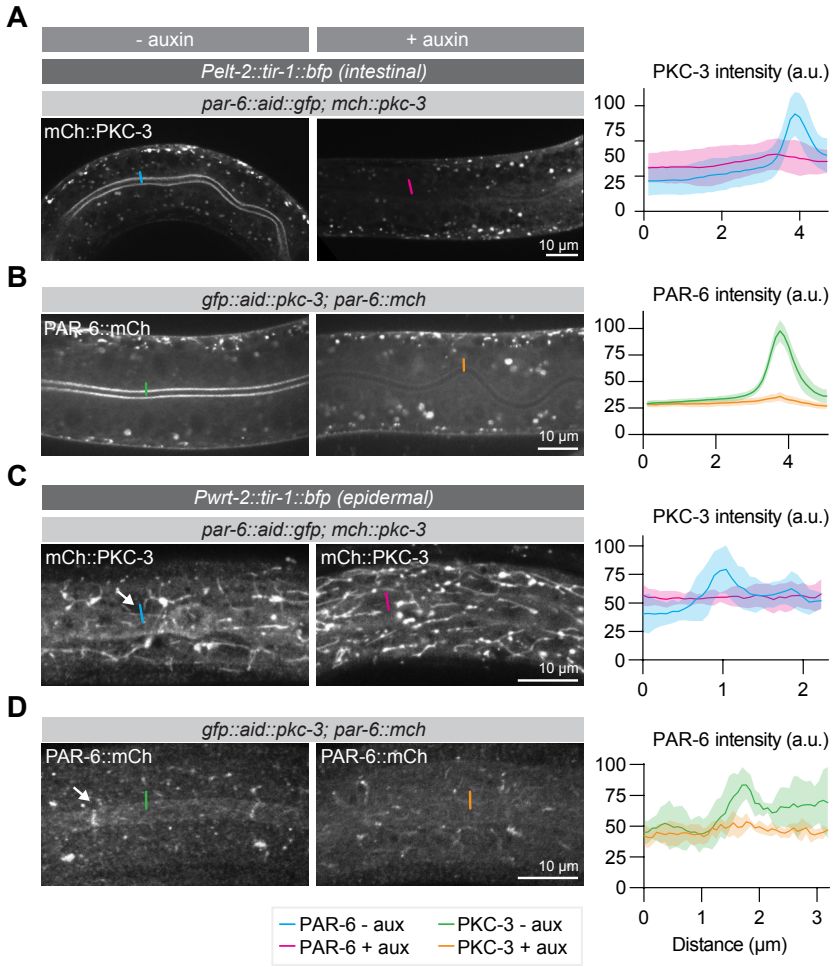

Figure 4—figure supplement 2. Localization dependencies of PAR-6 and, PKC-3. Left panels are of animals not exposed to auxin, right panels are of animals exposed to 1 mM auxin for 1 h. **(A, B)** Distribution and quantification of mCherry::PKC-3 upon intestinal depletion of PAR-6, and of PAR-6::mCherry upon instestinal depletion of PKC-3. Images are maximum intensity projections of the apical domain. **(C, D)** Distribution and quantification of mCherry::PKC-3 upon epidermal depletion of PAR-6, and of PAR-6::mCherry upon epidermal depletion of PKC-3. Images are maximum intensity projections of the apical domain from a z-stack. Short colored lines in microscopy images indicate the areas quantified in the graphs. Quantifications show mean apical GFP fluorescence intensity ± SD at the intestinal lumen (A, B) or the hyp7–seam cell junction (C, D). n = 8 animals for -aux and 4 animals for + aux in panel A, 8 animals for -aux and 4 animals for + aux in panel B, and 5 animals for both conditions in panels C and D.

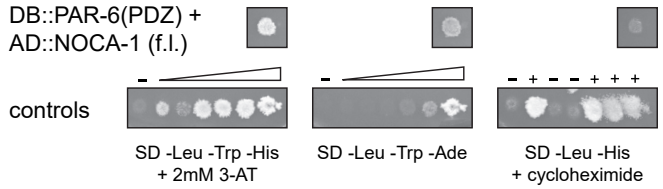

Figure 6—figure supplement 1. Interaction of PAR-6 and NOCA-1 in the yeast two hybrid system. The PAR-6 PDZ domain fused to the Gal4 DNA binding domain was co-expressed with full-length NOCA-1 fused to the Gal4 activation domain. Growth on -Leu -Trp -His + 2mM 3-AT, and on -Leu -Trp -Ade plates indicates presence of interaction. Lack of growth on -Leu -His + cycloheximide plate shows that DB::PAR-6 is not self-activating. Controls range from no reporter activation to strong reporter activation. On cycloheximide plates, (-) indicates no growth expected, and (+) indicates growth expected.

Video legends – available in the online published document

Video 1. Time-lapse imaging of PAR-6::AID::GFP and PKC-3::mCherry in animals expressing intestine-specific TIR1 upon addition of 1 mM Auxin.

Video 2. Time-lapse imaging of EBP-2::GFP in control animals and PAR-6 depleted animals. Freeze frame circles EBP-2 comets as an example of quantification. Final frames show a time projection as displayed in Figure 5E.

Video 3. Dual-color time-lapse imaging of EBP-2::mKate2 and MAPH-1.1::GFP. New microtubules largely grow along existing bundles.

Acknowledgements
We thank R. Schmidt and S. van den Heuvel for sharing strain SV1937, S. van den Heuvel for strain SV1009, J. Feldman for strains JLF15 and JLF173, K. Oegema for strain OD1652, A. Woollard for strain AW1015, A. Frand for strain GR1395, and D. Fay for strain RT3638. We thank S. van den Heuvel, M. Harterink, D. Fay and members of the S. van den Heuvel and M. Boxem groups for helpful discussions, M. Harterink for critical reading of the manuscript, and J. Cravo for generating the rose plots. We also thank Wormbase (Harris et al., 2020) and the Biology Imaging Center, Faculty of Sciences, Department of Biology, Utrecht University. Some strains were provided by the Caenorhabditis Genetics Center, which is funded by NIH Office of Research Infrastructure Programs (P40 OD010440).

Funding
This work was supported by the Netherlands Organization for Scientific Research (NWO)-ALW Open Program 824.14.021 and NWO-VICI 016.VICI.170.165 grants to M. Boxem, and the European Union's Horizon 2020 research and innovation programme under the Marie Skłodowska-Curie grant agreement No. 675407 – PolarNet.

Author contributions
Conceptualization: V.G.C., H.R.P., M.B.; Methodology: V.G.C., H.R.P.; Formal analysis: V.G.C., H.R.P., R.R.B.; Investigation: R.R.B., A.R., J.K.; Writing - original draft: V.G.C., H.R.P., M.B.; Visualization: V.G.C., H.R.P., M.B.; Supervision: M.B.; Project administration: M.B.; Funding acquisition: M.B.

Supplementary Materials
This manuscript is accompanied by Supplemental File 1 available in the online published document - DNA files.zip, a zip archive containing the DNA sequences of genome edits and plasmids described in this paper in genbank and SnapGene format.

"Science explains what is happening around us the whole time. So does religion, but science is better because it comes up with more understandable excuses when it's wrong."

Terry Pratchett

Characterization of the composition and functioning of the Crumbs complex in *C. elegans*

Victoria G Castiglioni[1], Hanna van Beuzekom[1], Jason Kroll[1], Riccardo Stucchi[2,3], Ruben Schmidt[1], Maarten Altelaar[3], Mike Boxem[1]

A version of this manuscript has been submitted to publication

[1] Division of Developmental Biology, Institute of Biodynamics and Biocomplexity, Department of Biology, Faculty of Science, Utrecht University, Utrecht, Netherlands.

[2] Cell Biology, Neurobiology and Biophysics, Institute of Biodynamics and Biocomplexity, Department of Biology, Faculty of Science, Utrecht University, Utrecht, the Netherlands

[3] Biomolecular Mass Spectrometry and Proteomics, Bijvoet Center for Biomolecular Research and Utrecht Institute for Pharmaceutical Sciences, Utrecht University, Utrecht, the Netherlands

Introduction

Epithelial tissues segregate their internal medium from the outside environment and are highly specialised for purposes such as absorption, secretion, protection, and transport. To perform these functions, epithelial cells are highly polarized: proteins and lipids of the plasma membrane are distributed asymmetrically into an apical domain that faces the external environment or lumen and a basolateral domain contacting neighbouring cells and the extracellular matrix. Cell-cell junctions at the boundary of the apical and basolateral domains seal the epithelial sheets to segregate the internal medium from the outside environment, and provide mechanical strength to the tissue. The establishment of these different domains relies on mutually antagonistic interactions between evolutionarily conserved polarity complexes. Members of the Par and Crumbs complexes establish apical identity and position cell junctions at the apical/lateral border, whilst basolateral identity is promoted by the Scribble group proteins and the Par1 kinase (Rodriguez-Boulan and Macara, 2014; Wen and Zhang, 2018).

The Crumbs complex is a key regulator of epithelial polarity that is crucial for the formation of the apical domain and the organization of junctions, and thus the boundary between the apical and basolateral domains (Klebes and Knust, 2000; Médina et al., 2002b; Tepass et al., 1990; Wodarz et al., 1995). There are multiple ways in which the Crumbs complex promotes epithelial polarity. For example, direct interactions between Crumbs and proteins that bind the actin cytoskeleton such as Moesin support the polarized organization of the cytocortex (Médina et al., 2002a). Moreover, Crumbs recruits β_{Heavy}-Spectrin to the apical membrane, contributing to apical membrane stability (Lee and Thomas, 2011; Pellikka et al., 2002). Finally, Crumbs promotes the apical localization and accumulation of the apical Par proteins, defining apical identity (Almeida et al., 2019; Lemmers et al., 2004). Loss of the Crumbs complex leads to severe polarity defects (Straight et al., 2004; Wodarz et al., 1993), disruption of cell junctions (Shin et al., 2005; Wang et al., 2006) and loss of tissue integrity (Jürgens et al., 1984). Nevertheless, the Crumbs complex is not essential in all epithelial tissues. For example, the Drosophila intestine and neuroblasts can withstand the absence of the Crumbs complex without apparent defects (Hong et al., 2001; Tepass et al., 1990).

The Crumbs complex is composed of three scaffolding proteins: the transmembrane protein Crumbs (Crb in Drosophila, CRB1, CRB2 or CRB3 in mammals and CRB-1, EAT-20 and CRB-3 in *C. elegans*), the MAGUK protein Pals1 (Protein associated with LIN7, Sdt in Drosophila), and the PDZ protein PatJ (Bhat et al., 1999; Knust et al., 1993; Nam and Choi, 2006; Tepass and Knust, 1993). Whereas Drosophila encodes one Crumbs gene, several orthologs can be found in the *C. elegans*, zebrafish, mouse, and human genomes. Mammalian CRB1 and CRB2 are composed of a large extracellular region, a transmembrane domain, and a small highly conserved intracellular region containing two protein-protein interaction domains: a C-terminal "ERLI" PDZ-binding motif (PBM) and a 4.1/Ezrin/Radixin/Moesin (FERM)-binding motif (FBM). CRB3 is similar to CRB1 and CRB2 but lacks the large extracellular region. Pals1 contains two L27 domains, a PDZ domain, a SH3 domain and a guanylate kinase (GUK) domain, whereas PATJ contains one N-terminal domain and multiple PDZ domains (Assémat et al., 2008).

Several protein-protein interactions are necessary for the formation of the Crumbs complex. Crumbs itself interacts with Pals1 through its PBM, and Pals1 in turn interacts with Crumbs through its PDZ and SH3 domains, additionally strengthening the interaction through its GUK domain (Bachmann et al., 2001; Hong et al., 2001). Assembly of the PatJ-Pals1 complex requires the formation of an L27 tetramer through the interaction between two units of Pals1-L27N—PatJ-L27 (Feng et al., 2005; Roh et al., 2002). The composition of the Crumbs complex can vary depending on the requirements. For example, in Drosophila embryonic epithelia and mature photoreceptor cells, Pals1 is necessary for apical Crumbs localization (Berger et al., 2007; Hong et al., 2001). However, in the embryonic posterior midgut and pupal photoreceptor, Pals1 decreases the apical levels of Crumbs by promoting its endocytosis (Almeida et al., 2019; Perez-Mockus et al., 2017). Moreover, the apical protein Par6 can interact with Crumbs through the PDZ domain of Crumbs (Lemmers et al., 2004), which is the domain used for the interaction between Pals1 and Crumbs, thereby generating an alternative complex. The interaction between Par6 and Crumbs has been reported to enable apical retention of the Crumbs complex (Almeida et al., 2019).

Previously, we showed that none of the Crumbs genes (*crb-1, eat-20,* and *crb-3*) are essential in *C. elegans*, as animals lacking all three genes are viable (Waaijers et al. 2015). However, a non-essential role for CRB-1 in apical junction formation has been described: CRB-1 provides a positional cue for junction formation in the intestine upon double depletion of HMP-1 α-catenin and LET-413 (Segbert et al., 2004). Moreover, the subcellular localization of the Crumbs proteins is strikingly similar to that of mammalian systems and Drosophila (Bossinger et al., 2001; Waaijers et al., 2015), suggesting that some aspects of spatial organization are conserved. Nevertheless, the function of the Crumbs complex in *C. elegans* remains elusive. Additionally, the composition of the *C. elegans* Crumbs complex has not been studied, even though candidate homologs of the main Crumbs complex components PatJ and Pals1 do exist. As a result, it is unknown if these putative homologs are part of a functional Crumbs complex.

In this study, we characterize the different components of the Crumbs complex in *C. elegans* and examine the effects of Crumbs overexpression. We demonstrate that *C. elegans* MAGU-2 shares key features with Pals1. MAGU-2 interacts with the three Crumbs proteins and is localized to the apical membrane domain in a Crumbs dependent manner. Like triple *crumbs* deletion

mutants, animals lacking *magu-2* are viable and show no overt polarity defects. Moreover, we find that MAGU-2 can interact with the putative PatJ ortholog MPZ-1. We conclude therefore that MAGU-2 is the *C. elegans* homolog of Pals1 and a member of the Crumbs complex. Finally, we show that overexpression of EAT-20 and CRB-3 in *C. elegans* leads to apical membrane expansion, as reported for overexpression of Drosophila Crumbs. Our results thus elucidate the composition of the Crumbs complex in *C. elegans* and indicate that the role of the Crumbs complex in promoting apical domain identity is conserved in *C. elegans*, albeit a high level of redundancy probably hinders our understanding of the complex.

Results

MAGU-2 is the ortholog of Pals1

The Crumbs complex has not been fully characterized in *C. elegans*. Whilst the role of the Crumbs homologs in organizing polarity has been investigated (Bossinger et al., 2001; Segbert et al., 2004; Waaijers et al., 2015), whether the orthologs of Pals1 and Patj exist and form a Crumbs complex is not known. To identify Pals1 homologs, we searched the predicted *C. elegans* proteome for candidate homologs using BLAST. Searches with the human Pals1 or Drosophila Sdt sequences yielded a significant *C. elegans* hit, MAGU-2 (Fig. 1A). MAGU-2 displayed 53% and 50% of amino acid sequence similarity with Pals1 and Sdt, respectively. MAGU-2 has two predicted isoforms, MAGU-2a of 830 amino acids (aa) and MAGU-2b of 668 aa. Both isoforms consist of a PDZ domain, an SH3 domain and a GUK domain, whilst MAGU-2A contains an extra N-terminal PDZ domain which is not present in Pals1 (Fig. 1B). The PDZ and SH3 domains of human Pals1 are involved in the interaction between Pals1 and Crumbs, whilst the GUK domain enhances the binding of Pals1 to Crumbs. Drosophila Crumbs, in turn, interacts with Pals1 through its intracellular PDZ-binding domain (Li et al., 2014). Most of the amino acids involved in the interaction between Pals1 and Crumbs are conserved in *C. elegans* MAGU-2 and CRB-1/EAT-20/CRB-3, consistent with MAGU-2 being the homolog of Pal1 (Fig. 1C).

To determine if MAGU-2 interacts with any of the three *C. elegans* Crumbs proteins, we performed a Y2H assay. We fused the intracellular domain of each of the three Crumbs proteins to the DNA binding domain of Gal4, and fused the following fragments of MAGU-2 to the activation domain: a full-length fragment (FL), an N-terminal fragment with the PDZ present in the long MAGU-2 isoform (1), an N-terminal fragment including both PDZ domains but lacking the SH3 domain (2), an N-terminal fragment that includes both PDZ domains and the SH3 domain (3), a fragment containing the second PDZ domain and the SH3 domain (4), a C-terminal fragment containing the SH3

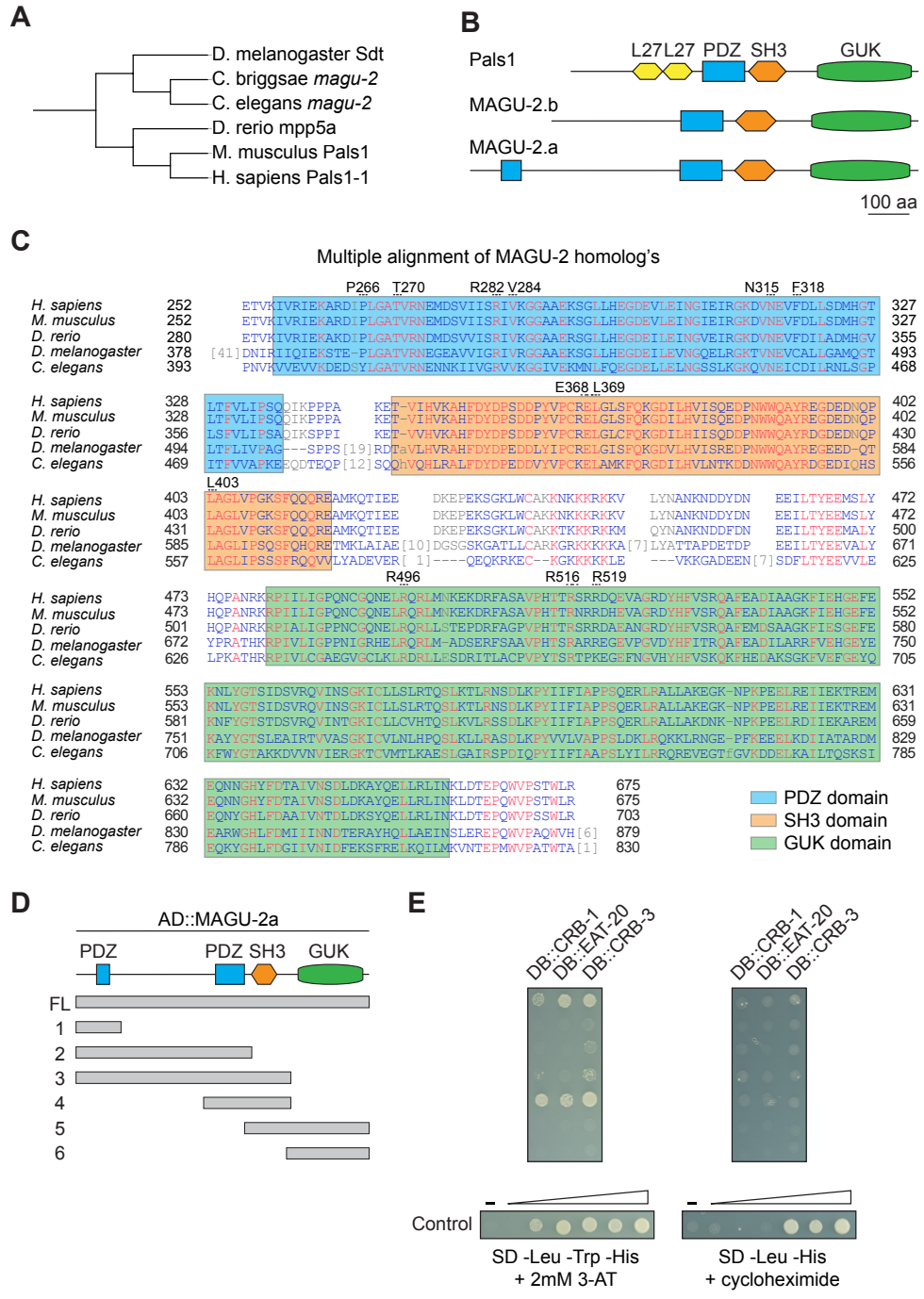

Figure 1. *magu-2* is the homolog of Pals1/Sdt. (A) Phylogenetic tree of Pals1 homologs, including *C. elegans magu-2*. **(B)** Schematic representation of predicted protein domains of Pals1 and MAGU-2. **(C)** Multiple alignment of *magu-2* homologs in *Homo Sapiens*, *Mus musculus*, *Danio rerio*, Drosophila *melanogaster* and *Caenorhabditis el-*

egans. Highlighted in black are the Pals1 residues involved in the interaction with Crumbs. **(D)** Schematic representation of the different fragments of MAGU-2 used for the Y2H assay. **(E)** Interaction of MAGU-2 and CRB-1, EAT-20 and CRB-3 in the yeast two-hybrid assay. Fragments of MAGU-2.b fused to the Gal4 activation domain were co-expressed with the intracellular domain of either CRB-1, EAT-20 or CRB-3 fused to the Gal4 DNA binding domain. Growth on the -Leu -Trp -His + 2 mM 3-AT plate indicates presence of interaction. Lack of growth on -Leu -His + cycloheximide plate shows that DB::CRB-1/EAT-20/CRB-3 are not self-activating. Controls range from no reporter activation to strong reporter activation. On cycloheximide plates "-" indicates no growth expected. Abbreviations: L27, Lin-2 and Lin-7 domain; PDZ, Postsynaptic density 95, Discs large, Zonula occludens-1; SH3 domain, SRC homology 3 domain; GUK, guanylate kinase-like domain.

and GUK domains (5) and a C-terminal fragment consisting of only the GUK domain (6) (Fig. 1D). The Y2H assay indicated that full length MAGU-2 interacts with each of the three Crumbs proteins (Fig. 1E). Consistent with previous analyses in other organisms (Li et al., 2014), both the conserved PDZ domain and the SH3 domain are required for the interaction. These results indicate that the interactions between MAGU-2 and CRB-1/EAT-20/CRB-2 are conserved.

MAGU-2 localizes apically in multiple epithelial tissues

To determine a potential role for MAGU-2 in organizing epithelial polarity, we first examined its expression pattern and subcellular localization. Mammalian Pals1 and Drosophila Std, localize at the apical cortex in epithelial tissues. If MAGU-2 is a functional ortholog, MAGU-2 would be expected to recapitulate the apical localization of these proteins. To visualize the localization of MAGU-2, we used CRISPR/Cas9 to insert the sequence encoding the green fluorescent protein (GFP) into the endogenous *magu-2* locus. The tag was inserted at the C-terminus such that all isoforms were tagged (Fig. 2A). We first detected MAGU-2::GFP in the intestine during early embryonic development, before apical-basal polarity is established, where it colocalized with the junctional protein DLG-1 (Fig. 2B). During later pharyngeal and intestinal development, MAGU-2 localized to the apical cortex, where it colocalized with the apical protein PAR-6 (Fig. 2C-D, F). Throughout larval development, MAGU-2::GFP localized to the nerve ring, and to the apical membrane domain of the pharynx and intestinal cells (Fig. 2E-F). The apical subcellular localization of MAGU-2 in polarized epithelial tissues, which matches the subcellular localization of the Crumbs proteins in these tissues (Shibata et al., 2000; Waaijers et al., 2015), strengthens our hypothesis that MAGU-2 is a Pals1 homolog and a member of the Crumbs complex.

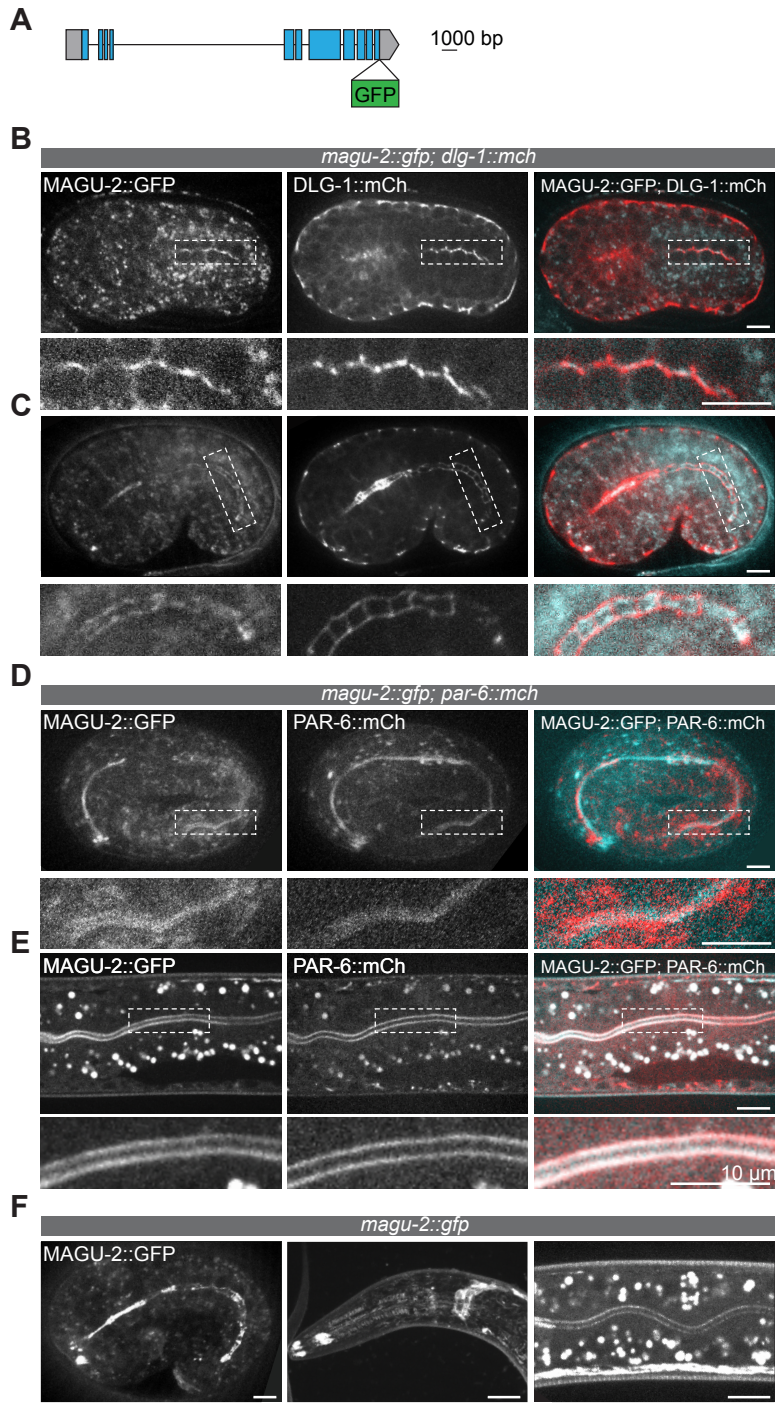

Figure 2. MAGU-2 localizes apically in epithelial tissues. (A) Schematic representation of endogenous tagging of magu-2 locus with the sequence encoding a green fluorescent protein (GFP). **(B-C)** Distribution of MAGU-2::GFP and DLG-1::mCh in the early

stages of intestinal polarization and in comma-shape embryos. **(D-E)** Distribution of MAGU-2::GFP and PAR-6::mCh in two-fold embryos and L3 larvae. **(F)** Distribution of MAGU-2::GFP in the pharynx and intestine of a comma-shape embryo, and the nerve ring and intestine of L2/L3 larvae.

The localization of MAGU-2 and Crumbs are not interdependent

We next examined the relationship between MAGU-2 and Crumbs. Mammalian Pals1 and Drosophila Sdt are dependent on Crumbs for their apical localization (Bachmann et al., 2001; Hong et al., 2001; Roh et al., 2002). We therefore examined MAGU-2 localization in the triple Crumbs deletion. Absence of the three Crumbs proteins resulted in a complete loss of MAGU-2 apical accumulation in the embryonic and larval intestine (Fig. 3A), indicating that Crumbs is necessary for apical enrichment of MAGU-2 in *C. elegans*. In some systems studied, Crumbs apical localization is also dependent on Pals1 or Sdt (Almeida et al., 2019; Berger et al., 2007; Hong et al., 2001; Perez-Mockus et al., 2017; Straight et al., 2004; van Rossum et al., 2006). To determine if this reciprocal requirement is conserved in *C. elegans*, we examined the localization of CRB-3 in a *magu-2* deletion generated previously in our lab (Ramalho, 2020). The resulting mutant (*mib6*) contains a deletion of 806 out of the 830 amino acids and introduces an early frame shift. To visualize CRB-3, we used a translational CRB-3::GFP fusion that closely mimics the endogenous expression pattern (Waaijers et al., 2015). In control worms, CRB-3 localizes to the apical side of the intestine in both embryos and larvae. Upon absence of *magu-2* the localization of CRB-3 was unaltered (Fig. 3B), indicating that MAGU-2 does not determine CRB-3 localization in *C. elegans*.

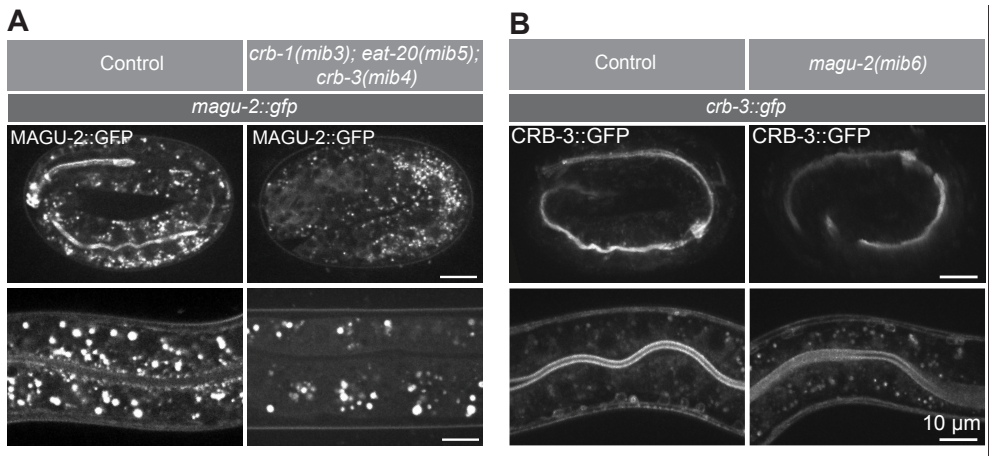

Figure 3. MAGU-2 is dependent on Crumbs for its localization. (A) Distribution of MAGU-2::GFP in control or *crb-1(mib3); eat-20(mib5); crb-3(mib4)* two-fold embryo or larvae. **(B)** Distribution of CRB-3::GFP in control or *magu-2* knock-out *(mib6)* three-fold embryos or larvae.

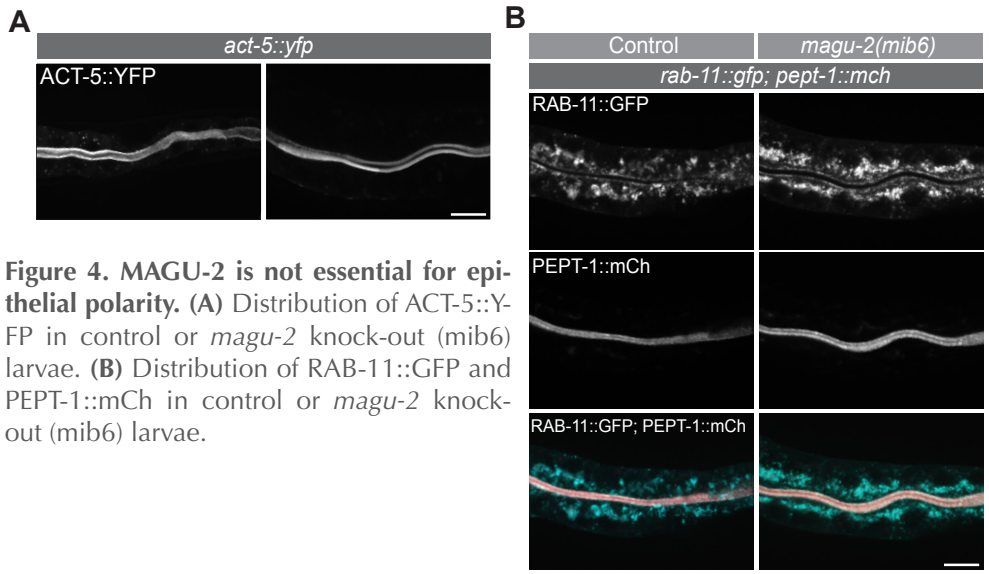

Figure 4. MAGU-2 is not essential for epithelial polarity. (A) Distribution of ACT-5::YFP in control or *magu-2* knock-out (mib6) larvae. **(B)** Distribution of RAB-11::GFP and PEPT-1::mCh in control or *magu-2* knock-out (mib6) larvae.

MAGU-2 is not essential for epithelial polarity

Loss of Pals1 in mammalian and Drosophila epithelia leads to severe polarity defects and disruption of cell junctions (Hong et al., 2001; Straight et al., 2004; Wang et al., 2006), and the phenotypes of Crumbs and Pals1 mutants are very similar, consistent with them forming a core complex (Hong et al., 2003; Nam and Choi, 2006; Tepass and Knust, 1993). Previous data from our group demonstrated that *magu-2(mib6)* deletion animals develop normally and have normal progeny numbers (Ramalho, 2020). Moreover, combining the *magu-2* deletion with the triple *crumbs* deletion did not exacerbate the phenotype of the *crumbs* deletion mutant, consistent with *magu-2* and the Crumbs proteins acting in the same pathway. To assess in more detail whether loss of *magu-2* disrupts apical membrane morphology, we examined the localization pattern of actin, the recycling endosome RAB-11 and the apical membrane transporter PEPT-1 in the absence of *magu-2*. Actin and PEPT-1 localize apically in control animals, and continued to localize apically in *magu-2* deletion mutants (Fig, 4A-B). Similarly, RAB-11, which is normally enriched in the cytoplasm, close to the apical lumen, maintained the same localization pattern in the absence of MAGU-2 (Fig. 4B). Taken together, these data indicate that *magu-2* is not necessary for apical polarity establishment/maintenance.

MAGU-2 interacts with MPZ-1, the homolog of PATJ

Having established that the *C. elegans* Crumbs complex contains a Pals1 homolog, we next investigated if *C. elegans* MAGU-2 interacts with a homolog of PatJ. For this purpose, we explored the interacting partners of MAGU-2 by performing affinity purification of the endogenous GFP::MAGU-2 from a mixed-

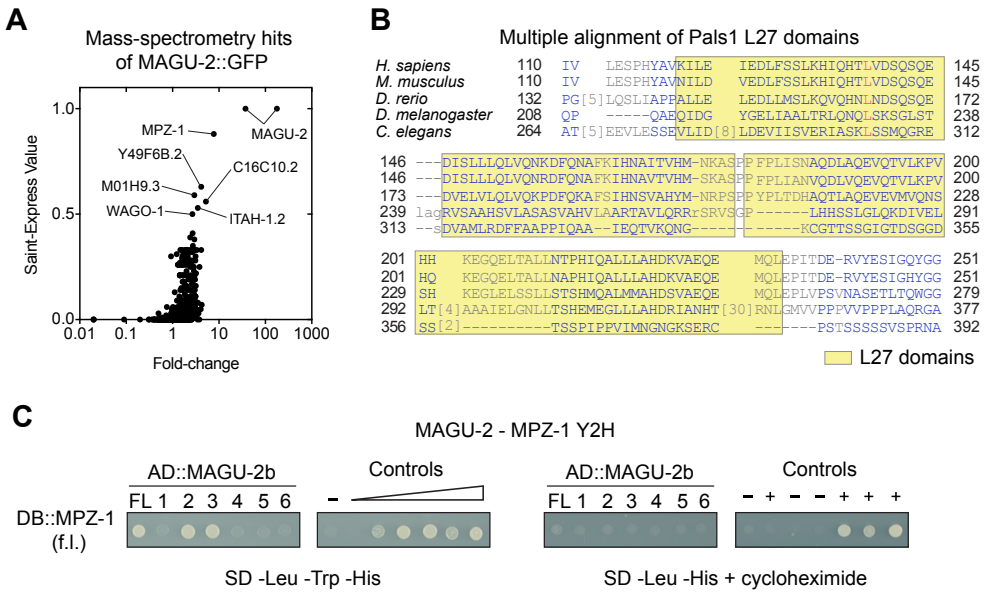

Figure 5. MAGU-2 interacts with MPZ-1. (A) Mass spectrometry hits for MAGU-2::GFP pull down plotted as correlation between fold-change score and Saint-Express Value. **(B)** Multiple alignment of the L27 domains in *Homo Sapiens*, *Mus musculus*, *Danio rerio*, Drosophila *melanogaster* and *Caenorhabditis elegans*. **(C)** Interaction of MAGU-2 and MPZ-1 in the yeast two-hybrid assay. Fragments of MAGU-2.b fused to the Gal4 activation domain were co-expressed with the full length of MPZ-1 fused to the Gal4 DNA binding domain. Growth on the -Leu -Trp -His plate indicates presence of interaction. Lack of growth on -Leu -His + cycloheximide plate shows that DB::MPZ-1 is not self-activating. Controls range from no reporter activation to strong reporter activation. On cycloheximide plates (-) indicates no growth expected.

stage population, followed by mass-spectrometry. The highest-ranking candidate interacting protein was MPZ-1, a putative *C. elegans* homolog of PatJ (Fig. 5A). Mammalian PatJ is characterized by having 10 PDZ domains. Similarly, the Drosophila homolog has four PDZ domains. Both human and Drosophila proteins also contain an N-terminal L27 domain, which interacts with the L27 domain of Pals1 (Roh et al., 2002). The putative *C. elegans* homolog, MPZ-1, is partially conserved: it is the only *C. elegans* protein with 10 PDZ domains, but lacks the N-terminal L27 domain. As the L27 domains through which PatJ and Pals1 interact are not conserved in MPZ-1 and MAGU-2 (Fig. 1B, 5B), we wanted to identify the MAGU-2 domain responsible for the interaction with MPZ-1. We fused the full length MPZ-1 coding sequence to the DNA binding domain of Gal4, and examined the interaction with the MAGU-2 activation domain fusions described above (Fig. 1D). Full length MAGU-2 interacted with MPZ-1, confirming the mass spectrometry result (Fig. 5C). MAGU-2 Fragments 2 and 3, which contain the region in which the L27 domain is located in mam-

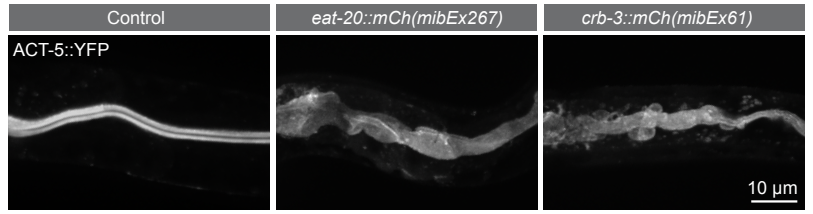

Figure 6. Crumbs overexpression results in apical domain expansion. Distribution of ACT-5::YFP in the intestine of larvae in control animals or upon EAT-20 or CRB-3 overexpression.

malian Pals1 and Drosophila Sdt, also interacted with MPZ-1. This suggests that the region between the first PDZ domain and the SH3 domain of MAGU-2 is necessary for the interaction between MAGU-2 and MPZ-1, despite lacking a recognizable L27 domain. Taken together, these data indicate that the interactions between Crumbs, Pals1, and PatJ are conserved in *C. elegans*.

Overexpression of Crumbs results in an apical membrane domain expansion

Deletion of all three *crumbs* genes demonstrated that the Crumbs complex is not essential in *C. elegans* (Waaijers et al., 2015). However, the effects of Crumbs overexpression, which is known to result in an enlarged apical domain in Drosophila (Wodarz et al., 1995), have not been investigated in *C. elegans*. In order to induce overexpression, we expressed EAT-20 Crb2 and CRB-3 Crb3 under the control of the intestine specific promoter *elt-2* (McGhee et al., 2009). To determine the effect on apical domain size, we examined the distribution of the actin marker YFP::ACT-5, which is highly enriched at the apical domain. Upon overexpression of either EAT-20 or CRB-3, the distribution of ACT-5 indicated an enlarged apical domain which bulged into the cytoplasm of the intestinal cells (Fig. 6). This indicates that overexpression of EAT-20 or CRB-3 results in apical domain expansion, and that the role of the Crumbs proteins in promoting apical domain identity are conserved in *C. elegans*.

Discussion

Here, we characterized the conservation of composition and functioning of the Crumbs complex in *C. elegans*. We identified MAGU-2 as the *C. elegans* ortholog of mammalian Pals1 and Drosophila Sdt. This conclusion is supported by the sequence conservation, the apical localization of MAGU-2, the dependency of MAGU-2 apical localization on Crumbs proteins, and the interactions with each Crumbs protein. We also identified MPZ-1 as a candi-

date ortholog of the Crumbs complex component PatJ, based on the interaction of MAGU-2 with MPZ-1 and the presence of multiple PDZ domains in MPZ-1. Finally, we demonstrate that overexpression of the *C. elegans* Crumbs proteins EAT-20 Crb2 or CRB-3 Crb3 can induce apical membrane overgrowth in the intestine.

The composition of the Crumbs complex, and the functioning of components besides Crumbs, had not been studied in *C. elegans*. Here, we focused on the homolog of Pals1, *magu-2*, which is a core member of the Crumbs complex in mammalian systems and Drosophila. MAGU-2 interacted with *C. elegans* CRB-1, EAT-20, and CRB-3 through its PDZ and SH3 domains, as has been shown for Sdt and Pals1 in Drosophila and mammals (Bachmann et al., 2001; Hong et al., 2001; Roh et al., 2002). MAGU-2 was enriched in the apical membrane and relied on CRB-1/EAT-20/CRB-3 for its localization. These results are in accordance with previous observations of Sdt and Pals1, both of which localize apically in a Crumbs dependent manner (Bachmann et al., 2001; Hong et al., 2001; Roh et al., 2002). CRB-3 did not, however, rely on MAGU-2 to become apically enriched. Mammalian Crb3 has been shown to localize apically independently of Pals1 (Straight et al., 2004), whereas Crb1 has been shown to require Pals1 to localize apically (van Rossum et al., 2006). In Drosophila, Crumbs has been shown to depend on Sdt in some tissues and developmental stages, such as the embryonic epithelia and mature photoreceptors (Berger et al., 2007; Hong et al., 2001). However in other tissues, such as the posterior midgut and pupal photoreceptors, Crumbs localization is independent of Sdt (Almeida et al., 2019; Perez-Mockus et al., 2017). Our efforts here focused on CRB-3, and it would be interesting to see if CRB-1 or EAT-20 require MAGU-2 to become apically localized in *C. elegans*.

In addition to the conservation of the interactions with the Crumbs family members, we demonstrated that MAGU-2 interacts with MPZ-1, the likely ortholog of PatJ. Pals1 and PatJ interact through their L27 domains (Feng et al., 2005; Roh et al., 2002), which are not conserved in *C. elegans* MAGU-2 and MPZ-1. However, the interaction with MPZ-1 was mediated by the region between the first PDZ domain and SH3 domain of MAGU-2, where the L27 domains are localized in Pals1 proteins in other species. This raises the possibility that MAGU-2 contains an L27-like structural fold that is not recognized at the primary amino acid sequence level. Altogether, we conclude that *magu-2* is the functional ortholog of Pals1/Sdt.

Despite their evolutionary conservation, none of the *C. elegans* Crumbs complex components have essential roles in the development of *C. elegans* (Bossinger et al., 2001; Ramalho, 2020). (Waaijers et al., 2015). One explanation for why protein inactivation can show no discernable phenotypes is redundancies with other proteins. Indeed, CRB-1 was shown to provide a positional cue for junction formation in the intestine upon double depletion of HMP-1 □-catenin and LET-413 (Segbert et al., 2004), suggesting that redundant

mechanisms ensure proper apical junction formation in the intestine. Further supporting a role for the *C. elegans* Crumbs complex in regulating apical-basal polarization, we observed that overexpression of either EAT-20 or CRB-3 resulted in apical membrane expansion.

Redundancy in the polarity network has been seen in other systems, such as Drosophila, where Crumbs is expressed in all embryonic epithelia derived from the ectoderm but tissues react differently to loss of Crumbs, from disintegration and apoptosis in the epidermis to no apparent defects in the hindgut (Chen et al., 2018; Tepass and Knust, 1990). These findings highlight that in order to understand the different functions of polarity regulators it is important to study them in a range of different systems and organisms. Although it remains uncertain what is the precise role in *C. elegans* of the Crumbs complex, and *magu-2* in particular, our characterization of the Crumbs complex provides further insight into the Crumbs complex in *C. elegans*.

Materials and Methods

Homology search

MAGU-2 was identified as the homolog of Pals1 and Sdt using BLAST homology search (Altschul et al., 1997; Altschul et al., 2005). The amino acid sequence of human Pals1 (Q8N3R9-1) was used as the input. Similarity was calculated using EMBL-EBI search and sequence analysis tools with the input sequences of MAGU-2 (C01B7.4b.1), Pals1(Q8N3R9-1), and Sdt (M9NG38-1) (Madeira et al., 2019). The homology tree was constructed using "Tree of Life" (https://itol.embl.de/itol.cgi).

Yeast two-hybrid analysis

Sequences encoding MAGU-2, CRB-1, EAT-20, CRB-3 and MPZ-1 were PCR amplified from a mixed-stage cDNA library using the primers found in Table 1. PCR products were digested with AscI and NotI, and cloned into Gal4-DB vector pMB28 and Gal4-AD vector pMB29, respectively (Koorman et al., 2016). The resulting plasmids were transformed into *Saccharomyces cerevisiae* strains Y8930 (MAT□) and Y8800 (MATa) (Yu et al., 2008) using the Te/LiAc transformation method (Schiestl and Gietz, 1989). Diploid yeast was generated by mating, and plated on synthetic defined (SD) medium plates lacking leucine, tryptophan, and histidine containing 2 mM 3-Amino-1,2,4-triazole (3-AT); and lacking leucine, tryptophan, and adenine to assess the presence of an interaction, and on an SD plate lacking leucine and histidine containing 1 µg/ml cycloheximide to test for self-activation. Controls of known reporter activation strength and behavior on cycloheximide were also added to all plates.

C. elegans strains

All C. elegans strains used in this study are derived from the N2 Bristol strain, and are listed in Table 2. All strains were maintained at 20 °C on Nematode Growth Medium (NGM) plates seeded with *Escherichiae coli* OP50 bacteria under standard conditions (Brenner, 1974).

CRISPR/Cas9 genome engineering

The *magu-2::gfp* fusion was done by homology-directed repair of CRISPR/Cas9-induced DNA double-strand breaks in an N2 background. The fusion was generated using plasmid-based expression of Cas9 and sgRNAs. The sequence targeted by the sgRNA was 5′ GTGAATACGGAGCCAATGT 3′. The *magu-2::gfp* repair template was cloned using SapTrap assembly into vector pDD379, and the fusion was repaired using a plasmid-based template with 550-600 bp homology arms. A self-excising cassette (SEC) was used for selection (Dickinson et al., 2015). The homology arms included mutations of the sgRNA recognition sites to prevent re-cutting after repair. The injection mix was prepared in MilliQ H_2O and contained 50 ng/µL Peft-3::cas9 (Addgene ID #46168) (Friedland et al., 2013), 65 ng/µL sgRNA-repair-template vector, and 2.5 ng/µL co-injection pharyngeal marker Pmyo-2::tdTomato to aid in visual selection of transgenic strains. Young adult hermaphrodites were injected in the germline using an inverted micro-injection setup (Eppendorf FemtoJet 4x mounted on a Zeiss Axio Observer A.1 equipped with an Eppendorf Transferman 4r). Candidate edited progeny were selected on plates containing 250 ng/µl of hygromycin (Dickinson et al., 2015), and correct genome editing was confirmed by PCR amplification of the edited genomic region. From correctly edited strains, the hygromycin selection cassette was excised by a heat shock of L1 larvae at 34 °C for 1 h in a water bath. Correct excision was confirmed by Sanger sequencing (Macrogen Europe) of PCR amplicons encompassing the edited genomic region. The sequence file of the final gene fusion in Genbank format is in Supplementary File 1.

Microscopy

Live imaging of *C. elegans* larvae was done by mounting larvae on 5% agarose pads in a 10 mM Tetramisole solution in M9 buffer to induce paralysis. Spinning disk confocal imaging was performed using a Nikon Ti-U microscope driven by MetaMorph Microscopy Automation & Image Analysis Software (Molecular Devices) and equipped with a Yokogawa CSU-X1-M1 confocal head and an Andor iXon DU-885 camera, using 60x or 100x 1.4 NA objectives. All stacks along the z-axis were obtained at 0.25 µm intervals, and all images were analyzed and processed using ImageJ(FIJI) and Adobe Photoshop.

GFP pull-down of MAGU-2::GFP.

Animals endogenously expressing GFP-tagged MAGU-2 or control animals expressing an integrated GFP transgene (Waaijers et al., 2016) were grown on 6–8 9 cm NGM plates until starvation, to enrich for L1 animals. Animals were then transferred into 250 ml of S-Medium supplemented with 1% Penn/Strep (Life Technologies), 0.1% nystatin (Sigma) and OP50 bacteria obtained from the growth of a 400 ml culture. Animals were grown at 20 °C at low shaking for 96 hours and were harvested and cleaned using a sucrose gradient, as previously described (Waaijers et al., 2016) with one exception being the inclusion of MgSO4 in the M9 medium. Worms were distributed into 15 ml TPX tubes (Diagenode) to reach 200–400 µl worm pellet per tube, and were washed with lysis buffer (25mM Tris-HCl pH 7.5, 150mM NaCl, 1mM EDTA, 0.5% IGEPAL CA-630, 1X Complete Protease Inhibitor Cocktail (Roche)). The liquid was removed, and the sample was flash frozen in liquid nitrogen for storage at -80 °C. To lyse the worms, tubes were thawed on ice and ice-cold lysis buffer was added to reach a total volume of 2 ml. Tubes were sonicated for 10 mins (sonication cycle: 30 sec ON, 30 sec OFF) at 4 °C in a Bioruptor ultrasonication bath (Diagenode) at high energy setting. After lysis, lysates were cleared by centrifugation and protein levels were measured using the Bradford BCA assay (Thermo Scientific). Immunoprecipitation was performed using GFP-Trap Magnetic Agarose beads (Chromotek) according to manufacturer's protocol, using 25 µl of beads per sample. To prep the beads, they were first equilibrated in wash buffer (10 mM Tris/Cl pH 7.5, 150 mM NaCl, 0.5 mM EDTA, 0.1% IGEPAL CA-630), blocked with 1% BSA for 1 hour, then washed 4 times with wash buffer. Next, lysate was added to the beads and they were incubated for 1 hour tumbling end-over-end. Lysate was then removed, and the beads were washed 4 times in wash buffer. After the final wash step, all liquid was removed, and the beads were flash frozen with liquid nitrogen. The experiment was performed in triplicate (biological replicates) and processed on independent days.

Mass spectrometry analysis for MAGU-2.

After affinity purification anti-GFP beads were resuspended in 15 µl of 4× Laemmli sample buffer (Biorad), boiled at 99 °C for 10 min and supernatants were loaded on 4–12% Criterion XT Bis–Tris precast gel (Biorad). The gel was fixed with 40% methanol and 10% acetic acid and then stained for 1 hour using colloidal coomassie dye G-250 (Gel Code Blue Stain, Thermo Scientific). Each lane from the gel was cut and placed in 1.5 ml tubes. Samples were then washed with 250 µl of water, followed by 15 min dehydration in acetonitrile. Proteins were reduced (10mM DTT, 1 hour at 56 °C), dehydrated and alkylated (55mM iodoacetamide, 1 hour in the dark). After two rounds

of dehydration, trypsin was added to the samples and incubated overnight at 37 °C. Peptides were extracted with acetonitrile, dried down and reconstituted in 10% formic acid prior to MS analysis.

Samples were analyzed on an Orbitrap Q-Exactive mass spectrometer (Thermo Fisher Scientific) coupled to an Agilent 1290 Infinity LC (Agilent Technologies). Peptides were loaded onto a trap column (Reprosil pur C18, Dr. Maisch, 100 µm × 2 cm, 3 µm; constructed in-house) with solvent A (0.1% formic acid in water) at a maximum pressure of 800 bar and chromatographically separated over the analytical column (Poroshell 120 EC C18, Agilent Technologies, 100 µm x 50 cm, 2.7 µm) using 90 min linear gradient from 7% to 30% solvent B (0.1% formic acid in acetonitrile) at a flow rate of 150 nl min^{-1}. The mass spectrometers were used in a data-dependent mode, which automatically switched between MS and MS/MS. After a survey scan from 375 to 1600m/z the 10 most abundant peptides were subjected to HCD fragmentation. MS spectra were acquired with a resolution > 30,000, whereas MS2 with a resolution > 17,500.

Raw data files were converted to mgf files using Proteome Discoverer 1.4 software (Thermo Fisher Scientif- ic). Database search was performed using the *C. elegans* database and Mascot (version 2.5.1, Matrix Science, UK) as the search engine. Carbamidomethylation of cysteines was set as a fixed modification and oxidation of methionine was set as a variable modification. Trypsin was set as cleavage specificity, allowing a maximum of two missed cleavages. Data filtering was performed using a percolator, resulting in 1% false discovery rate (FDR). Additional filters were search engine rank 1 and mascot ion score > 20.

Crapome (Mellacheruvu et al., 2013) was used to analyze MAGU-2 interacting proteins in three biological replicas, using proteins identified in the GFP pull downs as control. Significance analysis of interactome (SAINT) score (Choi et al., 2011) and simpler fold- change (FC) calculations FC-A and FC-B were derived from the Crapome analysis by averaging the spectral counts across the controls. FC-A averages the counts across all controls while the more stringent FC-B takes the average of the top 3 highest spectral counts for the abundance estimate.

Table 1. Primers used for Yeast-two-hybrid assay.

Primer	Sequence
oVGC342_mpz1_Y2H_FL_F	GGAGGCGCGCCATGCCGTTACAATCCGAGGA
oVGC343_mpz1_Y2H_FL_R	GGAGCGGCCGCTCATTGTTGAGGGATACTGT
oVGC348_magu2_Y2H_FL_F	GGAGGCGCGCCATGTCCAAGTCGGTGTCGAT
oVGC349_magu2_Y2H_FL_R	GGAGCGGCCGCTTAGCACGCTGTCCATGTAG
oVGC350_magu2_Y2H_1_R	GGAGCGGCCGCTTAATTCGAATTTGTGCAGTTAA
oVGC351_magu2_Y2H_2_R	GGAGCGGCCGCTTAAGACTTCTTTGCTGTGACAG
oVGC352_magu2_Y2H_3_R	GGAGCGGCCGCTTATGGAAGATTTTCCTCGTCAG
oVGC353_magu2_Y2H_4_F	GGAGGCGCGCCATGTCCCCCATCCCACCAGTTAT
oVGC354_magu2_Y2H_5_F	GGAGGCGCGCCATGGAACAAGACACCGAACAACC
oVGC355_magu2_Y2H_6_F	GGAGGCGCGCCATGGAGGTCAAAAAAGGGGCTGA
oVGC356_crb1_Y2H_intra_F	GGAGGCGCGCCATGCGGGGCAATAACGCCATGCA
oVGC357_crb1_Y2H_intra_R	GGAGCGGCCGCTCAGATAAGACGTTCTTGAGG
oVGC358_eat20_Y2H_intra_F	GGAGGCGCGCCATGTACATTCGCCAGTCACGTAA
oVGC359_eat20_Y2H_intra_R	GGAGCGGCCGCTTAGATCAGCCGCTCCTCCT
oVGC360_crb3_Y2H_intra_F	GGAGGCGCGCCATGAAATATGTGAAAGATAGAC-GAAAAAACC
oVGC361_crb3_Y2H_intra_R	GGAGCGGCCGCTTAGATAAGTCCTTCTACATTCGG

Table 2. Strain list

Strain	Genotype	Acknowledgement
JM125	*caIs[Pges-1p::YFP::ACT-5]*	James McGhee
BOX301	*magu-2(magu-2::GFP::loxP) V ; dlg-1(mib23) X*	
BOX300	*par-6(mib25[par-6::mCherry-LoxP]) I; magu-2(mib36) V*	
BOX267	*magu-2(magu-2::GFP::loxP) V*	
BOX42	*mibIs24[crb-3::GFP- Avi, Pmyo-3::mCherry] IV*	
BOX176	*magu-2(mib6) V; mibIs24[crb-3::GFP-2TEV-Avi; Pmyo-3::mCherry] IV*	
BOX198	*magu-2(mib6) V; caIs[Pges-1::YFP::ACT-5]*	
MZE1	*unc-119(ed3) III; cbgIs91[pPept-1:pept-1::DsRed;unc-119(+)]; cbgIs98[pPept-1:GFP::rab-11.1;unc-119(+)]*	Prof. M. Zerial
BOX182	*magu-2(mib6) V; unc-119(ed3) III; cbgIs91[pPept-1:pept-1::DsRed;unc-119(+)]; cbgIs98[pPept-1:GFP::rab-11.1;unc-119(+)]*	
BOX283	*magu-2(magu-2::GFP::loxP) V; crb-1(mib3), eat-20(mib5), crb-3(mib4) X*	

Acknowledgements

We thank members of the S van den Heuvel and M Boxem groups for helpful discussions and J. Ramalho for providing strains BOX176, BOX182 and BOX198. We also thank Wormbase (Harris et al., 2020) and the Biology Imaging Center, Faculty of Sciences, Department of Biology, Utrecht University. Some strains were provided by the Caenorhabditis Genetics Center, which is funded by NIH Office of Research Infrastructure Programs (P40 OD010440). This work was supported by the Netherlands Organization for Scientific Research (NWO)-ALW Open Program 824.14.021 and NWO-VICI 016.VICI.170.165 grants to M Boxem, and the European Union's Horizon 2020 research and innovation programme under the Marie Skłodowska-Curie grant agreement No. 675407 – PolarNet.

Author contributions

Victoria G Castiglioni, Conceptualization, Formal analysis, Investigation, Visualization, Methodology, Writing - original draft, Writing - review and editing; Hanna van Beuzekom, Jason Kroll, Formal analysis, Investigation; Ruben Schmidt, Investigation; Mike Boxem, Conceptualization, Supervision, Funding acquisition, Visualization, Project administration, Writing - review and editing.

"I love deadlines.
I love the whooshing noise they make as they go by."

Douglas Adams

The serine protease inhibitor coding gene *ZK287.4* is a genetic interactor of *crumbs*

Victoria G Castiglioni[1], Mike Boxem[1]

[1] Division of Developmental Biology, Institute of Biodynamics and Biocomplexity, Department of Biology, Faculty of Science, Utrecht University, Utrecht, Netherlands.

Abstract

Crumbs (Crb) is an evolutionarily conserved polarity protein localised to the apical membrane of epithelial cells. Loss or mislocalisation of Crb in *Drosophila* and mammalian systems is often associated with a disruption of apicobasal cell polarity. In *C. elegans*, no essential role for the for the three Crb family members has been described, suggesting that the Crumbs proteins may act redundantly with other pathways. Here, we aim to gain new insight into the Crumbs complex in *C. elegans*. In order to do so, we performed a forward genetic screen to identify alleles that have synthetic phenotypes with a triple *crumbs* deletion mutant. We identified 7 mutants that have synthetic defects with the *crumbs(triple null)* mutant, and performed whole genome sequencing to identify the causative mutations. One of the mutations is predicted to cause a loss of function of *zk287.4,* which encodes a predicted excreted serine protease inhibitor. By recreating the same mutation in a wild-type background using CRISPR/Cas9 we showed that *crumbs* has synthetic defects with *zk287.4*. Combined mutants display developmental and apical morphology defects. Our results indicate that the *C. elegans* Crumbs complex has functional redundancy with a predicted excreted serine protease inhibitor, is involved in apical domain homeostasis, and thus retains some functional conservation. Understanding the function of the genes that are redundant with Crumbs may continue shedding light into the function of this conserved polarity complex.

Introduction

Cell polarity, the asymmetric distribution of components and functions in a cell, is a fundamental property of animal cells. The establishment of cell polarity in epithelial cells depends on a complex interplay of interactions between evolutionary conserved apical and basolateral polarity regulators. The Crumbs/Pals1/PatJ and aPKC/Par6/Par3 complexes promote apical domain identity, whilst the Scribble/Dlg/Lgl module promotes basolateral identity. These cortical polarity complexes establish polarity through mutual inhibitory interactions and through their interactions with a number of other cellular components, such as lipids, junctional components and the cytoskeleton (Martin-Belmonte et al., 2016; Rodriguez-Boulan and Macara, 2014; Wen and Zhang, 2018).

Many polarity regulators have been identified through genetic studies in model organisms such as *Caenorhabditis elegans* and Drosophila *melanogaster* (Jürgens et al., 1984; Kemphues et al., 1988). Model organisms allow powerful genetic approaches to study basic biological processes due to their simplicity and stereotyped characteristics. Their genomes have been entirely sequenced and large-scale genetic studies are easy to execute (C. elegans Sequencing Consortium, 1998; Kutscher, 2014). Genetic screens have shown the existence of evolutionarily conserved proteins that regulate cell polarity in a variety of settings, such as Par6, Par3 and Crumbs (Jürgens et al., 1984; Kemphues et al., 1988; Tepass et al., 1990).

In order to understand how cell polarity controls tissue homeostasis, it is crucial to identify interactions between polarity proteins and other cellular pathways. The apical polarity protein Crumbs is important for several cellular processes. Apart from its well established role in apical domain formation, it has also been shown to be important for junction stability and tension, cell adhesion, endocytosis, and protection against oxidative damage (Flores-Benitez and Knust, 2015; Nemetschke and Knust, 2016; Spannl et al., 2017; Wodarz et al., 1993; Wodarz et al., 1995). The interactions between Crumbs and downstream cellular processes vary depending on tissue requirements, as do the expression and essentiality of Crumbs. For example, the large extracellular domain of Crumbs is dispensable for apical domain formation in Drosophila embryos (Klose et al., 2013), but is necessary for Crumbs stabilization and cell adhesion (Letizia et al., 2013). Crumbs is expressed in several epithelial tissues of Drosophila, such as the foregut, the tracheal system and the epidermis, as well as imaginal discs and photoreceptors. However, Crumbs appears to be absent in epithelial tissues derived from the endoderm, such as the midgut, indicating that the complement of proteins that controls apical domain formation varies between tissues (Chen et al., 2018; Tepass et al., 1990). Moreover, Crumbs is not essential in all tissues in which it is expressed. For example, while loss of Crumbs from the Drosophila epidermis greatly disrupts the tissue, loss of

Crumbs from the oesophagus or gonad causes only minor defects, implying that other apical polarity regulators play a central role there (Tepass and Knust, 1990). This variability reveals a high level of redundancy and robustness in the polarity network.

Mutations in functionally redundant genes show no obvious phenotypes by themselves but, when combined with specific mutations, can cause severe defects – a synthetic phenotype. Synthetic phenotypes can be the result of mutations in structurally related proteins or in genes involved in functionally connected pathways (Wagner, 2000). Uncovering synthetic phenotypes can be a very efficient way to increase our understanding of a particular process. Synthetic phenotypes with Crumbs genes have been reported before. Although Crumbs is conserved in *C. elegans*, a triple deletion mutant targeting the three *crumbs* homologs (*crumbs* from here on) results in viable animals with normal epithelial polarity (Waaijers et al., 2015). Interestingly, it has been shown that after inactivation of the junctional component HMP-1□-Catenin and the basolateral protein LET-413 Scribble, CRB-1 Crb1 provides a positional cue for the localization of apical junctions (Segbert et al., 2004). This synthetic phenotype may not be the only one, as it still remains uncertain what the exact role of the Crumbs complex in *C. elegans* is. It is possible that the observed lack of phenotype in the *crumbs* mutant is because Crumbs functions redundantly with other polarizing mechanisms.

Here, our aim is to gain new insight into the role of the Crumbs complex in *C. elegans*. In order to do so, we performed a forward genetic screen to identify alleles that have synthetic phenotypes with *crumbs* mutants. We observe that mutations in *crumbs* show synthetic defects when combined with loss of *ZK287.4*, which encodes a predicted excreted serine protease inhibitor, and that the combined mutants have developmental and apical morphology defects. These results show that the Crumbs complex is involved in apical domain homeostasis. While our understanding is still far from complete, the molecular details behind this interaction continue to be worked out.

Results

An F2 clonal screen identified synthetic mutations with a triple Crumbs deletion

Previous studies have observed that the Crumbs proteins are not essential for *C. elegans* development, suggesting that they function redundantly with other polarizing mechanisms (Segbert et al., 2004; Shibata et al., 2000; Waaijers et al., 2015). To explore this possibility, we performed an F2 clonal EMS screen to identify syntenic mutations with a *crumbs* deletion. The starting strain was a triple *crb-1(mib3); eat-20(mib5); crb-3(mib4)* deletion, from here on referred to as *crumbs(triple null)*, that contained an extrachromosomal (Ex) array

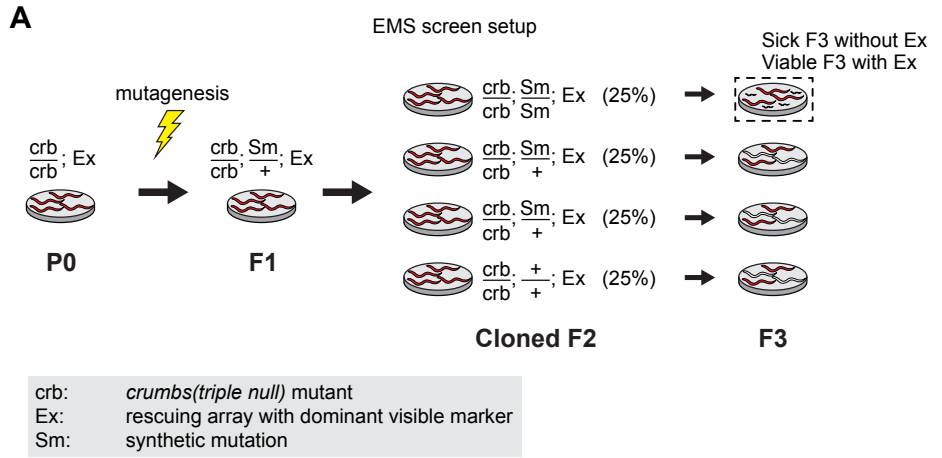

Figure 1. EMS screen for synthetic defects with the *crumbs(triple null)* mutant. (A) Outline of Crumbs synthetic screen. Following chemical mutagenesis, three consecutive generations of Ex+ animals were cloned and allowed to self-fertilize. Animals that acquired mutations that showed synthetic defects with *crumbs(triple null)* were identified by the detrimental phenotype in the absence of Ex. For further details, see text. **(B-C)** Progeny numbers and percentage of embryonic lethality of the selected mutants from the synthetic screen.

that expressed the three Crumbs proteins (Fig. S1) and a fluorescent co-injection marker in order to easily detect its presence or absence. The starting strain was mutagenized using EMS and the F2 progeny was analyzed in a clonal way (Fig. 1A). The presence or absence of the rescuing Ex array was used to identify candidate synthetic mutations (Sm). Candidate Sm were identified on plates where worms were viable if they expressed the Ex array and sick if they lacked it (Fig. 1A). In a screen of ~1680 haploid genomes, 7 independent Sm isolates were obtained (Fig. 1B-C). These mutants displayed reduced progeny numbers and enhanced embryonic lethality, and both of these phenotypes were rescued upon expression of the Ex array (Fig 1B-C).

In order to identify the mutations responsible for the synthetic defects observed with the *crumbs(triple null)* mutant, we sequenced the whole genome of the strains containing the variants. The genome of a strain treated with EMS contains on average 400 single nucleotide changes, of which 22% potentially disrupt gene function (Thompson et al., 2013). To distinguish the variants responsible for the synthetic defects from other variants, we used the Sibling Subtraction Method (SSM) (Joseph et al., 2018). We crossed each mutant to the original strain to obtain a heterozygous mutant. We then divided the progeny of the heterozygous mutants into mutant and a nonmutant pools based on phenotypic analysis. Heterozygous mutants were grouped together with non mutants due to the difficulty of distinguishing both phenotypes (Fig. 2A). We then sequenced the genome of both pools independently and performed a bioinformatic analysis in which we inspected the frequency of each variation in the mutant versus sibling pool. For any random mutant, we expected a ratio of 1, and for a synthetic phenotype causing mutant we expected a ratio above 2. (Fig. 2B). We focused on Sm8, which displayed a strong reduction in progeny numbers and a high embryonic lethality that was rescued with the Ex array. After the SSM was performed, Sm8 displayed an enrichment of variants in Chromosome V, suggesting that the variant responsible for the synthetic defects was located on Chr. V (Fig. 2C). Of the candidate mutants on Chr V, ten variants were located within protein coding regions, and one of them was predicted to cause a nonsense mutation (R338*) in the gene *ZK287.4* (Fig. 2D).

ZK287.4 has synthetic defects with *crumbs*

Having identified the candidate causal variants, we sought to validate the identity of the causal mutations of Sm8. To see whether the mutation in *ZK287.4* was responsible for the synthetic defects with the *crumbs(triple null)* mutant in Sm8, we injected a fosmid encoding the wild-type copy of ZK287.4 into Sm8. If a mutation in *ZK287.4* was responsible for the synthetic defects observed with the *crumbs(triple null)* mutant, providing a wild-type copy of ZK287.4 should rescue the synthetic defects. Upon extrachromosomal expression of ZK287.4, we indeed observed a rescue in the progeny numbers comparable to the rescue observed when expressing the Crumbs proteins, suggesting that *ZK287.4* was responsible for the synthetic defects observed in Sm8 (Fig. 3A). In order to confirm this hypothesis, we recreated the identical (C/T) mutation using CRISPR/Cas9. The mutation is predicted to change an Asparagine into a Stop codon in the 6th exon of the protein, resulting in a truncated protein (Fig. 3B). The resulting allele *ZK287.4(mib43)* did not have any progeny or growth abnormalities or delays (Fig. 3C-D). Combination of the *crumbs(triple null)* with *ZK287.4(mib43)* resulted in a strong decrease in progeny numbers, indicating that *ZK287.4* has synthetic defects with *crumbs*. From here on, all experiment were done with *ZK287.4(mib43)*. To confirm that the *ZK287.4* mutation creates a synthetic phenotype with the *crumbs(triple null)*, we an-

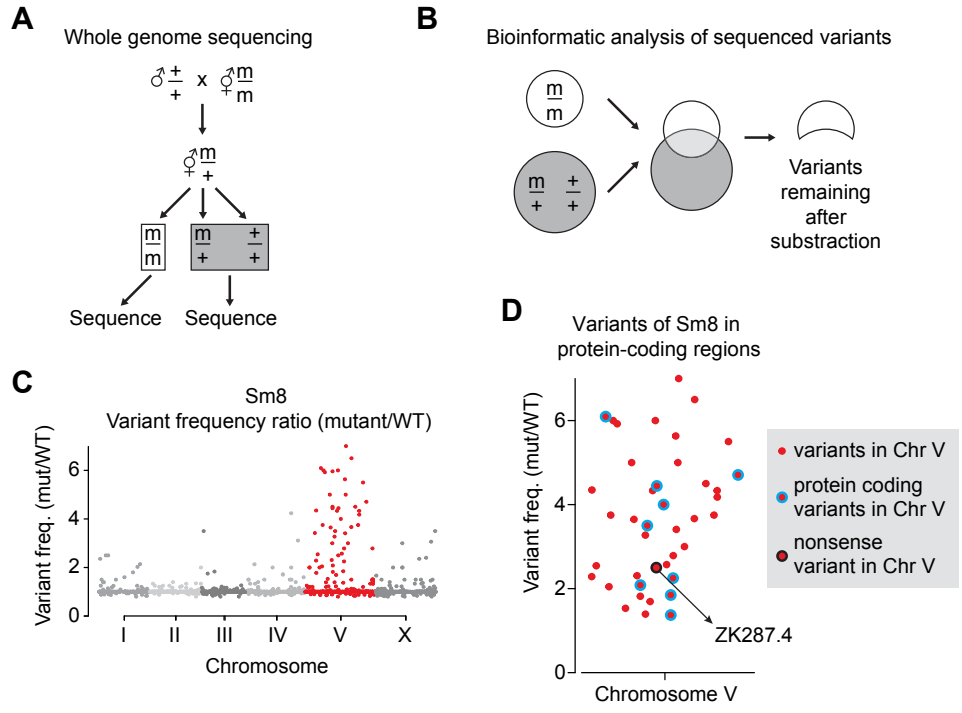

Figure 2. Identification of the causative mutation of Sm8. (A) Genetic crosses required for obtaining independent m/m and m/+ or +/+ siblings, which were combined to produce a mutant DNA pool and a nonmutant sibling DNA pool. **(B)** Simplified graphical representation of the bioinformatic analysis done to obtain the variants remaining after sibling subtraction. **(C)** Genetic variants of Sm8 plotted as correlation between chromosomal location and variant frequency (mut/WT). Highlighted in red are variants in Chr V. **(D)** Genetic variants of Chr V of Sm8 plotted as correlation between chromosomal location and variant frequency (mut/WT). Highlighted in blue are variants that result in an amino acid change and in black are variants that result in a nonsense mutation.

alyzed the development of the combined mutants. Whilst the single mutants of *crumbs(triple null)* and *ZK287.4* had a normal growth rate, we observed a strong reduction in the growth rate of the combined *ZK287.4; crumbs(triple null)* mutants, and a significant reduction in total body length (Fig. 3D-E). Together, these results indicate that mutations of *crumbs and ZK287.4* show synthetic interactions, with the combined mutations causing developmental defects.

ZK287.4 is a predicted excreted serine protease inhibitor

ZK287.4 is predicted to contain an N-terminal signal peptide and seven Kunitz domains (Fig. 4A). The N-terminal signal peptide should result in the excretion of the protein to the extracellular space, whilst the Kunitz domains are

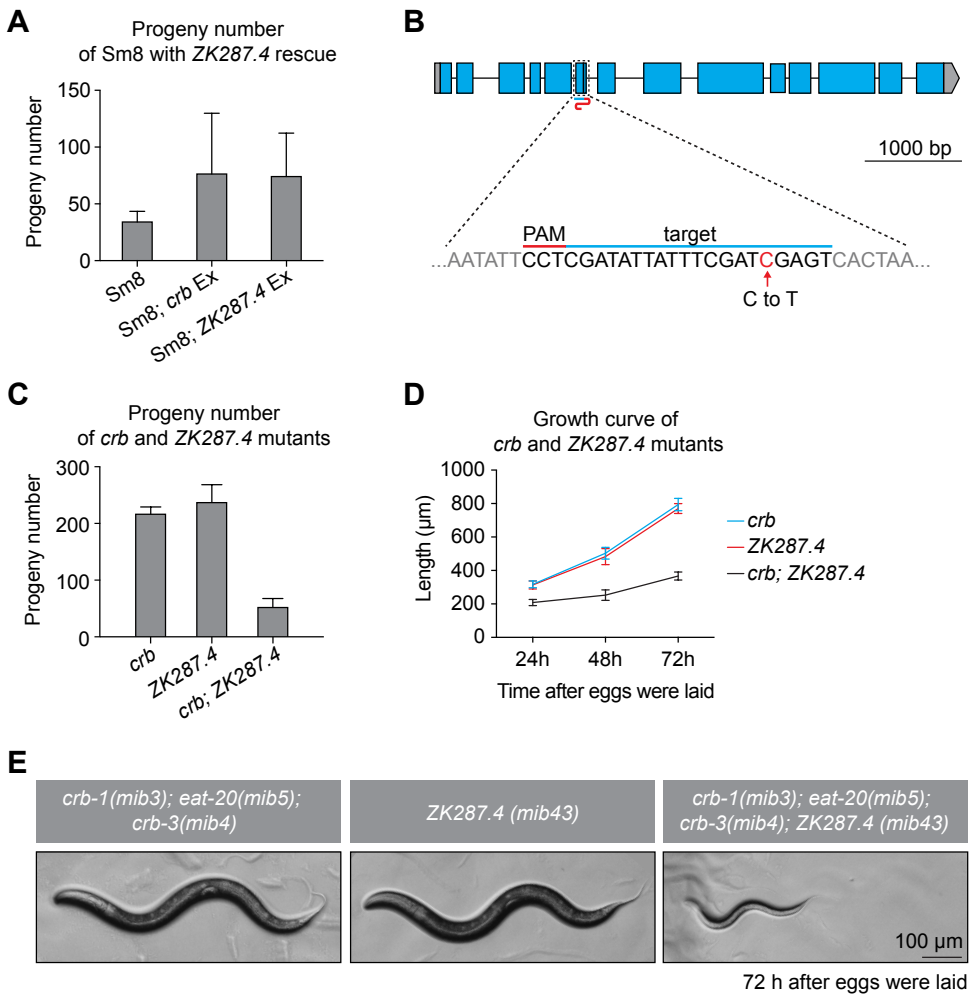

Figure 3. *ZK287.4* has synthetic defects with the *crumbs(triple null)* mutant. (A) Progeny numbers of Sm8 with an extrachromosomal array rescuing the three *crumbs* genes (*crb* Ex) or with with an extrachromosomal array rescuing *ZK287.4* (*ZK287.4* Ex). Data show mean ± SD. **(B)** Gene prediction of *ZK287.4* with sgRNA target site indicated by blue/red inverted S shape symbol. The single nucleotide change is highlighted by the red arrow. Grey boxes indicate untranslated regions. **(C)** Progeny numbers of *crb-1(mib3); eat-20(mib5); crb-3(mib4)*, *ZK287.4(mib43)* or the combined *crb-1(mib3); eat-20(mib5); crb-3(mib4)*; *ZK287.4(mib43)* mutants. Data show mean ± SD. **(D)** Growth curve of *crb-1(mib3); eat-20(mib5); crb-3(mib4)*, *ZK287.4(mib43)* or the combined *crb-1(mib3); eat-20(mib5); crb-3(mib4)*; *ZK287.4(mib43)* mutants from egg laying. Data show mean ± SD. **(E)** Transmitted light images of *crb-1(mib3); eat-20(mib5); crb-3(mib4)*, *ZK287.4(mib43)* or the combined *crb-1(mib3); eat-20(mib5); crb-3(mib4)*; *ZK287.4(mib43)* mutants whose eggs were laid 72 hr before.

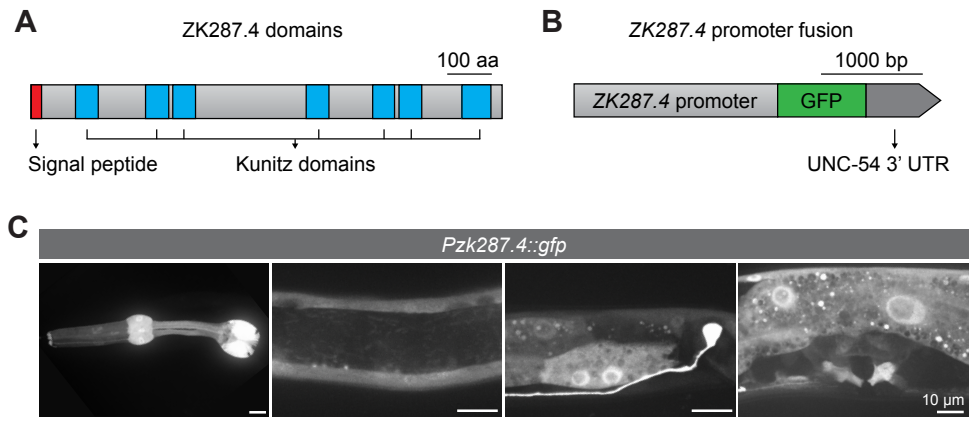

Figure 4. ZK287.4 is expressed in epithelial tissues. (A) Graphical representation of the predicted domains of ZK287.4. **(B)** Graphical representation of the ZK287.4 promoter fusion. The 2000 bp upstream of the start of *ZK287.4* were fused with the sequence encoding a green fluorescent protein (GFP) and the 3′ UTR of *unc-54*. **(C)** Distribution of GFP expressed from the *ZK287.4* promoter fusion explained in (B).

generally found in protease inhibitors (Kunitz and Northrop, 1936; Ranasinghe and McManus, 2013). To investigate the function of ZK287.4, we analyzed its expression pattern. We expressed GFP from the promoter region of *ZK287.4* (the 2000 bp upstream of the ZK287.4 start codon) using the UNC-54 3′ UTR in wild-type animals (Fig. 4B). The resulting transcriptional fusion allowed us to visualize the tissues in which ZK287.4 is being transcribed. *pZK287.4*-driven GFP expression was visible in the pharynx, body wall muscles, intestine, neurons, and vulva (Fig. 4C), indicating that the protein has a broad expression pattern.

ZK287.4; crumbs combined mutants have apical morphology defects

As the combined *ZK287.4; crumbs(triple null)* mutants show synthetic defects, we next examined these mutants in more detail. First we examined the localization pattern of a ubiquitously expressed PH::GFP fusion that labels all cell membranes. In wild-type animals, as well as in *crumbs(triple null)* and *ZK287.4* single mutants, the apical side of the intestine is seen as two parallel lines surrounding a lumen of approximately constant diameter. However, in the combined *ZK287.4; crumbs(triple null)* mutants, we observed abnormalities in the lumen such as short stretches showing a widened lumen (Fig. 5A). This defect, which varied in severity between animals, was also apparent when we used a YFP::ACT-5 actin marker to visualize the apical domain. YFP::ACT-5 localizes to the microvilli and the terminal web. Upon combined depletion of *crumbs(triple null)* and *ZK287.4*, we observe actin-containing bubbles bulging from the apical domain into the cytoplasm (Fig. 5B).

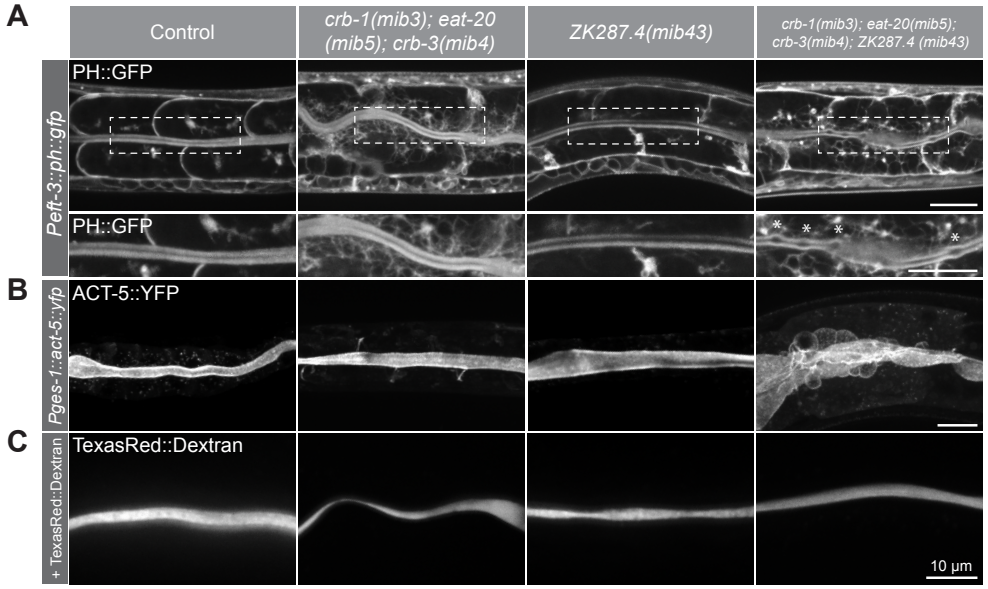

Figure 5. *crb-1(mib3); eat-20(mib5); crb-3(mib4); ZK287.4(mib43)* mutants have apical morphology defects. (A-C) Distribution of PH::GFP (A), ACT-5::YFP (B) or TexasRed::Dextran in control, *crb-1(mib3); eat-20(mib5); crb-3(mib4)*, *ZK287.4(mib43)* or the combined *crb-1(mib3); eat-20(mib5); crb-3(mib4)*; *ZK287.4(mib43)* mutants.

The defects observed in the apical side lead us to question whether epithelial integrity would be preserved in the combined *ZK287.4; crumbs(triple null)* mutants. In order to address this question, we fed the animals with a membrane impermeable Texas Red-dextran conjugate. In wild-type animals, as well as in *ZK287.4* and *crumbs(triple null)* mutants, Texas Red signal filled the lumen contiguously and was not detected outside of the lumen. The distribution of Texas Red signal was not altered in the combined *ZK287.4; crumbs(triple null)* mutants, indicating that epithelial integrity is preserved in *ZK287.4; crumbs(triple null)* mutants (Fig. 5C).

Taken together, these results indicate that even though ZK287.4 and Crumbs are not essential for the epithelial integrity of the lumen, they are necessary for apical domain homeostasis.

Discussion

Sythetic defects between a *crumbs* triple mutant and a mutation in the uncharacterized gene *ZK287.4*

In this work we have performed a forward genetic screen for synthetic interactions with a triple *crumbs* mutant, which is not essential in *C. elegans*. We identified seven mutations that show synthetic defects when combined with the triple *crumbs* mutant, and we showed that one of the causative mutations is located within the *ZK287.4* coding region. *ZK287.4; crumbs(triple null)* combined mutants are small in size and display apical morphology defects. The apical morphology defects were present in most, but not all, of the worms, and ranged from small lumen enlargements to bulges protruding into the cytoplasm of the intestinal cells. The continuity of the lumen and epithelial integrity of the intestine were not disrupted. Finally, we showed that ZK287.4 contains seven Kunitz domains and a signal peptide, predicting ZK287.4 to be excreted to the extracellular space. Expression analysis suggests that it has a wide expression pattern.

Kunitz domains are generally found in protease inhibitors, which are present in all metazoa. Kunitz inhibitors are serine protease inhibitors, and the specificity of the inhibition is determined by the amino acids at the reactive site. They act in a substrate-like manner, forming stable complexes of 1:1 stoichiometry with their target enzymes, which lose all activity (Kunitz and Northrop, 1936; Laskowski and Kato, 1980; Ranasinghe and McManus, 2013). Some Kunitz inhibitors, referred to as Kunitz-type toxins, block cation permeating channels (González et al., 2009; Harvey, 2001). ZK287.4 is most similar to Drosophila Papilin, human Tissue Factor Pathway Inhibitor (TFPI), and alpha-1-microglobulin/bikunin precursor (AMBP). Papilin is involved in cell rearrangement, crucial during development (Kramerova et al., 2000), whilst TFPI functions as a coagulation inhibitor (Brummel-Ziedins and Mann, 2018) and bikunin has anti-inflammatory capabilities. Due to the diverse function of the homologs, it is unclear what the function of ZK287.4 may be. However, the stable interactions that Kunitz inhibitors form with their substrates indicates that analyzing the interactors of ZK287.4 by mass spectrometry may shed light on to the function of ZK287.4.

The presence of multiple Kunitz domains strongly suggests that ZK287.4 is a serine protease inhibitor, a family that has been shown to be important in different pathways in *C. elegans*, such as cuticle remodeling, embryonic hypodermal enclosure and excretory canal morphology (Kramerova et al., 2000; Page et al., 2006). Moreover, serine proteases have been shown to be important in epithelia in different processes. They modulate barrier function in epithelial tissues by regulating ion permeability, direct cleavage of tight junction proteins or activation of proteinase activated receptors (PAR), which can induce a con-

traction of the actomyosin cortex and opening of the apical junction complex (Spaendonk et al., 2017; Swystun et al., 2005). We have shown here using a Texas Red-dextran conjugate that epithelial integrity does not seem to be disrupted in *C. elegans ZK287.4* mutants, although use of smaller sizes of dextran could provide additional information. It also remains to be investigated if ion permeability is disrupted or whether PARs are activated. Moreover, it is possible that due to its broad expression pattern, ZK287.4 does not only function in the intestine but in a wide variety of tissues.

In order to gain insight into the function of Crumbs it is crucial to understand the function of the genes with which *crumbs* acts redundantly, but also to study the phenotypes observed in the synthetic mutants. One of the most striking phenotypes of *crumbs(triple null); ZK287.4* double mutants is their small size. Whilst the animals are small, they are also relatively thin, different from the Dumpy phenotype which results in small and wide worms. Body length in *C. elegans* can be adversely affected by a number of defects: (1) abnormal pharyngeal neurotransmission, abnormal pharyngeal anatomy, or a defects in food uptake, which can result in long-term starvation (Mörck and Pilon, 2006), (2) defects in the TGFβ-related signaling pathway (Savage-Dunn et al., 2003), (3) defects in the spectrin pathway, causing impaired embryonic constriction, or (4) defects in the calcineurin pathway, causing impaired sensory neuron signaling (Mörck and Pilon, 2006). Mutation of *eat-20* Crb2 results in slightly smaller worms due to slower pharynx pumping rate, which results in a feeding defect (Shibata et al., 2000). However, the difference in size in comparison to wild type is minimal, and *ZK287.4* mutants show no defect in body length. Whilst we still do not know which pathway is affected in the *crumbs(triple null); ZK287.4* combined mutants, examining if any of these pathways is affected, or if the *crumbs(triple null); ZK287.4* mutants or the single mutants shows additive effect with mutants of the other pathways, which would indicate separate mechanisms, would be very informative in the understanding of the phenotype and of the functions of both Crumbs and ZK287.4.

A whole genome screen in *C. elegans* to identify synthetic defects with Crumbs

In this study we have performed a whole genome screen to identify synthetic defects with Crumbs and we have obtained 7 mutants, one of which we have characterized. With the same approach, several things could be done in order to increase our knowledge of Crumbs.

Firstly, EMS induces loss-of-function mutations in a given gene at an average frequency of one per 2000 mutagenized haploid genomes (Anderson, 1995; Brenner, 1974; Rosenbluth et al., 1983). In this work we have screened 1680 haploid genomes, meaning that we are unlikely to have seen a loss-of-function mutation in every gene. Moreover, in order to be confident with the number of genomes screened, screening double the number of haploid genomes that would give a mutation in each gene would be ideal. As a result, in order to be confident that we have looked at all the synthetic defects with the *crumbs(triple null)*, we would need to screen 4000 haploid genomes, or 2,4 times more than what we have done. This is if we do not take into consideration synthetic defects that require more than two genes to be mutated at the same time. It is likely then that there are many more genes that give synthetic defects with Crumbs and identifying them could increase greatly our knowledge of Crumbs' functions.

Secondly, we have identified 7 mutants in our screen, and we have confirmed the causative mutation of one of them, Sm8. Our average coverage in the WGS analysis was 50x, which should provide clear reads in order to identify the causative mutations of each mutant. However, identifying the causative mutations of the other mutants was not as straight forward as identifying the causative mutation of Sm8, which may be due to the fact that we did not back-cross the mutant strains before performing the whole-genome sequencing. In order to improve our analysis, it would be greatly recommended to back-cross the mutant strains to the starting strain 3 to 5 times, which would reduce the amount of mutations in each strain. Moreover, we pooled together the heterozygous progeny with the wild type progeny due to the difficulty of discerning both pools with a phenotypic analysis, which resulted in some causative mutant alleles in the "wild type" pool. It would be ideal to separate the heterozygous progeny from the wild-type progeny as it would prevent having causative mutant alleles in the "wild type" pool, facilitating the analysis and increasing the chances of identifying the causative mutations. Identifying the causative mutations of the other mutants could clarify the function of Crumbs.

Finally, we have used EMS to introduce mutations in the *C. elegans* genome. EMS is a chemical mutagen very widely used in *C. elegans* and has identified genes involved in numerous processes. It has the advantage that apart from loss of function mutations, it can also produce mutations that result in partial loss-of-function or gain-of-function (Anderson, 1995). However, there are other types of screens that can be done, each with its advantages and disadvantages. RNAi screens, for example, have the advantage that the gene that is targeted is known, bypassing the need for genetic mapping and sequencing. Recent technological advances have also simplified performing genome-wide RNAi screens. The disadvantage of RNAi screens is that feeding RNAi does not reduce protein levels in every tissue and may not be efficient enough to reduce levels of highly expressed proteins (Fire et al., 1998; Jagadeesan and Hakkim, 2018; Kamath and Ahringer, 2003). Taking into account the benefits and drawbacks of RNAi screens, and specially the ease at which a clonal screen to look for synthetic defects could be done, it would also be a suitable approach to gain insight into the function of redundant proteins. Lastly, protein-protein interaction studies, such as Y2H, affinity purification and proximity labeling could also be of great use in order to identify interactors of Crumbs.

Materials and Methods

C. elegans strains

All *C. elegans* strains used in this study are derived from the N2 Bristol strain, and are listed in Table 1. All strains were maintained at 20 °C on Nematode Growth Medium (NGM) plates seeded with *Escherichiae coli* OP50 bacteria under standard conditions (Brenner, 1974).

Generation of transgenic lines

Young adult hermaphrodites were injected in the germline using an inverted micro-injection setup (Eppendorf FemtoJet 4x mounted on a Zeiss Axio Observer A.1 equipped with an Eppendorf Transferman 4r).

To rescue the triple *crumbs* deletion with a wild-type copy of each *crumbs* gene, an extrachromosomal (Ex) array rescuing the three *crumbs* genes was injected into the *crb-1(mib3); eat-20(mib5); crb-3(mib4)* deletion background. The injection mix, prepared in MilliQ H_2O, contained 10 ng/µL of each fosmid (WRM066bF04 carrying crb-1, WRM062bD06 carrying *eat-20* and WRM0628dH07 carrying *crb-3)*, 50 ng/µL of lambda DNA and 2.5 ng/µL Pmyo-2::mCherry to generate multiple independent strains carrying stable extrachromosomal arrays.

To rescue Sm8 with a wild-type copy of *ZK287.4*, an extrachromosomal (Ex) array rescuing ZK287.4 was injected into the Sm8 background. The injection mix, prepared in MilliQ H_2O, contained 60 ng/µL of WRM0610cG12 fosmid, 50 ng/µL of lambda DNA and 5 ng/µL Pmyo-3::H2B::eGFP to generate multiple independent strains carrying stable extrachromosomal arrays.

The *ZK287.4* promoter fusion was generated in an N2 background. The 2000 bp upstream of the start codon of *ZK287.4* were amplified using the forward primer 5′-gcggCGCGccccaggatcgttcactgcgtg and reverse 3′- gcgcGGCCgcttctgacccattcgggccaa. The PCR product was digested using AscI/NotI and ligated into a pBSK backbone which contained GFP followed by the *unc-54* 3′ UTR.

Synthetic lethality screen

Synthetic mutants were obtained through an F2 clonal screen using standard EMS mutagenesis (Brenner, 1974; Kutscher, 2014) of strain BOX203. Shortly, young-adult hermaphrodites were collected and washed three times in M9 (0.22 M KH_2PO_4, 0.42 M Na_2HPO_4, 0.85 M NaCl, 0.001 M $MgSO_4$) buffer 0.05% Tween-20. After the last wash, animals were incubated in 4 mL of 50 mM ethyl methane sulfonate in M9 buffer for 4 h at 20 ºC with gentle constant agitation. Animals were washed several times with M9 buffer and placed on large NGM plates. F1 worms were transferred to new

plates and allowed to self-fertilize. Their progeny (F2) was subsequently picked to individual plates. The F3 was scored for synthetic mutations at the L4 stage. Synthetic mutants were identified by presenting detrimental phenotypes in the absence of the extrachromosomal array rescuing the three *Crumbs* genes.

Whole genome sequencing

Synthetic mutant strains were mated to BOX203 males and several F1 heterozygous cross-progeny were allowed to self-fertilize. 100 F2 self-progeny were subsequently picked to individual plates and scored for Sm/Sm; or Sm/+ and +/+. DNA was prepared using a DNeasy Blood & Tissue Kit (Qiagen) following the protocol of the Kaganovich lab. Libraries were prepared with Truseq DNA nano prep and sequenced using Illumina HiSeq X Ten system, obtaining paired reads of up to 150 bp. Variants were called and filtered as previously described (Joseph et al., 2018) and analyzed using the Integrative Genomics Viewer (Robinson et al., 2017).

CRISPR/Cas9 genome engineering

The ZK287.4 R338* mutation was generated by homology-directed repair of CRISPR/Cas9-induced DNA double-strand breaks in a *pha-1(e2123ts)* background. The fusion was generated using the PJW1285 plasmid, which contains Cas9 with a sgRNA targeting *pha-1* for co-conversion. The sgRNA targeting the *ZK287.4* locus was expressed from a plasmid under control of a U6 promoter. To generate sgRNA vector, antisense oligonucleotide pairs (5′-TCTTGACTCGATCGAAATAATATCG, 5′-AAACCGATATTATTTCGATCGAGTC) were annealed and ligated into BbsI-linearized pJJR50 (Addgene #75026) (Waaijers et al., 2016). Homology-directed repair was driven by a synthesized single-stranded oligodeoxynucleotide with 35 bp homology arms(5′-GGAATAGAAGAACCGTTCACATTTCTTAGTGACTCAGTCGAA GTAGTATCGAGGAATATTGAATGGCCCGTTGCCAATTGCTG). The homology arms included mutations of the sgRNA recognition sites to prevent re-cutting after repair. The injection mix was prepared in MilliQ H_2O and contained 60 ng/µL pJW1285 (U6::gRNA *pha-1* and Cas9 construct), 50 ng/µL ssODN repair template to correct pha-1(e2123), 50 ng/µL U6::sgRNA target construct and 50 ng/µL *ZK287.4* repair template. Young adult hermaphrodites were injected in the germline using an inverted micro-injection setup (Eppendorf FemtoJet 4x mounted on a Zeiss Axio Observer A.1 equipped with an Eppendorf Transferman 4r). Integration events were selected using *pha-1* co-CRISPR approach (Ward, 2015). Correct editing was confirmed by Sanger sequencing (Macrogen Europe) of PCR amplicons encompassing the edited genomic region.

Brood size and embryonic lethality

L4 animals (P0) were grown on individual plates at 20 °C and transferred to a fresh plate every 24 h for 6 consecutive days. Hatched and unhatched progeny were scored 24 h after removal of the P0, and embryonic lethality was scored 48 h after removal of the P0.

***C. elegans* growth curves**

In order to obtain synchronized worm populations, adults were placed in fresh plates for 1 hr. After that period, adults were carefully picked off to leave behind the eggs that were laid within that time span.

To measure growth curves, synchronized L1 animals were placed on NGM plates seeded with *E. coli* OP50. Images were taken in 24 hr intervals up to 72 hr, using a Zeiss Axio Zoom.V16 equipped with a PlanNeoFluar Z 1x/0.25 objective and Axiocam 506 color camera, driven by Zen Pro software. Animal length was quantified in ImageJ(FIJI) software by drawing a spline along the center line of the animal (Rueden et al., 2017; Schindelin et al., 2012).

Microscopy

Live imaging of *C. elegans* larvae was done by mounting larvae on 5% agarose pads in a 10 mM Tetramisole solution in M9 buffer to induce paralysis. Spinning disk confocal imaging was performed using a Nikon Ti-U microscope driven by MetaMorph Microscopy Automation & Image Analysis Software (Molecular Devices) and equipped with a Yokogawa CSU-X1-M1 confocal head and an Andor iXon DU-885 camera, using 60x or 100x 1.4 NA objectives. All stacks along the z-axis were obtained at 0.25 µm intervals, and all images were analyzed and processed using ImageJ(FIJI) and Adobe Photoshop. Imaging of plates was performed using a Zeiss Axio Zoom.V16 equipped with a PlanNeoFluar Z 1x/0.25 objective and Axiocam 506 color camera, driven by Zen Pro software.

Texas Red-dextran assay

Mixed-stage populations were collected in egg buffer (118 mM NaCl, 48 mM KCl, 2 mM MgCl2, 2 mM CaCl2, 25 mM HEPES pH 7.3) and washed three times. The worm pellet was concentrated and resuspended in a solution containing 1 mg/ml Texas Red-dextran (40,000 MW, D1829, Molecular Probes). The samples were incubated for 90 min while shaking at 300 rpm in the dark. The dye in solution was removed by washing the samples with egg buffer until the solution was clear, and animals were imaged directly.

Table 1. Strain list

Strain	Genotype	Acknowledgement
BOX142	*crb-1(mib3), eat-20(mib5), crb-3(mib4) X*	
BOX203	*crb-1(mib3), eat-20(mib5), crb-3(mib4) X; mibEx45[crb-1 fosmid 10ng/µL; eat-20 fosmid 10ng/µL; crb-3 fosmid 10ng/µL; Pmyo-2::mCherry 2.5ng/µL]*	
BOX312	*ZK287.4(mib43) V*	
BOX322	*ZK287.4(mib43) V; crb-1(mib3), eat-20(mib5), crb-3(mib4) X*	
SV1677	*CxTi 10816(he259[Peft-3::PH::eGFP::LOV::tbb-2]) IV*	Sander van den Heuvel
BOX334	*CxTi 10816(he259[Peft-3::PH::eGFP::LOV::tbb-2]) IV; crb-1(mib3), eat-20(mib5), crb-3(mib4) X*	
BOX338	*CxTi 10816(he259[Peft-3::PH::eGFP::LOV::tbb-2]) IV; ZK287.4(mib43) V*	
BOX335	*CxTi 10816(he259[Peft-3::PH::eGFP::LOV::tbb-2]) IV; ZK287.4(mib43) V; crb-1(mib3), eat-20(mib5), crb-3(mib4) X*	
JM125	*caIs[Pges-1p::YFP::ACT-5]*	James McGhee
BOX378	*crb-1(mib3), eat-20(mib5), crb-3(mib4) X; caIs[Pges-1p::YFP::ACT-5]*	
BOX682	*ZK287.4(mib43) V; caIs[Pges-1p::YFP::ACT-5]*	
BOX507	*ZK287.4(mib43) V; crb-1(mib3), eat-20(mib5), crb-3(mib4) X; caIs[Pges-1p::YFP::ACT-5]*	

Supplementary figure

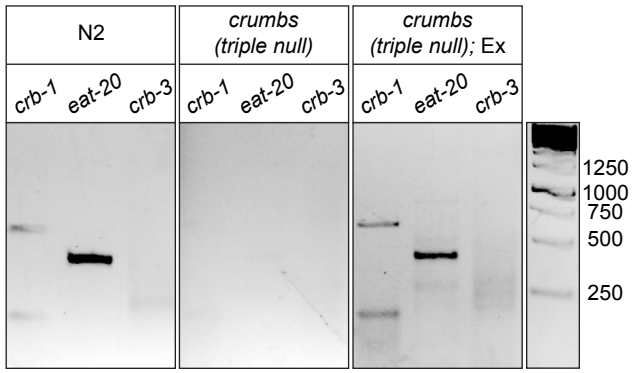

Figure S1. Expression of *crb-1*, *eat-20*, and *crb-3*. Expression of each Crumbs protein determined by reverse-transcriptase PCR in the following strains: wild type, triple *crumbs* deletion, and a triple *crumbs* deletion strain carrying an extrachromosomal array that expressed the three Crumbs proteins.

Acknowledgements

We thank members of the S van den Heuvel and M Boxem groups for helpful discussions, and J Ramalho for making strain BOX203. We also thank Wormbase (Harris et al., 2020) and the Biology Imaging Center, Faculty of Sciences, Department of Biology, Utrecht University. Some strains were provided by the Caenorhabditis Genetics Center, which is funded by NIH Office of Research Infrastructure Programs (P40 OD010440). This work was supported by the Netherlands Organization for Scientific Research (NWO)-ALW Open Program 824.14.021 and NWO-VICI 016.VICI.170.165 grants to M Boxem, and the European Union's Horizon 2020 research and innovation programme under the Marie Skłodowska-Curie grant agreement No. 675407 – PolarNet.

Author contributions

Victoria G Castiglioni, Conceptualization, Formal analysis, Investigation, Visualization, Methodology, Writing - original draft, Writing - review and editing; Mike Boxem, Conceptualization, Supervision, Funding acquisition, Visualization, Project administration, Writing - review and editing

"People who think they know everything are a great annoyance to those of us who do."

Isaac Asimov

Addendum

References

Abrams, J. and Nance, J. (2020). A polarity pathway for exocyst-dependent intracellular tube extension. *bioRxiv* 2020.10.05.327247.

Aceto, D., Beers, M. and Kemphues, K. J. (2006). Interaction of PAR-6 with CDC-42 is required for maintenance but not establishment of PAR asymmetry in C. elegans. *Dev. Biol.* **299**, 386–397.

Achilleos, A., Wehman, A. M. and Nance, J. (2010). PAR-3 mediates the initial clustering and apical localization of junction and polarity proteins during C. elegans intestinal epithelial cell polarization. *Dev. Camb. Engl.* **137**, 1833–1842.

Aguilar-Aragon, M., Elbediwy, A., Foglizzo, V., Fletcher, G. C., Li, V. S. W. and Thompson, B. J. (2018). Pak1 Kinase Maintains Apical Membrane Identity in Epithelia. *Cell Rep.* **22**, 1639–1646.

Ahmed, S. M. and Macara, I. G. (2017). The Par3 polarity protein is an exocyst receptor essential for mammary cell survival. *Nat. Commun.* **8**, 14867.

Albertson, R. and Doe, C. Q. (2003). Dlg, Scrib and Lgl regulate neuroblast cell size and mitotic spindle asymmetry. *Nat. Cell Biol.* **5**, 166–170.

Albertson, D. G. and Thomson, J. N. (1976). The pharynx of Caenorhabditis elegans. *Philos. Trans. R. Soc. Lond. B. Biol. Sci.* **275**, 299–325.

Ali, N. J. A., Dias Gomes, M., Bauer, R., Brodesser, S., Niemann, C. and Iden, S. (2016). Essential Role of Polarity Protein Par3 for Epidermal Homeostasis through Regulation of Barrier Function, Keratinocyte Differentiation, and Stem Cell Maintenance. *J. Invest. Dermatol.* **136**, 2406–2416.

Allam, A. H., Charnley, M. and Russell, S. M. (2018). Context-Specific Mechanisms of Cell Polarity Regulation. *J. Mol. Biol.* **430**, 3457–3471.

Almagor, L., Ufimtsev, I. S., Ayer, A., Li, J. and Weis, W. I. (2019). Structural insights into the aPKC regulatory switch mechanism of the human cell polarity protein lethal giant larvae 2. *Proc. Natl. Acad. Sci. U. S. A.*

Almeida, F. N. de, Walther, R. F., Pressé, M. T., Vlassaks, E. and Pichaud, F. (2019). Cdc42 defines apical identity and regulates epithelial morphogenesis by promoting apical recruitment of Par6-aPKC and Crumbs. *Development* **146**,.

Altschul, S. F., Madden, T. L., Schäffer, A. A., Zhang, J., Zhang, Z., Miller, W. and Lipman, D. J. (1997). Gapped BLAST and PSI-BLAST: a new generation of protein database search programs. *Nucleic Acids Res.* **25**, 3389–3402.

Altschul, S. F., Wootton, J. C., Gertz, E. M., Agarwala, R., Morgulis, A., Schäffer, A. A. and Yu, Y.-K. (2005). Protein database searches using compositionally adjusted substitution matrices. *FEBS J.* **272**, 5101–5109.

Altun, Z. F. and Hall, D. H. (2009). WormAtlas Hermaphrodite Handbook - Pericellular Structures. *WormAtlas*.

Anderson, P. (1995). Mutagenesis. *Methods Cell Biol.* **48**, 31–58.

Anderson, D. C., Gill, J. S., Cinalli, R. M. and Nance, J. (2008). Polarization of the C. elegans Embryo by RhoGAP-Mediated Exclusion of PAR-6 from Cell Contacts. *Science* **320**, 1771–1774.

Aono, S., Legouis, R., Hoose, W. A. and Kemphues, K. J. (2004). PAR-3 is required for epithelial cell polarity in the distal spermatheca of C. elegans. *Development* **131**, 2865.

Assémat, E., Bazellières, E., Pallesi-Pocachard, E., Le Bivic, A. and Massey-Harroche, D. (2008). Polarity complex proteins. *Biochim. Biophys. Acta BBA - Biomembr.* **1778**, 614–630.

Atherton, J., Luo, Y., Xiang, S., Yang, C., Rai, A., Jiang, K., Stangier, M., Vemu, A., Cook, A. D., Wang, S., et al. (2019). Structural determinants of microtubule minus end preference in CAMSAP CKK domains. *Nat. Commun.* **10**, 5236.

Atwood, S. X., Chabu, C., Penkert, R. R., Doe, C. Q. and Prehoda, K. E. (2007). Cdc42 acts downstream of Bazooka to regulate neuroblast polarity through Par-6 aPKC. *J. Cell Sci.* **120**, 3200–3206.

Atwood, S. X., Li, M., Lee, A., Tang, J. Y. and Oro, A. E. (2013). GLI activation by atypical protein kinase C ι/λ regulates the growth of basal cell carcinomas. *Nature* **494**, 484–488.

Bachmann, A., Schneider, M., Theilenberg, E., Grawe, F. and Knust, E. (2001). Drosophila Stardust is a partner of Crumbs in the control of epithelial cell polarity. *Nature* **414**, 638–643.

Bagnat, M., Cheung, I. D., Mostov, K. E. and Stainier, D. Y. R. (2007). Genetic control of single lumen formation in the zebrafish gut. *Nat. Cell Biol.* **9**, 954–960.

Bailey, M. J. and Prehoda, K. E. (2015). Establishment of Par-Polarized Cortical Domains via Phosphoregulated Membrane Motifs. *Dev. Cell* **35**, 199–210.

Balklava, Z., Pant, S., Fares, H. and Grant, B. D. (2007). Genome-wide analysis identifies a general requirement for polarity proteins in endocytic traffic. *Nat. Cell Biol.* **9**, 1066–1073.

Beatty, A., Morton, D. and Kemphues, K. (2010). The C. elegans homolog of Drosophila Lethal giant larvae functions redundantly with PAR-2 to maintain polarity in the early embryo. *Development* **137**, 3995–4004.

Beatty, A., Morton, D. G. and Kemphues, K. (2013). PAR-2, LGL-1 and the CDC-42 GAP CHIN-1 act in distinct pathways to maintain polarity in the C. elegans embryo. *Dev. Camb. Engl.* **140**, 2005–2014.

Beers, M. and Kemphues, K. (2006). Depletion of the co-chaperone CDC-37 reveals two modes of PAR-6 cortical association in C. elegans embryos. *Dev. Camb. Engl.* **133**, 3745–3754.

Bell, G. P., Fletcher, G. C., Brain, R. and Thompson, B. J. (2015). Aurora kinases phosphorylate Lgl to induce mitotic spindle orientation in Drosophila epithelia. *Curr. Biol. CB* **25**, 61–68.

Benton, R. and St Johnston, D. (2003). *Drosophila* PAR-1 and 14-3-3 inhibit Bazooka/PAR-3 to establish complementary cortical domains in polarized cells. *Cell* **115**, 691–704.

Berger, S., Bulgakova, N. A., Grawe, F., Johnson, K. and Knust, E. (2007). Unraveling the genetic complexity of Drosophila stardust during photoreceptor morphogenesis and prevention of light-induced degeneration. *Genetics* **176**, 2189–2200.

Betschinger, J., Mechtler, K. and Knoblich, J. A. (2003). The Par complex directs asymmetric cell division by phosphorylating the cytoskeletal protein Lgl. *Nature* **422**, 326–330.

Bhat, M. A., Izaddoost, S., Lu, Y., Cho, K.-O., Choi, K.-W. and Bellen, H. J. (1999). Discs Lost, a Novel Multi-PDZ Domain Protein, Establishes and Maintains Epithelial Polarity. *Cell* **96**, 833–845.

Bilder, D., Schober, M. and Perrimon, N. (2003). Integrated activity of PDZ protein complexes regulates epithelial polarity. *Nat. Cell Biol.* **5**, 53–58.

Blankenship, J. T., Fuller, M. T. and Zallen, J. A. (2007). The Drosophila homolog of the Exo84 exocyst subunit promotes apical epithelial identity. *J. Cell Sci.* **120**, 3099–3110.

Bonello, T. T. and Peifer, M. (2019a). Scribble: A master scaffold in polarity, adhesion, synaptogenesis, and proliferation. *J. Cell Biol.* **218**, 742–756.

Bonello, T. T. and Peifer, M. (2019b). Scribble and Discs-large direct adherens junction positioning and supermolecular assembly to establish apical-basal polarity. *bioRxiv* 654509.

Bossinger, O., Klebes, A., Segbert, C., Theres, C. and Knust, E. (2001a). Zonula adherens formation in Caenorhabditis elegans requires dlg-1, the homologue of the Drosophila gene discs large. *Dev Biol* **230**, 29–42.

Boxem, M., Maliga, Z., Klitgord, N., Li, N., Lemmens, I., Mana, M., de Lichtervelde, L., Mul, J. D., van de Peut, D., Devos, M., et al. (2008). A protein domain-based interactome network for *C. elegans* early embryogenesis. *Cell* **134**, 534–545.

Boyd, L., Guo, S., Levitan, D., Stinchcomb, D. T. and Kemphues, K. J. (1996). PAR-2 is asymmetrically distributed and promotes association of P granules and PAR-1 with the cortex in C. elegans embryos. *Development* **122**, 3075–3084.

Brajenovic, M., Joberty, G., Küster, B., Bouwmeester, T. and Drewes, G. (2004). Comprehensive proteomic analysis of human Par protein complexes reveals an interconnected protein network. *J. Biol. Chem.* **279**, 12804–12811.

Brenner, S. (1974). The Genetics of Caenorhabditis Elegans. *Genetics* **77**, 71–94.

Brooks, D. R., Appleford, P. J., Murray, L. and Isaac, R. E. (2003). An essential role in molting and morphogenesis of Caenorhabditis elegans for ACN-1, a novel member of the angiotensin-converting enzyme family that lacks a metallopeptidase active site. *J. Biol. Chem.* **278**, 52340–52346.

Brummel-Ziedins, K. and Mann, K. G. (2018). Chapter 126 - Molecular Basis of Blood Coagulation. In *Hematology (Seventh Edition)* (ed. Hoffman, R.), Benz, E. J.), Silberstein, L. E.), Heslop, H. E.), Weitz, J. I.), Anastasi, J.), Salama, M. E.), and Abutalib, S. A.), pp. 1885-1905.e8. Elsevier.

Bryant, D. M., Datta, A., Rodríguez-Fraticelli, A. E., Peränen, J., Martín-Belmonte, F. and Mostov, K. E. (2010). A molecular network for de novo generation of the apical surface and lumen. *Nat. Cell Biol.* **12**, 1035–1045.

Buechner, M., Yang, Z. and Al-Hashimi, H. (2020). A Series of Tubes: The C. elegans Excretory Canal Cell as a Model for Tubule Development. *J. Dev. Biol.* **8**,.

Bulgakova, N. A. and Knust, E. (2009). The Crumbs complex: from epithelial-cell polarity to retinal degeneration. *J. Cell Sci.* **122**, 2587–2596.

C. elegans Sequencing Consortium (1998). Genome sequence of the nematode C. elegans: a platform for investigating biology. *Science* **282**, 2012–2018.

Campbell, K., Knust, E. and Skaer, H. (2009). Crumbs stabilises epithelial polarity during tissue remodelling. *J. Cell Sci.* **122**, 2604–2612.

Cao, H., Xu, R., Shi, Q., Zhang, D., Huang, J. and Hong, Y. (2017). FERM domain phosphorylation and endogenous 3′UTR are not essential for regulating the function and subcellular localization of polarity protein Crumbs. *J. Genet. Genomics* **44**, 409–412.

Caria, S., Magtoto, C. M., Samiei, T., Portela, M., Lim, K. Y. B., How, J. Y., Stewart, B. Z., Humbert, P. O., Richardson, H. E. and Kvansakul, M. (2018). Drosophila melanogaster Guk-holder interacts with the Scribbled PDZ1 domain and regulates epithelial development with Scribbled and Discs Large. *J. Biol. Chem.* **293**, 4519–4531.

Carvalho, C. A. and Broday, L. (2020). Game of Tissues: How the Epidermis Thrones C. elegans Shape. *J. Dev. Biol.* **8**, 7.

Carvalho, C. A., Moreira, S., Ventura, G., Sunkel, C. E. and Morais-de-Sá, E. (2015). Aurora A triggers Lgl cortical release during symmetric division to control planar spindle orientation. *Curr. Biol. CB* **25**, 53–60.

Chabu, C. and Doe, C. Q. (2008). Dap160/intersectin binds and activates aPKC to regulate cell polarity and cell cycle progression. *Development* **135**, 2739–2746.

Chan, E. and Nance, J. (2013). Mechanisms of CDC-42 activation during contact-induced cell polarization. *J. Cell Sci.* **126**, 1692–1702.

Chen, X. and Macara, I. G. (2005). Par-3 controls tight junction assembly through the Rac exchange factor Tiam1. *Nat. Cell Biol.* **7**, 262–269.

Chen, J., Sayadian, A.-C., Lowe, N., Lovegrove, H. E. and St Johnston, D. (2018). An alternative mode of epithelial polarity in the Drosophila midgut. *PLoS Biol.* **16**, e3000041.

Chisholm, A. D. and Hardin, J. (2005). Epidermal morphogenesis. *WormBook*.

Chisholm, A. D. and Hsiao, T. I. (2012). The Caenorhabditis elegans epidermis as a model skin. I: development, patterning, and growth. *Wiley Interdiscip. Rev. Dev. Biol.* **1**, 861–878.

Chisholm, A. D. and Xu, S. (2012). The Caenorhabditis elegans epidermis as a model skin. II: differentiation and physiological roles. *Wiley Interdiscip. Rev. Dev. Biol.* **1**, 879–902.

Chuang, M., Hsiao, T. I., Tong, A., Xu, S. and Chisholm, A. D. (2016). DAPK interacts with Patronin and the microtubule cytoskeleton in epidermal development and wound repair. *eLife* **5**,.

Claret, S., Jouette, J., Benoit, B., Legent, K. and Guichet, A. (2014). PI(4,5)P2 produced by the PI4P5K SKTL controls apical size by tethering PAR-3 in Drosophila epithelial cells. *Curr. Biol. CB* **24**, 1071–1079.

Cohen, J. D. and Sundaram, M. V. (2020). C. elegans Apical Extracellular Matrices Shape Epithelia. *J. Dev. Biol.* **8**,.

Costa, M., Draper, B. W. and Priess, J. R. (1997). The role of actin filaments in patterning the Caenorhabditis elegans cuticle. *Dev. Biol.* **184**, 373–384.

Costa, M., Raich, W., Agbunag, C., Leung, B., Hardin, J. and Priess, J. R. (1998). A Putative Catenin–Cadherin System Mediates Morphogenesis of the Caenorhabditis elegans Embryo. *J. Cell Biol.* **141**, 297–308.

Cowan, C. R. and Hyman, A. A. (2004). Asymmetric cell division in C. elegans: cortical polarity and spindle positioning. *Annu. Rev. Cell Dev. Biol.* **20**, 427–453.

Cuenca, A. A., Schetter, A., Aceto, D., Kemphues, K. and Seydoux, G. (2003). Polarization of the C. elegans zygote proceeds via distinct establishment and maintenance phases. *Dev. Camb. Engl.* **130**, 1255–1265.

David, D. J. V., Wang, Q., Feng, J. J. and Harris, T. J. C. (2013). Bazooka inhibits aPKC to limit antagonism of actomyosin networks during amnioserosa apical constriction. *Dev. Camb.*

Engl. **140**, 4719–4729.

de Vreede, G., Schoenfeld, J. D., Windler, S. L., Morrison, H., Lu, H. and Bilder, D. (2014). The Scribble module regulates retromer-dependent endocytic trafficking during epithelial polarization. *Development* **141**, 2796–2802.

di Pietro, F., Echard, A. and Morin, X. (2016). Regulation of mitotic spindle orientation: an integrated view. *EMBO Rep.* **17**, 1106–1130.

Dickinson, D. J., Nelson, W. J. and Weis, W. I. (2011). A Polarized Epithelium Organized by β- and α-Catenin Predates Cadherin and Metazoan Origins. *Science* **331**, 1336–1339.

Dickinson, D. J., Pani, A. M., Heppert, J. K., Higgins, C. D. and Goldstein, B. (2015). Streamlined Genome Engineering with a Self-Excising Drug Selection Cassette. *Genetics* **200**, 1035–1049.

Dickinson, D. J., Schwager, F., Pintard, L., Gotta, M. and Goldstein, B. (2017). A Single-Cell Biochemistry Approach Reveals PAR Complex Dynamics during Cell Polarization. *Dev. Cell* **42**, 416-434.e11.

Dickinson, D. J., Slabodnick, M. M., Chen, A. H. and Goldstein, B. (2018). SapTrap assembly of repair templates for Cas9-triggered homologous recombination with a self-excising cassette. *MicroPublication Biol.* **2018**,.

Dimov, I. and Maduro, M. F. (2019). The C. elegans intestine: organogenesis, digestion, and physiology. *Cell Tissue Res.* **377**, 383–396.

Doerflinger, H., Vogt, N., Torres, I. L., Mirouse, V., Koch, I., Nüsslein-Volhard, C. and St Johnston, D. (2010). Bazooka is required for polarisation of the Drosophila anterior-posterior axis. *Dev. Camb. Engl.* **137**, 1765–1773.

Dong, W., Zhang, X., Liu, W., Chen, Y., Huang, J., Austin, E., Celotto, A. M., Jiang, W. Z., Palladino, M. J., Jiang, Y., et al. (2015). A conserved polybasic domain mediates plasma membrane targeting of Lgl and its regulation by hypoxia. *J. Cell Biol.* **211**, 273–286.

Dong, W., Lu, J., Zhang, X., Wu, Y., Lettieri, K., Hammond, G. R. and Hong, Y. (2019). A Polybasic Domain in aPKC Mediates Par-6-Dependent Control of Plasma Membrane Targeting and Kinase Activity. *bioRxiv* 588624.

Dong, W., Lu, J., Zhang, X., Wu, Y., Lettieri, K., Hammond, G. R. and Hong, Y. (2020). A polybasic domain in aPKC mediates Par6-dependent control of membrane targeting and kinase activity. *J. Cell Biol.* **219**,.

Dormoy, V., Tormanen, K. and Sütterlin, C. (2013). Par6γ is at the mother centriole and controls centrosomal protein composition through a Par6α-dependent pathway. *J. Cell Sci.* **126**, 860–870.

Ebnet, K., Iden, S., Gerke, V. and Suzuki, A. (2008). Regulation of epithelial and endothelial junctions by PAR proteins. *Front. Biosci. J. Virtual Libr.* **13**, 6520–6536.

Emptage, R. P., Lemmon, M. A. and Ferguson, K. M. (2017). Molecular determinants of KA1 domain-mediated autoinhibition and phospholipid activation of MARK1 kinase. *Biochem. J.* **474**, 385–398.

Emptage, R. P., Lemmon, M. A., Ferguson, K. M. and Marmorstein, R. (2018). Structural Basis for MARK1 Kinase Autoinhibition by Its KA1 Domain. *Struct. Lond. Engl. 1993* **26**, 1137-1143. e3.

Etemad-Moghadam, B., Guo, S. and Kemphues, K. J. (1995). Asymmetrically distributed PAR-3 protein contributes to cell polarity and spindle alignment in early C. elegans embryos. *Cell* **83**, 743–752.

Etienne-Manneville, S. (2004). Cdc42--the centre of polarity. *J. Cell Sci.* **117**, 1291–1300.

Etienne-Manneville, S. and Hall, A. (2001). Integrin-Mediated Activation of Cdc42 Controls Cell Polarity in Migrating Astrocytes through PKCζ. *Cell* **106**, 489–498.

Etienne-Manneville, S. and Hall, A. (2003). Cdc42 regulates GSK-3β and adenomatous polyposis coli to control cell polarity. *Nature* **421**, 753–756.

Feldman, J. L. and Priess, J. R. (2012). A Role for the Centrosome and PAR-3 in the Hand-Off of MTOC Function during Epithelial Polarization. *Curr. Biol.* **22**, 575–582.

Feng, W., Long, J. and Zhang, M. (2005). A unified assembly mode revealed by the structures of tetrameric L27 domain complexes formed by mLin-2/mLin-7 and Patj/Pals1 scaffold proteins. *Proc. Natl. Acad. Sci.* **102**, 6861–6866.

Feng, W., Wu, H., Chan, L.-N. and Zhang, M. (2008). Par-3-mediated junctional localization of the lipid phosphatase PTEN is required for cell polarity establishment. *J. Biol. Chem.* **283**, 23440–23449.

Ferrari, A., Veligodskiy, A., Berge, U., Lucas, M. S. and Kroschewski, R. (2008). ROCK-mediated contractility, tight junctions and channels contribute to the conversion of a preapical patch into apical surface during isochoric lumen initiation. *J. Cell Sci.* **121**, 3649–3663.

Fire, A., Xu, S., Montgomery, M. K., Kostas, S. A., Driver, S. E. and Mello, C. C. (1998). Potent and specific genetic interference by double-stranded RNA in Caenorhabditis elegans. *Nature* **391**, 806–811.

Flores-Benitez, D. and Knust, E. (2015). Crumbs is an essential regulator of cytoskeletal dynamics and cell-cell adhesion during dorsal closure in Drosophila. *eLife* **4**, e07398.

Folkmann, A. W. and Seydoux, G. (2019). Spatial regulation of the polarity kinase PAR-1 by parallel inhibitory mechanisms. *Development* **146**, dev171116.

Franz, A. and Riechmann, V. (2010). Stepwise polarisation of the Drosophila follicular epithelium. *Dev. Biol.* **338**, 136–147.

Friedland, A. E., Tzur, Y. B., Esvelt, K. M., Colaiácovo, M. P., Church, G. M. and Calarco, J. A. (2013). Heritable genome editing in C. elegans via a CRISPR-Cas9 system. *Nat. Methods* **10**, 741–743.

Gally, C., Wissler, F., Zahreddine, H., Quintin, S., Landmann, F. and Labouesse, M. (2009). Myosin II regulation during C. elegans embryonic elongation: LET-502/ROCK, MRCK-1 and PAK-1, three kinases with different roles. *Dev. Camb. Engl.* **136**, 3109–3119.

Gamblin, C. L., Hardy, É. J.-L., Chartier, F. J.-M., Bisson, N. and Laprise, P. (2014). A bidirectional antagonism between aPKC and Yurt regulates epithelial cell polarity. *J Cell Biol* **204**, 487–495.

Gamblin, C. L., Parent-Prévost, F., Jacquet, K., Biehler, C., Jetté, A. and Laprise, P. (2018). Oligomerization of the FERM-FA protein Yurt controls epithelial cell polarity. *J. Cell Biol.* **217**, 3853–3862.

Gao, L. and Macara, I. G. (2004). Isoforms of the Polarity Protein Par6 Have Distinct Functions*. *J. Biol. Chem.* **279**, 41557–41562.

Garrard, S. M., Capaldo, C. T., Gao, L., Rosen, M. K., Macara, I. G. and Tomchick, D. R. (2003). Structure of Cdc42 in a complex with the GTPase-binding domain of the cell polarity protein, Par6. *EMBO J.* **22**, 1125–1133.

Gendreau, S. B., Moskowitz, I. P. G., Terns, R. M. and Rothman, J. H. (1994). The Potential to Differentiate Epidermis Is Unequally Distributed in the AB Lineage during Early Embryonic Development in C. elegans. *Dev. Biol.* **166**, 770–781.

Georgiou, M., Marinari, E., Burden, J. and Baum, B. (2008). Cdc42, Par6, and aPKC regulate Arp2/3-mediated endocytosis to control local adherens junction stability. *Curr. Biol. CB* **18**, 1631–1638.

Gibson, D. G., Young, L., Chuang, R.-Y., Venter, J. C., Hutchison, C. A. and Smith, H. O. (2009). Enzymatic assembly of DNA molecules up to several hundred kilobases. *Nat. Methods* **6**, 343–345.

Gillard, G., Nicolle, O., Brugière, T., Prigent, S., Pinot, M. and Michaux, G. (2019). Force Transmission between Three Tissues Controls Bipolar Planar Polarity Establishment and Morphogenesis. *Curr. Biol. CB* **29**, 1360-1368.e4.

Gilleard, J. S., Barry, J. D. and Johnstone, I. L. (1997). cis regulatory requirements for hypodermal cell-specific expression of the Caenorhabditis elegans cuticle collagen gene dpy-7. *Mol. Cell. Biol.* **17**, 2301–2311.

Giot, L., Bader, J. S., Brouwer, C., Chaudhuri, A., Kuang, B., Li, Y., Hao, Y. L., Ooi, C. E., Godwin, B., Vitols, E., et al. (2003). A protein interaction map of *Drosophila melanogaster*. *Science* **302**, 1727–1736.

Goehring, N. W. and Grill, S. W. (2013). Cell polarity: mechanochemical patterning. *Trends Cell Biol.* **23**, 72–80.

Goldstein, B. and Hird, S. N. Specification of the anteroposterior axis in Caenorhabditis elegans. 8.

Goldstein, B. and Macara, I. G. (2007). The PAR proteins: fundamental players in animal cell polarization. *Dev. Cell* **13**, 609–622.

Gong, T., Yan, Y., Zhang, J., Liu, S., Liu, H., Gao, J., Zhou, X., Chen, J. and Shi, A. (2018). PTRN-1/CAMSAP promotes CYK-1/formin-dependent actin polymerization during endocytic recycling. *EMBO J.* **37**,.

González, S., Fló, M., Margenat, M., Durán, R., González-Sapienza, G., Graña, M., Parkinson, J., Maizels, R. M., Salinas, G., Alvarez, B., et al. (2009). A Family of Diverse Kunitz Inhibitors from Echinococcus granulosus Potentially Involved in Host-Parasite Cross-Talk. *PLoS ONE* **4**, e7009.

Goodwin, S. S. and Vale, R. D. (2010). Patronin regulates the microtubule network by protecting microtubule minus ends. *Cell* **143**, 263–274.

Gosens, I., Sessa, A., den Hollander, A. I., Letteboer, S. J. F., Belloni, V., Arends, M. L., Le Bivic, A., Cremers, F. P. M., Broccoli, V. and Roepman, R. (2007). FERM protein EPB41L5 is a novel member of the mammalian CRB–MPP5 polarity complex. *Exp. Cell Res.* **313**, 3959–3970.

Gotta, M., Dong, Y., Peterson, Y. K., Lanier, S. M. and Ahringer, J. (2003). Asymmetrically distributed C. elegans homologs of AGS3/PINS control spindle position in the early embryo. *Curr. Biol. CB* **13**, 1029–1037.

Graybill, C., Wee, B., Atwood, S. X. and Prehoda, K. E. (2012). Partitioning-defective protein 6 (Par-6) activates atypical protein kinase C (aPKC) by pseudosubstrate displacement. *J. Biol. Chem.* **287**, 21003–21011.

Green, J. L., Inoue, T. and Sternberg, P. W. (2008). Opposing Wnt pathways orient cell polarity during organogenesis. *Cell* **134**, 646–656.

Green, R. A., Kao, H.-L., Audhya, A., Arur, S., Mayers, J. R., Fridolfsson, H. N., Schulman, M., Schloissnig, S., Niessen, S., Laband, K., et al. (2011). A High-Resolution C. elegans Essential Gene Network Based on Phenotypic Profiling of a Complex Tissue. *Cell* **145**, 470–482.

Grossmann, A., Benlasfer, N., Birth, P., Hegele, A., Wachsmuth, F., Apelt, L. and Stelzl, U. (2015). Phospho-tyrosine dependent protein-protein interaction network. *Mol. Syst. Biol.* **11**, 794.

Guo, S. and Kemphues, K. J. (1995). par-1, a gene required for establishing polarity in C. elegans embryos, encodes a putative Ser/Thr kinase that is asymmetrically distributed. *Cell* **81**, 611–620.

Hannaford, M., Loyer, N., Tonelli, F., Zoltner, M. and Januschke, J. (2019). A chemical-genetics approach to study the role of atypical Protein Kinase C in Drosophila. *Dev. Camb. Engl.* **146**,.

Hao, Y., Boyd, L. and Seydoux, G. (2006). Stabilization of cell polarity by the C. elegans RING protein PAR-2. *Dev. Cell* **10**, 199–208.

Harris, T. J. C. (2017). Protein clustering for cell polarity: Par-3 as a paradigm. *F1000Research* **6**, 1620.

Harris, T. J. C. and Peifer, M. (2004). Adherens junction-dependent and -independent steps in the establishment of epithelial cell polarity in Drosophila. *J. Cell Biol.* **167**, 135–147.

Harris, T. J. C. and Peifer, M. (2005). The positioning and segregation of apical cues during epithelial polarity establishment in Drosophila. *J. Cell Biol.* **170**, 813–823.

Harris, T. J. C. and Peifer, M. (2007). aPKC controls microtubule organization to balance adherens junction symmetry and planar polarity during development. *Dev. Cell* **12**, 727–738.

Harris, K. P. and Tepass, U. (2008). Cdc42 and Par proteins stabilize dynamic adherens junctions in the Drosophila neuroectoderm through regulation of apical endocytosis. *J. Cell Biol.* **183**, 1129–1143.

Harris, T. W., Arnaboldi, V., Cain, S., Chan, J., Chen, W. J., Cho, J., Davis, P., Gao, S., Grove, C. A., Kishore, R., et al. (2020). WormBase: a modern Model Organism Information Resource. *Nucleic Acids Res.* **48**, D762–D767.

Harvey, A. L. (2001). Twenty years of dendrotoxins. *Toxicon* **39**, 15–26.

Hayes, G. D., Frand, A. R. and Ruvkun, G. (2006). The mir-84 and let-7 paralogous microRNA genes of Caenorhabditis elegans direct the cessation of molting via the conserved nuclear hormone receptors NHR-23 and NHR-25. *Dev. Camb. Engl.* **133**, 4631–4641.

Hein, M. Y., Hubner, N. C., Poser, I., Cox, J., Nagaraj, N., Toyoda, Y., Gak, I. A., Weisswange, I., Mansfeld, J., Buchholz, F., et al. (2015). A human interactome in three quantitative dimensions organized by stoichiometries and abundances. *Cell* **163**, 712–723.

Hendershott, M. C. and Vale, R. D. (2014). Regulation of microtubule minus-end dynamics by CAMSAPs and Patronin. *Proc. Natl. Acad. Sci. U. S. A.* **111**, 5860–5865.

Hirano, Y., Yoshinaga, S., Takeya, R., Suzuki, N. N., Horiuchi, M., Kohjima, M., Sumimoto, H. and Inagaki, F. (2005). Structure of a cell polarity regulator, a complex between atypical PKC and Par6 PB1 domains. *J. Biol. Chem.* **280**, 9653–9661.

Hirose, T., Izumi, Y., Nagashima, Y., Tamai-Nagai, Y., Kurihara, H., Sakai, T., Suzuki, Y., Yamanaka, T., Suzuki, A., Mizuno, K., et al. (2002). Involvement of ASIP/PAR-3 in the promotion of

epithelial tight junction formation. *J. Cell Sci.* **115**, 2485–2495.

Hirose, T., Karasawa, M., Sugitani, Y., Fujisawa, M., Akimoto, K., Ohno, S. and Noda, T. (2006). PAR3 is essential for cyst-mediated epicardial development by establishing apical cortical domains. *Dev. Camb. Engl.* **133**, 1389–1398.

Hoege, C., Constantinescu, A.-T., Schwager, A., Goehring, N. W., Kumar, P. and Hyman, A. A. (2010). LGL can partition the cortex of one-cell Caenorhabditis elegans embryos into two domains. *Curr. Biol.* **20**, 1296–1303.

Hollander, A. I. den, Davis, J., Velde-Visser, S. D. van der, Zonneveld, M. N., Pierrottet, C. O., Koenekoop, R. K., Kellner, U., Born, L. I. van den, Heckenlively, J. R., Hoyng, C. B., et al. (2004). CRB1 mutation spectrum in inherited retinal dystrophies. *Hum. Mutat.* **24**, 355–369.

Holly, R. W. and Prehoda, K. E. (2019). Phosphorylation of Par-3 by Atypical Protein Kinase C and Competition between Its Substrates. *Dev. Cell* **49**, 678–679.

Hong, Y. (2018). aPKC: the Kinase that Phosphorylates Cell Polarity. *F1000Research* **7**, 903.

Hong, Y., Stronach, B., Perrimon, N., Jan, L. Y. and Jan, Y. N. (2001). Drosophila Stardust interacts with Crumbs to control polarity of epithelia but not neuroblasts. *Nature* **414**, 634–638.

Hong, Y., Ackerman, L., Jan, L. Y. and Jan, Y.-N. (2003). Distinct roles of Bazooka and Stardust in the specification of Drosophila photoreceptor membrane architecture. *Proc. Natl. Acad. Sci. U. S. A.* **100**, 12712–12717.

Horikoshi, Y., Hamada, S., Ohno, S. and Suetsugu, S. (2011). Phosphoinositide binding by par-3 involved in par-3 localization. *Cell Struct. Funct.* **36**, 97–102.

Hsu, Y.-C., Willoughby, J. J., Christensen, A. K. and Jensen, A. M. (2006). Mosaic Eyes is a novel component of the Crumbs complex and negatively regulates photoreceptor apical size. *Dev. Camb. Engl.* **133**, 4849–4859.

Hughes, S., Wilkinson, H., Gilbert, S. P. R., Kishida, M., Ding, S. S. and Woollard, A. (2014). The C. elegans TPR Containing Protein, TRD-1, Regulates Cell Fate Choice in the Developing Germ Line and Epidermis. *PloS One* **9**, e114998.

Hung, T. J. and Kemphues, K. J. (1999). PAR-6 is a conserved PDZ domain-containing protein that colocalizes with PAR-3 in Caenorhabditis elegans embryos. *Development* **126**, 127–135.

Hurov, J. B., Watkins, J. L. and Piwnica-Worms, H. (2004). Atypical PKC phosphorylates PAR-1 kinases to regulate localization and activity. *Curr. Biol. CB* **14**, 736–741.

Hutterer, A., Betschinger, J., Petronczki, M. and Knoblich, J. A. (2004). Sequential roles of Cdc42, Par-6, aPKC, and Lgl in the establishment of epithelial polarity during Drosophila embryogenesis. *Dev. Cell* **6**, 845–854.

Huttlin, E. L., Ting, L., Bruckner, R. J., Gebreab, F., Gygi, M. P., Szpyt, J., Tam, S., Zarraga, G., Colby, G., Baltier, K., et al. (2015). The BioPlex Network: A Systematic Exploration of the Human Interactome. *Cell* **162**, 425–440.

Iden, S., van Riel, W. E., Schäfer, R., Song, J.-Y., Hirose, T., Ohno, S. and Collard, J. G. (2012). Tumor Type-Dependent Function of the Par3 Polarity Protein in Skin Tumorigenesis. *Cancer Cell* **22**, 389–403.

Izumi, Y., Hirose, T., Tamai, Y., Hirai, S., Nagashima, Y., Fujimoto, T., Tabuse, Y., Kemphues, K. J. and Ohno, S. (1998). An Atypical PKC Directly Associates and Colocalizes at the Epithelial Tight Junction with ASIP, a Mammalian Homologue of Caenorhabditis elegans Polarity Protein PAR-3. *J. Cell Biol.* **143**, 95–106.

Izumi, Y., Ohta, N., Itoh-Furuya, A., Fuse, N. and Matsuzaki, F. (2004). Differential functions of G protein and Baz-aPKC signaling pathways in Drosophila neuroblast asymmetric division. *J. Cell Biol.* **164**, 729–738.

Jagadeesan, S. and Hakkim, A. (2018). RNAi Screening: Automated High-Throughput Liquid RNAi Screening in Caenorhabditis elegans. *Curr. Protoc. Mol. Biol.* **124**, e65.

Jiang, K., Hua, S., Mohan, R., Grigoriev, I., Yau, K. W., Liu, Q., Katrukha, E. A., Altelaar, A. F. M., Heck, A. J. R., Hoogenraad, C. C., et al. (2014). Microtubule minus-end stabilization by polymerization-driven CAMSAP deposition. *Dev. Cell* **28**, 295–309.

Joberty, G., Petersen, C., Gao, L. and Macara, I. G. (2000). The cell-polarity protein Par6 links Par3 and atypical protein kinase C to Cdc42. *Nat. Cell Biol.* **2**, 531–539.

Johansson, A., Driessens, M. and Aspenstrom, P. (2000). The mammalian homologue of the Caenorhabditis elegans polarity protein PAR-6 is a binding partner for the Rho GTPases Cdc42 and Rac1. *J. Cell Sci.* **113**, 3267–3275.

Jones, T. A., Nikolova, L. S., Schjelderup, A. and Metzstein, M. M. (2014). Exocyst-mediated membrane trafficking is required for branch outgrowth in Drosophila tracheal terminal cells. *Dev. Biol.* **390**, 41–50.

Joseph, B. B., Blouin, N. A. and Fay, D. S. (2018). Use of a Sibling Subtraction Method for Identifying Causal Mutations in *Caenorhabditis elegans* by Whole-Genome Sequencing. *G3amp58 GenesGenomesGenetics* **8**, 669–678.

Joseph, B. B., Wang, Y., Edeen, P., Lažetić, V., Grant, B. D. and Fay, D. S. (2020). Control of clathrin-mediated endocytosis by NIMA family kinases. *PLoS Genet.* **16**, e1008633.

Jouette, J., Guichet, A. and Claret, S. B. (2019). Dynein-mediated transport and membrane trafficking control PAR3 polarised distribution. *eLife* **8**,.

Jürgens, G., Wieschaus, E., Nüsslein-Volhard, C. and Kluding, H. (1984). Mutations affecting the pattern of the larval cuticle inDrosophila melanogaster. *Wilhelm Rouxs Arch. Dev. Biol.* **193**, 283–295.

Kamath, R. S. and Ahringer, J. (2003). Genome-wide RNAi screening in Caenorhabditis elegans. *Methods San Diego Calif* **30**, 313–321.

Kemphues, K. J., Priess, J. R., Morton, D. G. and Cheng, N. S. (1988). Identification of genes required for cytoplasmic localization in early C. elegans embryos. *Cell* **52**, 311–320.

Klebes, A. and Knust, E. (2000). A conserved motif in Crumbs is required for E-cadherin localisation and zonula adherens formation in Drosophila. *Curr. Biol.* **10**, 76–85.

Klose, S., Flores-Benitez, D., Riedel, F. and Knust, E. (2013). Fosmid-Based Structure-Function Analysis Reveals Functionally Distinct Domains in the Cytoplasmic Domain of Drosophila Crumbs. *G3 GenesGenomesGenetics* **3**, 153–165.

Knight, C. G., Patel, M. N., Azevedo, R. B. R. and Leroi, A. M. (2002). A novel mode of ecdysozoan growth in Caenorhabditis elegans. *Evol. Dev.* **4**, 16–27.

Knoblich, J. A. (2010). Asymmetric cell division: recent developments and their implications for tumour biology. *Nat. Rev. Mol. Cell Biol.* **11**, 849–860.

Knoblich, J. A., Jan, L. Y. and Jan, Y. N. (1997). The N terminus of the Drosophila Numb protein directs membrane association and actin-dependent asymmetric localization. *Proc. Natl. Acad. Sci. U. S. A.* **94**, 13005–13010.

Knust, E., Tepass, U. and Wodarz, A. (1993). crumbs and stardust, two genes of Drosophila required for the development of epithelial cell polarity. *Development* **119**, 261–268.

Kodani, A., Tonthat, V., Wu, B. and Sütterlin, C. (2010). Par6α Interacts with the Dynactin Subunit p150Glued and Is a Critical Regulator of Centrosomal Protein Recruitment. *Mol. Biol. Cell* **21**, 3376–3385.

Kono, K., Yoshiura, S., Fujita, I., Okada, Y., Shitamukai, A., Shibata, T. and Matsuzaki, F. (2019). Reconstruction of Par polarity in apolar cells reveals a dynamic process of cortical polarization. *bioRxiv* 523589.

Koorman, T., Klompstra, D., van der Voet, M., Lemmens, I., Ramalho, J. J., Nieuwenhuize, S., van den Heuvel, S., Tavernier, J., Nance, J. and Boxem, M. (2016). A combined binary interaction and phenotypic map of *C. elegans* cell polarity proteins. *Nat. Cell Biol.* **18**, 337–346.

Krahn, M. P., Egger-Adam, D. and Wodarz, A. (2009). PP2A antagonizes phosphorylation of Bazooka by PAR-1 to control apical-basal polarity in dividing embryonic neuroblasts. *Dev. Cell* **16**, 901–908.

Krahn, M. P., Klopfenstein, D. R., Fischer, N. and Wodarz, A. (2010a). Membrane targeting of Bazooka/PAR-3 is mediated by direct binding to phosphoinositide lipids. *Curr. Biol. CB* **20**, 636–642.

Krahn, M. P., Bückers, J., Kastrup, L. and Wodarz, A. (2010b). Formation of a Bazooka–Stardust complex is essential for plasma membrane polarity in epithelia. *J. Cell Biol.* **190**, 751–760.

Kramerova, I. A., Kawaguchi, N., Fessler, L. I., Nelson, R. E., Chen, Y., Kramerov, A. A., Kusche-Gullberg, M., Kramer, J. M., Ackley, B. D., Sieron, A. L., et al. (2000). Papilin in development; a pericellular protein with a homology to the ADAMTS metalloproteinases. *Development* **127**, 5475–5485.

Kullmann, L. and Krahn, M. P. (2018). Redundant regulation of localization and protein stability of DmPar3. *Cell. Mol. Life Sci.* **75**, 3269–3282.

Kumfer, K. T., Cook, S. J., Squirrell, J. M., Eliceiri, K. W., Peel, N., O'Connell, K. F. and White, J. G. (2010). CGEF-1 and CHIN-1 regulate CDC-42 activity during asymmetric division in the Caenorhabditis elegans embryo. *Mol. Biol. Cell* **21**, 266–277.

Kunitz, M. and Northrop, J. H. (1936). ISOLATION FROM BEEF PANCREAS OF CRYSTALLINE TRYPSINOGEN, TRYPSIN, A TRYPSIN INHIBITOR, AND AN INHIBITOR-TRYPSIN COMPOUND. *J. Gen. Physiol.* **19**, 991–1007.

Kusakabe, M. and Nishida, E. (2004). The polarity-inducing kinase Par-1 controls Xenopus gastrulation in cooperation with 14-3-3 and aPKC. *EMBO J.* **23**, 4190–4201.

Kutscher, L. M. (2014). Forward and reverse mutagenesis in C. elegans. *WormBook* 1–26.

Lalli, G. (2009). RalA and the exocyst complex influence neuronal polarity through PAR-3 and aPKC. *J. Cell Sci.* **122**, 1499–1506.

Laprise, P. and Tepass, U. (2011). Novel insights into epithelial polarity proteins in Drosophila. *Trends Cell Biol.* **21**, 401–408.

Laprise, P., Beronja, S., Silva-Gagliardi, N. F., Pellikka, M., Jensen, A. M., McGlade, C. J. and Tepass, U. (2006). The FERM Protein Yurt Is a Negative Regulatory Component of the Crumbs Complex that Controls Epithelial Polarity and Apical Membrane Size. *Dev. Cell* **11**, 363–374.

Laprise, P., Lau, K. M., Harris, K. P., Silva-Gagliardi, N. F., Paul, S. M., Beronja, S., Beitel, G. J., McGlade, C. J. and Tepass, U. (2009). Yurt, Coracle, Neurexin IV and the Na(+),K(+)-ATPase form a novel group of epithelial polarity proteins. *Nature* **459**, 1141–1145.

Laskowski, M. and Kato, I. (1980). Protein inhibitors of proteinases. *Annu. Rev. Biochem.* **49**, 593–626.

Lažetić, V. and Fay, D. S. (2017). Molting in C. elegans. *Worm* **6**, e1330246.

Lee, S.-K. and Thomas, G. H. (2011). Rac1 modulation of the apical domain is negatively regulated by βHeavy-spectrin. *Mech. Dev.* **128**, 116–128.

Lee, J. D., Silva-Gagliardi, N. F., Tepass, U., McGlade, C. J. and Anderson, K. V. (2007). The FERM protein Epb4.1l5 is required for organization of the neural plate and for the epithelial-mesenchymal transition at the primitive streak of the mouse embryo. *Dev. Camb. Engl.* **134**, 2007–2016.

Leibfried, A., Fricke, R., Morgan, M. J., Bogdan, S. and Bellaiche, Y. (2008). Drosophila Cip4 and WASp define a branch of the Cdc42-Par6-aPKC pathway regulating E-cadherin endocytosis. *Curr. Biol. CB* **18**, 1639–1648.

Lemmers, C., Michel, D., Lane-Guermonprez, L., Delgrossi, M.-H., Médina, E., Arsanto, J.-P. and Le Bivic, A. (2004). CRB3 Binds Directly to Par6 and Regulates the Morphogenesis of the Tight Junctions in Mammalian Epithelial Cells. *Mol. Biol. Cell* **15**, 1324–1333.

Lenfant, N., Polanowska, J., Bamps, S., Omi, S., Borg, J.-P. and Reboul, J. (2010). A genome-wide study of PDZ-domain interactions in C. elegans reveals a high frequency of non-canonical binding. *BMC Genomics* **11**, 671.

Letizia, A., Ricardo, S., Moussian, B., Martín, N. and Llimargas, M. (2013). A functional role of the extracellular domain of Crumbs in cell architecture and apicobasal polarity. *J. Cell Sci.* **126**, 2157–2163.

Leung, B., Hermann, G. J. and Priess, J. R. (1999). Organogenesis of the Caenorhabditis elegans intestine. *Dev. Biol.* **216**, 114–134.

Li, J., Kim, H., Aceto, D. G., Hung, J., Aono, S. and Kemphues, K. J. (2010a). Binding to PKC-3, but not to PAR-3 or to a conventional PDZ domain ligand, is required for PAR-6 function in C. elegans. *Dev. Biol.* **340**, 88–98.

Li, B., Kim, H., Beers, M. and Kemphues, K. (2010b). Different domains of *C. elegans* PAR-3 are required at different times in development. *Dev. Biol.* **344**, 745–757.

Li, Y., Wei, Z., Yan, Y., Wan, Q., Du, Q. and Zhang, M. (2014). Structure of Crumbs tail in complex with the PALS1 PDZ–SH3–GK tandem reveals a highly specific assembly mechanism for the apical Crumbs complex. *Proc. Natl. Acad. Sci. U. S. A.* **111**, 17444–17449.

Lin, D., Edwards, A. S., Fawcett, J. P., Mbamalu, G., Scott, J. D. and Pawson, T. (2000). A mammalian PAR-3–PAR-6 complex implicated in Cdc42/Rac1 and aPKC signalling and cell polarity. *Nat. Cell Biol.* **2**, 540–547.

Ling, J., Sckaff, M., Tiwari, M., Chen, Y., Li, J., Jones, J. and Sen, G. L. (2020). RAS-mediated suppression of PAR3 and its effects on SCC initiation and tissue architecture occur independently of hyperplasia. *J. Cell Sci.* **133**,.

Liu, X.-F., Ishida, H., Raziuddin, R. and Miki, T. (2004). Nucleotide exchange factor ECT2 interacts with the polarity protein complex Par6/Par3/protein kinase Czeta (PKCzeta) and regulates PKCzeta activity. *Mol. Cell. Biol.* **24**, 6665–6675.

Liu, X. F., Ohno, S. and Miki, T. (2006). Nucleotide exchange factor ECT2 regulates epithelial cell polarity. *Cell. Signal.* **18**, 1604–1615.

Liu, H., Wang, S., Hang, W., Gao, J., Zhang, W., Cheng, Z., Yang, C., He, J., Zhou, J., Chen, J., et al. (2018). LET-413/Erbin acts as a RAB-5 effector to promote RAB-10 activation during endocytic recycling. *J. Cell Biol.* **217**, 299–314.

Luck, K., Kim, D.-K., Lambourne, L., Spirohn, K., Begg, B. E., Bian, W., Brignall, R., Cafarelli, T., Campos-Laborie, F. J., Charloteaux, B., et al. (2020). A reference map of the human binary protein interactome. *Nature* **580**, 402–408.

Macara, I. G. and Mili, S. (2008). Polarity and Differential Inheritance – Universal Attributes of Life? *Cell* **135**, 801–812.

Madeira, F., Park, Y. mi, Lee, J., Buso, N., Gur, T., Madhusoodanan, N., Basutkar, P., Tivey, A. R. N., Potter, S. C., Finn, R. D., et al. (2019). The EMBL-EBI search and sequence analysis tools APIs in 2019. *Nucleic Acids Res.* **47**, W636–W641.

Mango, S. (2007). The C. elegans pharynx: a model for organogenesis. *WormBook*.

Martin-Belmonte, F., Gassama, A., Datta, A., Yu, W., Rescher, U., Gerke, V. and Mostov, K. (2007). PTEN-mediated apical segregation of phosphoinositides controls epithelial morphogenesis through Cdc42. *Cell* **128**, 383–397.

Martin-Belmonte, F., Bernascone, I. and Galvez-Santisteban, M. (2016). Cell Polarity. In *Encyclopedia of Cell Biology* (ed. Bradshaw, R. A.) and Stahl, P. D.), pp. 741–750. Waltham: Academic Press.

Mathew, D., Gramates, L. S., Packard, M., Thomas, U., Bilder, D., Perrimon, N., Gorczyca, M. and Budnik, V. (2002). Recruitment of scribble to the synaptic scaffolding complex requires GUK-holder, a novel DLG binding protein. *Curr. Biol. CB* **12**, 531–539.

McCaffrey, L. M. and Macara, I. G. (2009). Widely conserved signaling pathways in the establishment of cell polarity. *Cold Spring Harb. Perspect. Biol.* **1**, a001370.

McCarter, J., Bartlett, B., Dang, T. and Schedl, T. (1999). On the control of oocyte meiotic maturation and ovulation in Caenorhabditis elegans. *Dev. Biol.* **205**, 111–128.

McGhee, J. D., Fukushige, T., Krause, M. W., Minnema, S. E., Goszczynski, B., Gaudet, J., Kohara, Y., Bossinger, O., Zhao, Y., Khattra, J., et al. (2009). ELT-2 is the predominant transcription factor controlling differentiation and function of the C. elegans intestine, from embryo to adult. *Dev. Biol.* **327**, 551–565.

McKinley, R. F. A. and Harris, T. J. C. (2012). Displacement of basolateral Bazooka/PAR-3 by regulated transport and dispersion during epithelial polarization in Drosophila. *Mol. Biol. Cell* **23**, 4465–4471.

McKinley, R. F. A., Yu, C. G. and Harris, T. J. C. (2012). Assembly of Bazooka polarity landmarks through a multifaceted membrane-association mechanism. *J. Cell Sci.* **125**, 1177–1190.

McMahon, L., Legouis, R., Vonesch, J. L. and Labouesse, M. (2001). Assembly of C. elegans apical junctions involves positioning and compaction by LET-413 and protein aggregation by the MAGUK protein DLG-1. *J. Cell Sci.* **114**, 2265–2277.

Médina, E., Williams, J., Klipfell, E., Zarnescu, D., Thomas, G. and Le Bivic, A. (2002a). Crumbs interacts with moesin and βHeavy-spectrin in the apical membrane skeleton of Drosophila. *J. Cell Biol.* **158**, 941–951.

Médina, E., Lemmers, C., Lane-Guermonprez, L. and Le Bivic, A. (2002b). Role of the Crumbs complex in the regulation of junction formation in Drosophila and mammalian epithelial cells. *Biol. Cell* **94**, 305–313.

Mehalow, A. K., Kameya, S., Smith, R. S., Hawes, N. L., Denegre, J. M., Young, J. A., Bechtold, L., Haider, N. B., Tepass, U., Heckenlively, J. R., et al. (2003). CRB1 is essential for external limiting membrane integrity and photoreceptor morphogenesis in the mammalian retina. *Hum. Mol. Genet.* **12**, 2179–2189.

Meli, V. S., Osuna, B., Ruvkun, G. and Frand, A. R. (2010). MLT-10 Defines a Family of DUF644 and Proline-rich Repeat Proteins Involved in the Molting Cycle of Caenorhabditis elegans. *Mol. Biol. Cell* **21**, 1648–1661.

Mertens, A. E. E., Rygiel, T. P., Olivo, C., van der Kammen, R. and Collard, J. G. (2005). The Rac activator Tiam1 controls tight junction biogenesis in keratinocytes through binding to and activation of the Par polarity complex. *J. Cell Biol.* **170**, 1029–1037.

Michaux, G., Legouis, R. and Labouesse, M. (2001). Epithelial biology: lessons from Caenorhabditis elegans. *Gene* **277**, 83–100.

Michaux, G., Massey-Harroche, D., Nicolle, O., Rabant, M., Brousse, N., Goulet, O., Bivic, A. L. and Ruemmele, F. M. (2016). The localisation of the apical Par/Cdc42 polarity module is specifically affected in microvillus inclusion disease. *Biol. Cell* **108**, 19–28.

Minor, P. J. and Sternberg, P. W. (2019). C. elegans LRP-2 functions in vulval precursor cell polarity. *MicroPublication Biol.* **2019**,.

Minor, P. J., He, T.-F., Sohn, C. H., Asthagiri, A. R. and Sternberg, P. W. (2013). FGF signaling regulates Wnt ligand expression to control vulval cell lineage polarity in C. elegans. *Dev. Camb. Engl.* **140**, 3882–3891.

Montell, D. J., Yoon, W. H. and Starz-Gaiano, M. (2012). Group choreography: mechanisms orchestrating the collective movement of border cells. *Nat. Rev. Mol. Cell Biol.* **13**, 631–645.

Montoyo-Rosario, J. G., Armenti, S. T., Zilberman, Y. and Nance, J. (2020). The Role of pkc-3 and Genetic Suppressors in *Caenorhabditis elegans* Epithelial Cell Junction Formation. *Genetics*.

Morais-de-Sá, E., Mirouse, V. and St Johnston, D. (2010). aPKC phosphorylation of Bazooka defines the apical/lateral border in Drosophila epithelial cells. *Cell* **141**, 509–523.

Mörck, C. and Pilon, M. (2006). *C. elegans* feeding defective mutants have shorter body lengths and increased autophagy. *BMC Dev. Biol.* **6**, 39.

Moreira, S., Osswald, M., Ventura, G., Gonçalves, M., Sunkel, C. E. and Morais-de-Sá, E. (2019). PP1-Mediated Dephosphorylation of Lgl Controls Apical-basal Polarity. *Cell Rep.* **26**, 293-301.e7.

Morin, X. and Bellaïche, Y. (2011). Mitotic Spindle Orientation in Asymmetric and Symmetric Cell Divisions during Animal Development. *Dev. Cell* **21**, 102–119.

Motegi, F. and Seydoux, G. (2013). The PAR network: redundancy and robustness in a symmetry-breaking system. *Philos. Trans. R. Soc. B Biol. Sci.* **368**, 20130010.

Motegi, F. and Sugimoto, A. (2006). Sequential functioning of the ECT-2 RhoGEF, RHO-1 and CDC-42 establishes cell polarity in Caenorhabditis elegans embryos. *Nat. Cell Biol.* **8**, 978–985.

Motegi, F., Zonies, S., Hao, Y., Cuenca, A. A., Griffin, E. and Seydoux, G. (2011). Microtubules induce self-organization of polarized PAR domains in *Caenorhabditis elegans* zygotes. *Nat. Cell Biol.* **13**, 1361–1367.

Munro, E., Nance, J. and Priess, J. R. (2004). Cortical flows powered by asymmetrical contraction transport PAR proteins to establish and maintain anterior-posterior polarity in the early C.

elegans embryo. *Dev. Cell* **7**, 413–424.

Myers, T. R. and Greenwald, I. (2005). lin-35 Rb Acts in the Major Hypodermis to Oppose Ras-Mediated Vulval Induction in C. elegans. *Dev. Cell* **8**, 117–123.

Nagai-Tamai, Y., Mizuno, K., Hirose, T., Suzuki, A. and Ohno, S. (2002). Regulated protein-protein interaction between aPKC and PAR-3 plays an essential role in the polarization of epithelial cells. *Genes Cells Devoted Mol. Cell. Mech.* **7**, 1161–1171.

Nam, S.-C. and Choi, K.-W. (2006). Domain-specific early and late function of Dpatj in Drosophila photoreceptor cells. *Dev. Dyn.* **235**, 1501–1507.

Nance, J. and Priess, J. R. (2002). Cell polarity and gastrulation in C. elegans. *Dev. Camb. Engl.* **129**, 387–397.

Nance, J., Munro, E. M. and Priess, J. R. (2003). *C. elegans* PAR-3 and PAR-6 are required for apicobasal asymmetries associated with cell adhesion and gastrulation. *Development* **130**, 5339–5350.

Nelson, W. J. (2009). Remodeling Epithelial Cell Organization: Transitions Between Front–Rear and Apical–Basal Polarity. *Cold Spring Harb. Perspect. Biol.* **1**, a000513.

Nemetschke, L. and Knust, E. (2016). Drosophila Crumbs prevents ectopic Notch activation in developing wings by inhibiting ligand-independent endocytosis. *Development* **143**, 4543–4553.

Niessen, M. T., Scott, J., Zielinski, J. G., Vorhagen, S., Sotiropoulou, P. A., Blanpain, C., Leitges, M. and Niessen, C. M. (2013). aPKCλ controls epidermal homeostasis and stem cell fate through regulation of division orientation. *J. Cell Biol.* **202**, 887–900.

Nishimura, K., Fukagawa, T., Takisawa, H., Kakimoto, T. and Kanemaki, M. (2009). An auxin-based degron system for the rapid depletion of proteins in nonplant cells. *Nat. Methods* **6**, 917–922.

Osada, S.-I., Minematsu, N., Oda, F., Akimoto, K., Kawana, S. and Ohno, S. (2015). Atypical Protein Kinase C Isoform, aPKCλ, Is Essential for Maintaining Hair Follicle Stem Cell Quiescence. *J. Invest. Dermatol.* **135**, 2584–2592.

Ozdamar, B., Bose, R., Barrios-Rodiles, M., Wang, H.-R., Zhang, Y. and Wrana, J. L. (2005). Regulation of the polarity protein Par6 by TGFbeta receptors controls epithelial cell plasticity. *Science* **307**, 1603–1609.

Oztan, A., Silvis, M., Weisz, O. A., Bradbury, N. A., Hsu, S.-C., Goldenring, J. R., Yeaman, C. and Apodaca, G. (2007). Exocyst requirement for endocytic traffic directed toward the apical and basolateral poles of polarized MDCK cells. *Mol. Biol. Cell* **18**, 3978–3992.

Page, B. D., Zhang, W., Steward, K., Blumenthal, T. and Priess, J. R. (1997). ELT-1, a GATA-like transcription factor, is required for epidermal cell fates in Caenorhabditis elegans embryos. *Genes Dev.* **11**, 1651–1661.

Page, A. P., McCormack, G. and Birnie, A. J. (2006). Biosynthesis and enzymology of the Caenorhabditis elegans cuticle: Identification and characterization of a novel serine protease inhibitor. *Int. J. Parasitol.* **36**, 681–689.

Pellikka, M., Tanentzapf, G., Pinto, M., Smith, C., McGlade, C. J., Ready, D. F. and Tepass, U. (2002). Crumbs, the Drosophila homologue of human CRB1/RP12, is essential for photoreceptor morphogenesis. *Nature* **416**, 143–149.

Perez-Mockus, G., Roca, V., Mazouni, K. and Schweisguth, F. (2017). Neuralized regulates

Crumbs endocytosis and epithelium morphogenesis via specific Stardust isoforms. *J. Cell Biol.* **216**, 1405–1420.

Persa, O. D., Koester, J. and Niessen, C. M. (2021). Regulation of Cell Polarity and Tissue Architecture in Epidermal Aging and Cancer. *J. Invest. Dermatol.* **0**,.

Peterson, F. C., Penkert, R. R., Volkman, B. F. and Prehoda, K. E. (2004). Cdc42 regulates the Par-6 PDZ domain through an allosteric CRIB-PDZ transition. *Mol. Cell* **13**, 665–676.

Pichaud, F., Walther, R. F. and Nunes de Almeida, F. (2019). Regulation of Cdc42 and its effectors in epithelial morphogenesis. *J. Cell Sci.* **132**,.

Pickett, M. A., Naturale, V. F. and Feldman, J. L. (2019). A Polarizing Issue: Diversity in the Mechanisms Underlying Apico-Basolateral Polarization In Vivo. *Annu. Rev. Cell Dev. Biol.* **35**, 285–308.

Pieczynski, J. and Margolis, B. (2011). Protein complexes that control renal epithelial polarity. *Am. J. Physiol. Renal Physiol.* **300**, F589-601.

Pinal, N., Goberdhan, D. C. I., Collinson, L., Fujita, Y., Cox, I. M., Wilson, C. and Pichaud, F. (2006). Regulated and polarized PtdIns(3,4,5)P3 accumulation is essential for apical membrane morphogenesis in photoreceptor epithelial cells. *Curr. Biol. CB* **16**, 140–149.

Pinheiro, E. M. and Montell, D. J. (2004). Requirement for Par-6 and Bazooka in Drosophila border cell migration. *Development* **131**, 5243–5251.

Plant, P. J., Fawcett, J. P., Lin, D. C. C., Holdorf, A. D., Binns, K., Kulkarni, S. and Pawson, T. (2003). A polarity complex of mPar-6 and atypical PKC binds, phosphorylates and regulates mammalian Lgl. *Nat. Cell Biol.* **5**, 301–308.

Plyte, S. E., Hughes, K., Nikolakaki, E., Pulverer, B. J. and Woodgett, J. R. (1992). Glycogen synthase kinase-3: functions in oncogenesis and development. *Biochim. Biophys. Acta BBA - Rev. Cancer* **1114**, 147–162.

Polgar, N. and Fogelgren, B. (2018). Regulation of Cell Polarity by Exocyst-Mediated Trafficking. *Cold Spring Harb. Perspect. Biol.* **10**, a031401.

Ramalho, J. M., de Amil da Costa Jacob (2020). Untangling the animal plumbing : Apical domain formation in C. elegans tubular epithelia.

Ramalho, J. J., Sepers, J. J., Nicolle, O., Schmidt, R., Cravo, J., Michaux, G. and Boxem, M. (2020). C-terminal phosphorylation modulates ERM-1 localization and dynamics to control cortical actin organization and support lumen formation during C. elegans development. *Dev. Camb. Engl.*

Ramanujam, R., Han, Z., Zhang, Z., Kanchanawong, P. and Motegi, F. (2018). Establishment of the PAR-1 cortical gradient by the aPKC-PRBH circuit. *Nat. Chem. Biol.* **14**, 917–927.

Ranasinghe, S. and McManus, D. P. (2013). Structure and function of invertebrate Kunitz serine protease inhibitors. *Dev. Comp. Immunol.* **39**, 219–227.

Reina-Campos, M., Linares, J. F., Duran, A., Cordes, T., L'Hermitte, A., Badur, M. G., Bhangoo, M. S., Thorson, P. K., Richards, A., Rooslid, T., et al. (2019). Increased Serine and One-Carbon Pathway Metabolism by PKCλ/ι Deficiency Promotes Neuroendocrine Prostate Cancer. *Cancer Cell* **35**, 385-400.e9.

Renschler, F. A., Bruekner, S. R., Salomon, P. L., Mukherjee, A., Kullmann, L., Schütz-Stoffregen, M. C., Henzler, C., Pawson, T., Krahn, M. P. and Wiesner, S. (2018). Structural basis for the interaction between the cell polarity proteins Par3 and Par6. *Sci. Signal.* **11**,.

Robinson, J. T., Thorvaldsdóttir, H., Wenger, A. M., Zehir, A. and Mesirov, J. P. (2017). Variant Review with the Integrative Genomics Viewer. *Cancer Res.* **77**, e31–e34.

Rodriguez, J., Peglion, F., Martin, J., Hubatsch, L., Reich, J., Hirani, N., Gubieda, A. G., Roffey, J., Fernandes, A. R., St Johnston, D., et al. (2017). aPKC Cycles between Functionally Distinct PAR Protein Assemblies to Drive Cell Polarity. *Dev. Cell* **42**, 400-415.e9.

Rodriguez-Boulan, E. and Macara, I. G. (2014). Organization and execution of the epithelial polarity programme. *Nat. Rev. Mol. Cell Biol.* **15**, 225–242.

Roeth, J. F., Sawyer, J. K., Wilner, D. A. and Peifer, M. (2009). Rab11 Helps Maintain Apical Crumbs and Adherens Junctions in the Drosophila Embryonic Ectoderm. *PLOS ONE* **4**, e7634.

Roh, M. H., Makarova, O., Liu, C.-J., Shin, Lee, S., Laurinec, S., Goyal, M., Wiggins, R. and Margolis, B. (2002). The Maguk protein, Pals1, functions as an adapter, linking mammalian homologues of Crumbs and Discs Lost. *J. Cell Biol.* **157**, 161–172.

Roignot, J., Peng, X. and Mostov, K. (2013). Polarity in mammalian epithelial morphogenesis. *Cold Spring Harb. Perspect. Biol.* **5**,.

Rosa, A., Vlassaks, E., Pichaud, F. and Baum, B. (2015). Ect2/Pbl acts via Rho and polarity proteins to direct the assembly of an isotropic actomyosin cortex upon mitotic entry. *Dev. Cell* **32**, 604–616.

Rosenbluth, R. E., Cuddeford, C. and Baillie, D. L. (1983). Mutagenesis in Caenorhabditis elegans: I. A rapid eukaryotic mutagen test system using the reciprocal translocation, eTI(III;V). *Mutat. Res. Mol. Mech. Mutagen.* **110**, 39–48.

Rosse, C., Formstecher, E., Boeckeler, K., Zhao, Y., Kremerskothen, J., White, M. D., Camonis, J. H. and Parker, P. J. (2009). An aPKC-Exocyst Complex Controls Paxillin Phosphorylation and Migration through Localised JNK1 Activation. *PLOS Biol.* **7**, e1000235.

Rueden, C. T., Schindelin, J., Hiner, M. C., DeZonia, B. E., Walter, A. E., Arena, E. T. and Eliceiri, K. W. (2017). ImageJ2: ImageJ for the next generation of scientific image data. *BMC Bioinformatics* **18**, 529.

Russel, S., Frand, A. R. and Ruvkun, G. (2011). Regulation of the C. elegans molt by pqn-47. *Dev. Biol.* **360**, 297–309.

Sailer, A., Anneken, A., Li, Y., Lee, S. and Munro, E. (2015). Dynamic Opposition of Clustered Proteins Stabilizes Cortical Polarity in the C. elegans Zygote. *Dev. Cell* **35**, 131–142.

Sallee, M. D., Zonka, J. C., Skokan, T. D., Raftrey, B. C. and Feldman, J. L. (2018). Tissue-specific degradation of essential centrosome components reveals distinct microtubule populations at microtubule organizing centers. *PLOS Biol.* **16**, e2005189.

Sallee, M. D., Pickett, M. A. and Feldman, J. L. (2020). Apical PAR complex proteins protect against epithelial assaults to create a continuous and functional intestinal lumen. *bioRxiv* 2020.10.28.359299.

Sánchez, N. S. and Barnett, J. V. (2012). TGFβ and BMP-2 regulate epicardial cell invasion via TGFβR3 activation of the Par6/Smurf1/RhoA pathway. *Cell. Signal.* **24**, 539–548.

Sanchez, A. D. and Feldman, J. L. (2017). Microtubule-organizing centers: from the centrosome to non-centrosomal sites. *Curr. Opin. Cell Biol.* **44**, 93–101.

Savage-Dunn, C., Maduzia, L. L., Zimmerman, C. M., Roberts, A. F., Cohen, S., Tokarz, R. and Padgett, R. W. (2003). Genetic screen for small body size mutants in C. elegans reveals many TGFβ pathway components. *genesis* **35**, 239–247.

Schell, C., Rogg, M., Suhm, M., Helmstädter, M., Sellung, D., Yasuda-Yamahara, M., Kretz, O., Küttner, V., Suleiman, H., Kollipara, L., et al. (2017). The FERM protein EPB41L5 regulates actomyosin contractility and focal adhesion formation to maintain the kidney filtration barrier. *Proc. Natl. Acad. Sci.* **114**, E4621–E4630.

Schiestl, R. H. and Gietz, R. D. (1989). High efficiency transformation of intact yeast cells using single stranded nucleic acids as a carrier. *Curr. Genet.* **16**, 339–346.

Schindelin, J., Arganda-Carreras, I., Frise, E., Kaynig, V., Longair, M., Pietzsch, T., Preibisch, S., Rueden, C., Saalfeld, S., Schmid, B., et al. (2012). Fiji: an open-source platform for biological-image analysis. *Nat. Methods* **9**, 676–682.

Schlüter, M. A., Pfarr, C. S., Pieczynski, J., Whiteman, E. L., Hurd, T. W., Fan, S., Liu, C.-J. and Margolis, B. (2009). Trafficking of Crumbs3 during Cytokinesis Is Crucial for Lumen Formation. *Mol. Biol. Cell* **20**, 4652–4663.

Schneikert, J. and Behrens, J. (2007). The canonical Wnt signalling pathway and its APC partner in colon cancer development. *Gut* **56**, 417–425.

Schober, M., Schaefer, M. and Knoblich, J. A. (1999). Bazooka recruits Inscuteable to orient asymmetric cell divisions in Drosophila neuroblasts. *Nature* **402**, 548–551.

Schonegg, S. and Hyman, A. A. (2006). CDC-42 and RHO-1 coordinate acto-myosin contractility and PAR protein localization during polarity establishment in C. elegans embryos. *Dev. Camb. Engl.* **133**, 3507–3516.

Schrader, K. A., Masciari, S., Boyd, N., Wiyrick, S., Kaurah, P., Senz, J., Burke, W., Lynch, H. T., Garber, J. E. and Huntsman, D. G. (2008). Hereditary diffuse gastric cancer: association with lobular breast cancer. *Fam. Cancer* **7**, 73–82.

Schwartz, M. L. and Jorgensen, E. M. (2016). SapTrap, a Toolkit for High-Throughput CRISPR/Cas9 Gene Modification in *Caenorhabditis elegans*. *Genetics* **202**, 1277–1288.

Segbert, C., Johnson, K., Theres, C., van Fürden, D. and Bossinger, O. (2004). Molecular and functional analysis of apical junction formation in the gut epithelium of Caenorhabditis elegans. *Dev. Biol.* **266**, 17–26.

Shafaq-Zadah, M., Brocard, L., Solari, F. and Michaux, G. (2012). AP-1 is required for the maintenance of apico-basal polarity in the C. elegans intestine. *Development* **139**, 2061–2070.

Shahab, J., Tiwari, M. D., Honemann-Capito, M., Krahn, M. P. and Wodarz, A. (2015). Bazooka/PAR3 is dispensable for polarity in Drosophila follicular epithelial cells. *Biol. Open* **4**, 528–541.

Shelton, C. A., Carter, J. C., Ellis, G. C. and Bowerman, B. (1999). The Nonmuscle Myosin Regulatory Light Chain Gene mlc-4 Is Required for Cytokinesis, Anterior-Posterior Polarity, and Body Morphology during Caenorhabditis elegans Embryogenesis. *J. Cell Biol.* **146**, 439–451.

Sherrard, K. M. and Fehon, R. G. (2015). The transmembrane protein Crumbs displays complex dynamics during follicular morphogenesis and is regulated competitively by Moesin and aPKC. *Dev. Camb. Engl.* **142**, 2226.

Shibata, Y., Fujii, T., Dent, J. A., Fujisawa, H. and Takagi, S. (2000). EAT-20, a novel transmembrane protein with EGF motifs, is required for efficient feeding in Caenorhabditis elegans. *Genetics* **154**, 635–646.

Shin, K., Straight, S. and Margolis, B. (2005). PATJ regulates tight junction formation and polarity in mammalian epithelial cells. *J. Cell Biol.* **168**, 705–711.

Sigurbjörnsdóttir, S., Mathew, R. and Leptin, M. (2014). Molecular mechanisms of de novo lumen formation. *Nat. Rev. Mol. Cell Biol.* **15**, 665–676.

Smith, C. A., Lau, K. M., Rahmani, Z., Dho, S. E., Brothers, G., She, Y. M., Berry, D. M., Bonneil, E., Thibault, P., Schweisguth, F., et al. (2007). aPKC-mediated phosphorylation regulates asymmetric membrane localization of the cell fate determinant Numb. *EMBO J.* **26**, 468–480.

Soriano, E. V., Ivanova, M. E., Fletcher, G., Riou, P., Knowles, P. P., Barnouin, K., Purkiss, A., Kostelecky, B., Saiu, P., Linch, M., et al. (2016). aPKC Inhibition by Par3 CR3 Flanking Regions Controls Substrate Access and Underpins Apical-Junctional Polarization. *Dev. Cell* **38**, 384–398.

Sotillos, S., Díaz-Meco, M. T., Caminero, E., Moscat, J. and Campuzano, S. (2004). DaPKC-dependent phosphorylation of Crumbs is required for epithelial cell polarity in Drosophila. *J. Cell Biol.* **166**, 549–557.

Spaendonk, H. V., Ceuleers, H., Witters, L., Patteet, E., Joossens, J., Augustyns, K., Lambeir, A.-M., Meester, I. D., Man, J. G. D. and Winter, B. Y. D. (2017). Regulation of intestinal permeability: The role of proteases. *World J. Gastroenterol.* **23**, 2106–2123.

Spannl, S., Kumichel, A., Hebbar, S., Kapp, K., Gonzalez-Gaitan, M., Winkler, S., Blawid, R., Jessberger, G. and Knust, E. (2017). The Crumbs_C isoform of Drosophila shows tissue- and stage-specific expression and prevents light-dependent retinal degeneration. *Biol. Open* **6**, 165–175.

St Johnston, D. (2018). Establishing and transducing cell polarity: common themes and variations. *Curr. Opin. Cell Biol.* **51**, 33–41.

St Johnston, D. and Ahringer, J. (2010). Cell polarity in eggs and epithelia: parallels and diversity. *Cell* **141**, 757–774.

Stephens, R., Lim, K., Portela, M., Kvansakul, M., Humbert, P. O. and Richardson, H. E. (2018). The Scribble Cell Polarity Module in the Regulation of Cell Signaling in Tissue Development and Tumorigenesis. *J. Mol. Biol.* **430**, 3585–3612.

Sternberg, P. W. (2005). Vulval development. *WormBook*.

Straight, S. W., Shin, K., Fogg, V. C., Fan, S., Liu, C.-J., Roh, M. and Margolis, B. (2004). Loss of PALS1 Expression Leads to Tight Junction and Polarity Defects. *Mol. Biol. Cell* **15**, 1981–1990.

Sundaram, M. V. and Buechner, M. (2016). The Caenorhabditis elegans Excretory System: A Model for Tubulogenesis, Cell Fate Specification, and Plasticity. *Genetics* **203**, 35–63.

Suzuki, A., Hirata, M., Kamimura, K., Maniwa, R., Yamanaka, T., Mizuno, K., Kishikawa, M., Hirose, H., Amano, Y., Izumi, N., et al. (2004). aPKC acts upstream of PAR-1b in both the establishment and maintenance of mammalian epithelial polarity. *Curr. Biol. CB* **14**, 1425–1435.

Swystun, V., Chen, L., Factor, P., Siroky, B., Bell, P. D. and Matalon, S. (2005). Apical trypsin increases ion transport and resistance by a phospholipase C-dependent rise of Ca2+. *Am. J. Physiol.-Lung Cell. Mol. Physiol.* **288**, L820–L830.

Tabuse, Y., Izumi, Y., Piano, F., Kemphues, K. J., Miwa, J. and Ohno, S. (1998). Atypical protein kinase C cooperates with PAR-3 to establish embryonic polarity in Caenorhabditis elegans. *Development* **125**, 3607–3614.

Taffoni, C., Omi, S., Huber, C., Mailfert, S., Fallet, M., Rupprecht, J.-F., Ewbank, J. J. and Pujol, N. (2020). Microtubule plus-end dynamics link wound repair to the innate immune response. *eLife* **9**,.

Tapia, R., Kralicek, S. E. and Hecht, G. A. (2017). Modulation of epithelial cell polarity by bacterial pathogens. *Ann. N. Y. Acad. Sci.* **1405**, 16–24.

Tenlen, J. R., Molk, J. N., London, N., Page, B. D. and Priess, J. R. (2008). MEX-5 asymmetry in one-cell C. elegans embryos requires PAR-4- and PAR-1-dependent phosphorylation. *Dev. Camb. Engl.* **135**, 3665–3675.

Tepass, U. (2012). The apical polarity protein network in Drosophila epithelial cells: regulation of polarity, junctions, morphogenesis, cell growth, and survival. *Annu. Rev. Cell Dev. Biol.* **28**, 655–685.

Tepass, U. and Knust, E. (1990). Phenotypic and developmental analysis of mutations at the crumbs locus, a gene required for the development of epithelia in Drosophila *melanogaster*. *Rouxs Arch. Dev. Biol.* **199**, 189–206.

Tepass, U. and Knust, E. (1993). crumbs and stardust Act in a Genetic Pathway That Controls the Organization of Epithelia in Drosophila melanogaster. *Dev. Biol.* **159**, 311–326.

Tepass, U., Theres, C. and Knust, E. (1990). crumbs encodes an EGF-like protein expressed on apical membranes of Drosophila epithelial cells and required for organization of epithelia. *Cell* **61**, 787–799.

Thompson, B. J. and McDonald, N. Q. (2019). Competitive Inhibition of aPKC by Par-3/Bazooka and Other Substrates. *Dev. Cell* **49**, 680.

Thompson, O., Edgley, M., Strasbourger, P., Flibotte, S., Ewing, B., Adair, R., Au, V., Chaudhry, I., Fernando, L., Hutter, H., et al. (2013). The million mutation project: a new approach to genetics in Caenorhabditis elegans. *Genome Res.* **23**, 1749–1762.

Tinevez, J.-Y., Perry, N., Schindelin, J., Hoopes, G. M., Reynolds, G. D., Laplantine, E., Bednarek, S. Y., Shorte, S. L. and Eliceiri, K. W. (2017). TrackMate: An open and extensible platform for single-particle tracking. *Methods* **115**, 80–90.

Totong, R., Achilleos, A. and Nance, J. (2007). PAR-6 is required for junction formation but not apicobasal polarization in C. elegans embryonic epithelial cells. *Dev. Camb. Engl.* **134**, 1259–1268.

Uppaluri, S. and Brangwynne, C. P. (2015). A size threshold governs Caenorhabditis elegans developmental progression. *Proc. R. Soc. B Biol. Sci.* **282**, 20151283.

van Rossum, A. G. S. H., Aartsen, W. M., Meuleman, J., Klooster, J., Malysheva, A., Versteeg, I., Arsanto, J.-P., Le Bivic, A. and Wijnholds, J. (2006). Pals1/Mpp5 is required for correct localization of Crb1 at the subapical region in polarized Müller glia cells. *Hum. Mol. Genet.* **15**, 2659–2672.

Vijay, G. V., Zhao, N., Den Hollander, P., Toneff, M. J., Joseph, R., Pietila, M., Taube, J. H., Sarkar, T. R., Ramirez-Pena, E., Werden, S. J., et al. (2019). GSK3β regulates epithelial-mesenchymal transition and cancer stem cell properties in triple-negative breast cancer. *Breast Cancer Res. BCR* **21**, 37.

Visco, I., Hoege, C., Hyman, A. A. and Schwille, P. (2016). In vitro Reconstitution of a Membrane Switch Mechanism for the Polarity Protein LGL. *J. Mol. Biol.* **428**, 4828–4842.

von Stein, W., Ramrath, A., Grimm, A., Müller-Borg, M. and Wodarz, A. (2005). Direct

association of Bazooka/PAR-3 with the lipid phosphatase PTEN reveals a link between the PAR/aPKC complex and phosphoinositide signaling. *Development* **132**, 1675–1686.

Von Stetina, S. E. and Mango, S. E. (2015). PAR-6, but not E-cadherin and β-integrin, is necessary for epithelial polarization in C. elegans. *Dev. Biol.* **403**, 5–14.

Von Stetina, S. E., Liang, J., Marnellos, G. and Mango, S. E. (2017). Temporal regulation of epithelium formation mediated by FoxA, MKLP1, MgcRacGAP, and PAR-6. *Mol. Biol. Cell* **28**, 2042–2065.

Vorhagen, S., Kleefisch, D., Persa, O.-D., Graband, A., Schwickert, A., Saynisch, M., Leitges, M., Niessen, C. M. and Iden, S. (2018). Shared and independent functions of aPKCλ and Par3 in skin tumorigenesis. *Oncogene* **37**, 5136–5146.

Waaijers, S., Ramalho, J. J., Koorman, T., Kruse, E. and Boxem, M. (2015). The *C. elegans* Crumbs family contains a CRB3 homolog and is not essential for viability. *Biol. Open* **4**, 276–284.

Waaijers, S., Muñoz, J., Berends, C., Ramalho, J. J., Goerdayal, S. S., Low, T. Y., Zoumaro-Djayoon, A. D., Hoffmann, M., Koorman, T., Tas, R. P., et al. (2016). A tissue-specific protein purification approach in Caenorhabditis elegans identifies novel interaction partners of DLG-1/Discs large. *BMC Biol.* **14**,.

Wagner, A. (2000). Robustness against mutations in genetic networks of yeast. *Nat. Genet.* **24**, 355–361.

Walck-Shannon, E., Lucas, B., Chin-Sang, I., Reiner, D., Kumfer, K., Cochran, H., Bothfeld, W. and Hardin, J. (2016). CDC-42 Orients Cell Migration during Epithelial Intercalation in the Caenorhabditis elegans Epidermis. *PLOS Genet.* **12**, e1006415.

Walther, R. F. and Pichaud, F. (2010). Crumbs/DaPKC-dependent apical exclusion of Bazooka promotes photoreceptor polarity remodeling. *Curr Biol* **20**, 1065–74.

Wang, H.-R., Zhang, Y., Ozdamar, B., Ogunjimi, A. A., Alexandrova, E., Thomsen, G. H. and Wrana, J. L. (2003). Regulation of cell polarity and protrusion formation by targeting RhoA for degradation. *Science* **302**, 1775–1779.

Wang, Q., Chen, X.-W. and Margolis, B. (2006). PALS1 Regulates E-Cadherin Trafficking in Mammalian Epithelial Cells. *Mol. Biol. Cell* **18**, 874–885.

Wang, S., Wu, D., Quintin, S., Green, R. A., Cheerambathur, D. K., Ochoa, S. D., Desai, A. and Oegema, K. (2015). NOCA-1 functions with γ-tubulin and in parallel to Patronin to assemble non-centrosomal microtubule arrays in C. elegans. *eLife* **4**, e08649.

Wang, S.-C., Low, T. Y. F., Nishimura, Y., Gole, L., Yu, W. and Motegi, F. (2017). Cortical forces and CDC-42 control clustering of PAR proteins for Caenorhabditis elegans embryonic polarization. *Nat. Cell Biol.* **19**, 988–995.

Ward, J. D. (2015). Rapid and precise engineering of the Caenorhabditis elegans genome with lethal mutation co-conversion and inactivation of NHEJ repair. *Genetics* **199**, 363–377.

Watts, J. L., Etemad-Moghadam, B., Guo, S., Boyd, L., Draper, B. W., Mello, C. C., Priess, J. R. and Kemphues, K. J. (1996). par-6, a gene involved in the establishment of asymmetry in early C. elegans embryos, mediates the asymmetric localization of PAR-3. *Dev. Camb. Engl.* **122**, 3133–3140.

Weis, W. I., Nelson, W. J. and Dickinson, D. J. (2013). Evolution and Cell Physiology. 3. Using Dictyostelium discoideum to investigate mechanisms of epithelial polarity. *Am. J. Physiol.-Cell Physiol.* **305**, C1091–C1095.

Welchman, D. P., Mathies, L. and Ahringer, J. (2007). Similar requirements for CDC-42 and the PAR-3/PAR-6/PKC-3 complex in diverse cell types. *Dev. Biol.* **305**, 347–357.

Wen, W. and Zhang, M. (2018). Protein Complex Assemblies in Epithelial Cell Polarity and Asymmetric Cell Division. *J. Mol. Biol.* **430**, 3504–3520.

Whitney, D. S., Peterson, F. C. and Volkman, B. F. (2011). A conformational switch in the CRIB-PDZ module of Par-6. *Struct. Lond. Engl. 1993* **19**, 1711–1722.

Whitney, D. S., Peterson, F. C., Kittell, A. W., Egner, J. M., Prehoda, K. E. and Volkman, B. F. (2016). Binding of Crumbs to the Par-6 CRIB-PDZ Module Is Regulated by Cdc42. *Biochemistry* **55**, 1455–1461.

Wildwater, M., Sander, N., de Vreede, G. and van den Heuvel, S. (2011). Cell shape and Wnt signaling redundantly control the division axis of *C. elegans* epithelial stem cells. *Development* **138**, 4375–4385.

Wilson, M. I., Gill, D. J., Perisic, O., Quinn, M. T. and Williams, R. L. (2003). PB1 domain-mediated heterodimerization in NADPH oxidase and signaling complexes of atypical protein kinase C with Par6 and p62. *Mol. Cell* **12**, 39–50.

Winter, J. F., Höpfner, S., Korn, K., Farnung, B. O., Bradshaw, C. R., Marsico, G., Volkmer, M., Habermann, B. and Zerial, M. (2012). *Caenorhabditis elegans* screen reveals role of PAR-5 in RAB-11-recycling endosome positioning and apicobasal cell polarity. *Nat. Cell Biol.* **14**, 666–676.

Wirtz-Peitz, F., Nishimura, T. and Knoblich, J. A. (2008). Linking cell cycle to asymmetric division: Aurora-A phosphorylates the Par complex to regulate Numb localization. *Cell* **135**, 161–173.

Wodarz, A., Grawe, F. and Knust, E. (1993). CRUMBS is involved in the control of apical protein targeting during Drosophila epithelial development. *Mech. Dev.* **44**, 175–187.

Wodarz, A., Hinz, U., Engelbert, M. and Knust, E. (1995). Expression of crumbs confers apical character on plasma membrane domains of ectodermal epithelia of drosophila. *Cell* **82**, 67–76.

Wodarz, A., Ramrath, A., Kuchinke, U. and Knust, E. (1999). Bazooka provides an apical cue for Inscuteable localization in Drosophila neuroblasts. *Nature* **402**, 544–547.

Wodarz, A., Ramrath, A., Grimm, A. and Knust, E. (2000). Drosophila atypical protein kinase C associates with Bazooka and controls polarity of epithelia and neuroblasts. *J. Cell Biol.* **150**, 1361–1374.

Wu, Y. and Griffin, E. E. (2017). Regulation of Cell Polarity by PAR-1/MARK Kinase. *Curr. Top. Dev. Biol.* **123**, 365–397.

Yamanaka, T. and Ohno, S. (2008). Role of Lgl/Dlg/Scribble in the regulation of epithelial junction, polarity and growth. *Front. Biosci. J. Virtual Libr.* **13**, 6693–6707.

Yamanaka, T., Horikoshi, Y., Suzuki, A., Sugiyama, Y., Kitamura, K., Maniwa, R., Nagai, Y., Yamashita, A., Hirose, T., Ishikawa, H., et al. (2001). PAR-6 regulates aPKC activity in a novel way and mediates cell-cell contact-induced formation of the epithelial junctional complex. *Genes Cells Devoted Mol. Cell. Mech.* **6**, 721–731.

Yamanaka, T., Horikoshi, Y., Sugiyama, Y., Ishiyama, C., Suzuki, A., Hirose, T., Iwamatsu, A., Shinohara, A. and Ohno, S. (2003). Mammalian Lgl forms a protein complex with PAR-6 and aPKC independently of PAR-3 to regulate epithelial cell polarity. *Curr. Biol. CB* **13**, 734–743.

Yin, X., Gower, N. J. D., Baylis, H. A. and Strange, K. (2004). Inositol 1,4,5-Trisphosphate Signaling Regulates Rhythmic Contractile Activity of Myoepithelial Sheath Cells in Caenorhabditis elegans. *Mol. Biol. Cell* **15**, 3938–3949.

Yochem, J., Tuck, S., Greenwald, I. and Han, M. (1999). A gp330/megalin-related protein is required in the major epidermis of Caenorhabditis elegans for completion of molting. *Dev. Camb. Engl.* **126**, 597–606.

Yu, F., Morin, X., Cai, Y., Yang, X. and Chia, W. (2000). Analysis of partner of inscuteable, a novel player of Drosophila asymmetric divisions, reveals two distinct steps in inscuteable apical localization. *Cell* **100**, 399–409.

Yu, H., Braun, P., Yildirim, M. A., Lemmens, I., Venkatesan, K., Sahalie, J., Hirozane-Kishikawa, T., Gebreab, F., Li, N., Simonis, N., et al. (2008). High-quality binary protein interaction map of the yeast interactome network. *Science* **322**, 104–110.

Zhang, H., Abraham, N., Khan, L. A., Hall, D. H., Fleming, J. T. and Göbel, V. (2011). Apicobasal domain identities of expanding tubular membranes depend on glycosphingolipid biosynthesis. *Nat. Cell Biol.* **13**, 1189–1201.

Zhang, H., Kim, A., Abraham, N., Khan, L. A., Hall, D. H., Fleming, J. T. and Gobel, V. (2012). Clathrin and AP-1 regulate apical polarity and lumen formation during C. elegans tubulogenesis. *Dev. Camb. Engl.* **139**, 2071–2083.

Zhang, L., Ward, J. D., Cheng, Z. and Dernburg, A. F. (2015). The auxin-inducible degradation (AID) system enables versatile conditional protein depletion in C. elegans. *Dev. Camb. Engl.* **142**, 4374–4384.

Zheng, Z., Zhu, H., Wan, Q., Liu, J., Xiao, Z., Siderovski, D. P. and Du, Q. (2010). LGN regulates mitotic spindle orientation during epithelial morphogenesis. *J. Cell Biol.* **189**, 275–288.

Zhu, J., Shang, Y., Wan, Q., Xia, Y., Chen, J., Du, Q. and Zhang, M. (2014). Phosphorylation-dependent interaction between tumor suppressors Dlg and Lgl. *Cell Res.* **24**, 451–463.

Zihni, C., Vlassaks, E., Terry, S., Carlton, J., Leung, T. K. C., Olson, M., Pichaud, F., Balda, M. S. and Matter, K. (2017). An apical MRCK-driven morphogenetic pathway controls epithelial polarity. *Nat. Cell Biol.* **19**, 1049–1060.

Zilberman, Y., Abrams, J., Anderson, D. C. and Nance, J. (2017). Cdc42 regulates junctional actin but not cell polarization in the Caenorhabditis elegans epidermis. *J Cell Biol* **216**, 3729–3744.

Zonies, S., Motegi, F., Hao, Y. and Seydoux, G. (2010). Symmetry breaking and polarization of the C. elegans zygote by the polarity protein PAR-2. *Development* **137**, 1669–1677.

Zuo, X., Guo, W. and Lipschutz, J. H. (2009). The exocyst protein Sec10 is necessary for primary ciliogenesis and cystogenesis in vitro. *Mol. Biol. Cell* **20**, 2522–2529.

Nederlandse samenvatting

Celpolariteit is een fundamentele en universele eigenschap van cellen. Epitheelcellen, één van de meest voorkomende gepolariseerde dierlijke celtypen, polariseren over een apicaal-basale as en delen moleculair- en functioneel-verschillende apicale, laterale en basale membraandomeinen in. De overgang tussen de apicale en laterale domeinen wordt gekenmerkt door de aanwezigheid van cel-cel contacten die cellen met elkaar verbinden en de ongewenste uitwisseling van moleculen tussen de cellen door cellen voorkomt. Polariteit komt tot stand door onderling tegenwerkende interacties tussen apicale en basale polariteitseiwitten, waaronder de apicale Par- en Crumbs-complexen en de basolaterale Scribble module.
Ondanks dat de veelvoorkomende polariteitseiwitten, zoals onderdelen van het Par-complex, een cruciale rol spelen in de meest bestudeerde weefsels, zijn er grote verschillen tussen celtypen: sommige cellen kunnen polariseren zonder sommige van deze factoren, hun partners en functies zijn contextafhankelijk en ze voeren taken uit die los staan van polariteit. Om beter te begrijpen hoe celpolarisatie werkt, is het belangrijk om te bestuderen hoe celpolariteit varieert tussen celtypen en of er alternatieve routes in werking treden onder verschillende omstandigheden. In **Hoofdstuk 2** hebben we recente bevindingen in het celpolariteitsveld belicht, waaronder de mechanismen die de activiteit en lokalisatie van apicaal-basale polariteitsregulatoren besturen.

In Hoofdstuk 3-5 hebben we ons gericht op de functies van de apicale polariteitscomplexen in *C. elegans* larvale weefsels. We startten met de apicale PAR eiwitten, die geconserveerd zijn van *C. elegans* tot hogere organismen. In *C. elegans* hebben de meeste onderzoeken die zich op het Par-complex richtten het *C. elegans*-embryo geanalyseerd, waarbij de nadruk lag op de eicel of de polarisatie van de darm of epidermis tijdens de embryonale ontwikkeling. Het is welomschreven dat PAR-3/PAR-6/PKC-3 betrokken zijn bij het opzetten en onderhouden van anterieure-posterieure polariteit, evenals bij het opzetten van de apicale-basale polariteit in de embryonale darm, farynx en epidermis, en in de larvale spermatheca. Er wordt gesuggereerd dat PAR-6 een rol vervult in de larvale epidermis en PAR-3 en PKC-3 in de spermatheca. Echter, aangezien het moeilijk is om deze essentiële eiwitten te onderzoeken – mutanten overlijden tijdens embryogenese en RNAi is niet sterk genoeg – is de functie van het Par-complex in larvale weefsels grotendeels onbekend. In **Hoofdstuk 3** hebben we hulpmiddelen ontwikkeld om het Par-complex in larvaal epitheel af te breken en hiermee nieuwe inzichten te krijgen in de rol van het Par-complex tijdens de larvale ontwikkeling. We hebben laten zien dat PAR-6 en PKC-3, maar niet PAR-3, essentieel zijn voor de larvale ontwikkeling en in het bijzonder de epidermis. Verder hebben we gezien dat naast hun standaard rol in

polariteit, die geconserveerd is in de larvale epidermis, PAR-6 en PKC-3 ook essentieel zijn voor vervelling, de deling van cellend die de onderhuid vormen en celdifferentiatie. Als laatste hebben we laten zien dat PAR-6 interacteert met de microtubulus organisator NOCA-1/Ninein en een fysieke aanwijzing geeft voor de apicale lokalisatie van NOCA-1. Deze resultaten geven aan dat PAR-6 niet-centrosomale microtubuli organiseert via de lokalisatie met NOCA-1 en een directe link biedt tussen het PAR-complex en microtubulus-organisatie.

In Hoofdstuk 4 en 5 hebben we ons gericht op de functie van het Crumbs-complex, wat een mysterie blijft in *C. elegans*. Ondanks dat het geconserveerd is, spelen de Crumbs-eiwitten waarnaar het complex is vernoemd geen essentiële rol bij de totstandbrenging of de instandhouding van polariteit. Tot op heden is niet onderzocht of andere leden van het complex geconserveerd zijn in *C. elegans*. In **Hoofdstuk 4** hebben we de conservering in samenstelling en functie van het Crumbs-complex in *C. elegans* beoordeeld. We hebben de homoloog van Pals1, *magu-2*, geïdentificeerd en deze bleek sterk geconserveerd. MAGU-2 is verrijkt aan het apicale domein en is, net zoals de drie Crumbs homologen, niet essentieel voor het opzetten of onderhouden van epitheelpolariteit. We hebben ook een interactie tussen MAGU-2 en de homoloog van PatJ, *mpz-1* geïdentificeerd. Als laatste hebben we gekeken naar het effect van overexpressie van de homologen van CRB2 en CRB3, respectievelijk *eat-20* en *crb-3*, om meer inzicht te krijgen in de functie van het Crumbs-complex. Overexpressie van EAT-20 en CRB-3 resulteerde in een vergroot apicaal domein, wat aangeeft dat het Crumbs-complex apicale identiteit in *C. elegans* kan stimuleren. De niet-essentiële rol van de Crumbs homologen in *C. elegans* kan komen door overlappende functies binnen het apicale polariteitsnetwerk. Om deze mogelijkheid te onderzoeken en om inzicht te krijgen in de functie van het Crumbs-complex, hebben we gedetailleerd gekeken naar de functie van de drie Crumbs homologen in **Hoofdstuk 5** door middel van een genetische screen voor synthetische defecten met een driedubbele Crumbs knock-out. We hebben synthetische defecten gevonden tussen de driedubbele Crumbs knock-out en een nonsense-mutatie in een vermoedelijke serine-proteaseremmer, *zk287.4*. De gecombineerde mutanten van ZK287.4 en de drie Crumbs eiwitten hadden ontwikkelings- en morfologiedefecten die we niet zagen in de individuele mutanten. Deze resultaten suggereren dat de driedubbele *Crumbs* mutanten geen defecten tonen door overlap met andere eiwitroutes en dat het Crumbs-complex betrokken is bij het opzetten en onderhouden van het apicale domein.

Al met al hebben we de apicale Par- en Crb-complexen in *C. elegans* epithelia in detail bestudeerd, nieuwe functies voor beide complexen blootgelegd en ons begrip van het apicale polariteitsnetwerk vergroot. Bovendien hebben we nieuwe inzichten gekregen over de interactie tussen celpolariteit en andere

cellulaire processen. Naarmate er meer bekend wordt over de mechanismen die celpolariteit bevorderen, wordt het duidelijk dat de organisatie van celpolariteit niet in alle weefsels en organismen hetzelfde is. Doordat er veel geavanceerde genetische hulpmiddelen beschikbaar zijn voor werk in *C. elegans* en doordat de ontwikkeling van het organisme uitstekend in kaart is gebracht, biedt *C. elegans* een aantrekkelijk modelsysteem voor onderzoek naar celpolariteit, de interactie tussen celpolariteit en andere processen en hoe celpolariteit nauw verbonden is met weefselhomeostase en de ontwikkeling van een organisme.

English summary

Cell polarity is a fundamental and universal property of cells. Epithelial cells, one of the major polarized animal cell types, polarize along an apical-basal axis and establish molecularly and functionally distinct apical, basal, and junctional domains. Polarity establishment is mediated by mutually antagonistic interactions between apical and basal polarity regulators, including the apical Par and Crumbs complex and the basolateral Scribble module.
Although canonical polarity regulators, such as members of the Par complex, have crucial roles in most studied tissues, there is a high degree of diversity among cell types: some cells can polarize in the absence of some these factors, their partners and functions are context-dependent, and they have roles that are independent on polarization. Thus, in order to understand the process of cell polarization it is key to study how the cell polarization varies between cell-types and whether alternative pathways operate in specific contexts (Pickett et al., 2019; St Johnston, 2018).

The Par complex

The role of the apical Par complex in *C. elegans* larval tissues remains unclear. Most studies focusing on the Par complex have analyzed the *C. elegans* embryo, focusing on the oocyte or the polarization of the intestine or epidermis during embryonic development (Achilleos et al., 2010; Totong et al., 2007). It has been suggested that PAR-6 has a role in the larval epidermis (Welchman et al., 2007) and PAR-3 and PKC-3 in the spermatheca (Aono et al., 2004; Montoyo-Rosario et al., 2020), but the details remain largely unknown.
In chapter 3 we have gained new insights into the role of the Par complex during larval development. We have shown that PAR-6 and PKC-3, but not PAR-3, are essential for larval development, and in particular in the epidermis. Furthermore, we saw that apart from having a canonical polarity role, which is conserved in the larval epidermis, PAR-6 and PKC-3 are essential for the processes of molting, seam cell division and differentiation. Whilst Par6 and aPKC have been shown to have a function in spindle positioning and asymmetric cell division in Drosophila and mammalian systems (Knoblich, 2010), the mechanistic details have only been resolved in Drosophila (Izumi et al., 2004; Knoblich et al., 1997; Smith et al., 2007; Wirtz-Peitz et al., 2008; Wodarz et al., 2000; Yu et al., 2000). Understanding why cell division and differentiation are affected in *C. elegans* could shed light into how cell polarity is involved in such a key process.
Moreover, we have shown that PAR-6 interacts with the microtubule organizer NOCA-1 Ninein and provides a physical cue for the apical localization of NOCA-1, as well as that of GIP-1 and PTRN-1. These results indicate that PAR-6 organizes non-centrosomal microtubule arrays through localization of

NOCA-1 and provide a direct link between the PAR complex and microtubule organization. Whilst there have been some studies linking cell polarity and the Par proteins to microtubule organization (St Johnston, 2018), a direct link between the polarity complex and the microtubule cytoskeleton had not been identified until now. It would be interesting to know whether the interaction between PAR-6 and NOCA-1 that we have described here also plays a role in the assembly of the non-centrosomal microtubule organizing center in other tissues and organisms.
Importantly, we have developed tools to degrade the Par complex in larval epithelia. Whilst we have focused on the epidermis, the Par complex is likely to have essential roles in different tissues. For example, a recent study described a novel role for the Par complex in the excretory canal, where PAR-6 and PKC-3 interact with the exocyst pathway (Abrams and Nance, 2020). In chapter 3 we have described several roles for the Par complex that are likely tissue specific, such as the defects on molting and the growth arrest observed upon degradation of PAR-6/PKC-3. Whilst these defects may arise from the microtubule defects that we observed, this remains unclear. Studying the role of these proteins in different tissues may shed light into different interactions between the Par complex and other cellular processes, increasing our understanding of the effector pathways of cell polarity.

The Crumbs complex

The Crumbs complex remains a mystery in *C. elegans*. Despite being conserved, it has no essential role in polarity establishment or maintenance (Waaijers et al., 2015). Furthermore, it has not been studied whether the different members of the complex are conserved in *C. elegans*. Interestingly, Crumbs has been suggested to have a redundant role with the junctional component HMP-1α-Catenin and the basolateral protein LET-413 Scribble. After inactivation of HMP-1 and LET-413, CRB-1 Crb1 provides a positional cue for the localization of apical junctions (Segbert et al., 2004). These results suggest that Crumbs is functional. In chapter 4 and 5 we have strived to increase our understanding of the complex.
In chapter 4 we characterized the conservation of composition and functioning of the Crumbs complex in *C. elegans*. We identified *magu-2* as a functional homolog of mammalian Pals1, a core member of the Crumbs complex, and *mpz-1* as a putative homolog of PatJ. As would be expected, MAGU-2 interacts with the Crumbs proteins and with MPZ-1 and depends on Crumbs for its apical localization. Similarly to the Crumbs proteins, which are not essential for polarity establishment or *C. elegans* development (Waaijers et al., 2015), neither is MAGU-2. These results suggest that the Crumbs complex is conserved in *C. elegans*. We also overexpressed EAT-20 Crb2 and CRB-3 Crb3 in the larval intestine and observed apical membrane overgrowth, indicating that the Crumbs complex can perform a traditional apical identity promoting function

in *C. elegans*.
In chapter 5 we sought to gain new insights into the functioning of the Crumbs complex. We performed an EMS screen to identify synthetic interactions with the three Crumbs proteins, and identified a putative serine protease inhibitor, ZK287.4, as a synthetic interactor. Combined mutants of ZK287.4 and the three Crumbs proteins display developmental and morphological defects not seen in the individual mutants. These results further confirm that Crumbs is functional in wild-type animals and suggest that a triple *Crumbs* mutant appears to show no defects due to redundancy with other pathways. It would be very interesting to know the precise function of ZK287.4, as it would also help us understand the function of the Crumbs complex.

Altogether, we have studied in detail the apical Par and Crb complexes in *C. elegans* epithelia, uncovering new functions for both complexes and increasing our understanding of the apical polarity network. Moreover, we have gained new insights on the interaction between cell polarity and other cellular processes. As more becomes clear about the mechanisms that promote cell polarity, it becomes apparent that the organization of cell polarity is not the same in all tissues and organisms. The model system *C. elegans*, with its advanced genetic tools and characterized development, provides an attractive system to study cell polarity and its interaction with other processes, as well as how cell polarity is intertwined with tissue homeostasis and the development of an organism.

Curriculum vitae

María Victoria García Castiglioni was born in Montevideo, Uruguay, on September 14th 1993. She studied a bachelor's degree in Biotechnology at the Universidad Politécnica de Valencia (UPV), majoring in Biomedicine. During her bacherlor she spent one year at Wageningen University, as part of an Erasmus programme. Later on she carried out a master's degree in Neuroscience at the Universidad Autónoma de Barcelona (UAB). On September 2016 Victoria started her doctorate degree in the group of Prof. Boxem at Utrecht University, in the department of Developmental Biology. Her doctorate was part of Polarnet, a Marie Skłodowska-Curie Actions Innovative Training Network. The results of her research, which was carried out until February 2021, are presented in this thesis.

List of Publications

Castiglioni VG, Ramalho JJ, Kroll J, Stucchi R, van Beuzekom H, Schmidt R, Altelaar M, Boxem M. (2021) Characterization of the composition and functioning of the Crumbs complex in *C. elegans*. *bioRxiv 2021.08.10.455623*

Riga A, Cravo J, Schmidt R, Pires HR, **Castiglioni VG**, van den Heuvel S, Boxem M. (2021) *Caenorhabditis elegans* LET-413 Scribble is essential in the epidermis for growth, viability, and directional outgrowth of epithelial seam cells. *bioRxiv 2021.04.11.439327*

Castiglioni VG*, Pires HR*, Bertolini RR, Riga A, Kerver J, Boxem M. (2020) Epidermal PAR-6 and PKC-3 are essential for larval development of *C. elegans* and organize non-centrosomal microtubules. *eLife 62067*

Castiglioni VG*, Riga A*, Boxem M. (2019) New insights into apical-basal polarization in epithelia. *Current Opinion in Cell Biology 62:1–8*

* co-authorship

Acknowledgements

There is an African proverb that says “It takes a village to raise a child”. Similarly, it takes a whole lot of people to complete a PhD.

First and foremost, I’d like to thank **Mike**. You have always been kind, patient and understanding with me. From explaining basic genetic crosses and CRISPR during my first months, to giving me freedom to design my experiments at the end, you have always encouraged me to think for myself and to become an independent researcher. You’ve always been open to every type of question, making me feel safe to ask whatever I didn’t understand and taking the time to explain it in detail - even during your busiest periods, you were always available when I had questions or when I needed encouragement. And apart from all the serious supervising you had to do, you were always up to having a beer with us and even playing ping-pong in the office. Completing a PhD is not easy, and I’m very thankful that I have so many good memories during the time in your lab.

I’d also like to thank **Sander**, my earliest promotor. During the first meetings were I presented my work to the group I was always afraid of what you’d ask – knowing that they will be good questions and may be hard to answer. With time that fear subsided, and I was looking forward to your very helpful input. Thank you for making time to participate in my projects. I’d also like to thank you for your work in the department, where you and Inge have always strived to create a friendly environment, introducing us to the American Thanksgiving and Dutch Sinterklaas traditions.

Coming from abroad can be hard, and luckily for me the department of Developmental Biology became a makeshift foster family. The week after we arrived there was an annual barbecue, where we got to meet everyone well and got introduced to the social side of the department. Since then (and before covid hit us), there have been dinners and galas, lab outings, climbing sessions, and board game nights.

Closest to my heart will always be the southern girls. There is no way I could have made it through the PhD without the support that you offered. You’ve made the lab a fun place, you’ve supported me when things were hard, and you were always up to grabbing a coffee to leave the Kruyt for a few minutes. **Helena**, I have no idea where this thesis would be without you. When I was struggling with my project and needed help you embraced me without a doubt, welcoming me into your project as a full member since the first day. You’ve been the best cheerleader and the best listener, and working with you made work feel nothing like work! There are so many things I’m happy to have

learned from you, from critical thinking, scientific writing and experimental design, to how to be a good colleague and a good friend. I'm so happy that our paths crossed during these years, and know that as our paths manage to cross again during the coming years everything will be just as it was when we saw each other every single day. **Amalia**, you've been such an essential piece to the puzzle. I can't even begin to describe how lucky I feel that Mike hired you as the other PolarNet member of the lab. I remember our first day, we arranged to meet each other before meeting Mike but we bumped into him and he invited us to come to the lab early… we've become so much better at sneaking out of the lab since then! These years have been difficult for both of us in countless different ways, and we've been there for each other through it all. And if there's something I love about you is that you can make anything fun, we'll never not laugh together. So apart from doing all these incredible things like a PhD and travelling around for courses, conferences, and internships (like, how incredibly lucky were we? And how cool that we got to do all those things together?), we've had so much fun. I can't believe that going out for drinks or for a coffee is not part of our everyday life anymore. But I know the good memories will keep coming, and I'm really excited to have you in my life from hereon. **Janine**, since I arrived to the lab you've been by my side. We were office mates, had lunch together almost every day, drinks on Fridays. You're always up to do something fun, and always had time to discuss life or lab things. I've learned from you that some things in life shouldn't be taken seriously and also, a crazy amount of perseverance - you are incredibly hard working, and it's been great to be by your side all this time!

Not to appear like I discriminate nationalities, there's quite a few non-southern people which I'm incredibly thankful for. **Sanne**, you came into the lab with so much energy and life. It's been great to see how you approach your PhD and incredible to think that you're also almost done! I've had so much fun with you, in the lab and outside. I missed you a lot during covid, but I'm glad that we kept meeting up online. Hopefully we'll keep meeting up in different places in the future ;) **Jorian**, I'm so glad that you came back after your internship! It's been so nice to work with you for so many years, you're also always up for doing fun things, for having a break, gossiping a bit, and it's so incredibly easy to tease you! I'll miss you so much!! I do expect to see you back in your favorite city though, I promise I'll be a great tour guide! **Vincent**, I've thought about how I'd thank you for all these years and I'm not sure what to say. You've been so incredibly kind and helpful, it's been so nice to seat across from you, to grab coffees, to discuss things when they were hard. You are so incredibly patient too, explaining for the thousandths time the same thing. I don't know how I'd have managed without all your scientific, but also non-scientific, advice. **Ruben**, you've been my office and lab mate during these 4+ years. In the office you're kind of quiet, but in the lab you become much more chatty, and

it's been really fun to speak about life and try to find music which we both like. It's also been really fun to meet you outside As Vincent's F1, it perhaps makes sense that you were also so helpful explaining things when I was new in the lab! Thank you for that! **Molly**, it's crazy to think you've been gone for a while now. I'm really happy we got to work together for a while, it's so inspiring to see with how much energy and passion you approach everything in life, from work to climbing. I miss your positive attitude towards everything! **Ben**, joining a teaching position we coincided less than with other members, but your friendliness and openness made for an instant fit into dev bio. Your love for teaching and science is really inspiring, and I'm glad we got to know each other. **Jason**, you've been such a good addition to the lab! It's been really nice to see how you approach your work and I'm really glad that your stories are working out! **Lars** and **Suzanne**, I started when you guys were finishing so we didn't overlap that much. Still, as a new PhD student you learn a lot from the ones coming before you, and I'm thankful for all the wise advice you passed on before graduating. Good luck in your current endeavors! **Suzan**, we've only shared the lab for a few months yet it's been really nice to get to know you. You're so passionate about what you do and it's really inspiring to speak to you and to see how you're now supervising so many students. I wish you all the success in your future research! **Inge**, I'd like to thank you for all the insight you've shared on group meetings, all the nice conversations during lab borrels, dinners and galas, as well as for inviting us to your home and making us feel welcome. **Tessa**, **Alex** and **Elise**, the new generation, it seems like the lab is in great hands now! I hope you have fun in the lab!

A decent part of my PhD was devoted to teaching, where I taught as much as I learned. I'd like to thank my master students, **Hanna** and **Rodrigo**, for choosing to do their internships with us, for their patience and for their hard work! I hope you took as much from the experience as I did and that you succeed in your next steps. I'd also like to thank all the other master students that spent time in the lab, especially Olga and Nik, for all the nice conversations and bringing a breath of fresh air to the lab

This book would probably not have come to existence without a little help from my friends. **Eva**... no se que habría sido de mi sin ti en Utrecht. De verdad que no se poner en palabras lo agradecida que estoy de que nos hayamos conocido y de tenerte ahora en mi vida. Te echo de menos, always. Y gracias por ser mi Paranimf. **Tal**, otro de mis pilares, sin el cuál no sé cómo habría sido de mi en Utrecht. Siempre has estado ahí para mi cuando lo he necesitado, me alegro tanto de que se hayan cruzado nuestros caminos y de tenerte como amiga de aquí en más. Haber acabado el doctorado, esta etapa de la vida, hubiera sido muchísimo más fácil si no significara que ya no vivimos todas a 10 minutos de cada una, ya que por mucho que me alegre de teneros en mi vida,

estoy igualmente triste de ya no teneros cerca. Aunque si queréis hacemos un Utrecht 2.0 - un poco más soleado - por aquí. And of course, I'm so thankful for the CSnD girls. **Jet, Arwa, Maya, Marta** and **Helena**. It's been so fun to spend these years with you... brunches, dinners, coffees and drinks, and some travelling here and there. I'm so thankful we all came together because of the PhD programme, as these years would have been very dull without you in my life. I'm really excited to see where life takes us now! And also, to party in all our defenses... we deserve it!
Y gracias también a mis amigas de España, por el apoyo, por visitar, por seguir estando ahí a pesar que soy malísima manteniendo el contacto, y por la recibida/re-acogida que me habeis dado después de una larga ausencia <3

Y por último, quiero agradecer a mi familia. **Mamá** y **Papá**, que siempre han creído en mi con una fé absoulta, y me dicen que lo que tengo me lo merezco y no es todo suerte. Dieron todo por nosotros y cada día siguen dandonos todo su amor y apoyo. Hacer un doctorado no habría sido posible sin su ejemplo de trabajo y perseverancia. **Belu**, que has venido a visitarme más que nadie y has estado ahí para hablar por teléfono unas tropecientas veces más. Gracias por todo el apoyo que me has dado durante estos años y por siempre ayudarme a solucionar cualquier problema que me surja. **Pancho**, por pensar que lo que hago está re bueno, dibujarme gusanitos y ser el hermano más divertido. Y last but not least, **Jack**, por estar a mi lado todos los días, escucharme hasta incluso conseguir aprender a describir bastante bien lo que hago, y por apoyarme cuando más lo necesito.

“τούτου μὲν τοῦ ἀνθρώπου ἐγὼ σοφώτερός εἰμι·
κινδυνεύει μὲν γὰρ ἡμῶν οὐδέτερος οὐδὲν καλὸν
κἀγαθὸν εἰδέναι, ἀλλ᾽ οὗτος μὲν οἴεταί τι εἰδέναι
οὐκ εἰδώς, ἐγὼ δέ, ὥσπερ οὖν οὐκ οἶδα, οὐδὲ οἴομαι·
ἔοικα γοῦν τούτου γε σμικρῷ τινι αὐτῷ τούτῳ
σοφώτερος εἶναι, ὅτι ἃ μὴ οἶδα οὐδὲ οἴομαι εἰδέναι”

I am wiser than this man,
for neither of us appears to know anything great and good;
but he fancies he knows something, although he knows nothing;
whereas I, as I do not know anything, so I do not fancy I do.
In this trifling particular, then, I appear to be wiser than he,
because I do not fancy I know what I do not know

“ὁ ... ἀνεξέταστος βίος οὐ βιωτὸς ἀνθρώπῳ”

The unexamined life is not worth living

Socrates